Appendix 3A

PLANT DESIGN ASSESSMENT REPORT FOR SAFETY/RELIEF VALVES AND LOSS-OF-COOLANT ACCIDENT LOADS

TABLE OF CONTENTS

Appendix 3A

**PLANT DESIGN ASSESSMENT REPORT FOR
SAFETY/RELIEF VALVES AND LOSS-OF-COOLANT
ACCIDENT LOADS**

TABLE OF CONTENTS (Continued)

Appendix 3A

**PLANT DESIGN ASSESSMENT REPORT FOR
SAFETY/RELIEF VALVES AND LOSS-OF-COOLANT
ACCIDENT LOADS**

TABLE OF CONTENTS (Continued)

Appendix 3A

**PLANT DESIGN ASSESSMENT REPORT FOR
SAFETY/RELIEF VALVES AND LOSS-OF-COOLANT
ACCIDENT LOADS**

<u>TABLE OF CONTENTS</u> (Continued)

<u>Section</u>   <u>Page</u>

Appendix 3A

**PLANT DESIGN ASSESSMENT REPORT FOR
SAFETY/RELIEF VALVES AND LOSS-OF-COOLANT
ACCIDENT LOADS**

TABLE OF CONTENTS (Continued)

Appendix 3A

**PLANT DESIGN ASSESSMENT REPORT FOR
SAFETY/RELIEF VALVES AND LOSS-OF-COOLANT
ACCIDENT LOADS**

TABLE OF CONTENTS (Continued)

Appendix 3A

**PLANT DESIGN ASSESSMENT REPORT FOR
SAFETY/RELIEF VALVES AND LOSS-OF-COOLANT
ACCIDENT LOADS**

TABLE OF CONTENTS (Continued)

Appendix 3A

**PLANT DESIGN ASSESSMENT REPORT FOR
SAFETY/RELIEF VALVES AND LOSS-OF-COOLANT
ACCIDENT LOADS**

TABLE OF CONTENTS (Continued)

Appendix 3A

PLANT DESIGN ASSESSMENT REPORT FOR SAFETY/RELIEF VALVES AND LOSS-OF-COOLANT ACCIDENT LOADS

LIST OF TABLES

Appendix 3A

**PLANT DESIGN ASSESSMENT REPORT FOR
SAFETY/RELIEF VALVES AND LOSS-OF-COOLANT
ACCIDENT LOADS**

<u>LIST OF TABLES</u> (Continued)

Appendix 3A

**PLANT DESIGN ASSESSMENT REPORT FOR
SAFETY/RELIEF VALVES AND LOSS-OF-COOLANT
ACCIDENT LOADS**

LIST OF TABLES (Continued)

Appendix 3A

**PLANT DESIGN ASSESSMENT REPORT FOR
SAFETY/RELIEF VALVES AND LOSS-OF-COOLANT
ACCIDENT LOADS**

LIST OF FIGURES

Appendix 3A

PLANT DESIGN ASSESSMENT REPORT FOR
SAFETY/RELIEF VALVES AND LOSS-OF-COOLANT
ACCIDENT LOADS

LIST OF FIGURES (Continued)

Appendix 3A

PLANT DESIGN ASSESSMENT REPORT FOR
SAFETY/RELIEF VALVES AND LOSS-OF-COOLANT
ACCIDENT LOADS

<u>LIST OF FIGURES</u> (Continued)

Appendix 3A

**PLANT DESIGN ASSESSMENT REPORT FOR
SAFETY/RELIEF VALVES AND LOSS-OF-COOLANT
ACCIDENT LOADS**

<u>LIST OF FIGURES</u> (Continued)

Appendix 3A

**PLANT DESIGN ASSESSMENT REPORT FOR
SAFETY/RELIEF VALVES AND LOSS-OF-COOLANT
ACCIDENT LOADS**

LIST OF FIGURES (Continued)

Appendix 3A

**PLANT DESIGN ASSESSMENT REPORT FOR
SAFETY/RELIEF VALVES AND LOSS-OF-COOLANT
ACCIDENT LOADS**

LIST OF FIGURES (Continued)

Appendix 3A

**PLANT DESIGN ASSESSMENT REPORT FOR
SAFETY/RELIEF VALVES AND LOSS-OF-COOLANT
ACCIDENT LOADS**

<u>LIST OF FIGURES</u> (Continued)

Appendix 3A

**PLANT DESIGN ASSESSMENT REPORT FOR
SAFETY/RELIEF VALVES AND LOSS-OF-COOLANT
ACCIDENT LOADS**

<u>LIST OF FIGURES</u> (Continued)

Appendix 3A

PLANT DESIGN ASSESSMENT REPORT FOR
SAFETY/RELIEF VALVES AND LOSS-OF-COOLANT
ACCIDENT LOADS

This third revision of the "Plant Design Assessment Report," (DAR) together with the
safety/relief valve (SRV), condensation oscillation and chugging reports, finalizes the
Columbia Generating Station load definition, load application, load combination, and design
margins for hydrodynamic loading conditions.

In July 1993 Energy Northwest requested an amendment to the operating license to allow an
increase in the power level of the plant. The effects of power uprate on the containment
system response are described in NEDC-32141-P. Specifically, Section 4.1 of
NEDC-32141-P states that for short-term containment pressure response, the peak pressure
values are below design values and remain virtually unaffected by power uprate and extended
load line limit. The loss-of-coolant accident (LOCA) containment dynamic loads are not
affected by power uprate, and SRV containment loads will remain below their design
allowables. Appendix 3A has not been updated to reflect the minor changes to the LOCA and
SRV load analyses described in NEDC-32141-P.

3A.1.1   CONFORMANCE TO NRC ACCEPTANCE CRITERIA

The DAR specifies the Columbia Generating Station position for each of the pool dynamic
loads. The table further provides a detailed description of each load, the NRC evaluation, and
the Columbia Generating Station position on the acceptance for each load. The Columbia
Generating Station positions (Attachment 3A.H) were discussed, reviewed, and approved by
NRC at various meetings with Energy Northwest. The NRC acceptance was formalized in the
Columbia Generating Station Safety Evaluation Report (SER).

3A.1.2   ROLE OF THE DESIGN ASSESSMENT REPORT

The Columbia Generating Station DAR serves the primary purpose of assessing the adequacy of structures and equipment affected during SRV actuation or a postulated LOCA. This report utilizes the load definition data from the SRV report, chugging report, DFFR (Reference 3A.3.2-2), and applicable NRC guidelines as outlined in Attachment 3A.H.

Specifically Revision 3 of the DAR serves the following purposes:

   a.   Summarize the loads and effects agreed upon with NRC which are most
        important to the design of the plant,

   b.   Identify the design modifications implemented to withstand these loads, and

   c.   Identify the design margins for hydrodynamic loading conditions.

3A.1.3   ASSESSMENT APPROACH

The information developed in the SRV and Chugging Reports (References 3A.3.1-1 and 3A.3.2-15 respectively) together with other information available as outlined in Attachment 3A.H, was used to assess all major structures, systems, and components in the wetwell region. The effects of hydrodynamic loads outside the wetwell region are discussed in the appropriate sections of the FSAR.

3A.1.4   SUMMARY OF DESIGN ASSESSMENT REPORT CONTENT

The DAR, Revision 3 is summarized as follows:

Chapter 1

      a.   Introduction to CGS Loads,
      b.   Review of the purpose of the plant specific loads, and
      c.   Discussion of the assessment of containment components since DAR Revision 2.

Chapter 2

      a.   General description of the CGS containment, and
      b.   Summary and conclusions.

Chapter 3

A discussion of the manner in which the plant specific loads for CGS are determined, based on information provided in the SRV and chugging reports, DFFR, and other associated and referenced documents.

Chapter 4

A review of the design assessment for the CGS containment system. Assessment and conclusions are included for suppression pool boundary structures (steel containment, vertical and horizontal tees, basemat, pedestal, diaphragm floor, and diaphragm floor seal) and for suppression pool major structures (downcomer bracing, columns, downcomers, SRV piping systems, quenchers, and platforms), and for suppression pool miscellaneous piping systems.

Chapter 5

Provides the building response due to SRV discharge, LOCA.

Attachments

The attachments to this report provide

      a.   Attachment not utilized,

      b.   Theoretical formulation for the calculation of three dimensional source flows in exact containment geometry,

c.   A method to calculate drag forces on submerged structures caused by hydrodynamic flow fields,

d.   Calculation models for short term LOCA phenomena,

e.   Description of the suppression pool temperature monitoring system,

f.   Description of computer programs utilized for CGS load definition and plant assessment,

g.   Attachment not utilized,

h.   Table of conformance of CGS design to NRC acceptance criteria, and

i.   Summary of the methodologies used for defining SRV and LOCA loads on submerged structures.

3A.2   SUMMARY AND CONCLUSIONS

3A.2.1   GENERAL DESCRIPTION OF PLANT

The Energy Northwest Nuclear Project No. 2 (CGS) is a nuclear fueled electrical generating station which utilizes a General Electric Company BWR-5 (1969 product line) nuclear reactor.

The primary containment utilizes a Mark II over/under pressure-suppression configuration (see Figure 3A.2.1-1). The primary containment consists of a steel pressure vessel enclosed by a concrete shield wall both supported by a concrete basemat. The primary containment is enclosed by the reactor building, a reinforced-concrete structure functioning as a secondary containment.

The drywell is connected to the suppression chamber by 99 downcomer pipes. Originally 102 downcomer pipes were provided but three were capped, as discussed in Sections 3A.3.2.1 and 3A.3.2.2. Steam that could be released in the drywell during a postulated loss-of-coolant accident (LOCA) is channeled through these downcomer pipes into the suppression pool where it is condensed thus effecting pressure-suppression.

Eighteen safety/relief valves (SRVs) are mounted on the four main steam lines. When SRVs are actuated, steam from the reactor pressure vessel (RPV) flows through the SRV discharge lines into the suppression pool where the steam is condensed. The discharge lines from all 18 SRVs are routed inside selected downcomers into the suppression chamber (Figures 3A.2.1-6 through 3A.2.1-8). Each discharge line terminates with a quencher device having four arms. Seven of the 18 SRVs are part of the automatic depressurization system (ADS) (Table 3A.3.1-1) which is designed to function, under certain conditions, following a postulated intermediate or small size line break.

3A.2.1.1   Structures, Piping, and Components Directly Affected by Pool Dynamic Loads

The structures in the suppression chamber are shown in Figures 3A.2.1-2 through 3A.2.1-8. The structures, piping and components directly affected by the hydrodynamic events associated with the LOCA pressure suppression and the SRV discharge are identified below. The applicable hydrodynamic loads are identified in Section 3A.4.

    a.   Boundary elements

        The suppression chamber boundary elements are: the steel containment including the vertical and horizontal tee stiffeners (Figure 3A.4.1-4), the concrete basemat, the concrete pedestal, the diaphragm floor and the diaphragm floor seal;

b.   Major structures and components

The major vertical structures are shown in Figure 3A.2.1-2. They are the
102 downcomers, the 18 SRV lines including quenchers and support towers,
and the 17 concrete columns supporting the diaphragm floor. The major
horizontal structures are the steel truss shown in Figure 3A.2.1-3 which
provides lateral support to the downcomers and the SRV lines, and the platform
at el. 472 ft 4 in. shown in Figures 3A.2.1-3 and 3A.2.1-8. The downcomer
bracing truss is submerged and the platform is located in the pool swell zone;
and

c.   Miscellaneous piping systems

A developed elevation of the CGS containment showing the location of the
containment penetrations is shown in Figure 3A.2.1-9. The piping systems of
the suppression pool are classified as described below.

1.   Fully submerged piping systems

Eleven piping systems are fully submerged in the suppression pool (see
Figure 3A.2.1-2). Seven systems enter the pool through containment
penetrations at el. 452 ft 0 in. One pipe [4 in.-fuel pool cooling and
cleanup (FPC)] enters the pool through the pedestal at el. 451 ft 8.25 in.
Two short lengths of pipe (instrumentation stubs) enter the pool at
el. 462 ft 0 in. A third (instrumentation line) enters at el. 455 ft 0 in.
Pipes below the downcomer vent exit at el. 454 ft 4.75 in.

2.   Partially submerged piping systems

Thirteen partially submerged piping systems enter the suppression
chamber through containment penetrations at el. 467 ft 9 in. (see
Figure 3A.2.1-3) and enter the pool vertically within 3 ft 0 in. distance
from the containment as shown in Figures 3A.2.1-6 through 3A.2.1-8.

3.   Piping systems in pool swell zone

The pool swell zone is identified in Section 3A.3.2.3 to be between the
elevations of the initial pool surface (466 ft 4.75 in.) and the maximum
pool rise during a LOCA (design basis accident) (484 ft 4.75 in.).

Piping systems in the pool swell zone include short projections into the chamber from the containment at one access hatch and 10 miscellaneous piping systems as shown in Figure 3A.2.1-3 and Figures 3A.2.1-6 through 3A.2.1-8.

4.   Piping systems above the pool swell zone

Piping systems above the pool swell zone include short lengths of pipe entering at el. 491 ft 0 in. and two penetrations for the wetwell spray header also at el. 491 ft 0 in. as shown in Figure 3A.2.1-4 and Figures 3A.2.1-6 through 3A.2.1-8.

3A.2.1.2   Structures, Piping, and Components Indirectly Affected by Pool Dynamic Loads

In the drywell region the containment structures, piping, and components are also affected by pool dynamic loads. This is a result of loading applied to the suppression chamber boundary (basemat, pedestal, and containment shell) which would result in vibratory motion transmitted through the reactor pedestal and the primary containment. This is commonly referred to as "building response."

High Point Top of Steel El. 668'-9 1/4"

Top Of Parapet Steel El. 671' - 2"

Roof Truss

125 Ton Bridge Crane

Crane Runway Girder

Refueling Platform

Bridge Girder

26'-3 1/8"

El. 606' - 10 1/2"

Dryer & Separator Storage Pool

El. 598' - 8"

Fuel Storage Pool

7'-10 3/4"

Reactor Well Pool Cavity

7'-8"

31' - 8" I.D.

3'-6 3/4"

El. 581-10 1/2"

39'-6 1/2"

El. 583' - 1/4"

El. 572' 0"

Storage Area

Stabilizer Truss

Steel Primary Containment Vessel

Sacrificial Shield

El. 548

R.P.V.

Reactor Building

47' - 9 3/4"

Columns

22'-8 7/8" O.D.

Drywell Area

El. 521' - 0 1/4"

El. 519'-2 1/4"

El. 522' - 0"

Biological Shield Wall

18' - 9" I.D.

El. 499' - 6"

20' - 3" I.D.

El. 501'

El. 492'-8 1/4"

Drywell Floor

Drywell Floor Seal

85' - 9" I.D.

Suppression Chamber

Reactor Pedestal

Down Comer Vents

El. 471

El. 466' - 4 3/4" (Max) Suppression Pool Water Level

Columns

Sand Filled Pockets

El. 446' - 0"

El. 435' - 3"

El. 435' - 3"

Outer Skirt

El. 428' - 3 1/4"

Inner Skirt

El. 422' - 3" Bldg. Ins. Dia. 127'-0" x 143'-0"

Foundation Mat

77' - 0"

143' - 0"

Section Looking South

Columbia Generating Station
Final Safety Analysis Report

Primary and Secondary Containment Structure

Draw. No. 950021.60 | **Rev.** | **Figure 3A.2.1-1**

Form No. 960690

GENERAL NOTES:

1. SEE SM 168 FOR CONTAINMENT COMPOSITE DWG'S.

NOTES:

1. WORK THIS DWG. WITH DWG'S SM 247, SM 250, SM 251 & SM 260.

SUPPRESSION POOL DWG LIST:

SM-246 SUPPRESSION POOL COMPOSITE PLAN AT EL. 435'-3", REACTOR BLDG.
SM-247 SUPPRESSION POOL COMPOSITE PLAN AT EL. 455'-4", REACTOR BLDG.
SM-248 SUPPRESSION POOL COMPOSITE PLAN AT EL. 486'-8", REACTOR BLDG.
SM-249 SUPPRESSION POOL COMPOSITE PLAN AT EL. 494'-5¼", REACTOR BLDG.
SM-250 SUPPRESSION POOL COMPOSITE SECTIONS & DETAILS, REACTOR BLDG.
SM-251 SUPPRESSION POOL COMPOSITE SECTION & DETAILS, REACTOR BLDG.
SM-260 SUPPRESSION POOL COMPOSITE SECTION & DETAILS, REACTOR BLDG.

REFERENCE DWGS:

M701 RHR, LPCS, RCC, FPC, SLC, CDR PLAN, SECT'S & DTL'S, EL.422'-3' REACTOR BLDG.
M702 RHR, LPCS, RCC, FPC, SLC, CDR PLAN, SECT'S & DTL'S, EL.444'-0' REACTOR BLDG.
M712 RFW, RCIC, HPCS, SW, RWCU, RRC & TSW REACTOR BLDG. EL.441'-0'
M733 COMPR.AIR, FIRE PROT.COND, DEMIN, WATER, SUMP DISCH.&MISC.PIPING-PLAN, SECT'S & DTL'S EL.441'-0' REACTOR BLDG.
M789 REACTOR BLDG. REACTOR PEDESTAL SH.1 THRU 4
S794 CONTAINMENT VESSEL SH. 1 THRU 8
S1057 CONTAINMENT VESSEL-PART PLAN & SECT'S MISC. PIPING SUPPORT.
S1066 CONTAINMENT VESSEL PLAN OF QUENCHER SUPPORTS
S1067 CONTAINMENT VESSEL SECT'S & DETL'S OF QUENCHER SUPPORT
S1068 CONTAINMENT VESSEL PLAN OF MISC. PIPING SUPPORTS
S1069 CONTAINMENT VESSEL SECT'S & DETL'S MISC. PIPING SUPPORT
S1070 CONTAINMENT VESSEL MISC.DETAILS-MISC PIPING SUPPORT
M200 SH. 73 - QUENCHER ASSEMBLY & DETAILS
M290 SH.76 THRU 93-MAIN STEAM PIPING FROM JET DEFLECTOR TO QUENCHER

KEY PLAN
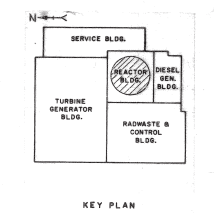
Columbia Generating Station Final Safety Analysis Report	Suppression Pool Composite Plan at El. 435 ft 3 in.		
	Draw. No. SM246	Rev. 0	Figure 3A.2.1-2

Form No. 960690FH
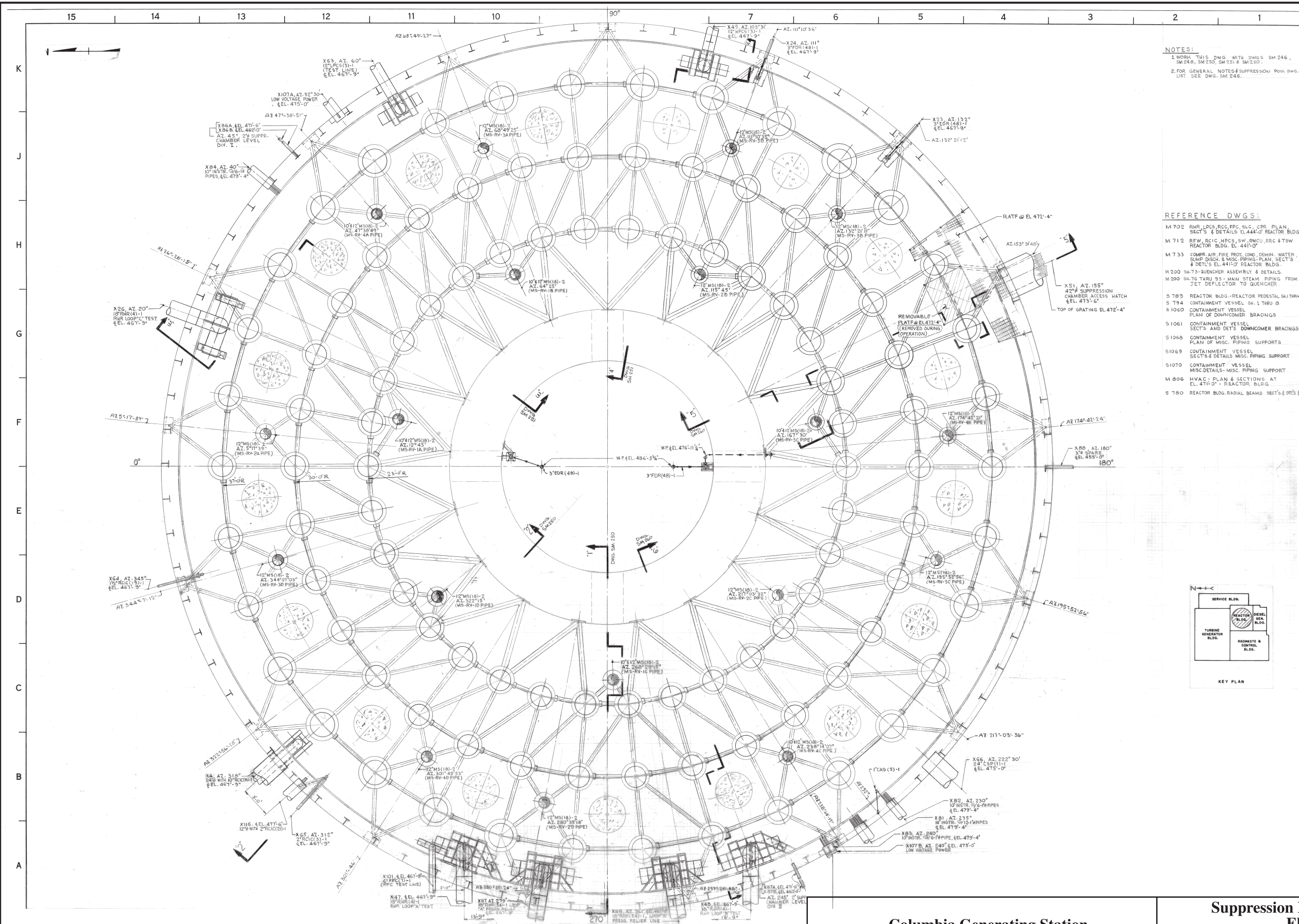
NOTES:

1. WORK THIS DWG. WITH DWGS. SM 246, SM 248, SM 250, SM 251 & SM 280.

2. FOR GENERAL NOTES & SUPPRESSION POOL DWG. LIST, SEE DWG. SM 246.

REFERENCE DWGS:

M 702   RWR, LPCS, RCC, FPC, SLC, CRR PLAN, SECT'S & DETAILS EL 441'-0 REACTOR BLDG.

M 712   RFW, RCIC, HPCS, SW, RWCU, RRC & TSW REACTOR BLDG. EL 441'-0

M 733   COMPR. AIR, FIRE PROT, COND, DEMIN, WATER SUMP DISCH. & MISC. PIPING PLAN, SECT'S & DET'L'S EL 441'-0 REACTOR BLDG.

M 200 SH 73 - QUENCHER ASSEMBLY & DETAILS

M 200 SH 76 THRU 93 - MAIN STEAM PIPING FROM JET DEFLECTOR TO QUENCHER

S 783   REACTOR BLDG.-REACTOR PEDESTAL SH 1 THRU 4

S 794   CONTAINMENT VESSEL SH. 1 THRU 8

S 1060   CONTAINMENT VESSEL PLAN OF DOWNCOMER BRACINGS

S 1061   CONTAINMENT VESSEL SECT'S AND DET'S DOWNCOMER BRACINGS

S 1068   CONTAINMENT VESSEL PLAN OF MISC. PIPING SUPPORTS.

S 1069   CONTAINMENT VESSEL SECT'S & DETAILS MISC. PIPING SUPPORT

S 1070   CONTAINMENT VESSEL MISC. DETAILS - MISC. PIPING SUPPORT

M 806   HVAC PLAN & SECTIONS AT EL. 471'-0 - REACTOR BLDG.

S 780   REACTOR BLDG. RADIAL BEAMS SECT'S & DET'S
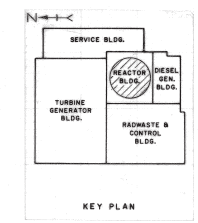
KEY PLAN

Columbia Generating Station
Final Safety Analysis Report

Suppression Pool Composite Plan at El. 455 ft 4 in.

| Draw. No. SM247 | Rev. 0 | Figure 3A.2.1-3 |

Form No. 960690FH

NOTES:

REFERENCE DWGS:

GRAPHIC SCALE

KEY PLAN

Columbia Generating Station Final Safety Analysis Report	Suppression Pool Composite Plan at El. 486 ft 8 in.		
	Draw. No. SM248	Rev. C	Figure 3A.2.1-4

Form No. 960690

NOTES:

REFERENCE DWGS:

Columbia Generating Station
Final Safety Analysis Report

Suppression Pool Composite Plan at
El. 494 ft 5-1/4 in.

| Draw. No. | SM249 | Rev. | B | Figure | 3A.2.1-5 |
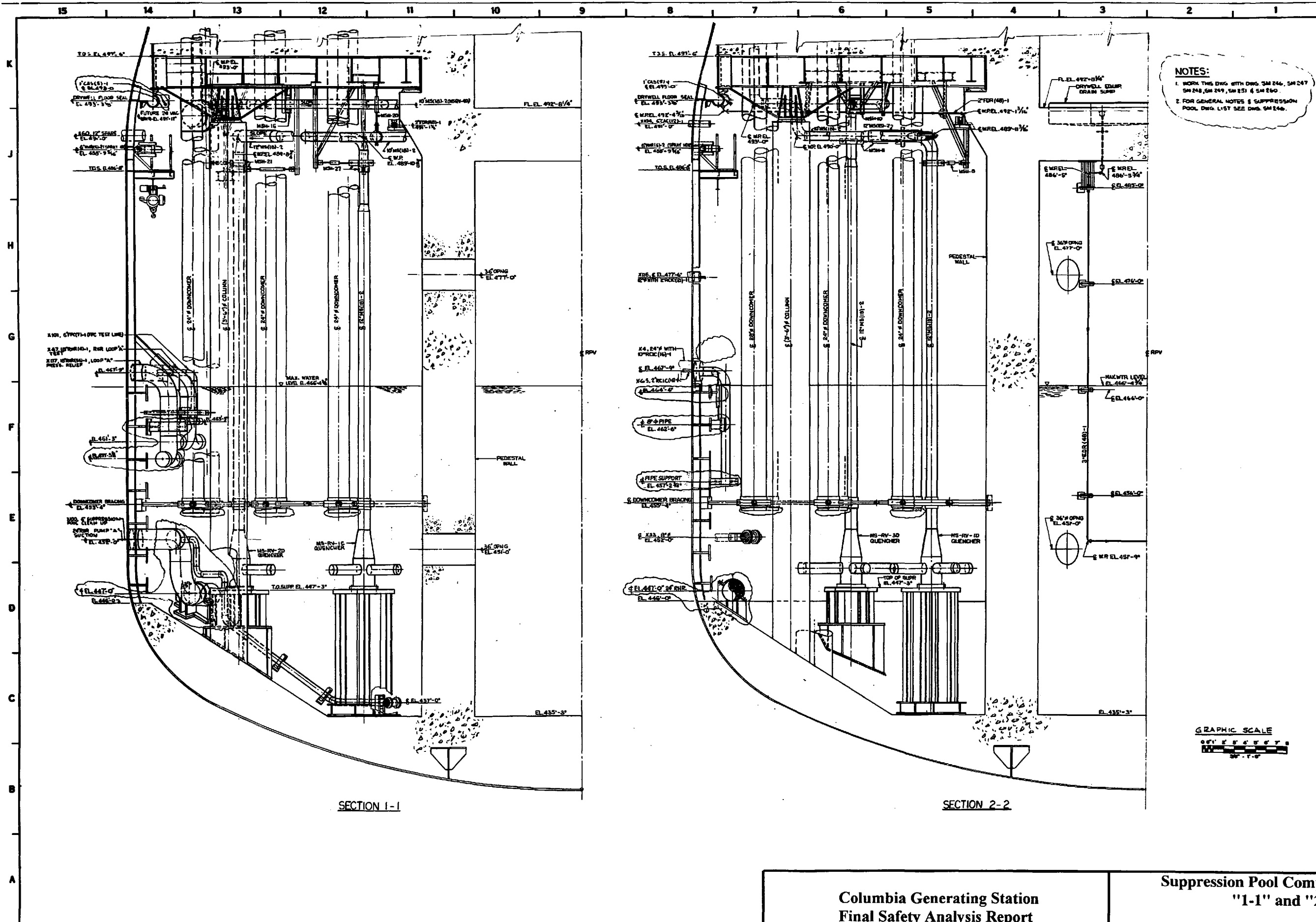
NOTES:
1. WORK THIS DWG. WITH DWG. SM 246, SM 247, SM 248, SM 249, SM 251 & SM 260.
2. FOR GENERAL NOTES & SUPPRESSION POOL DWG. LIST SEE DWG. SM 246.
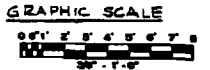
SECTION 1-1

SECTION 2-2

GRAPHIC SCALE

Columbia Generating Station Final Safety Analysis Report	Suppression Pool Composite Sections "1-1" and "2-2"		
	Draw. No. SM250	Rev. B	Figure 3A.2.1-6
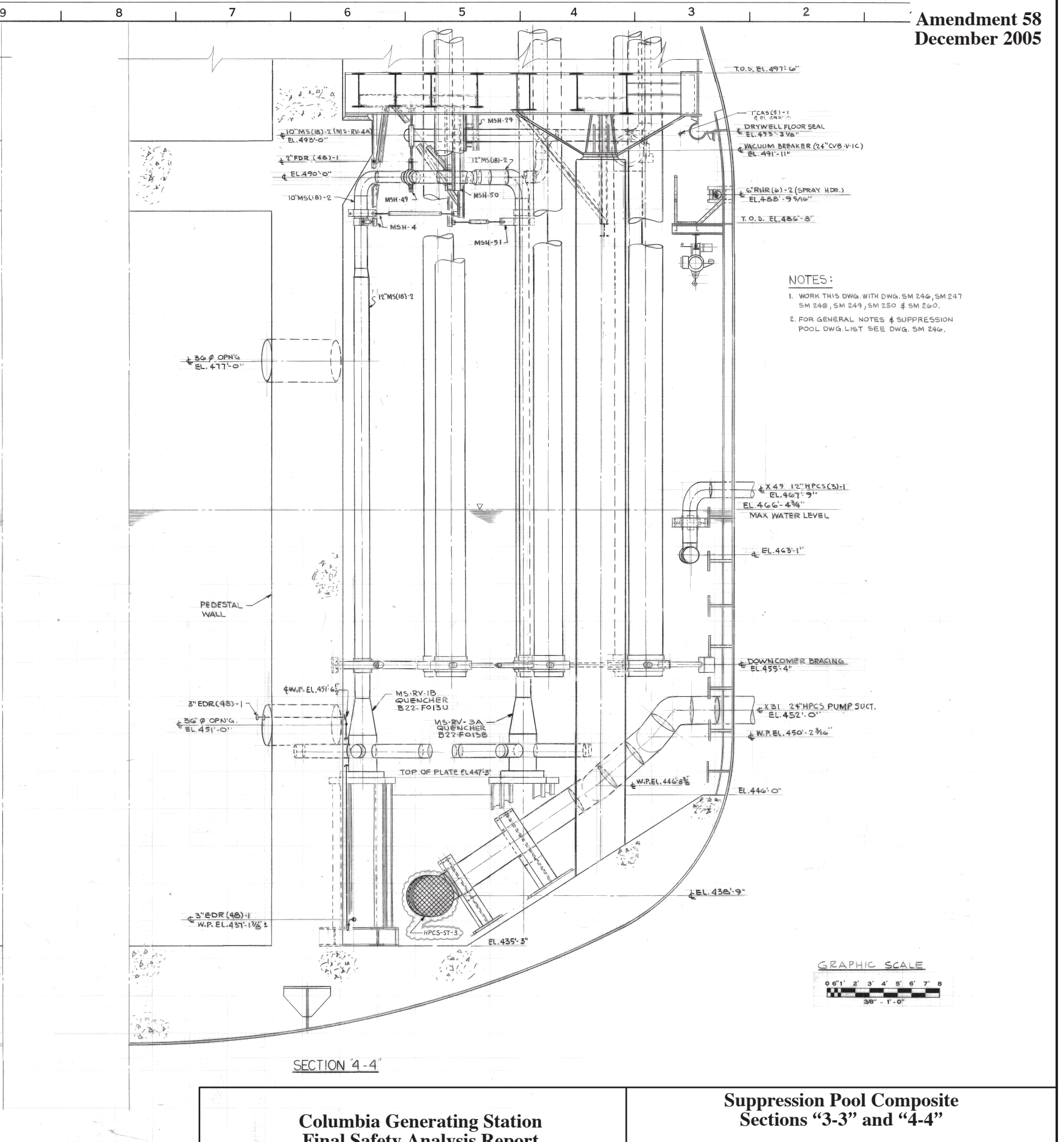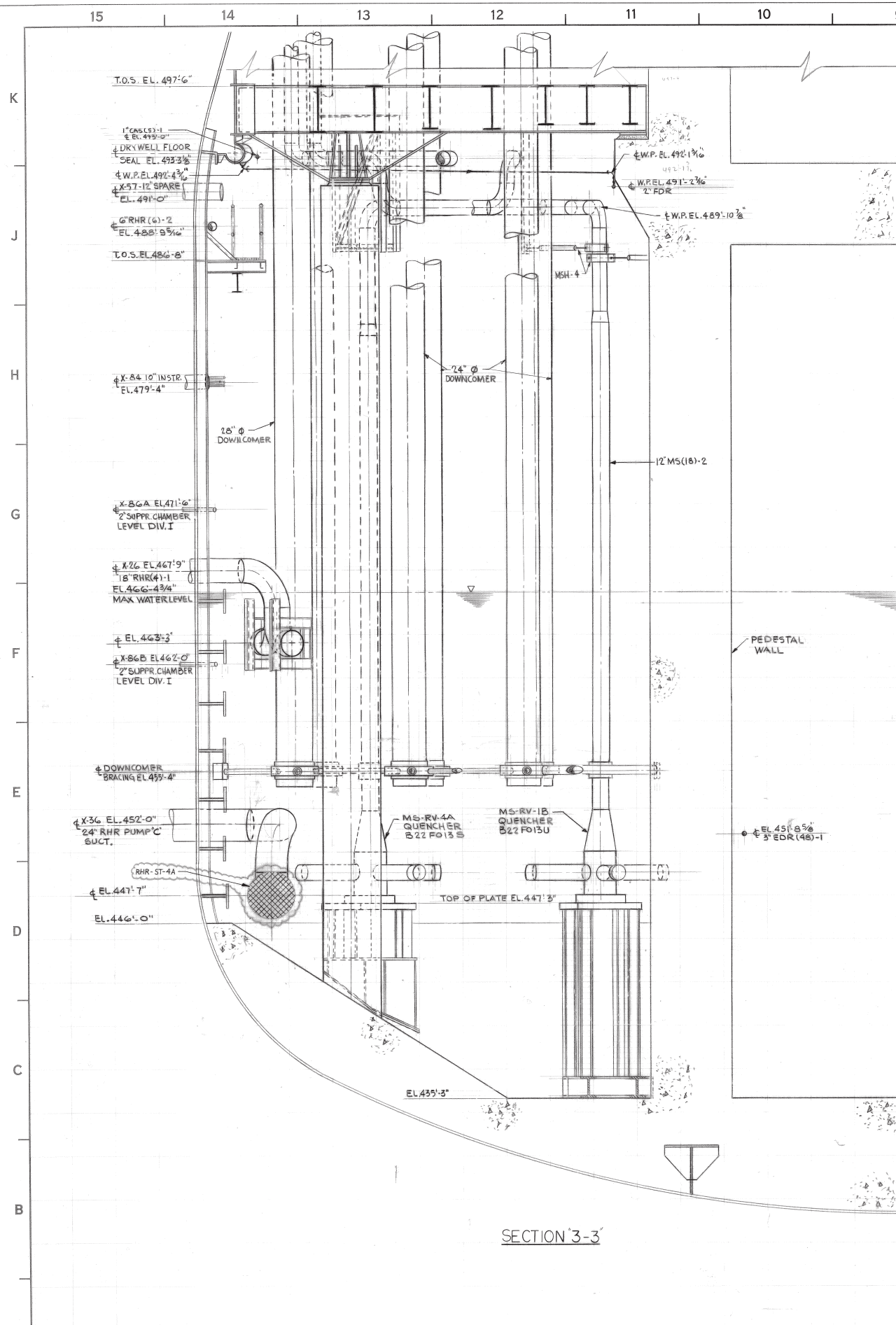
Form No. 960690

SECTION "3-3"

SECTION "4-4"

NOTES:
1. WORK THIS DWG. WITH DWG. SM 246, SM 247 SM 248, SM 249, SM 250 & SM 260.
2. FOR GENERAL NOTES & SUPPRESSION POOL DWG. LIST SEE DWG. SM 246.

GRAPHIC SCALE
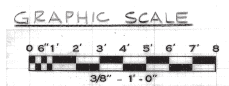
Columbia Generating Station
Final Safety Analysis Report

Suppression Pool Composite Sections "3-3" and "4-4"

| Draw. No. SM251 | Rev. 0 | Figure 3A.2.1-7 |

Form No. 960690FH

SECTION "6-6"

SECTION "5-5"

NOTES:
1. WORK THIS DWG. WITH DWG. SM 246, SM 247, SM 248, SM 249, SM 250 & SM 260.
2. FOR GENERAL NOTES & SUPPRESSION POOL DWG. LIST SEE DWG. SM 246.

GRAPHIC SCALE

3/8" = 1'-0"

Columbia Generating Station
Final Safety Analysis Report

Suppression Pool Composite
Sections "5-5" and "6-6"

| Draw. No. SM260 | Rev. 0 | Figure 3A.2.1-8 |

Form No. 960690FH

3A.2.2   SUMMARY OF CHANGES AND CONCLUSIONS

3A.2.2.1   Summary of Changes to Preserve Design Margins

Structures, piping, and components which were affected by pool dynamic loads were divided into two general categories, i.e., those directly affected by pool dynamic loads (those in and bounded by the suppression chamber) and those affected only indirectly by pool dynamic loads (outside the suppression chamber). The Design Assessment Report (DAR) addressed the structures, piping, and components in and bounding the suppression chamber. For these structures several changes in design were implemented as a result of consideration of SRV discharge and LOCA hydrodynamic loads. Table 3A.2.2-1 provides a list of the structures and components that were impacted by the DAR and includes the design margins, controlling load combination, and the design changes that have been made. The steel containment structure has been reinforced by the addition of seven horizontal rows of tee stiffeners as shown in Figure 3A.4.1-1. The downcomer bracing system has been redesigned from a system of radial beams to a pipe truss system. This bracing system also is designed to provide lateral restraint for the SRV discharge pipes. Quenchers have been provided as exit devices for the SRV discharge pipes. Additions and modifications of pipe supports for miscellaneous piping systems have been provided. Other miscellaneous changes are noted in Table 3A.2.2-1.

3A.2.2.2   Conclusions

The DAR, Revision 3 concluded that the modified design of the wetwell for CGS is capable of withstanding the effects of the hydrodynamic loads resulting from SRV actuation and postulated LOCA events in conjunction with other applicable loads.

The effects due to hydrodynamic loads outside the wetwell region are discussed in the FSAR.

Table 3A.2.2-1

Suppression Pool Assessment Summary

Structure	Controlling Margin[a]	Controlling Load Combination[b]	Changes to Structures Due to SRV and LOCA Loads
Steel containment	1.26	3	Added horizontal tee stiffeners, revised platform location, and connection to containment.
Basemat	Bending - 1.14 Shear - 1.27	7	None
Pedestal diaphragm floor	1.11 Downward - 1.62 Uplift - 1.27	4 4a	None None
Diaphragm floor seal	See Section 3A.4.1.5.5	See Section 3A.4.1.5	None
Downcomer	1.68	5	Redesigned bracing system as a pipe truss system
Columns	1.19	1	None
Downcomers	1.08	See Section 3A.4.2.3	Added stainless-steel spool piece, provided local reinforcement where SRV pipe penetrates downcomer, raised the vacuum breaker valves out of the pool swell zone. Capped three downcomers.
SRV piping systems	1.05	See Section 3A.4.2.4	Provided lateral restraint at downcomer bracing system, rerouted SRV lines.
Quenchers	1.25	See Table 3A.4.2-3	Added quencher device and support to the end of SRV lines

Table 3A.2.2-1

Suppression Pool Assessment Summary (Continued)

Structure	Controlling Margin[a]	Controlling Load Combination[a]	Changes to Structures Due to SRV and LOCA Loads
Platforms and ladders	1.18	5a	Removed floor plate, replaced with grating, revised locations and connections to containment, added platform supports to service vacuum breaker valves; strengthened grating connections and supports.
Miscellaneous wetwell piping system	See Section 4.3	See Section 3A.4.3	Added and modified pipe supports. Stiffened penetrations. Relocated two piping systems.

[a] See Section 3A.4 for a complete discussion.

[b] See Section 3A.3.5 for a complete discussion.

3A.3   CONTAINMENT DYNAMIC FORCING FUNCTIONS

3A.3.1   LOADS ASSOCIATED WITH SAFETY/RELIEF VALVE ACTUATION

3A.3.1.1   Description of the Safety/Relief System

The safety/relief system is comprised of 18 safety/relief valves (SRVs) connected to the main steam lines in the drywell chamber. From each of the valves, a discharge line with two vacuum breakers is routed from the drywell into the wetwell where it terminates in a quencher in the suppression pool, as shown in Figures 3A.2.1-3 to 3A.2.1-8. To pass through the drywell floor, the discharge lines are routed through selected downcomers to about el. 490 ft. At this elevation, they exit the downcomers and are routed horizontally, as shown in Figure 3A.2.1-4, to points directly above their respective quenchers. They then are routed vertically down into the suppression pool, as shown in Figures 3A.2.1-6 to 3A.2.1-8. Under normal operating conditions, each quencher is filled with water and its discharge line is filled to the same level as the surface of the suppression pool. The remaining volume of the discharge line up to the SRV is filled with air. Table 3A.3.1-1 summarizes the characteristics of the safety/relief system.

3A.3.1.2   Description of the Phenomena and Resulting Loads

During plant operation, if one or more of the SRVs is actuated, three transient events occur consecutively for each:

      a.   The water in each quencher and discharge line is expelled into the suppression pool through the holes in the quencher arms,

      b.   The air which fills each discharge line is expelled into the suppression pool, and

      c.   The steam from the discharge line being vented is expelled into the suppression pool and condensed.

Each of these events creates disturbances in the suppression pool. The first creates water jets, the second creates air discharge related pressure oscillations and the third creates pressure fluctuations as the steam is condensed. These disturbances, in turn, produce hydrodynamic loads both on the structures which are submerged in the suppression pool and on the pool boundaries. Sections 3A.3.1.2.1, 3A.3.1.2.2, and 3A.3.1.2.3 briefly describe the characteristics of the load producing phenomena, while Section 3A.3.1.3 discusses the loads produced.

3A.3.1.2.1   Water Clearing Loads

When an SRV opens and permits steam to pass, the steam flow compresses the air above the water standing in the discharge line increasing the line pressure. The increased air pressure forces the water into the suppression pool through the holes in each side of the quencher arms. As the water flows from the adjacent sides of the quencher arms, it coalesces into four turbulent jets. These jets flow away from the quencher producing acceleration and standard drag loads on structures in their paths. Due to the turbulent nature of the jets, their momentum diffuses rapidly and their effective velocity decreases to zero in a distance comparable to a quencher arm length.

Based on the results of scaled experiments and Caorso test results (Reference 3A.3.1-3), the region throughout which the jets produce a significant load is small, at most existing to a distance comparable to a quencher arm length. There are no structures located in this region except a small intrusion of the concrete column which is designed for significantly higher air clearing loads. Detailed definition of water clearing loads therefore is unnecessary for the purposes of this report. It is noted that a clear demarcation between the water clearing loads and air clearing loads is not possible from the recorded Caorso test data. For the purpose of this report it is assumed that significant pressure peaks represent air clearing loads and that the slowly rising pressure before the first significant peak represents water clearing loads.

3A.3.1.2.2   Air Clearing Loads

Following the expulsion of water from the SRV discharge line, the air trapped in the line is forced through the holes in the sides of the quencher arms into the suppression pool. As a result of this disturbance of the pool, oscillations are produced in the pool which induce time varying pressure and velocity fields. These fields create acceleration drag loads on the submerged structures and time varying loads on the pool boundaries. The definition of these air clearing loads is provided in Section 3A.3.1.3.

3A.3.1.2.3   Steam Condensation Loads

After the water and air have been expelled from the SRV discharge line, high pressure, high temperature, high mass flux steam is discharged into the suppression pool. As the steam condenses and collapses, vibrations or small pressure fluctuations are produced in the water. Suppression pool temperature transient analyses were performed for CGS, for a stuck open relief valve, isolation scram, and small break accident (SBA), in accordance with the requirements of NUREG-0783. The peak pool temperature for each of these cases is maintained within the limits of NUREG-0783. As a result unstable steam condensation due to extended SRV discharge to the suppression pool will not occur. Details of this analysis are provided in Reference 3A.3.1-7. The suppression pool temperature monitoring system is discussed in FSAR Appendix 3A Attachment 3A.E.

3A.3.1.3   Safety/Relief Valve Air Clearing Loads

Testing and analytical efforts have been performed by the Mark II Owners' Group to define the loads resulting from discharge through a quencher device upon actuation of the SRV. The SRV testing carried out at the Caorso plant in Italy represents the most extensive test program to date with geometry and plant conditions similar to CGS. An analytical effort was undertaken by Burns and Roe to evaluate the data taken during the Caorso Phase I and II tests (References 3A.3.1-3 and 3A.3.1-4) which resulted in an improved SRV load definition and application methodology for Mark II containments (Reference 3A.3.1-1). These results and a detailed description of the analysis have been submitted, reviewed, and approved by the NRC (Reference 3A.3.1-6) as part of the SRV reports (Reference 3A.3.1-1).

Hydrodynamic loads due to an SRV discharge affect both pool boundaries and submerged structures. A summary of the improved load definition for the specific applications is provided in Sections 3A.3.1.3.1 and 3A.3.1.3.2.

3A.3.1.3.1   Boundary Loads

Expulsion of water and air in a discharge line during an SRV discharge creates disturbances in the suppression pool which induce dynamic pressure loads on the pool boundary. Resulting dynamic effects depend upon the definition of a rigid wall pressure incident on this boundary. Analytical interpretations and subsequent definitions of the spatial pressure distribution, pressure wave forms, and maximum pressure amplitudes recorded during the Caorso tests are the basis for defining the design boundary pressure load. Conversion of these Caorso results for application to CGS requires a correlation between the test conditions at Caorso and the design condition at CGS. Reference 3A.3.1-1 details this correlation along with the derivation of the design boundary pressure with regard to all the possible SRV discharge events that may occur during the life of the plant (see 3A.4.1.1.1.1). Sections 3A.3.1.3.1.1, 3A.3.1.3.1.2, and 3A.3.1.3.1.3 summarize the more important aspects of the derivation.

3A.3.1.3.1.1   Spatial Distribution of Boundary Pressures. The spatial distribution of boundary pressures during an SRV discharge contributes to a complete definition of the design boundary pressure load. Based on analytical studies of data recorded at Caorso, it was concluded that the spatial distribution of pressure is independent of the time variable. As stated in Reference 3A.3.1-1, this implies that the maximum pressure amplitude can be representatively used when studying the spatial distributions.

The circumferential pressure distribution (Figure 3A.3.1-1) as well as the vertical pressure distribution (Figure 3A.3.1-2) adopted for the SRV load specification is obtained through comparisons of various available distributions (Reference 3A.3.1-1). It should be noted that both distributions have been normalized for 1 psi peak pressure.

3A.3.1.3.1.2   Pressure Wave Forms. The SRV boundary pressure load specification depends on the evaluation of the pressure wave forms measured during the Caorso tests. Based on the experimental data recorded, two distinct characteristic wave forms prevail, the multiple frequency pressure (MFP) wave form and the single frequency pressure (SFP) wave form.

The design MFP wave form, shown in Figure 3A.3.1-3, reflects the characteristics of all such MFP wave forms measured at Caorso. Initially, there are several pressure spikes as the pressure wave reaches the pool boundary. They exhibit a frequency content in the range of 15.0 Hz to 40 Hz. Following the pressure spikes are damped oscillations exhibiting primarily a single frequency in the range of 6.0 Hz to 10.0 Hz. Maximum pressure amplitude occurs in the initial period and decays rapidly thereafter. Figure 3A.3.1-4 illustrates the frequency spectrum of the pressure amplitude trace indicating rich frequency content in the range of 15.0 Hz to 40.0 Hz and a distinct peak in the range of 6.0 Hz to 10.0 Hz. There is negligible frequency content beyond 40.0 Hz.

The design SFP wave form, shown in Figure 3A.3.1-5, reflects the characteristics of all such SFP wave forms measured at Caorso.

Unlike the MFP wave form, a single characteristic frequency of oscillation predominates for the entire time history. As shown in the corresponding frequency spectrum (Figure 3A.3.1-6), the dominant frequency is in the range of 6.0 Hz to 10.0 Hz. Again, there is negligible frequency content beyond 40.0 Hz.

Due to the randomness and variability in the characteristic/dominant frequencies of the pressure wave forms recorded, the time histories of the design pressure wave forms are compacted and expanded to obtain a characteristic frequency covering the range of 4.0 Hz to 12.0 Hz at intervals of 1.0 Hz. As a result, each type of wave form (MFP and SFP) is depicted by nine separate pressure time histories (see Reference 3A.3.1-1 for details).

3A.3.1.3.1.3   Design Maximum Pressure Amplitude. Conversion of the Caorso maximum pressure amplitude computed for application to CGS yields a design maximum pressure amplitude of 15.0 psi (References 3A.3.1-1 and 3A.3.1-5). This is the rigid wall pressure incident on the suppression pool boundary resulting from an SRV actuation. Application of this design boundary pressure for all SRV discharge cases that may possibly occur during the life of the CGS plant, as specified in the DFFR (Reference 3A.3.1-2), is discussed in Section 3A.4.1.1.1.1. As discussed in Reference 3A.3.1-2, the design pressure reflects a 90% confidence level and 90% probability of nonexceedence.

3A.3.1.3.2   Submerged Structure Loads

The methodology for calculating the loads on submerged structures during SRV discharge uses the predicted pressure time histories directly rather than the velocity and acceleration

transients. The pressure predictions are based on the pressures measured on submerged structures in Caorso tests and their correlation with the boundary pressure loads.

3A.3.1.3.2.1 <u>Peak Safety/Relief Valve Dynamic Loads.</u> The methodology used to define peak SRV dynamic loads on submerged structures is outlined in Attachment 3A.I (see also Reference 3A.3.1-8).

3A.3.1.3.2.2 <u>Time Dependence of Safety/Relief Valve Loads and Dynamic Load Factors.</u>
The pressure time histories recorded on submerged structures at Caorso show waveform characteristics similar to those recorded at pool boundary. As indicated in Reference 3A.3.1-1, boundary pressure time histories consist of SFP time histories and MFP time histories.

Dynamic load factor (DLF) versus frequency curves are presented in Figure 3A.3.1-10. A typical curve, such as the curve labeled SFP, 1% damping, was calculated as follows:

  a.   Response spectra that correspond to all the SFP time histories described in Section 3A.3.1.3.1.2 are computed using 1% damping,

  b.   The response spectra obtained in (a) are enveloped, and

  c.   The DLF curve is obtained from the response spectrum envelope by dividing the responses at various frequencies by the zero period response.

3A.3.1.3.2.3 <u>Safety/Relief Valve Loads on Structures.</u> Loads on submerged structures are shown for the submerged structures listed below. Unless otherwise noted, calculation of an equivalent static load is completed via a DLF as obtained from Figure 3A.3.1-10.

  a.   Downcomers

         Figure 3A.3.1-7 shows dynamic load on a downcomer;

  b.   Columns

         Figure 3A.3.1-8 shows dynamic load on a concrete column. Note, for the subsequent actuation load case the maximum direct pressure load is shown (see Reference 3A.3.1-8). Reference 3A.3.1-9 computes the maximum dynamic reaction of the column, and these time-history analyses results are applied in Reference 3A.3.1-10 for final column structural (i.e., code) qualification. Table 3A.4.2-2 tabulates maximum column reaction load results;

c.   Safety/relief valve line and quencher supports

Figure 3A.3.1-9 shows dynamic load on SRV line and the quencher support. Horizontal flow past an SRV line due to actuation of its quencher is negligible; and

d.   Piping, supports, and bracing truss

Figure 3A.3.1-11 shows equivalent static loads on piping, supports, and bracing truss.

3A.3.1.4   <u>References</u>

3A.3.1-1   "SRV Loads - Improved Definition and Application Methodology for Mark II Containments," Technical Report, Burns and Roe, Inc., July 1980. Transmitted to NRC by letter GO2-80-172, of August 8, 1980.

3A.3.1-2   "Mark II Containment Dynamic Forcing Functions Information Report (DFFR)," General Electric Company, <u>NEDO-21061</u>, Revision 4, November 1981.

3A.3.1-3   "Mark II Containment Supporting Program Caorso SRV Discharge Tests, Phase I Test Report," General Electric Company, <u>NEDE-25100-P</u>, May 1979.

3A.3.1-4   "Mark II Containment Supporting Program Caorso SRV Discharge Tests, Phase II ATR Report," General Electric Company, <u>NEDE-25118</u>.

3A.3.1-5   Letter, GO2-82-35, 1/13/82, "Responses to CSB Open Items 44 through 48," G. D. Bouchey (WPPSS) to A. Schwencer (NRC).

3A.3.1-6   "Safety Evaluation Report Related to the Operation of WPPSS Nuclear Project No. 2," NUREG-0892, Supplement No. 1, USNRC, August 1982.

3A.3.1-7   "Suppression Temperature Analysis," Stone and Webster Report 14057-4 (D-1). Transmitted to NRC by letter GO2-81-524 of December 15, 1981.

3A.3.1-8   Supply System Calculation No. ME-02-93-22, "SRV Air Clearing Loads on Diaphragm Slab Columns."

3A.3.1-9   Supply System Calculation No. CE -02-93-12, "Diaphragm Slab Column Evaluation for SRV Air Clearing Loads."

3A.3.1-10   Burns & Roe Calculation No. 6.19.36, Book SV-830, "Calculation for Reactor Building Diaphragm Floor Column and Plant DAR for Hydrodynamic Loads, Rev. 3."

Table 3A.3.1-1

Summary of Safety/Relief System Characteristics

1.	Number of SRVs	18	
2.	SRV manufacturer	Crosby	P.S.P
3.	Designations of SRVs and pressure setpoints (Refer to Figure 3A.2.1-2)	<u>Valves</u>	<u>(psi)</u>
		1B[a], 1C[a]	1165
		1A[a], 2B[a], 2C[a], 1D[a]	1175
		2A, 3B, 3C, 2D	1185
		3A, 4B, 4C, 3D	1195
		4A, 5B, 5C, 4D	1205
4.	Number of automatic depressurization valves [automatic depressurization system (ADS)]	7	
5.	Designations of automatic depressurization valves	MS-RV-3D, 4A, 4B, 4C, 4D, 5B, 5C	
6.	Nominal range of valve opening times (ms)	20-150	
7.	Nominal range of nameplate steam rates (lbm/sec)	236.33-251.81	
8.	Number of vacuum breakers per discharge line	2 (in parallel)	
9.	Size of each vacuum breaker (in.)	10	
10.	Each discharge line pipe sizes (in./schedule)	10/80 expanded to 12/80 at approximate el. 493 ft	
11.	Discharge line rage of lengths to normal water level (ft)	107.99-161.99	
12.	Discharge line range of air volumes to normal water level (ft^3)	57.2-88.1	
13.	Depth of suppression pool at RPV pedestal to normal water level (ft)	31.0	
14.	Submergence of quenchers to high water level (ft)	17.4	

Table 3A.3.1-1

Summary of Safety/Relief System Characteristics (Continued)

15. Elevation of inner/outer ring quenchers above basemat (ft) 13.6-8.2

16. Quencher area defined by circumscribed circle (ft^2) 74.6

---

[a] These valves are the low setpoint valves which are prone to subsequent actuation. However, subsequent actuation may occur (though unlikely) in the higher set pressure SRV groups (see also discussion contained in Reference 3A.3.1-8).

1.0

Quencher

R = 39.5'

Normalized Design Circumferential Distribution of
Pool Boundary Pressures at Containment

Draw. No. 950021.64   Rev.   Figure 3A.3.1-1

Form No. 960690

Normalized Design Vertical Distribution of Pool Boundary Pressures at Containment

Columbia Generating Station Final Safety Analysis Report	Normalized Design Vertical Distribution of Pool Boundary Pressures at Containment		
	Draw. No. 950021.65	Rev.	Figure 3A.3.1-2

Form No. 960690

	MFP Design Wave Form (Normalized)		
Columbia Generating Station Final Safety Analysis Report	Time History		
	Draw. No. 950021.66	Rev.	Figure 3A.3.1-3
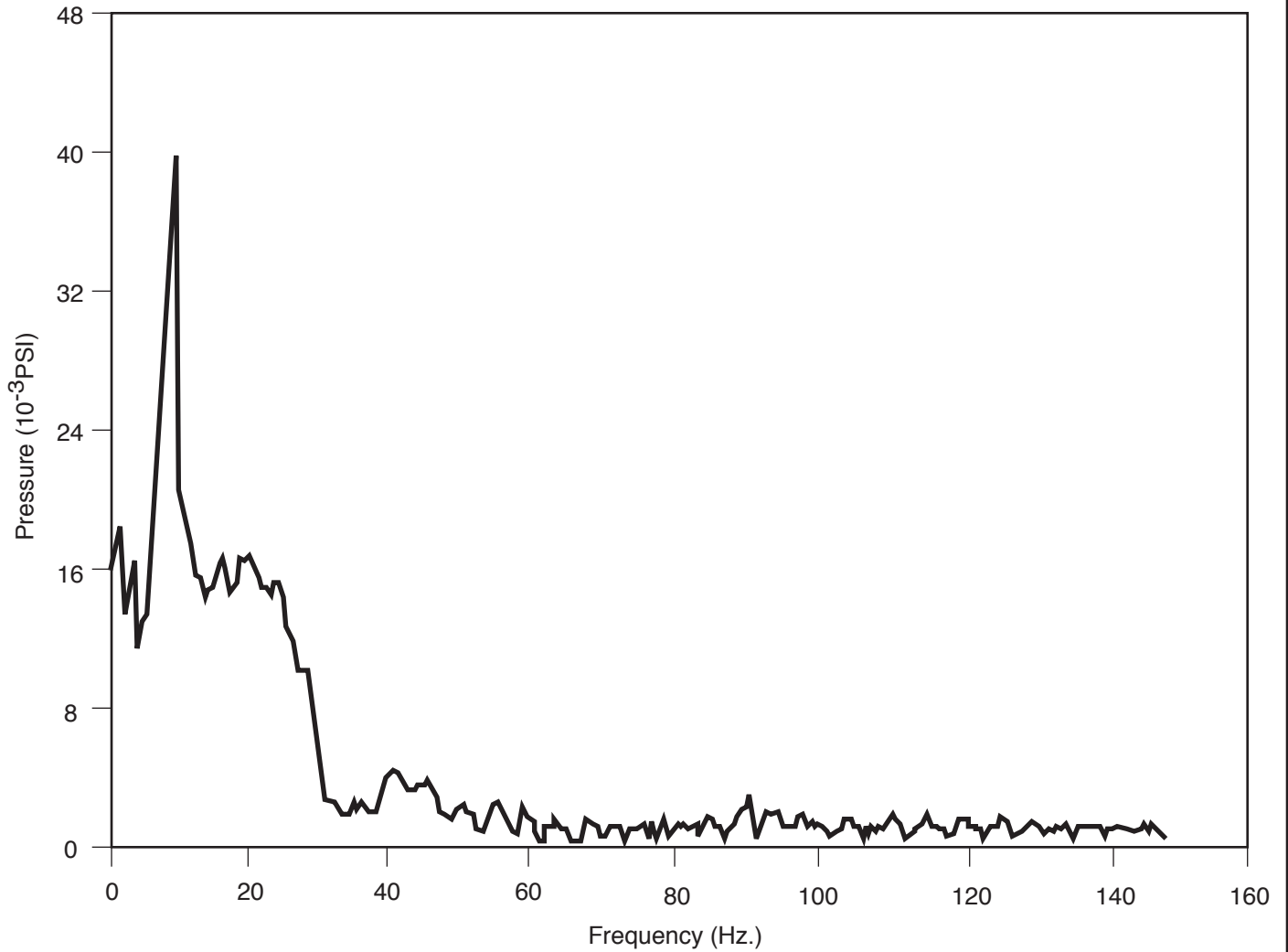
	MFP Design Wave Form (Normalized) Amplitude of Frequency Spectrum		
Columbia Generating Station **Final Safety Analysis Report**			
	Draw. No. 950021.67	**Rev.**	**Figure** 3A.3.1-4

SFP Design Wave Form (Normalized)
Time History

Columbia Generating Station
Final Safety Analysis Report

| Draw. No. 950021.68 | Rev. | Figure 3A.3.1-5 |

Pressure (10^{-3} psi)
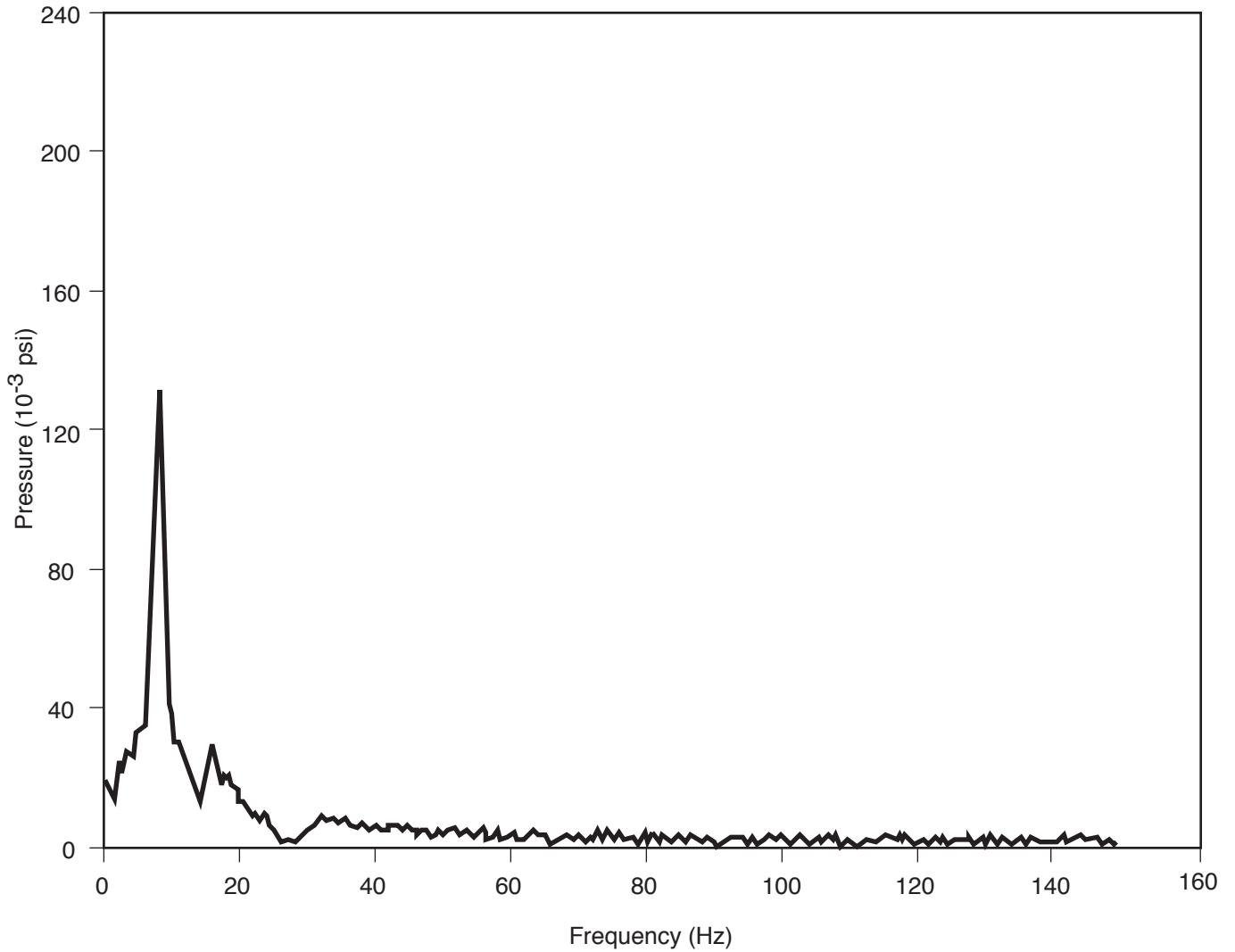
Frequency (Hz)

Columbia Generating Station Final Safety Analysis Report	SFP Design Wave Form (Normalized) Amplitude of Frequency Spectrum

| Draw. No. 950021.69 | Rev. | Figure 3A.3.1-6 |

C 24" or 28" Downcomer

El. 466' - 4 3/4"

El. 454' - 4 3/4"

Initial Actuation Loading Cases

Subsequent Actuation Loading Cases

3.0 psi

El. 461 - 0"

0.75 psi

Submergence (ft)

Horizontal Dynamic Load (psi)
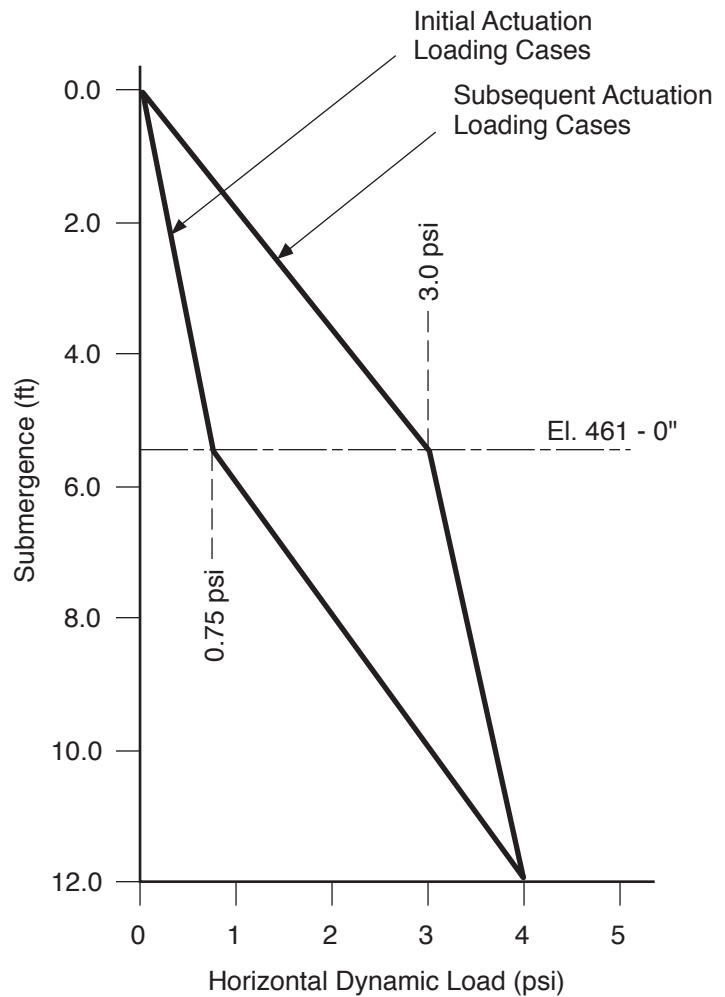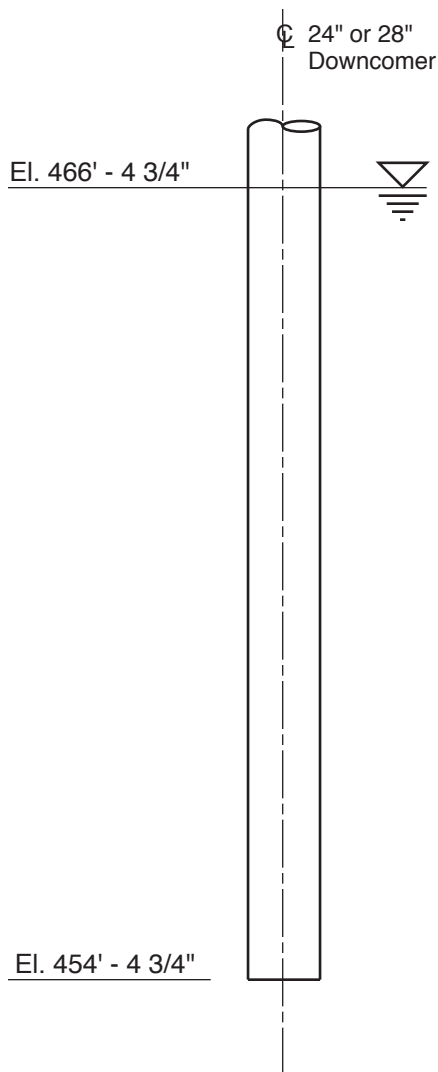
Notes:

1. Dynamic load factors are obtained from Figure 3A.3.1-10.

2. Horizontal loads on downcomers are applied in any horizontal direction producing maximum load effects.

Columbia Generating Station Final Safety Analysis Report	SRV Air Clearing Load Distribution on a Downcomer		
	Draw. No. 950021.70	Rev.	Figure 3A.3.1-7

C̶ 42" Concrete Column

EL. 466' - 4 3/4"

Subsequent Actuation Loading Case -
Effective max Column Frontal Pressure Based
on Nodal Forces of Ref 3A.3.1-8 on 3 ft
Column Increments.

1.67 psi

EL. 461 - 0"

Initial Actuation
Loading Cases

1.33 PSI

8.61 psi

12"

13.05 psi

EL. 449' - 0"

5.67 psi

8.33 psi

Submergence (ft)

0.0 2.0 4.0 6.0 8.0 10.0 12.0 14.0 16.0 18.0 20.0 22.0 24.0

0 2 4 6 8 10 12 14

Horizontal Dynamic Load (psi)

EL. 442' - 4 3/4"

Notes

1. Dynamic load factors for initial actuation load cases are obtained from
Figure 3A.3.1-10, dynamic load response reactions for the subsequent actuation
case are tabulated in Table 3A.4.2-2 (see also References 3A.3.1-9 and 3A.3.1-10).

2. Horizontal loads on concrete column are applied in any
horizontal direction producing maximum load effects.

Columbia Generating Station
Final Safety Analysis Report

SRV Air Clearing Load
Distribution on a Concrete Column

| **Draw. No.** 950021.71 | **Rev.** | **Figure** 3A.3.1-8 |

Form No. 960690

12" SRV
Discharge Line

EL. 466' - 4 3/4"

0.8 psi

0.3 psi

EL. 461' - 0"

Subsequent actuation
Loading Cases

Initial
Actuation
Loading Cases

EL. 449' - 0"

12"

1.5 psi

3.0 psi

0.8 psi

1.2 psi

EL. 435' - 3"

Submergence (ft)

Horizontal Dynamic Load (psi)
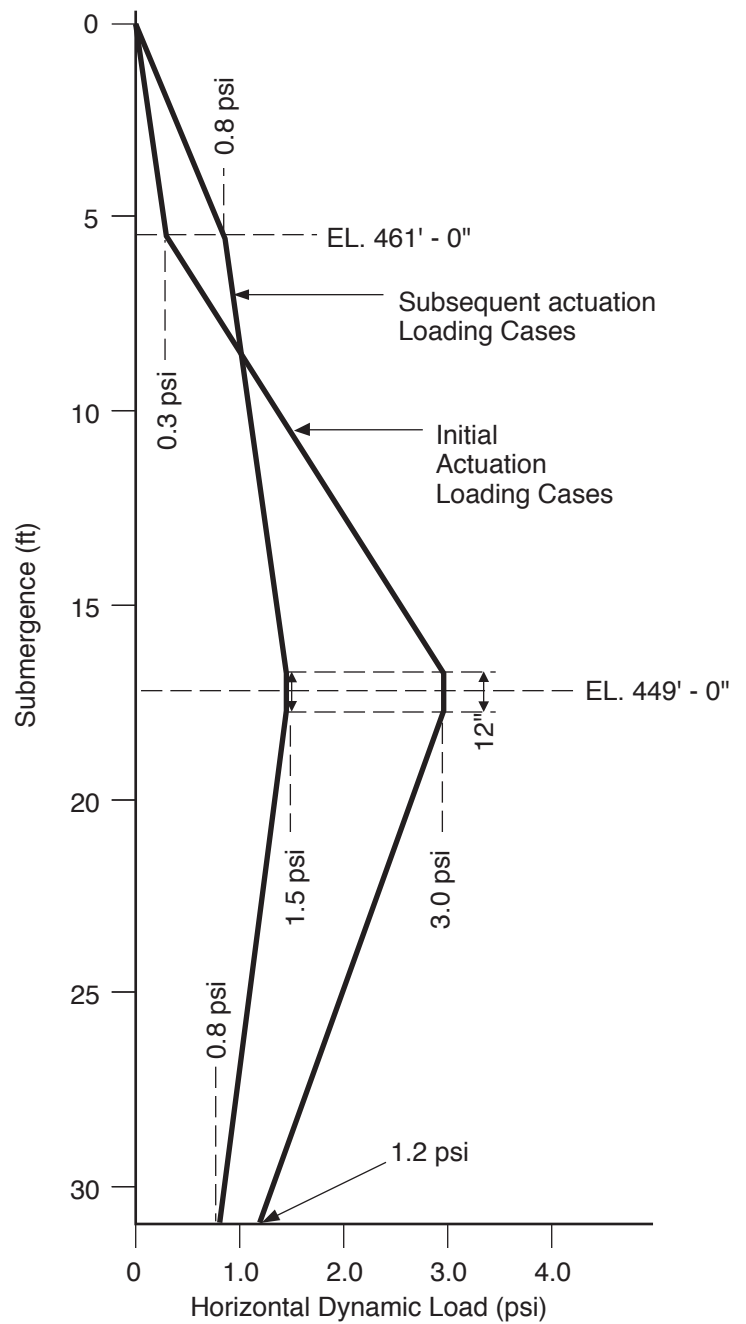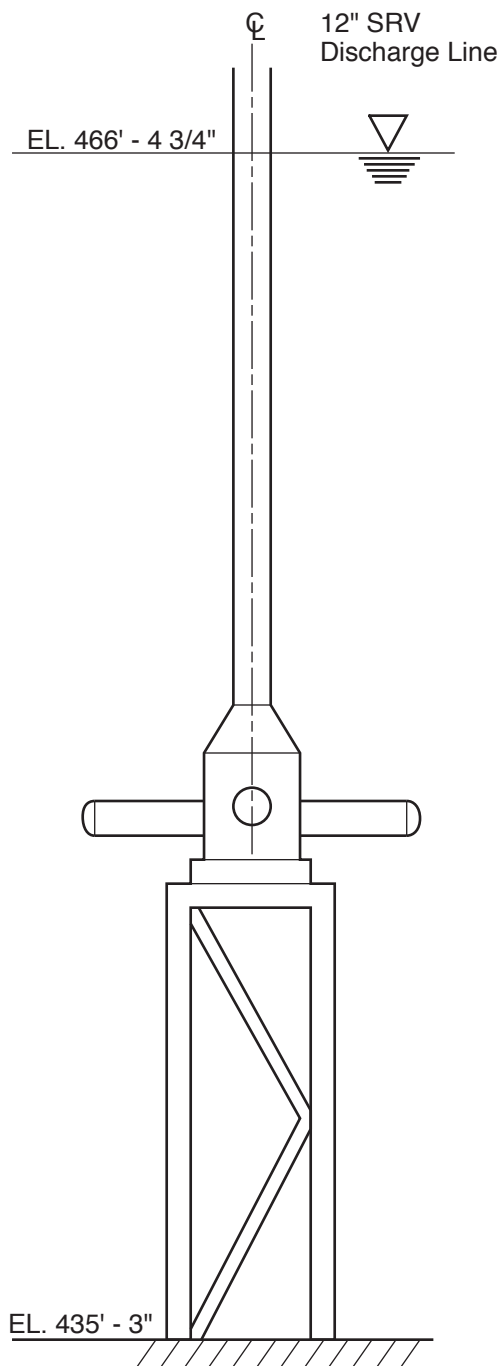
Notes

1. Dynamic load factors are obtained from Figure 3A.3.1-10.

2. Horizontal loads on SRV lines are applied in any horizontal
   direction producing maximum load effects.

Columbia Generating Station
Final Safety Analysis Report

SRV Air Clearing Load Distribution on an
SRV Discharge Line and Quencher Support

| Draw. No. 950021.72 | Rev. | Figure 3A.3.1-9 |

Note:

1. The curve labeled as MFP is used with initial actuation cases and the curves labeled as SFP are used with the subsequent actuation cases.

SFP, 1% Damping for Pipes ≤ 12" Diameter

5.1

SFP, 2% Damping for Pipes > 12" Diameter

4.2

SFP, 4% Damping for Concrete Column

3.25

2.52

2.34

2.6

MFP, 1% Damping for all Structures and Piping

2.2

2.1

2.24

2.05

1.92

1.76

1.52

1.4

1.3

1.08

Dynamic Load Factor (vertical axis: 1, 2, 3, 4, 5)

Frequency (Hz) (horizontal axis: 0, 20, 40, 60, 80, 100)

Columbia Generating Station Final Safety Analysis Report	Dynamic Load Factor Versus Frequency to be Used for Defining SRV Load on Submerged Structures		
	Draw. No. 950021.73	Rev.	Figure 3A.3.1-10

Form No. 960690

Containment Wall

Pedestal

El. 466' - 4 3/4"

Pipe Support (Typ.)

Bracing Truss
El. 455' - 4"

El. 449' - 0"

El. 446' - 0"

Segment of
Interest (Typ.)

El. 435' - 3"

ELEVATION

Containment Wall

Pedestal

Vertical Pipe

Segment of
Interest (Typ.)

Vertical Pipe

PLAN

Columbia Generating Station Final Safety Analysis Report	SRV Air Clearing Load Distribution on Piping, Supports and Bracing Truss		
	Draw. No. 950021.74	Rev.	Figure 3A.3.1-11a

Notes:

1. The load is applied along the line joining the center of the nearest actuating quencher and the geometric center of the pipe segment as shown in Fig. 3A.3.1-11a.

2. The equivalent static load ($p_1$lb) on piping, supports and bracing truss is:

   $P = \pm0.32D^2L$ for initial actuation.

   $P = \pm0.25KD^2L$ for subsequent actuation and for pipes near containment or pool bottom.

   $P = \pm0.64KD^2L$ for subsequent actuation and for pipes near pedestal.

   where:

   D = diameter of pipe or the cylinder circumscribing a non-circular cross-section, in units of inches.

   L = length of segment, in units of inches

   K = see note 5

3. For load on piping, supports and bracing truss, the load component parallel to the pipe is neglected.

4. Since the load direction on piping, supports and bracing truss generally varies from one point to another, segmentation of the piping or structural component may be needed.

5. If the fundamental natural frequency of the piping, support or bracing truss member is greater than or equal to 17HZ, K = 1. This is applicable in most cases.

   If the fundamental natural frequency is less than 17HZ, then $K = \frac{DLF}{2.6}$,

   where DLF is the dynamic load facor and is determined from Fig. 3A.3.1-10. If K, as calculated above, is less than 1, K = 1 is used.

Columbia Generating Station **Final Safety Analysis Report**	**SRV Air Clearing Load Distribution on** **Piping, Supports and Bracing Truss**

Draw. No. 950021.75	Rev.	Figure 3A.3.1-11b

3A.3.2   LOADS ASSOCIATED WITH LOSS-OF-COOLANT ACCIDENT

A loss-of-coolant accident (LOCA) occurs when the integrity of the reactor coolant pressure boundary is breached and coolant is released. In order to contain the coolant which flashes to steam, CGS utilizes a GE Mark II pressure suppression system. The LOCA loading phenomena are discussed in Section 3A.3.2.2. The short-term and long-term LOCA loads are discussed in detail in Sections 3A.3.2.3 and 3A.3.2.4, respectively. Section 3A.3.2.5 describes the LOCA pressure and temperature transients and Section 3A.3.2.6 describes the CGS building response to the LOCA loads.

3A.3.2.1   Description of Pressure Suppression System

The CGS primary containment utilizes a GE Mark II over/under pressure-suppression configuration (see Figure 3A.2.1-1). The drywell and suppression chamber (or wetwell) are large sealed volumes designed to contain and condense escaping reactor coolant. Both contain structures and piping systems with the suppression chamber approximately half filled with water (suppression pool) for steam quenching. The drywell is connected to the suppression pool by 99 downcomer pipes that channel steam released during a LOCA for quenching and pressure suppression. Details of the downcomers, other piping systems and structures in the suppression chamber are shown in Figures 3A.2.1-2 through 3A.2.1-8.

Originally, 102 downcomer pipes were provided. During the assessment of the wetwell piping for hydrodynamic loads, it was found that the LOCA water jet loads on three containment vessel penetrations and their supports were excessive. To eliminate these loads, three of the 102 downcomers are capped in the drywell region, leaving 99 for venting steam to the wetwell.

The piping systems involved are at penetration X-31, X-34, and X-36. The three capped downcomers are on the outer circle of downcomers closest to the containment vessel, at azimuths 95°, 63°, and 42° (Figures 3A.2.1-2 and 3A.2.1-4).

3A.3.2.2   Description of the Phenomena and Resulting Loads

The sequence of LOCA-generated hydrodynamic events described below cause dynamic loads on the containment and on structures and components located in the wetwell. These transient dynamic forces (see Table 3A.3.2-1) are termed dynamic forcing functions and are discussed in detail in Reference 3A.3.2-2 and summarized below. Section 3A.3.4 discusses the sequence of LOCA generated loads.

Following a postulated LOCA, released coolant causes the drywell pressure to rise rapidly and to accelerate the column of water in each downcomer downward due to the pressure rise. As the water exits the downcomers and enters the suppression pool, it forms a jet-pool interface which rolls into a mushroom shaped vortex ring. Expulsion of water out of each of the

downcomers results in a water jet which produces loads on submerged structures and suppression pool boundary pressure loads. Because bulk pool velocities are small during vent clearing, the corresponding impact and induced flow field drag loads are generally small. However, locally, significant drag loads may result.

Immediately after vent clearing, air[*] in the downcomer vents from the drywell beings to flow into the suppression pool. The LOCA air[*] bubbles are formed at the exits of the vents which charge and expand under the entire pool surface causing three dimensional drag loads on submerged structures. On contact with each other, the individual bubbles coalesce and accelerate the pool water above the downcomer vent exit plane vertically with no significant horizontal water motion.

Pool swell is the upward movement of suppression pool water above the exit plane of the vents due to injection of drywell air[*] below the pool surface. The velocity and acceleration of the water slug associated with this phenomenon produces impact, drag, and lift forces on structures within the swell zone.

The containment boundaries also experience loads due to drywell pressurization, air bubble pressure and wetwell free airspace compression. The rising pool surface motion is slowed due to the compression of air in the suppression chamber airspace. At about this time the rising bubbles break up the remaining pool slug which falls back to its original position terminating pool swell.

During pool swell, the bottom of the rising water slug continually falls back to the suppression pool due to instabilities at the bubble/water slug interface. This phenomenon and the large scale falling back of the remaining water slug at pool swell termination is known as fallback and causes drag and lift loads on structures in the pool swell zone, but a negligible containment boundary load.

Pool swell and the subsequent fallback of the remaining water slug are followed by an air/steam mixture flow through the downcomers until the drywell air is completely purged and the mass flux becomes pure steam. The loading phenomena associated with a high or medium steam mass flux is termed steam condensation oscillation (CO).

The air content and steam mass flow rate along with the pool temperature determines the behavior of the steam/suppression pool water interface. At high steam flow the interface location is essentially constant. As the flow rate decreases, due to reactor depressurization and associated drywell pressure decrease, the interface takes on an oscillatory character. The rate

---

[*] During a LOCA an air (nitrogen)/steam mixture would be blown down the downcomer vents; however, the analytical models of LOCA phenomena conservatively assume that only noncondensables are injected into the suppression pool.

of change of the displacement of the interface is reflected in submerged structure and suppression pool boundary loads.

When the steam mass flux decreases below a critical level a hydrodynamic phenomenon termed chugging occurs. Chugging is associated with low steam mass flow and high suppression pool boundary pressure spikes relative to CO. The phenomenon appears to be random in time and is caused by the complex interaction of water/steam condensation surface instabilities with the physical properties of the downcomers, the suppression pool, and the suppression pool boundaries. Chugging causes loads on the suppression pool boundary and submerged structures.

To determine the effects of downcomer capping on the hydrodynamic load definition, displacement time histories due to chugging are obtained at selected nodes on the containment vessel. Two sets of time histories are obtained. The first includes the effects of downcomer capping and the second excludes these effects. A comparison of the maximum displacements indicates that capping results in a slight reduction in the maximum displacements. Since lower displacements are associated with lower loads and stresses, it is conservative to assume uncapped downcomers for establishing the chugging load definition. The Containment Functional Design Analysis described in Section 6.2 was based on the venting capacity of 99 downcomers.

3A.3.2.3   Short-Term Loss-of-Coolant Accident Loads

Short-term LOCA loads are associated with hydrodynamic related phenomena that occur within a few seconds after LOCA initiation. The short-term loading phenomena include downcomer vent clearing, LOCA bubble charging, pool swell, and fallback. Figure 3A.3.2-1 illustrates the short-term loading phenomena. The flow fields during downcomer vent clearing and LOCA bubble charging are three-dimensional. Flow fields during pool swell and fallback are vertical and exist only above the vent exit elevation. Loads on submerged structures due to downcomer vent clearing and LOCA bubble charging are compared and the larger loads are employed for subsequent evaluations.

Section 3A.3.2.3.1 and Table 3A.H-1 provide a detailed summary of the short-term LOCA loading phenomenon and load calculation procedures used to assess CGS structures.

3A.3.2.3.1   Analytical Models and Supporting Test Data

3A.3.2.3.1.1 Vent Clearing Jet and Induced Flow Field Model. To calculate the CGS vent clearing jet and induced flow field, a LOCA Water Jet Analytical Model was developed for CGS. The model development and supporting test data are documented in Reference 3A.3.2-9. The calculation is performed for a unit cell with a downcomer at the center. Input data included the downcomer vent water clearing time history.

In order to calculate the downcomer vent water clearing time history and to provide a continuous pool surface displacement time history, a VENT computer code was developed. The model development and supporting test data for VENT are discussed in detail in Attachment 3A.D.2.

CGS input data for the LOCA water jet model and the VENT computer code are shown in Tables 3A.3.2-2 and 3A.3.2-3, respectively. As appropriate, maximums or minimums of CGS parameters are used to make the input data conservative in order to maximize vent water clearing velocities.

The vent exit water velocity and acceleration calculated by VENT are increased by 10% as requested by the NRC in Reference 3A.3.2-1. The velocity and acceleration time histories (including the 10% increase) are shown in Figures 3A.3.2-2 and 3A.3.2-3, respectively. As indicated in Reference 3A.3.2-9, tests have shown that LOCA jet continues to propagate downward for a short duration beyond the vent clearing instant due to rapidly charging air. Although the vent clearing time for CGS is 0.654 sec, the jet tip reaches a maximum velocity of about 15.8 ft/sec at t = 0.704 sec.

Submerged boundary loads during downcomer vent water clearing is specified to be a static addition of an overpressure of 24 psi to the local hydrostatic pressure below the downcomer vent exit (walls and basemat) with a linear attenuation to zero at the pool surface.

3A.3.2.3.1.2 Loss-of-Coolant Accident Bubble Charging Model. In order to calculate the flow field associated with the LOCA bubble charging phenomenon, a LOCA bubble charging model was developed. The model development and supporting test data are discussed in detail in Attachment 3A.D.4.

As discussed in Attachment 3A.D.4, the LOCA bubble charging flow field is calculated using a numerical technique for potential flows in the exact CGS suppression pool geometry. The uniformly charging LOCA bubbles are modeled as equal strength point sources located one downcomer radius below the CGS vent exit at el. 453 ft-4.75 in. Figure 3A.B-2 shows the modeled geometry for the CGS LOCA bubble charging phenomenon and Figures 3A.3.2-4 through 3A.3.2-6 show contour plots of the maximum radial, tangential, and vertical components of the gradient of the velocity potential.

The growth rate of the CGS LOCA bubble and the corresponding source strengths of the point sources are determined by continuity from the rate of displacement of the pool surface after vent clearing. The rate of displacement of the pool surface is determined from the pool swell analytical model (PSAM) (see 3A.3.2.3.1.3). Figure 3A.3.2-7 shows the velocity source strength, Q(t), the acceleration source strength, Q(t), and the radius, R(t), of the CGS LOCA bubbles charging process. Section 3A.B.4.2 discusses how to determine the CGS LOCA bubble charging transient flow field using the data in Figures 3A.3.2-4 through

3A.3.2-7. Tables 3A.3.2-4 and 3A.D-5 summarize results from the LOCA bubble charging
analysis for CGS.

Since LOCA bubble charging represents the early portion of pool swell, the associated
suppression pool boundary loads are discussed in Section 3A.3.2.3.1.3.

3A.3.2.3.1.3 Pool Swell Analytical Model. The pool swell transient is conservatively defined
for CGS by the computer code SWELL based on the model presented in Reference 3A.3.2-10.
The model development and supporting test data are discussed in Section 3A.C.3.

The CGS input data for SWELL are given in Tables 3A.3.2-3 and 3A.3.2-5. As appropriate,
maximums and minimums of CGS parameters are used to make the input data conservative in
order to maximize pool swell velocities. The CGS pool swell velocity, acceleration,
displacement, bubble pressure, and wetwell air pressure versus time are given in Figures
3A.3.2-8 through 3A.3.2-12, respectively. Figure 3A.3.2-13 shows the pool lug velocity vs.
displacement and Table 3A.3.2-6 shows results from the pool swell analysis for CGS.
Velocities and accelerations calculated by the computer code SWELL are multiplied by a factor
of 1.1, as requested by the NRC in Reference 3A.3.2-1. The 10% increase in velocities and
accelerations is included in Figures 3A.3.2-8, 3A.3.2-9, and 3A.3.2-13.

Test results indicate that no significant froth will occur when the water slug breaks up during
pool swell in Mark II containments. Hence, the load due to froth is negligible
(Reference 3A.3.2-11) and no froth impingement is considered in the assessment of the design
of structures.

Loads on submerged boundaries during pool swell are calculated by specifying that basemat
and wall loads be determined from static addition of the maximum bubble pressure predicted
by the PSAM to the local hydrostatic pressure below the downcomer vent exit plane and with a
linear attenuation to the maximum wetwell air space pressure at maximum pool swell
elevation.

Wetwell wall loads due to air compression during pool swell are specified by the direct
application of the PSAM calculated wetwell air compression pressure to the wetwell walls
above the pool surface.

The short-term drywell pressure history during pool swell is specified as the drywell pressure
transient presented in Table 3A.3.2-5.

Test data have shown that a small short duration upward pressure differential on the diaphragm
floor may occur due to rapid pressurization of the wetwell air space during the pool swell
transient. The 4T Test results, discussed in Section 4.4.6.6 of Reference 3A.3.2-11, show a
net upward load on the diaphragm floor of less than 2.2 psi. These low value 4T test results

were confirmed by small scale pool swell tests which showed an average scaled up net upward pressure differential of 1.83 psi. However, as discussed in Section 4.4.6.6 of Reference 3A.3.2-11, the Bodega Bay test data, for a wide variety of blowdown conditions, shows that the wetwell air space pressure never exceeds the drywell pressure.

Conservatively, therefore, the CGS diaphragm floor is assessed for an uplift pressure, P, of 5.5 psi. This is a maximum dynamic load and is in agreement with the loads specified in References 3A.3.2-2 and 3A.3.2-8.

3A.3.2.3.1.4 Fallback Model. The model presented in Reference 3A.3.2-11 is used to calculate the CGS fallback phenomenon. The model development and supporting test data are discussed in Reference 3A.3.2-11. The fallback model conservatively assumes the pool swell slug remains intact during pool swell and falls back from its maximum height $1.5 \times H_o$, where H_o is the pre-LOCA downcomer submergence, at full water density and under the constant acceleration due to gravity. Figure 3A.3.2-14 shows a plot of the fallback water slug velocity vs. elevation of water slug top surface.

Reference 3A.3.2-10 indicates that fallback loads on submerged boundaries are negligible and are therefore not specified. This is based on review of existing fallback data.

3A.3.2.3.2   Boundary Loads

The analytical models used to describe containment boundary loads during short-term LOCA loading phenomena are discussed in Section 3A.3.2.3.1. Figures 3A.3.2-15 through 3A.3.2-17 show the duration and distribution of the short-term containment boundary loads.

3A.3.2.3.3   Structure Loads

The CGS structures affected by short-term LOCA loading phenomena are identified in Section 3A.2.1.1 and shown in Figures 3A.2.1-2 through 3A.2.1-8. Short-term LOCA loads on submerged structures are given in Tables 3A.3.2-8, 3A.3.2-9, and Figure 3A.3.2-18.

Piping and structural components below el. 454.4 ft are subjected to loads caused by water clearing/air charging. Piping and structural components between elevations 454.4 ft and 434.4 ft are subjected to drag and lift loads caused by pool swell/fallback. Also, piping and structural components between elevations 466.4 ft and 484.4 ft are subjected to impact loads caused by pool swell. Direct hydrodynamic loads do not exist for piping and structures above el. 484.4 ft.

The following is a description of how the short-term LOCA definition models, discussed in Section 3A.3.2.3.1, are applied to CGS structures.

a.   Vent clearing jet load

The loads on submerged structures located inside the jet boundaries are calculated using the vent exit velocity and acceleration at t = 0.654 sec. The loads on submerged structures located outside the jet boundaries are calculated using velocity and acceleration fields at t = 0.704 sec.

For elbows of 24-in. diameter pipes, the impact load for full momentum transfer of the intercepted jet (K=2) (Reference 3A.3.2-10) is calculated to be smaller than the drag load. Hence, drag load is used in the assessment.

Submerged structures located below the vent exit elevation are subjected to drag loads caused by the vent clearing jet. The types of drag loads and the formulas for calculating them are presented in item c below and in Attachment 3A.C. For the case of the vent clearing jet, the standard drag coefficient, C_D, is equal to 1.2; the acceleration drag coefficient, C_M, is equal to 2.0; and the lift coefficient, C_L, is equal to 0. In order to account for the dynamic nature of the loading phenomenon, a multiplier of 2.0 is used to calculate the equivalent static pressure.

b.   Loss-of-coolant accident bubble load

Submerged structures located below the vent exit elevation are subjected to drag loads caused by LOCA bubble charging. The types of drag loads and the formulas for calculating them are presented in Item c below and in Attachment 3A.C. The velocity and acceleration at any point in the pool are calculated by applying the methods outlined in 3A.3.2.3.1.2.

For the case of LOCA bubble charging, the standard drag coefficient, C_D, is equal to 1.2; the acceleration drag coefficient, C_M, is equal to 2.0; and the lift coefficient, C_L, is equal to 0. These numerical values are consistent with References 3A.3.2-4 and 3A.3.2-6. In order to account for the dynamic nature of the LOCA bubble charging load phenomenon, a DLF of 2.0 is used to calculate the equivalent static pressure.

c.   Pool swell load

The structures above the initial pool surface and below the maximum pool swell height are subject to impact loads due to the rising pool surface. The maximum dynamic pressure due to pool swell impact is calculated by using the methodology outlined in Reference 3A.3.2-2 and in Section III.B.3.c.1 of Reference 3A.3.2-1. In order to account for the dynamic nature of the pool swell loading phenomenon, the equivalent static pressure is obtained by

multiplying the maximum dynamic impact pressure by a DLF. The DLF is given in Figure 5 of Reference 3A.3.2-3. No impact loads on grating surfaces are specified since the CGS grating bars are narrow (typically 3/16-in. wide).

Structures located above the vent exit elevation and below the maximum pool swell height are subjected to drag forces during the pool swell transient. Drag loads have three components: standard drag, acceleration drag, and lift. Formulas for calculating these three types of load are presented in Attachment 3A.C. Standard drag load is velocity square dependent and acts in the flow direction. Acceleration drag load is proportional to the flow acceleration and acts in the flow direction. Lift load is velocity square dependent and is normal to the flow direction.

In order to calculate the three components of drag load, three coefficients are determined. These are: standard drag coefficient, C_D; acceleration drag coefficient, C_M; and lift coefficient, C_L. For circular cross-sections, coefficients C_D, C_M, and C_L are calculated using Reference 3A.3.2-6. For non-circular cross-sections, coefficients C_D and C_M are calculated using Reference 3A.3.2-7, and C_L is assumed equal to 1.6 as indicated in Reference 3A.3.2-5. Interference effects from adjacent structures are taken into account by using the methodology presented in Reference 3A.3.2-4. In order to account for the dynamic nature of the pool swell loading phenomenon, appropriate DLFs are used to calculate the equivalent static loads.

The gratings are subject to drag loads during pool swell due to resistance to the flow through them. The dynamic drag load is determined by the product of the differential pressure across the grating and the total plan area of the grating. The open area fraction for the grating is greater than 60%. The peak dynamic differential pressure across the grating is obtained from Figure 4-1 of Reference 3A.3.2-2. This figure is based on a pool swell approach velocity of 40 fps. Since the maximum pool swell velocity for CGS is smaller than 40 fps, the differential pressure values in Figure 4-1 of Reference 3A.3.2-2 are multiplied by a factor equal to the square of the ratio given by the maximum velocity divided by 40 fps. The maximum pool swell velocity is given in Table 3A.3.2-6 (plus a velocity multiplier of 1.1). In order to account for the dynamic nature of the pool swell loading phenomenon, a multiplier of 2.0 is used to calculate the equivalent static pressure.

Vertical drag pressure and horizontal lift pressure are applied simultaneously to the projected area of a cylinder circumscribing the structural member under consideration. The projection is always made on a plane normal to the direction of pressure. Vertical impact load is applied separately (not in combination with drag and lift loads) to structures located between elevations 466.4 ft and

484.4 ft on the projected area of the structure on the horizontal plane. Impact load is not used to check local bending effects of flanges or webs or ovaling effects of a pipe. The full drag, lift, or impact load calculated as outlined above is applied normal to a pipe or a structural component. There are no loads parallel to the longitudinal axis of the structure.

d. Fallback load

Structures located above the vent exit elevation and below the maximum pool swell height are subjected to drag and lift forces during fallback. The same methodology and the same drag and lift coefficients used in calculating pool swell drag and lift loads reused to define fallback drag and lift loads. To account for the dynamic nature of the fallback loading phenomenon, a multiplier of 2.0 is used to calculate the equivalent static load. No impact loads are specified during fallback (Reference 3A.3.2-11).

Fallback drag loads on gratings are specified to be equal in magnitude to the pool swell drag loads but opposite in direction.

The method of applying drag and lift pressure on a structural member is the same as that outlined at the end of Item c above.

3A.3.2.3.3.1 Loads on Major Structures. The major vertical structures are shown in Figure 3A.2.1-2. They are: the 102 downcomers (three were capped), the 18 SRV lines including quenchers and support towers, and the 17 concrete columns supporting the diaphragm floor. The major horizontal structures are the steel truss shown in Figure 3A.2.1-3, which provides lateral support to the downcomers and the SRV lines, and the platform at el. 472 ft 4 in. shown in Figures 3A.2.1-3 and 3A.2.1-8. The truss is submerged and the platform is located in the pool swell zone.

Hydrodynamic loads on the vertically oriented columns may occur only due to horizontal flow across the columns. Since the columns are vertical, pool swell and fallback loads are negligible. The columns are located along circumferential and radial lines of symmetry between downcomers; however, some asymmetry is created because some of the downcomers have a diameter of 24 in. while others have a diameter of 28 in. This small asymmetry in the downcomer arrangement causes small loads on the columns during water clearing/air charging. The magnitude and distribution of loads on the columns are shown in Table 3A.3.2-8 and Figure 3A.3.2-18 respectively.

As with the columns, hydrodynamic loads on the vertically oriented downcomers may occur only due to horizontal flow across the downcomers since the downcomers are located along circumferential and radial lines of symmetry between other downcomers and the suppression pool boundaries, the LOCA water jet, LOCA bubble charging, pool swell, and fallback

horizontal flows are small. Because the horizontal flows are small the resulting loadings are negligible.

Table 3A.3.2-8 and Figure 3A.3.2-18 show the magnitude and distribution of loads on a vertical SRV line as well as quencher arms during the water clearing/air charging phases of LOCA. Since quencher supports are below el. 448 ft-0 in., they are not subjected to short-term LOCA (Figure 3A.3.2-18). Pool swell and fallback exert negligible loads on the SRV lines due to the vertical orientation of the SRV lines above the downcomer vent exit plane. Because of their location below the downcomer vent exit plane, no pool swell or fallback loads are experienced by the quencher supports and quencher arms.

The downcomer bracing truss is oriented in a horizontal plane one foot above the downcomer vent exit plane. Since the truss is located above the downcomer vent exit the induced flow field and, therefore, drag load due to LOCA water jet during vent clearing is small. Horizontal LOCA bubble load on the bracing truss is small. Because the truss is above the downcomer vent exit plane, pool swell and fallback loads are experienced.

The only major horizontal structure in the pool swell zone is a platform at el. 472 ft-4 in. The platform consists of a grating with an open area fraction of 0.776 and is supported by 0.5-in. thick vertical members. The dynamic drag load is calculated to be 4.2 psi for pool swell and fallback induced loads and is multiplied by a DLF of 2.0. The equivalent static load is then applied to the total plan area of the platform. Because the platform is above the initial pool surface it does not experience vent clearing or LOCA bubble loads.

3A.3.2.3.3.2 Loads on Fully Submerged Piping Systems Below Elevation 454.4 ft. The 24-in. high-pressure core spray (HPCS) (X-31), 24-in. residual heat removal (RHR)-B (X-32), 8-in. reactor core isolation cooling (RCIC) (X-33), 24-in. low-pressure core spray (LPCS) (X-34), 24-in. RHR-A (X-35), 24-in. RHR-C (X-36), 6-in. suppression pool cleanup (X-100) and the 4-in. fuel pool cooling and cleanup (FPC) are the eight piping systems fully submerged in the CGS suppression pool. Seven systems enter the pool through containment penetrations at el. 452 ft 0 in. as shown in Figure 3A.2.1-2. The 4-in. FPC enters the pool through the pedestal at el. 451 ft 6 in. and is also shown in Figure 3A.2.1-2. Each of these pipes runs along the CGS suppression pool boundaries with a maximum distance between pipe centerline and boundaries of 46 in. Since these pipes are below the downcomer vent exit el. 454 ft 4.75 in. they are not subjected to pool swell or fallback loads during a LOCA. The magnitude and distribution of short-term LOCA loads on submerged pipes are given in Table 3A.3.2-8 and Figure 3A.3.2-18 respectively.

3A.3.2.3.3.3 Loads On Partially Submerged Piping Systems. The 13 partially submerged piping systems enter the suppression chamber through containment penetrations at el. 467 ft 9 in. as shown in Figure 3A.2.1-3 and enter the pool vertically within a 39 in. distance from the containment as shown in Figures 3A.2.1-6 through 3A.2.1-8.

The pipes' horizontal portions are subjected to vertical drag and horizontal lift loads caused by pool swell/fallback. Also, the pipes' horizontal portions experience vertical impact pressure due to pool swell. Inclined braces above the penetrations are not subjected to pool swell impact since they are shielded by the pipes. Horizontal supports below penetrations do not experience pool swell impact since these supports are below el. 466.4 ft.

3A.3.2.3.3.4 Loads on Piping Systems and Structural Components Between Elevations 454.4 ft and 484.4 ft. The portion of the wetwell between elevations 454.4 ft and 484.4 ft is affected by pool swell and fallback only. Piping systems located in this zone are subjected to drag, and lift loads. In addition piping between the normal pool surface, el. 466.4 ft, and el. 484.4 ft is subjected to impact loads unless shielded by pipe supports below. These piping systems include penetration sleeves, pipe stubs, pipes, and pipe supports.

3A.3.2.4   Long-Term Hydrodynamic Loads

Long-term hydrodynamic loads refer to the LOCA related loads exerted on the pool boundaries and on submerged wetwell structures following the fallback transient. These loads are associated with steam condensation at the downcomer vent exits as steam from the drywell flows into the suppression chamber via the vents. Depending on the steam mass flux through the vents, two types of loading conditions are anticipated. During high or medium mass flux so-called COs occur. During low mass flux, chugging loads occur. Chugging loads and CO loads are discussed in the following sections.

3A.3.2.4.1   Analytical Models and Supporting Test Data

3A.3.2.4.1.1 Chugging Loads. The design specification for chugging loads herein is based on the major test programs on the effects of CO and chugging, which were conducted for the Mark II Containment Program during the period of 1975 to 1981 (References 3A.3.2-16 and 3A.3.2-17). It takes account of the generic chugging load definition developed for the Mark II type plants (References 3A.3.2-18 and 3A.3.2-19), but departs from the generic definition in order to provide for important structural differences between the CGS plant and the generic plant. The design specification (Reference 3A.3.2-15) is called the Revised Definition as it represents a revision of an earlier definition called the Improved Definition (Reference 3A.3.2-20) which was based only on the first stage of the test results, the 4T Program (Reference 3A.3.2-16). The current design specification, i.e., the Revised Definition, was submitted to and approved by the NRC (Reference 3A.3.1-6). The scope of the design specification covers both single vent loads and multiple vent loads applicable to the CGS plant.

The single vent load definition is based on two series of full scale single vent tests, namely, the 4T tests and the 4TCO tests (References 3A.3.2-16 and 3A.3.2-17). The load is defined in terms of a series of source loads located at the vent exit with significant load features selected on the basis of the pressure readings at the test tank and the characteristics disclosed by the

vent-pool-tank system. Both test programs indicate the impulsive and random strength nature of chugging, and it is noted that the strength, although random, is related to system conditions. The greater chugs of the 4TCO program are controlling relative to pressure amplitude, frequency content, and spatial distribution of pressure. Thus, the Revised Definition is a group of seven source loads selected on the basis of the seven greatest chugs from the 4TCO data. A design load envelope is obtained by applying the source loads in turn at the vent exit; each load consists of an impulsive pressure gradient with appropriate system parameter values. To calculate results at the wetwell tank, the theory of acoustic fluids is used with a fully coupled model consisting of the vent steam, the pool water, and the wetwell tank. The calculated results, due to application of the defining source loads, envelope both the 4TCO data and the 4T data, relative to all pertinent characteristics.

The multiple vent load definition utilizes the preceding single vent definition in conjunction with the 102 vents in the CGS plant. It is described in Section 3A.3.2.4.2.1.

3A.3.2.4.1.2 Condensation Oscillation Loads. The generic definition of CO loads, as developed for the Mark II Containment Program, is given in Reference 3A.3.2-21. The definition is based on direct application of the bounding pressure measurements from full-scale single vent 4TCO tests to the Mark II containment boundaries.

A comparison has been made between this load definition for CO loads, the JAERI CO results, and the preceding definition for chugging loads. The comparison, as reported in Reference 3A.3.2-12 shows that the CO loads and the chugging loads are similar with respect to pertinent characteristics such as randomly varying amplitude, frequency content, and desynchronization of vent loads. However, it is also shown (References 3A.3.2-12 and 3A.3.2-23), that in a Mark II multivent containment, the controlling boundary pressures due to the CO load are less than those due to the chugging load. It is therefore concluded that the CO load does not represent a governing load and that it need not be considered in the assessment of the design adequacy of the CGS structures.

3A.3.2.4.2   Boundary Loads

3A.3.2.4.2.1 Chugging Loads. The current design specification, i.e., the Revised Definition (Reference 3A.3.2-15), includes definition of the chugging boundary loads due to multivent chugging together with the associated application methodology. The chugging pressures on the suppression pool boundary are defined as resulting from the application of the single vent design chugging loads at all 102 vent exits in the CGS pool-containment structure. To determine the boundary pressures, the analysis is based on a fully coupled model which accounts for all important plant parameters: vent length, three-dimensional multivent pool geometry, pool with sloped bottom, and flexibility of pool structural boundaries. Detailed analytical methods are described in Reference 3A.3.2-15.

The methodology for application of the source loads to the 102 vents is generally similar to that of the generic load definition (Reference 3A.3.2-19), and reflects the characteristics of multivent behavior disclosed by the JAERI and CREARE test programs. Two deterministic spatial distributions of chug strengths, similar to but not the same as the generic distributions, are specified to maximize axisymmetric and nonaxisymmetric responses. Random variation of chug initiation tines from vent to vent is recognized with desynchronization of the start times as in the generic definition. The seven basic single vent loads of the design specification are applied in turn at the 102 vents with variation of strength and initiation time between vents as previously noted; an envelope of containment pressures is calculated. The calculated results exceed the test results in the 4TC0 and the JAERI tests with respect to maximum containment pressures and the Fourier amplitude spectra for containment pressures.

3A.3.2.4.2.2 Condensation Oscillation Loads. The discussion in Section 3A.3.2.4.1.2 on the relative magnitudes of chugging loads and CO loads is applicable. As noted therein, the controlling boundary pressures due to chugging exceed those due to CO. Hence, the CO load is not a governing load and it is not considered in the assessment of the design adequacy of the CGS structure.

3A.3.2.4.3   Submerged Structure Loads

Loads on submerged structures caused by CO and chugging are presented in the following sections.

3A.3.2.4.3.1 Condensation Oscillation Loads. There is no need to assess the CGS plant for a CO load definition since CO loading is less critical and is bounded by the chugging load.

3A.3.2.4.3.2 Chugging Loads. The LOCA chugging loads on submerged structures are defined consistently with the load definition for the pool boundary. Pressure field in the fluid is obtained using chugging design sources developed for pool boundary loads (Reference 3A.3.2-15). From the pressure field, pressure gradients and loads on submerged structures are calculated.

In the method described above, it is assumed that the flow in the vicinity of the vent during chugging is unaffected by the presence of pool boundaries or other sources in the pool. Therefore, fluid pressures in a single cell/single vent pool are representative of pressures near the vent in the CGS pool.

For structures located beyond a distance of 4R (R being the downcomer radius) from the vent exit center, the chugging loads are negligible and need not be considered in the design assessment of the structures. Equivalent static chugging loads for structures located within a distance of 4R from the vent exit center are calculated by using the formula:

$$p = C_m \frac{\pi}{4} D \times DLF \times \frac{\partial p}{\partial n}$$

where

  p   = equivalent static pressure on structure (psi)

  C_m = hydrodynamic mass coefficient = 2.0

  DLF   = dynamic load factor = 1.5

  D   = diameter in inches of the pipe or of the cylinder circumscribing the cross-section of a support member

  $\frac{\partial p}{\partial n}$ = pressure gradient across a submerged structure (psi/in). Numerical values for this term are given in Figure 3A.3.2-19.

Chugging loads calculated as outlined above are listed as follows:

a.   Bracing Truss Members: A load of 10 psi is applied vertically upward or downward. This load is applied simultaneously to all members connecting to a downcomer. Chugging event under each vent occurs with random phasing from events at other vents. Therefore, this load is not applied simultaneously to all members of the truss;

b.   Inner Row SRV Line: A load of 12 psi is applied radially outward or inward from the vent axis of the adjacent inner row downcomer. The load distribution is assumed uniform between el. 454.4 ft and el. 452.4 ft and then linearly decreasing to zero at Point A (Figure 3A.3.2-19); and

c.   Pipes and Supports: A pressure is applied vertically upward or downward. The magnitude and distribution of the vertical pressure are calculated using Equation 3A.3.2-1 and Figure 3A.3.2-19. The maximum vertical pressure is 2.4D psi. Simultaneously, a radial pressure is applied inward or outward from the vent axis of the adjacent outer row downcomer. The magnitude and distribution of the radial pressure are calculated using Equation 3A.3.2-1 and Figure 3A.3.2-19. The radial load is assumed zero above the vent exit.

The pressure loads listed above are multiplied by the projected area of the structure segment normal to the direction of the loading to obtain the total force on each segment. The total load on each segment of the structure is applied at the geometric center of the segment

3A.3.2.4.4   Lateral Loads on Downcomer Vents

This section provides the definition of the lateral loads which occur near the downcomer exits during chugging. The definition conforms with the requirements for such loads as prescribed in NUREG-0808 (Reference 3A.3.2-8). These lateral loads are defined herein in relation to the downcomer bracing system which is described and assessed in Section 3A.4.2.1. The principal features included in the definition are single vent loads, loads on multiple vents, overall loading of the bracing system, and loads and downcomer size.

> a.   Single Vent Load - The maximum lateral exit load on one 24-in. downcomer is defined as a dynamic single pulse load having a half sine wave shape with load amplitude of 65 klbf (kips) and duration of 3 msec. For the assessment of the bracing system, a dynamic analysis of the system acted on by this single vent load is made.

> b.   Loads on Multiple Vents - With multiple vent loading, the force on each loaded vent is also defined as a single pulse half sine wave dynamic load. However, in line with NUREG-0808, the pulse duration is taken to vary over a range of values and the force amplitude is taken to depend on the pulse duration, T, and on the number of loaded vents. The vent force, F(t), is evaluated by the expression:

$$F(t) = M \, A(T) \sin (t/T) \quad 0 \leq t \leq T \qquad \text{(Eq. 3A.3.2-2)}$$

> where

$$A(T) = (50 - 20 \, T/3) \text{ klbf} \quad 3 \leq T < 6 \text{ ms} \qquad \text{(Eq. 3A.3.2-3)}$$

> The factor M is a load reduction factor which depends on the number of loaded vents and the required level of exceedence probability. For a given number of loaded downcomers, it is evaluated at the exceedence probability level of 10^{-4} using the diagram specified in NUREG-0808.

> To determine the controlling value of the amplitude factor A, the bracing system was analyzed over the range of the duration, T. Thus, values of T in the range of 3 to 6 ms and the associated values of A were utilized. It was determined that the controlling value of T was always 3 ms. Consequently, the associated value of A in the above equation for F(t) is evaluated as 30 kips.

For the assessment under multiple vent loading, the bracing system is analyzed dynamically with lateral loads on a given set of vents. In the analysis, the force on each loaded vent is defined by Equation 3A.3.2-2 where M is obtained as previously described, A equals 30 klbf, and T equals 3 ms.

c. Overall Loading of the Bracing System - The design assessment of the downcomer bracing system under multiple lateral exit loads in 3A.4.2.1 describes the method used to determine the controlling number of loaded vents and the controlling direction of the loads. The methodology is generally similar to that of Section 2.3.2.2 of NUREG-0808.

d. Loads and Downcomer Size - The downcomer system consists of 102 downcomers of which 84 are 24-in. diameter and 18 are 28-in. diameter. The lateral loads on the 24-in. diameter vents have been defined above in paragraphs a and b for the cases of single vent loading and multiple vent loading. In line with NUREG-0808, the lateral loads on the 28-in. vents are defined as 1.34 times as great as those on the 24-in. vents.

3A.3.2.5   Pressure and Temperature Transients

A LOCA causes a pressure and temperature transient in the drywell and wetwell due to mass and energy released from the line break. The drywell and wetwell pressure and temperature histories are employed to establish the structural loading conditions in the containment. The response must be determined for a range of parameters such as break size, reactor pressure, and initial (preincident) containment conditions. The analytical models used to evaluate the pressure and temperature response of the containment have been developed by GE (References 3A.3.2-13 and 3A.3.2-14).

The assumptions made for analyzing the LOCA transients were based on conservatively predicting the blowdown mass and energy rates into the drywell and suppression pool. The following assumptions were made:

a. Initial drywell pressure of 0.75 psig,

b. Downcomer submergence at high water level,

c. Minimum drywell free air volume,

d. Minimum wetwell free air volume,

e. Minimum water volume in wetwell, and

      f.   Suppress ion pool initial temperature and service water temperature at the maximum Technical Specifications limit.

(Assumptions b, d, and e are inconsistent with each other but provide conservative results.)

For the intermediate size breaks, it was assumed that all the mass and energy releases from the broken pipe discharge via the drywell into the suppression pool. Normally, a portion of the mass and energy release will be dispersed over the drywell volume causing the drywell pressure and temperature to rise.

3A.3.2.5.1   Results for CGS

The drywell pressure transients have been calculated with inventory effects included in the analysis. The results for the recirculation and main steam line breaks are presented in Figures 3A.3.2-20 through 3A.3.2-28.

The plant parameters used are given in Table 3A.3.2-7. The spectrum of accident conditions covered are:

      a.   Large double-ended break of a recirculation line,
      b.   Large double-ended break of one main steamline, and
      c.   Intermediate recirculation line break (0.1 ft^2 break area).

Table 3A.3.2-5 provides the drywell pressure transient during the 2 sec period immediately following a recirculation line break. This table differs from the values plotted in Figure 3A.3.2-20, since it includes the influence of reactor subcooling on the initial blowdown flow rate from the break. This is a short-term effect that occurs during the first few seconds of the accident and does not influence the maximum drywell pressure. Since this LOCA leads to the most severe short-term pressure conditions, the data in Table 3A.3.2-5 are used to calculate the pool swell velocities and associated effects.

Figures 3A.3.2-20 through 3A.3.2-24 give the pressure/temperature transients resulting from a large recirculation line break. As shown in Figure 3A.3.2-20, the drywell pressure increases to a maximum value of 35 psig in about 20 sec. Also, the pressure of the wetwell air, while increasing with time, is less than the drywell pressure until the ECCS flow starts to spill from the break. The drywell temperature increases to about 280°F (Figure 3A.3.2-23), while the temperature of the suppression pool increases to about 220°F. Similar response curves for a main steam line break are also shown in Figures 3A.3.2-25 and 3A.3.2-26, and those for an intermediate break accident (IBA) are shown in Figures 3A.3.2-27 and 3A.3.2-28.

3A.3.2.5.2   Differential Pressure Load on the Diaphragm Floor

As illustrated in Figures 3A.3.2-20, 3A.3.2-21, 3A.3.2-25, and 3A.3.2-28, the net pressure on the diaphragm floor is downward throughout a LOCA transient (refer to FSAR Section 6.2.1). However, the diaphragm floor is conservatively designed for a net uplift pressure of 5.5 psi as discussed in 3A.3.2.3.1.3. The maximum net downward pressure on the diaphragm occurs during the short-term part of the large break LOCA transients and reaches a maximum value of 20 psi.

During the initial phase of a LOCA transient, drywell air is blown down through the downcomer vents into the wetwell by the steam from the break. The steam rapidly replaces the air in the drywell.

Initially, a steam-air fixture flows through the vents into the suppression pool and forms bubbles that rise to the pool's surface. Condensation of the steam in the bubbles allows only the air component to reach the wetwell airspace. As the air collects, the air space becomes pressurized and heated.

As the reactor vessel blowdown ends, the emergency core cooling system floods the core with water which starts to spill out of the break into the drywell. This results in rapid condensation of the steam, which has replaced the air, and consequent rapid drywell depressurization below that in the wetwell. Before the net upward pressure becomes large, however, nine 24-in. vacuum breakers, which are attached to nine selected downcomers, open to equalize the pressure difference by returning the air (nitrogen) collected in the wetwell to the drywell. These vacuum breakers are adjusted to open when the differential pressure across them is in the range of 0.15 to 0.35 psi.

3A.3.2.6   Building Response to Loss-of-Coolant Accident Loads

The analysis and response of the reactor building under the action of long-term LOCA loads is discussed in Section 3A.5.2.

3A.3.2.7   References

3A.3.2-1   "Mark II Containment Lead Plant Program Load Evaluation and Acceptance Criteria," NUREG-0487, NRC, October 1978.

3A.3.2-2   Mark II Containment Dynamic Forcing Functions Information Report (DFFR), General Electric Company, NEDO-21061, Revision 4, November 1981.

3A.3.2-3   "Impact Loads on Structures Above Mark II Containment Pools," G. Maise, Brookhaven National Laboratory, February 28, 1978.

3A.3.2-4   "Submerged Structure Methodology," Appendix G, Zimmer Power Station, Unit 1, DAR Amendment No. 13, October 1980.

3A.3.2-5   "Mark II Containment Lead Plant Program Load Evaluation and Acceptance Criteria," NUREG-0487, Supplement No.1, NRC, September 1980.

3A.3.2-6   "In-Line and Transverse Forces on Cylinders in Oscillatory Flow at High Reynolds Number," Journal of Ship Research, Volume 21, No. 4, pp. 200-216, December 1977.

3A.3.2-7   "Forces on Cylinders and Plates in an Oscillating Fluid," G. H. Keulegan and L. H. Carpenter, Journal of Research of the National Bureau of Standards, Volume 60, No. 5, May 1958.

3A.3.2-8   "Mark II Containment Program Load Evaluation and Acceptance Criteria," NUREG-0808, USNRC, August 1981.

3A.3.2-9   "An Analytical Model for LOCA Water Jet in Mark II Containments (The Ring Vortex Model)," Burns and Roe, Inc., September 1980.

3A.3.2-10   Mark II Containment Dynamic Forcing Functions Information Report (DFFR), General Electric Company, NEDO-21061, Revision 3, June 1978.

3A.3.2-11   Mark II Containment Dynamic Forcing Functions Information Report (DFFR), General Electric Company, NEDO-21061, Revision 2, September 1976.

3A.3.2-12   "Comparison of Condensation Oscillation and Chugging Loads for Assessment of WPPSS Nuclear Project No. 2," Summary Report, Proprietary, Burns and Roe, Inc., December 1981 transmitted to NRC by letter GO2-81-552 dated December 24, 1981.

3A.3.2-13   The General Electric Pressure Suppression Containment Analytical Model, General Electric Company, NEDO-10320, April 1971.

3A.3.2-14   Safe System Analysis for Standby Core Cooling Equipment, General Electric Company, NEDE-10169, Proprietary, September 1977.

3A.3.2-15   "Chugging Loads - Revised Definition and Application Methodology for Mark II Containments (Based on 4TCO Test Results)," Technical Report, Burns and Roe, Inc., July 1981. Transmitted to NRC by letter GO2-81-189 of July 22, 1981.

3A.3.2-16   "Mark II Pressure Suppression Test Program - Phase I, II, and III of the 4T Tests - Application Memo," NEDE-23678-P, Rev. 0, General Electric Company, January 1977.

3A.3.2-17   "4T Condensation Oscillation Test Program Final Test Report," NEDE-24811-P, General Electric Company, May 1980.

3A.3.2-18   "Mark II Improved Chugging Methodology," NEDE-24822-P, General Electric Company, May 1980.

3A.3.2-19   "Generic Chugging Load Definition Report," NEDE-24302-P, General Electric Company, April 1981.

3A.3.2-20   "Chugging Loads - Improved Definition and Application Methodology to Mark II Containments," Technical Report, Proprietary, Burns and Roe, Inc., June 1979.

3A.3.2-21   "Generic Condensation Oscillation Load Definition Report," NEDO-24288, General Electric Company, February 1981.

3A.3.2-22   "Mass Energy Report," General Electric Report, GEWP-2-77-533, March 15, 1977.

3A.3.2-23   Letter report on C.O. loads GO2-82-351 of April 1, 1982.

3A.3.2-24   "WPPSS Nuclear Project No. 2, Final Safety Analysis Report," Washington Public Power Supply System, Chapter 6.2.

3A.3.2-25   AEC-TR-6630, "Handbook of Hydraulic Resistance - Coefficients of Local Resistance And Friction," I. E. Idel'chik, 1960.

3A.3.2-26   "Flow of Fluids Through Valves, Fittings, and Pipe," Technical Paper No. 410, Crane Company, 1980.

3A.3.2-27   "CONTEMPT-LT--A Computer Program For Predicting Containment Pressure-Temperature Response to A Loss-of-Coolant Accident," Aerojet Nuclear Company, June 1975.

3A.3.2-28   "Mark II Pressure Suppression Containment Systems: An Analytical Model of the Pool Swell Phenomenon," NEDE-21544-P, General Electric Company, December 1976.

3A.3.2-29   Response to NRC Question 020.071, transmitted via letter MFN-275-78 to
              Mr. J. F. Stolz, Chief, Light Water Reactor Branch No. 1, USNRC, from
              Mr. L. J. Sobon, Manager BWR Containment Licensing, General Electric
              Company on "Responses to NRC Request for Additional Information
              (Round 3 Questions)," dated June 30, 1978.

Table 3A.3.2-1

Summary of Loss-of-Coolant Accident Affected Structures

| | Type of Loading Condition | | | | | |
| | Short-Term LOCA | | | | Long-Term LOCA | |
Structures Experiencing LOCA Loads	Water Jet	LOCA Bubble	Pool Swell	Fallback	Condensation Oscillations	Chugging
Fully submerged piping systems	3A.3.2.3.1.1/ 3A.3.2.3.3.2	3A.3.2.3.1.2/ 3A.3.2.3.3.2			3A.3.2.4.1.2/ 3A.3.2.4.3.1	3A.3.2.4.1.1/ 3A.3.2.4.3.2
Partially submerged piping systems	3A.3.2.3.1.1/ 3A.3.2.3.3.3	3A.3.2.3.1.2/ 3A.3.2.3.3.3	3A.3.2.3.1.3/ 3A.3.2.3.3.3	3A.3.2.3.1.4/ 3A.3.2.3.3.3	3A.3.2.4.1.2/ 3A.3.2.4.3.1	3A.3.2.4.1.1/ 3A.3.2.4.3.2
Piping systems fully above initial pool surface			3A.3.2.3.1.3/ 3A.3.2.3.3.4	3A.3.2.3.1.4/ 3A.3.2.3.3.4		
Grating			3A.3.2.3.1.3/ 3A.3.2.3.3.1	3A.3.2.3.1.4/ 3A.3.2.3.3.1		
Drywell floor			3A.3.2.3.2			
Containment wall	3A.3.2.3.1.1		3A.3.2.3.2	3A.3.2.3.2	3A.3.2.4.2.2	3A.3.2.4.2.1
Pedestal	3A.3.2.3.1.1		3A.3.2.3.2	3A.3.2.3.2	3A.3.2.4.2.2	3A.3.2.4.2.1
Basemat	3A.3.2.3.1.1	3A.3.2.3.2	3A.3.2.3.2	3A.3.2.3.2	3A.3.2.4.2.2	3A.3.2.4.2.1
Columns	3A.3.2.3.1.1/ 3A.3.2.3.3.1	3A.3.2.3.1.2/ 3A.3.2.3.3.1				
Downcomers	3A.3.2.3.1.1/ 3A.3.2.3.3.1	3A.3.2.3.1.2/ 3A.3.2.3.3.1			3A.3.2.4.1.2/ 3A.3.2.4.3.1	3A.3.2.4.1.1/ 3A.3.2.4.3.2
Downcomers bracing system			3A.3.2.3.1.3/ 3A.3.2.3.3.1	3A.3.2.3.1.4/ 3A.3.2.3.3.1	3A.3.2.4.1.2/ 3A.3.2.4.3.1	3A.3.2.4.1.1/ 3A.3.2.4.3.2
SRV system	3A.3.2.3.1.1/ 3A.3.2.3.3.1	3A.3.2.3.1.2/ 3A.3.2.3.3.1			3A.3.2.4.1.2/ 3A.3.2.4.3.1	3A.3.2.4.1.1/ 3A.3.2.4.3.2

Note: Numbers refer to section of Appendix 3A.

Table 3A.3.2-2

CGS Data for Loss-of-Coolant Accident
Water Jet Analysis

Unit cell diameter	40.87 in.
Unit cell depth	354.0 in.
Downcomer inner radius	13.625 in.
Downcomer submergence	144.0 in.
Downcomer water clearing velocity time history	Figure 3A.3.2-2

Table 3A.3.2-3

CGS Data for Vent Clearing And Pool Swell Analysis

Drywell

1. Temperature (initial)   135°F

2. Drywell pressure transient   Table 3A.3.2-5

3. Relative humidity   0%

Suppression Chamber

1. Free air volume (maximum)   147,290 ft^3

2. Net suppression pool surface area   4520 ft^2

3. Pressure (initial)   0.7 psig

4. Air specific heat ratio   1.4[a]/1.2[b]

Downcomer vent system

1. Submergence (minimum/maximum)   11 ft-8 in./12 ft[a]

2. Nominal diameter   2 ft

3. Number of vents   102

4. Vent exit area   321 ft^2

5. Vent loss coefficient   1.9

[a] Value used to determine maximum pool swell elevation.

Table 3A.3.2-4

Results from Loss-of-Coolant Accident
Bubble Charging Analysis for CGS

	Downcomers		
	Inner Radius	Middle Radius	Outer Radius
Bubble coalescence time (sec)[a]	0.09	0.16	0.24
Bubble radius at coalescence (ft)	2.12	2.77	3.41

[a] Times represent time after vents have cleared.

Table 3A.3.2-5

CGS Drywell Pressure as a Function of Time for
Loss-of-Coolant Accident[a]
(Effects of Pipe Inventory and Subcooling Included)

Time After Loss-of-Coolant Accident (sec)	Drywell Pressure (psia)
0.0	15.45
0.00159	15.32
0.00171	15.30
0.00549	14.72
0.0641	17.61
0.127	20.18
0.252	24.83
0.502	33.27
0.720	35.69
0.740	35.42
1.099	35.11
1.537	35.84
1.568	35.92
2.037	36.00

[a] See Reference 3A.3.2-22.

Table 3A.3.2-6

Results of Pool Swell Analysis for CGS

Vent clearing time[a] - t_c	0.65 sec
Pool water surface velocity[b] at time t_c	5.3 ft/sec
Time of maximum pool swell velocity	1.12 sec
Maximum pool swell velocity[b]	28.7 ft/sec
Time of maximum pool height[a]	1.48 sec
Maximum pool swell height (H_{max})	18.0 ft
Ratio of H_{max} to H_o (downcomer submergence)	1.5
Maximum air bubble pressure	35.75 psia
Maximum wetwell airspace pressure	47.55 psia
Maximum pool swell elevation	484 ft 4.75 in. msl
Pool swell termination[a]	1.48 sec

[a] Times represent time after LOCA initiation.
[b] Does not include velocity multiplier of 1.1.

Table 3A.3.2-7

CGS Plant Parameters for
Loss-of-Coolant Accident Transient Analysis

1. Drywell
   a. Free air volume .... $200,540 \text{ ft}^3$
   b. Temperature (initial) .... 135°F
   c. Pressure (initial) .... 0.75 psig
   d. Relative humidity 50%

2. Wetwell
   a. Free air volume .... $144,184 \text{ ft}^3$
   b. Water volume[a] .... $107,850 \text{ ft}^3$
   c. Pool temperature (initial) .... 90°F
   d. Pressure (initial) .... 0.75 psig
   e. Relative humidity 100%

3. Break area
   a. Design basis accident (DBA) - .... 3.106 ft^2
      recirculation line
   b. DBA - steam line .... 3.92 ft^2
   c. Intermediate break .... 0.1 ft^2

4. Main vent
   a. Maximum submergence .... 12 ft
   b. Nominal diameter .... 2 ft
   c. Number of vents .... 102[b]
   d. Vent entrance flow area .... 304.6 ft^2
   e. Downcomer loss factor 1.9

[a] Water volume
[b] Refer to Section 3A.3.2.2 for a discussion of the effect of capping three downcomers.

Table 3A.3.2-8

Short-Term Loss-of-Coolant Accident Loads
on Structures Below Elevation 454.4 ft

| | Radial Location r of Geometric Center of the Structure or Segment of Structure | | | |
| | Zone I $0 \leq r < 2.3R$ | | Zone II $2.3R \leq r < 5.0R$ | |
Structure	p_r max (psi)	p_v max (psi)	p_r max (psi)	p_v max (psi)
42 in. diameter vertical column			+2	
12 in. diameter vertical SRV line	±20 inner row		+2 outer row	
Pipes and Supports				
Diameter[a] > 12 in. (X-31,32,34,35,36)	±60	+212	+6	-45
Diameter[a] ≤ 12 in. (X-33,100,4 in. FPC, quencher arm)	±60	+100	+6	-25

[a] For noncylindrical structures, the diameter of a cylinder circumscribing the cross section of the structure is used.

Notes:

1. Vertical load is positive in the downward direction. Radial load is positive in the radially outward direction from the axis of symmetry of the downcomer.

2. The vertical distribution associated with the tabulated peak values is shown in Figure 3A.3.2-18. The distribution in the radial direction in each zone is uniform and is aximsymmetric in the circumferential direction.

3. Long structures are divided into smaller segments, L ≤ D; D being the diameter of the structure, and L being the segment length.

Table 3A.3.2-8

Short-Term Loss-of-Coolant Accident Loads
on Structures Below Elevation 454.4 ft (Continued)

4.   Radial or vertical load is calculated at the geometric center of each structure or segment
(see Figure 3A.3.2-18) by multiplying the pressure value at the geometric center
(obtained from this table) with the length and the diameter of the structure.

For noncylindrical structures, diameter of the circumscribing cylinder is used.

5.   Radial or vertical load has, in general, two components. One is parallel and the other
is normal to the structure or segment. All components of load that are parallel to the
structure or segment are neglected.

6.   The radial location, r, of the structure or segment is taken from the nearest vent. Since
the flow from vents occurs in-phase during water clearing/air charging phases of
LOCA, the flow field calculations and the above specified loads have already accounted
for the multi-vents effect. Therefore, effects of flow from other adjacent vents need
not be added or subtracted.

7.   The loads specified are equivalent static and utilize a DLF equal to 2.

Table 3A.3.2-9

Short-Term Loss-of-Coolant Accident Loads on
Structures Between Elevations 454 ft 4.75 in. and 484 ft 4.75 in.

Structures Located Between El. 454 ft 4.75 in. and El. 484 ft 4.75 in.	Equivalent Static Load		
	Pool Swell/ Impact ±Pψ (psi)	Pool Swell Fallback Drag ±Pψ (psi)	Pool Swell/ Fallback Horizontal Lift ±Ph (psi)
I. Downcomer bracing truss		25	5
II. Platform at el. 472 ft 4 in.: grating perimeter members		8.4	25
III. Piping at 467 ft 9 in. and supports			
A. Horizontal portions of pipes			
a. X-48,118,117,47,26,63,49,101, X-23,24, X-4 (pipe and sleeve)	41	25	15
b. X-64,65	16	20	15
B. Inclined braces above penetrations		50	25
C. Horizontal supports below penetrations		60	25
IV. Penetration sleeves, pipe stubs, and electrical box protective structures			
a. X-51,66 sleeves for: X-81,82,83,84,116	209	25	5
b. X-87A	166	25	5
c. X-86A	62	25	5
d. X-88,87B,86B,116 (piping)		25	5
e. X-81,82,83,84 (piping except X-82e)	209	20	5
f. X-107A, X-107B (electrical box protective structures)	116	25	5

Increasing
Drywell
Pressure

Wetwell Air
Compression

Initial
Pool
Surface
Elevation
(Typ.)

1. VENT CLEARING

Increasing
Drywell
Pressure

Air Bubble Pressure

2. LOCA BUBBLE CHARGING

Increasing
Drywell
Pressure

Wetwell Air
Compression

Maximum
Pool Swell
Height

Water
Slug

Air Bubble
Pressure

3. POOL SWELL

4. FALLBACK

Columbia Generating Station Final Safety Analysis Report	Short Term Hydrodynamic Processes Associated with a LOCA
	Draw. No. 950021.76 Rev. Figure 3A.3.2-1

Time = 0.654 Sec.
Velocity = 82.22 Ft/Sec

Vent Clearing Velocity (Ft/Sec)

Time After LOCA (Sec)

Columbia Generating Station **Final Safety Analysis Report**	**Downcomer Vent Water Clearing Velocity** **Versus Time**		
	Draw. No. 950021.77	Rev.	Figure 3A.3.2-2
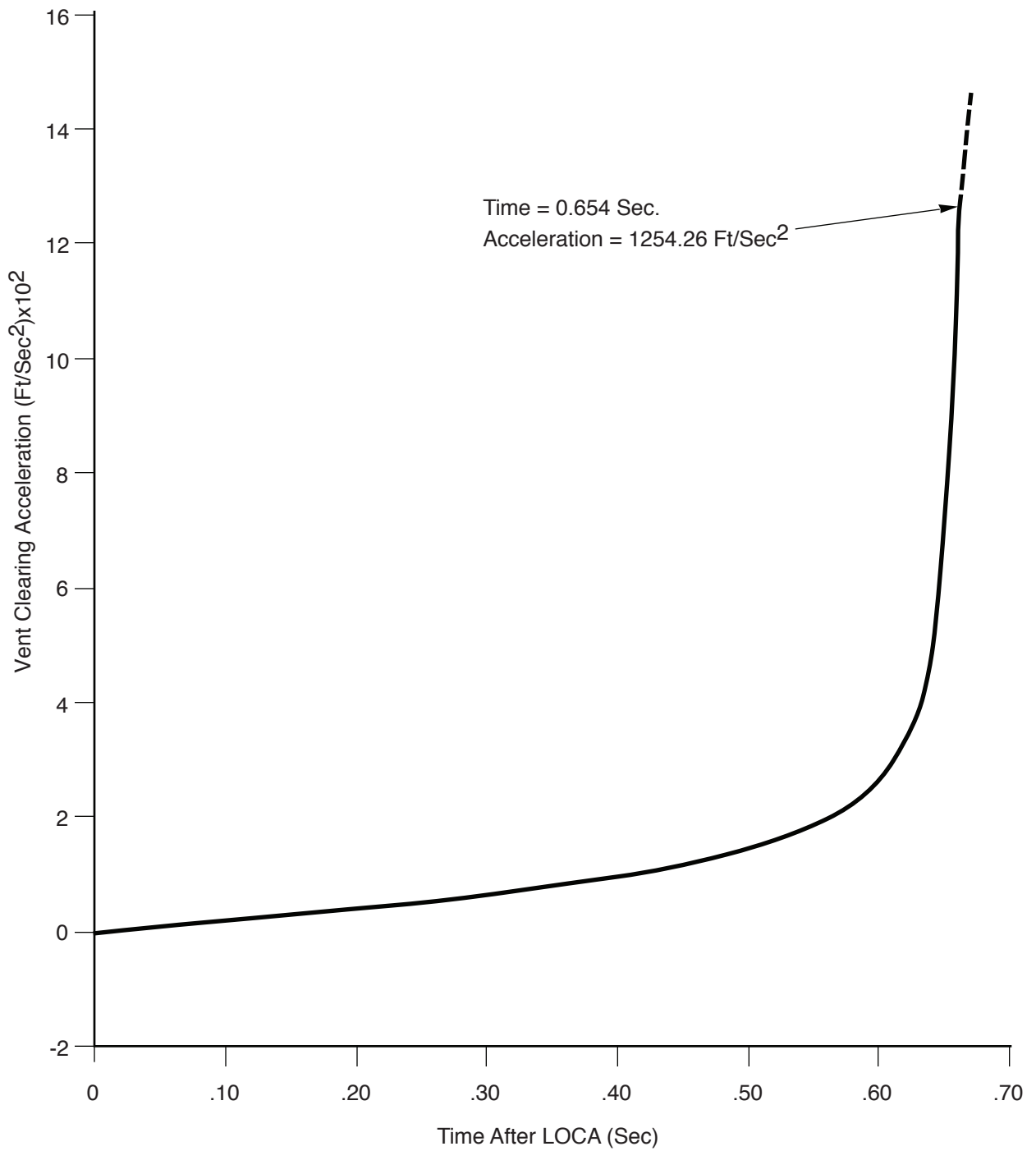
Form No. 960690

Time = 0.654 Sec.
Acceleration = 1254.26 Ft/Sec^2

Vent Clearing Acceleration (Ft/Sec^2)x10^2

Time After LOCA (Sec)

Columbia Generating Station Final Safety Analysis Report	Downcomer Vent Water Clearing Acceleration Versus Time		
	Draw. No. **950021.78**	Rev.	Figure **3A.3.2-3**

∇Φ Units: in/sec for a Point Source of Strength 10+⁴ in³/sec

Radial Distance from Reactor Building Centerline (inches)
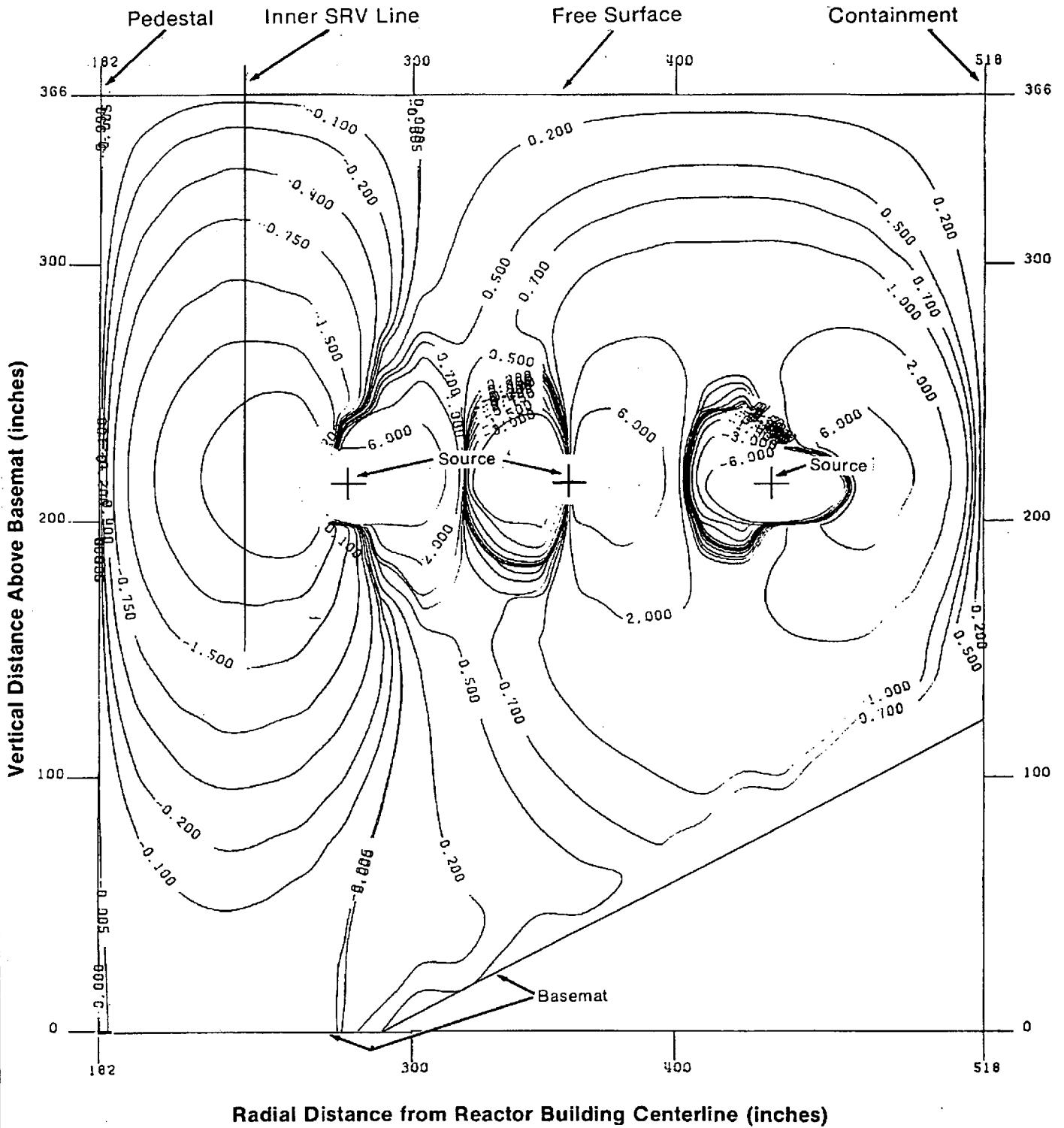
Columbia Generating Station Final Safety Analysis Report	LOCA Bubble Charging Radial Component of ∇Φ in Radial Plane Containing Downcomers		
	Draw. No. 020361.16	**Rev.**	**Figure 3A.3.2-4**

∇Φ Units: in/sec for a Point Source of Strength |10+⁴ in³/sec

Θ = 5°-17′ -39″
Plane of Symmetry
Between Downcomers

Θ = 0°, Plane Containing Downcomers

Free Surface

Vertical Distance Above Basemat (inches)

Tangential Distance From Plane Containing Downcomers (Inches)

Basemat
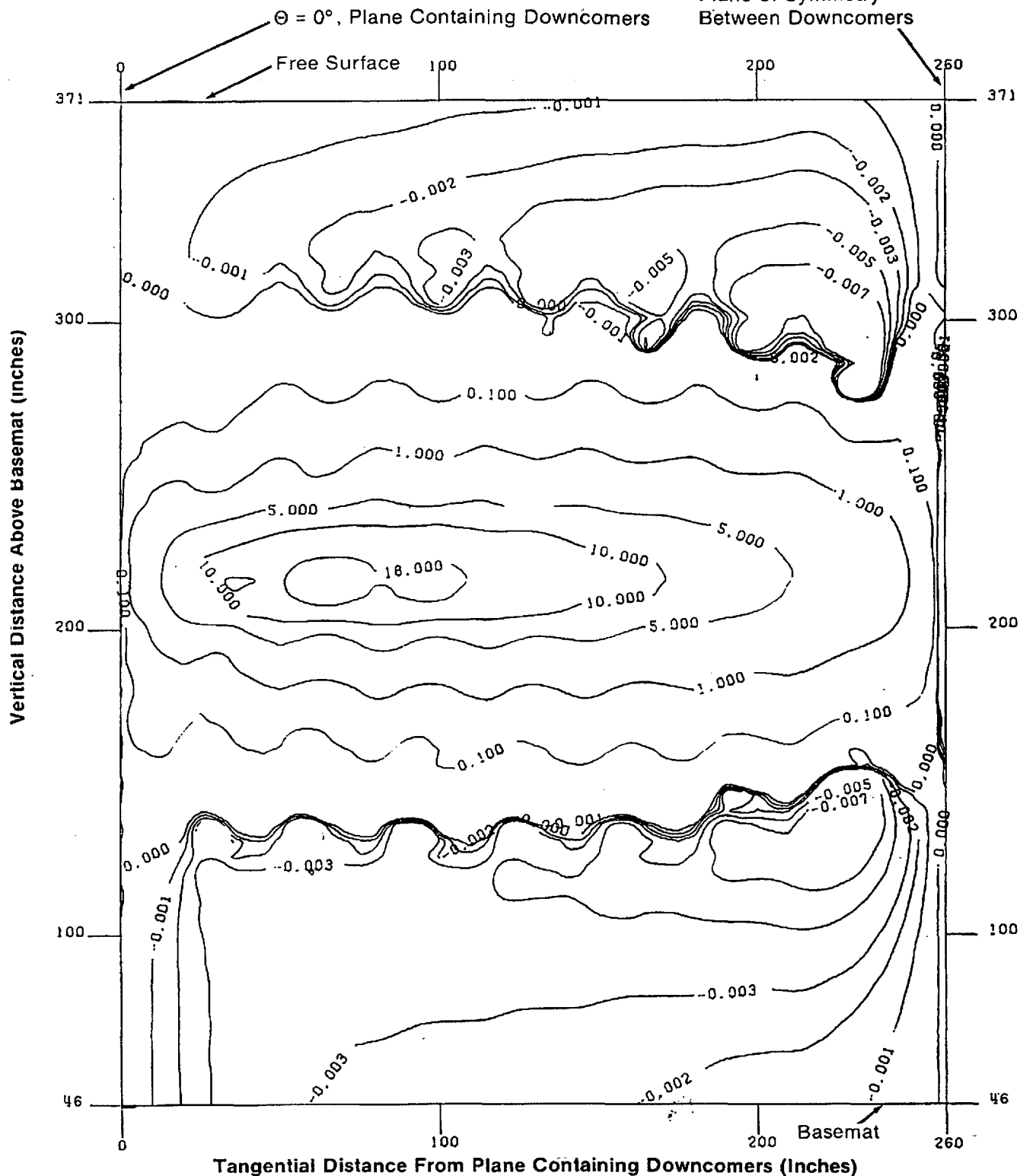
Columbia Generating Station Final Safety Analysis Report	LOCA Bubble Charging Tangential Component of ∇Φ in Vertical Cylindrical Surface Through Middle Downcomers		
	Draw. No. 020361.17	Rev.	Figure 3A.3.2-5

Form No. 960690

$\nabla \Phi$ Units: in/sec for a Point Source of Strength 10^{+4} in^3/sec

Radial Distance From Reactor Building Centerline (inches)
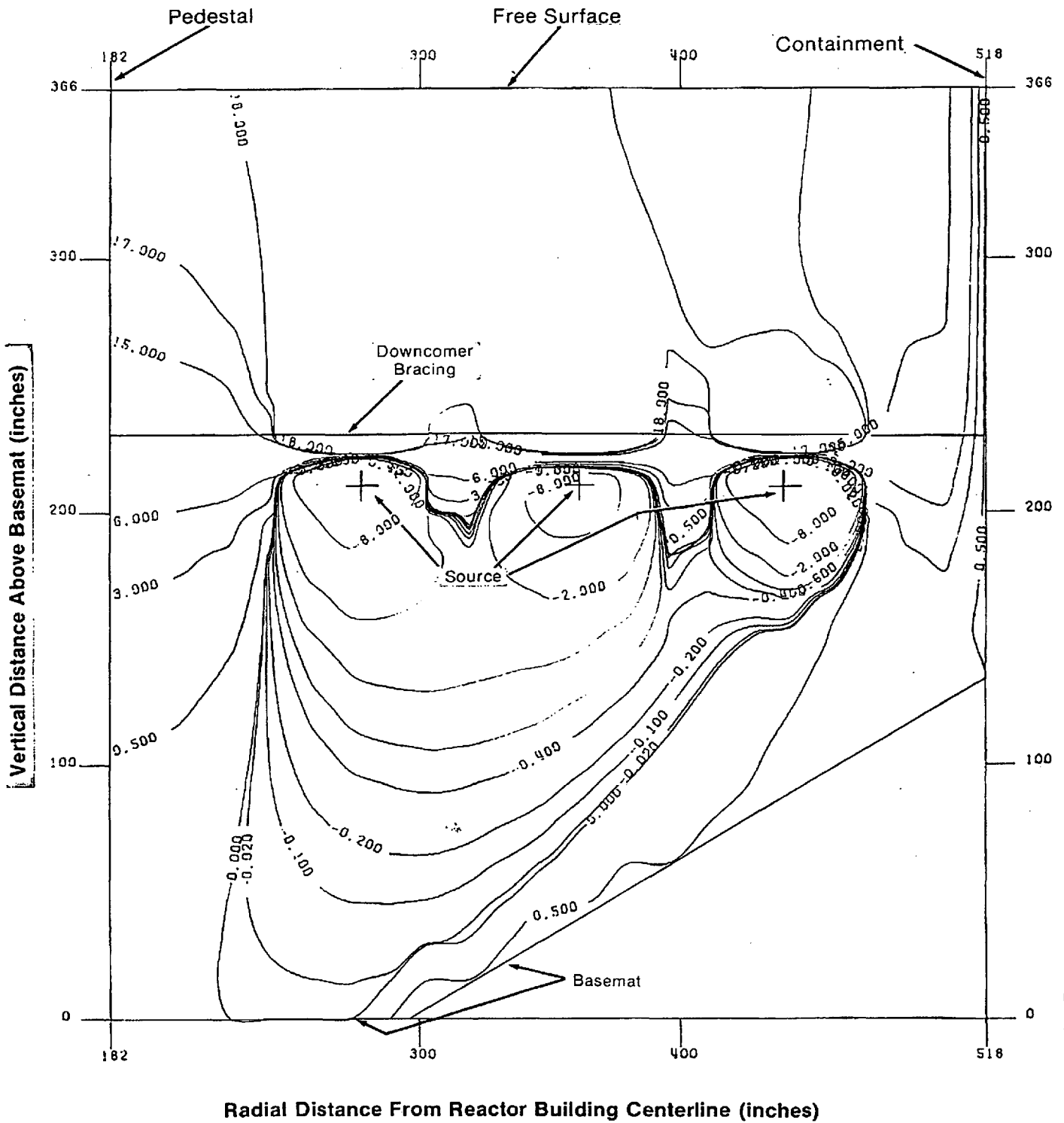
Columbia Generating Station Final Safety Analysis Report	LOCA Bubble Charging Vertical Component of $\nabla\Phi$ in Radial Plane Containing Downcomers		
	Draw. No. 020361.18	Rev.	Figure 3A.3.2-6

Form No. 960690
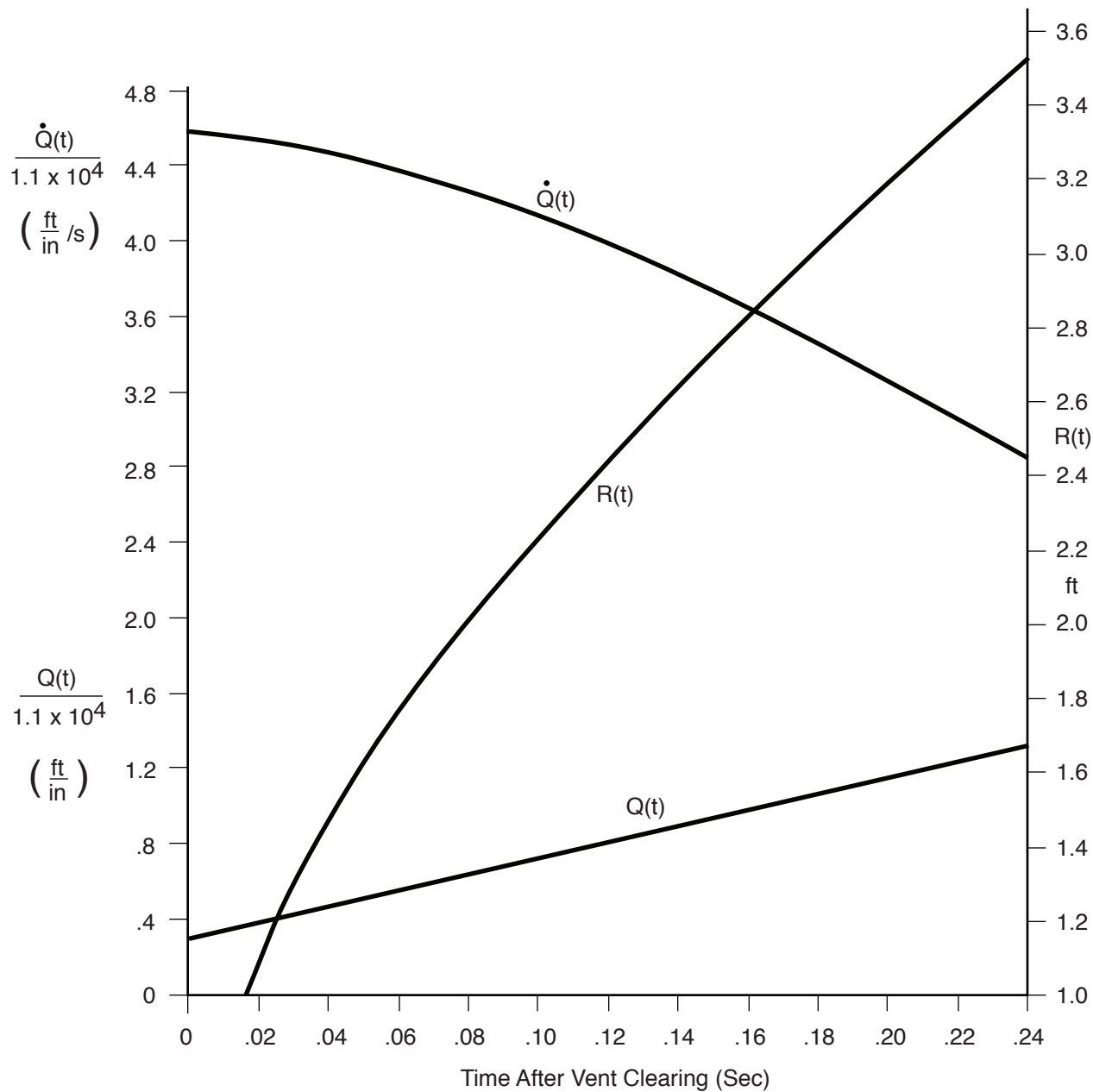
LOCA Bubble Radius and Source Strength Time Histories by PSAM Method

Columbia Generating Station
Final Safety Analysis Report

Draw. No. 950021.79	Rev.	Figure 3A.3.2-7
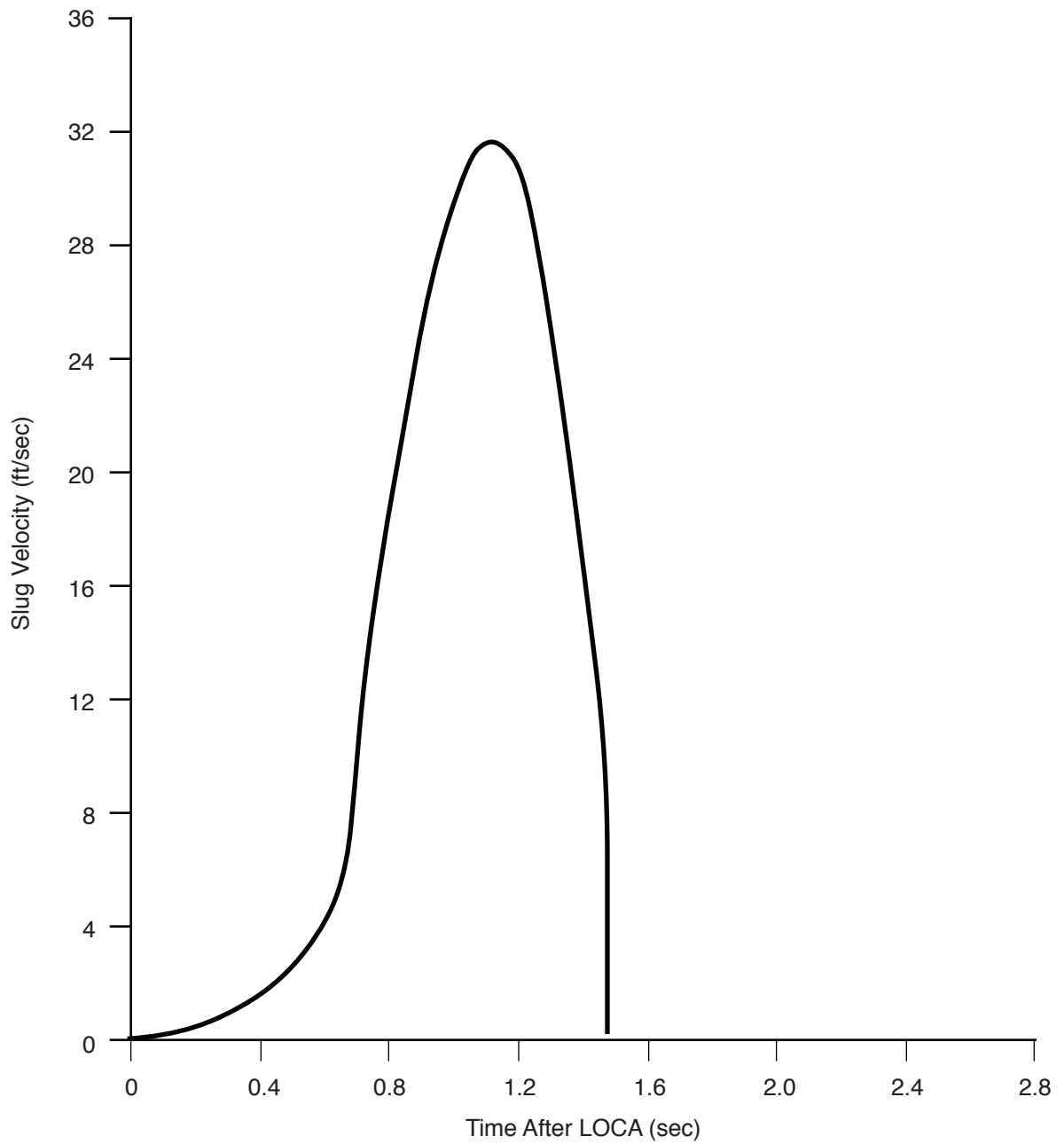
Form No. 960690

Slug Velocity (ft/sec)

Time After LOCA (sec)

Columbia Generating Station Final Safety Analysis Report	Pool Swell Water Slug Velocity Versus Time
	Draw. No. **950021.80** Rev. Figure **3A.3.2-8**

Form No. 960690

200 —

160 —

120 —

80 —

40 —

0 —

-40 —

-80 —

-120 —

-160 —

Slug Acceleration (Ft/Sec^2)

0   0.4   0.8   1.2   1.6   2.0   2.4   2.8

Time After LOCA (Sec)
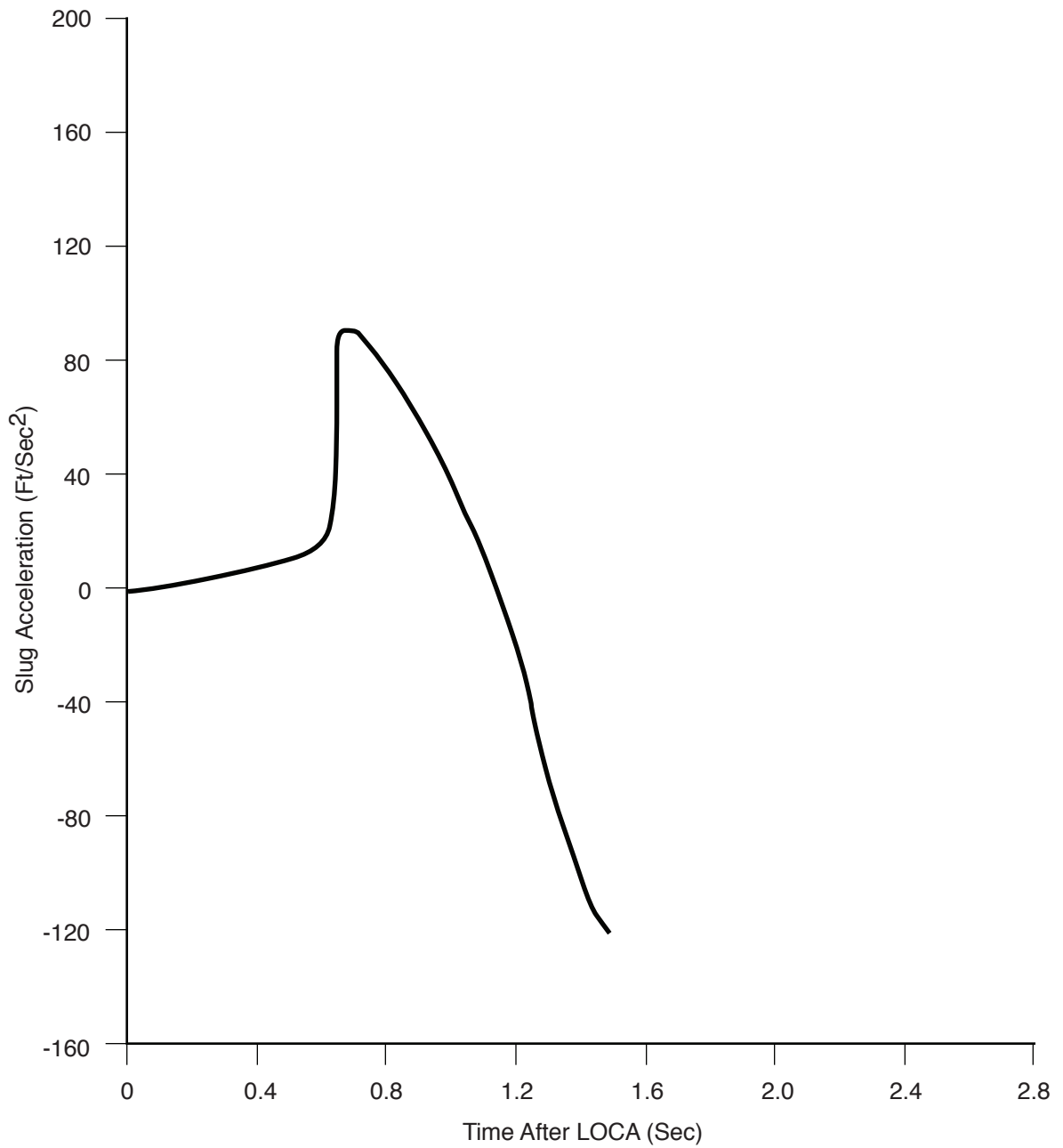
Columbia Generating Station
Final Safety Analysis Report

Pool Swell Water Slug Acceleration Versus Time

Draw. No. **950021.81** | Rev. | Figure **3A.3.2-9**
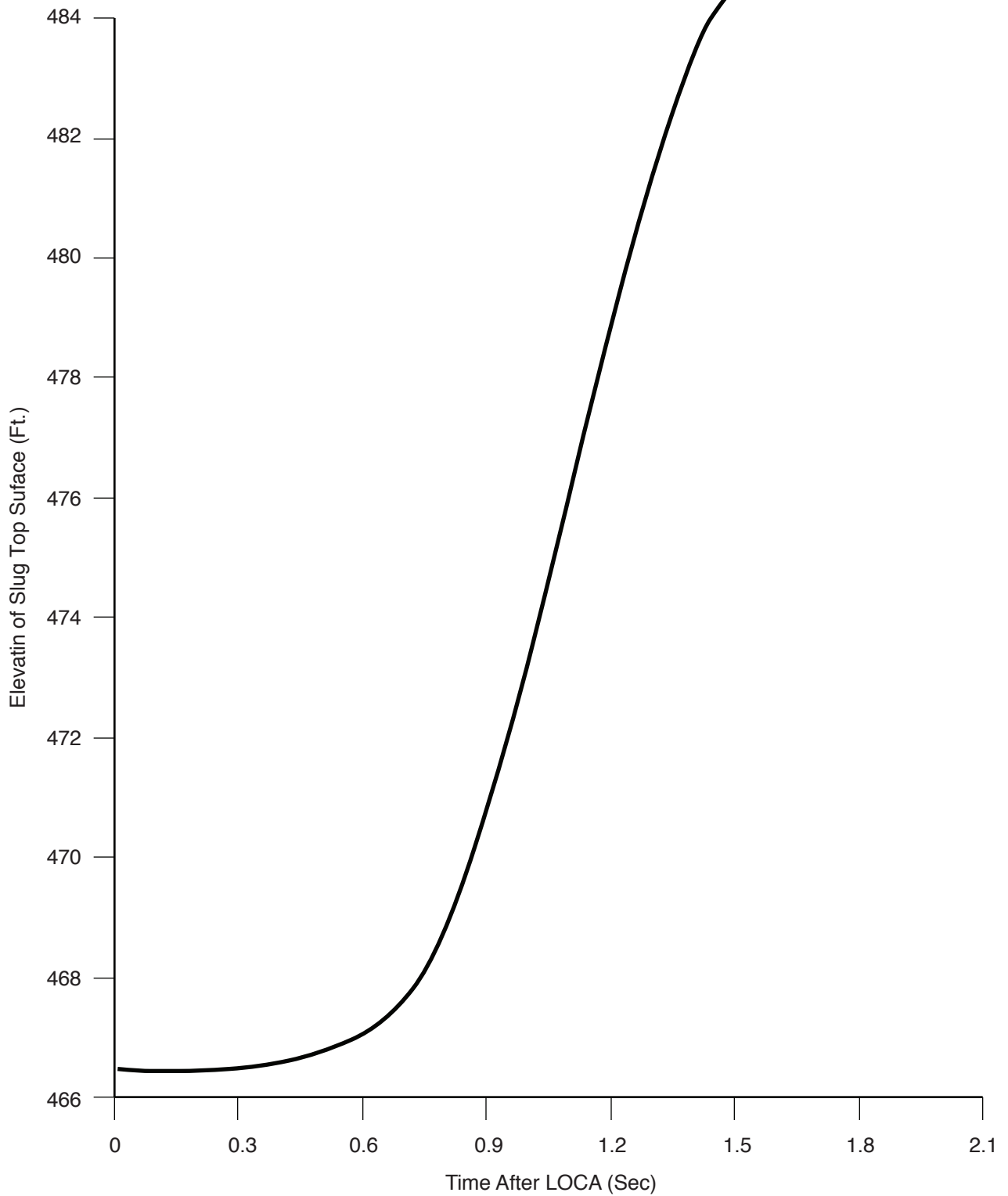
Pool Swell Water Slug Elevation
(Top Surface) Versus Time

Columbia Generating Station **Final Safety Analysis Report**	**Pool Swell Water Slug Elevation** **(Top Surface) Versus Time**

Draw. No. 950021.82	Rev.	Figure 3A.3.2-10

Pressure (psia)

Time After LOCA (sec)
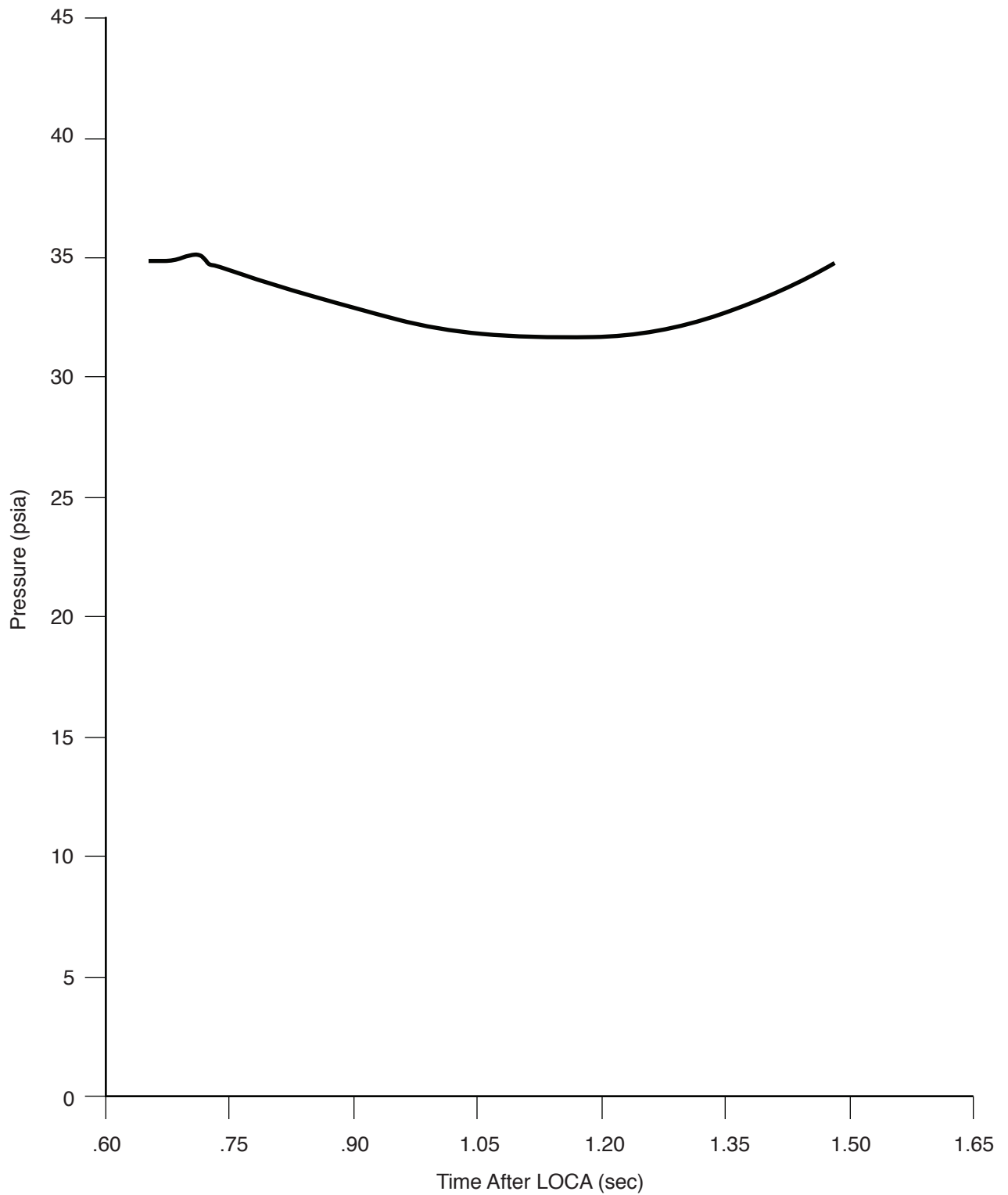
Columbia Generating Station Final Safety Analysis Report	Pool Swell Air Bubble Pressure Versus Time

| Draw. No. 950021.83 | Rev. | Figure 3A.3.2-11 |

Form No. 960690

Pressure (psia)

Time After LOCA (Sec)
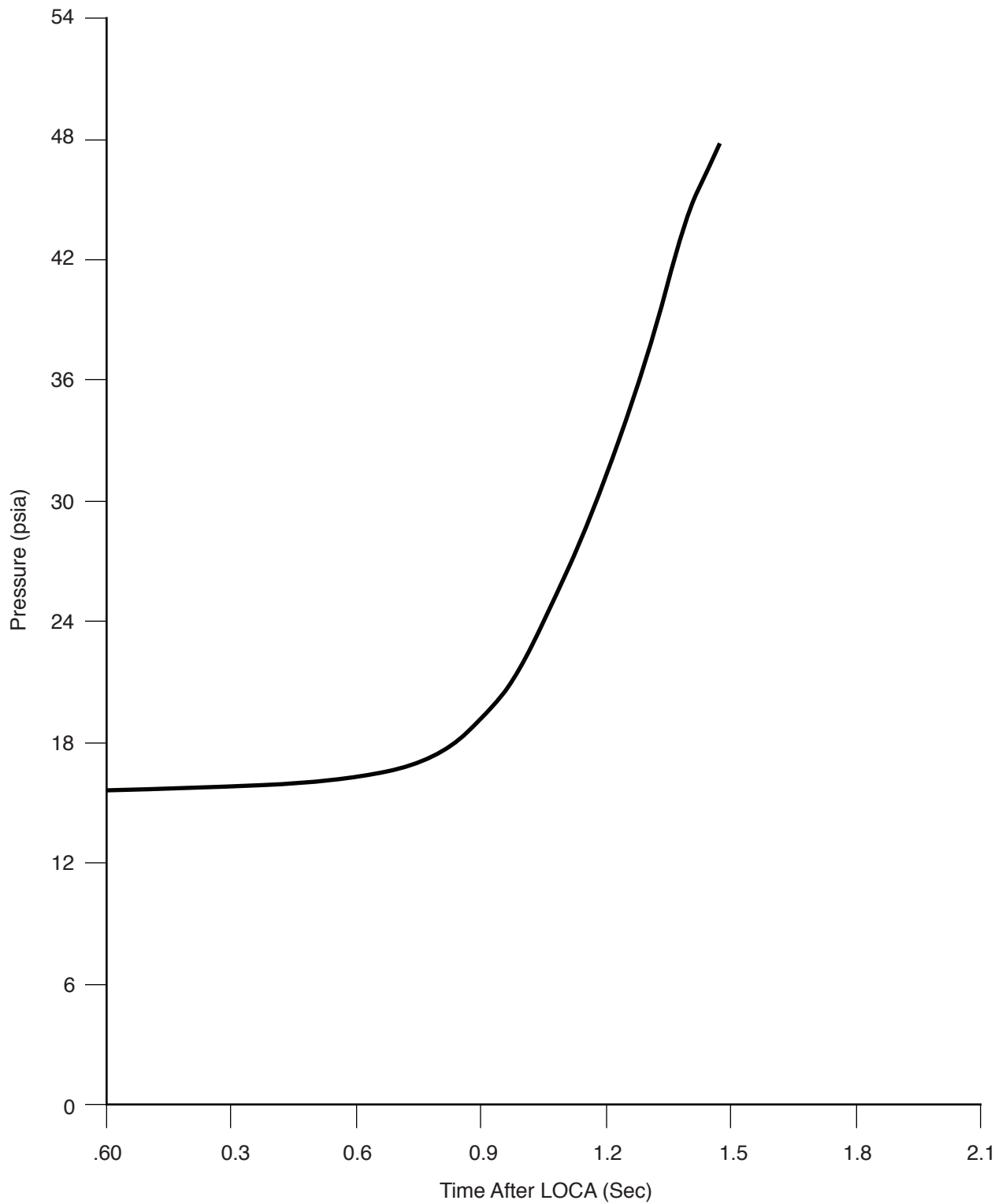
| Columbia Generating Station | **Pool Swell Wetwell Air Pressure Versus Time** |
| **Final Safety Analysis Report** | |

| **Draw. No.** 950021.84 | **Rev.** | **Figure** 3A.3.2-12 |
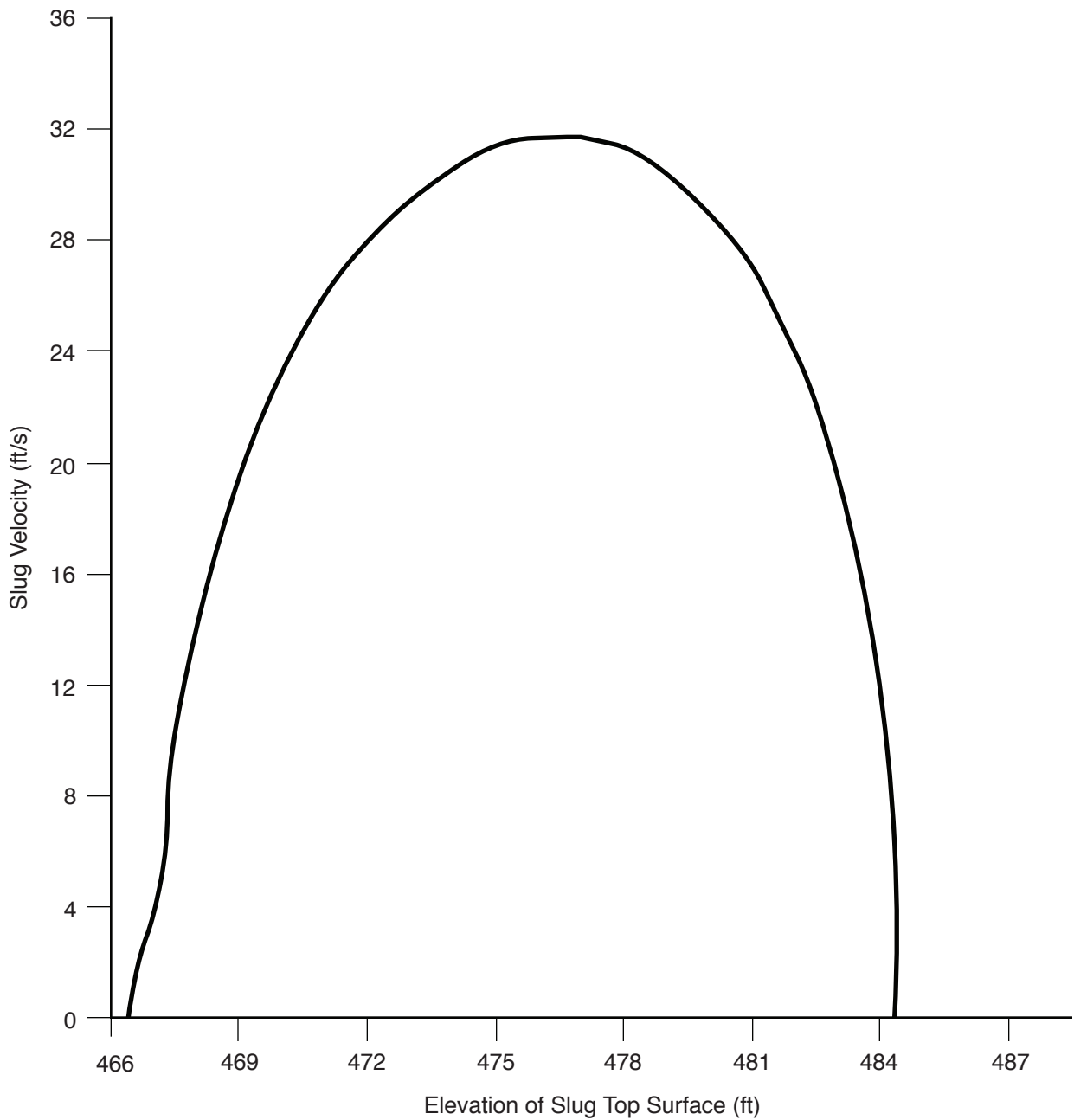
Form No. 960690

Slug Velocity (ft/s)

Elevation of Slug Top Surface (ft)

Columbia Generating Station Final Safety Analysis Report	Pool Swell Water Slug Velocity Versus Elevation of Slug Top Surface
	Draw. No. **950021.85** Rev. Figure **3A.3.2-13**

Form No. 960690

Fallback Water Slug Velocity (Ft/Sec)

40

35

30

25

20

15

10

5

0

El. 484' - 4 3/4"

El. 466' - 4 3/4"

Elevation of Water
Slug Top Surface (Ft)
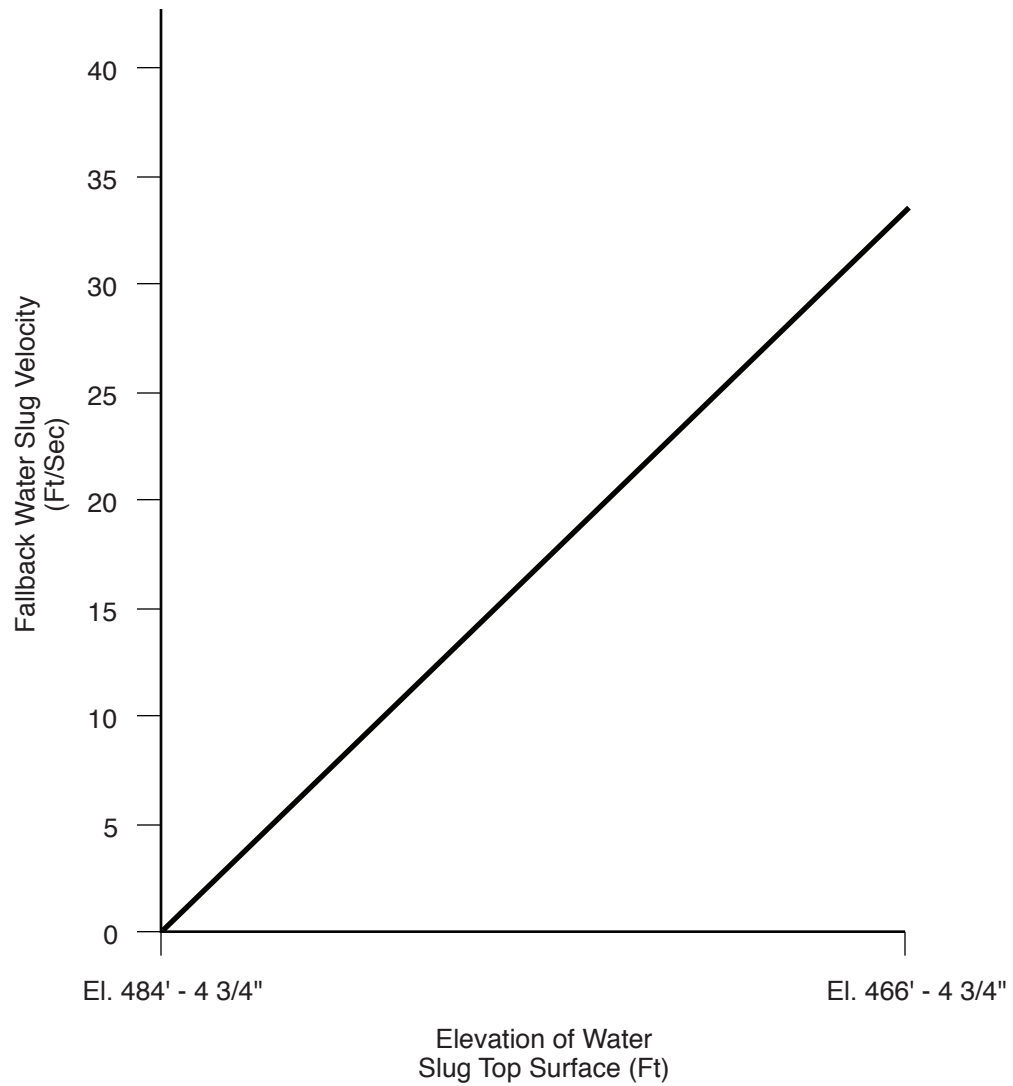
Columbia Generating Station Final Safety Analysis Report	Fallback Water Slug Velocity Versus Elevation of Water Slug Top Surface
	Draw. No. **950021.86** Rev. Figure **3A.3.2-14**

Form No. 960690

D

C

Event

B

A

| 0 | 0.5 | 1.0 | 1.5 | 2.0 |

Time After Break (Sec)
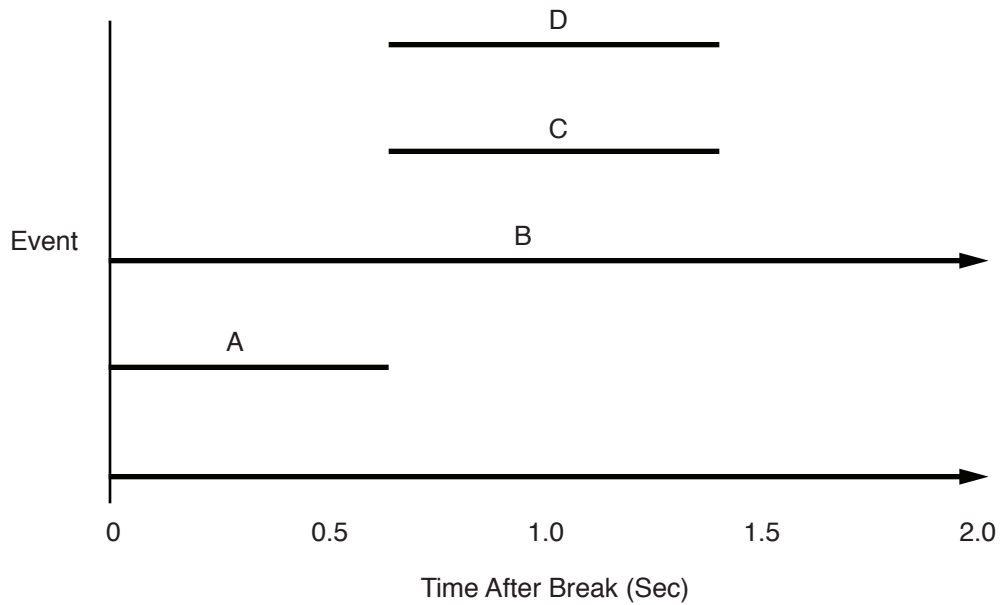
Event   Loading Phenomenon

A   Submerged Boundary Loads During Vent Clearing

B   Drywell Pressurization

C   Loads on Submerged Boundaries During Pool Swell

D   Wetwell Air Compression
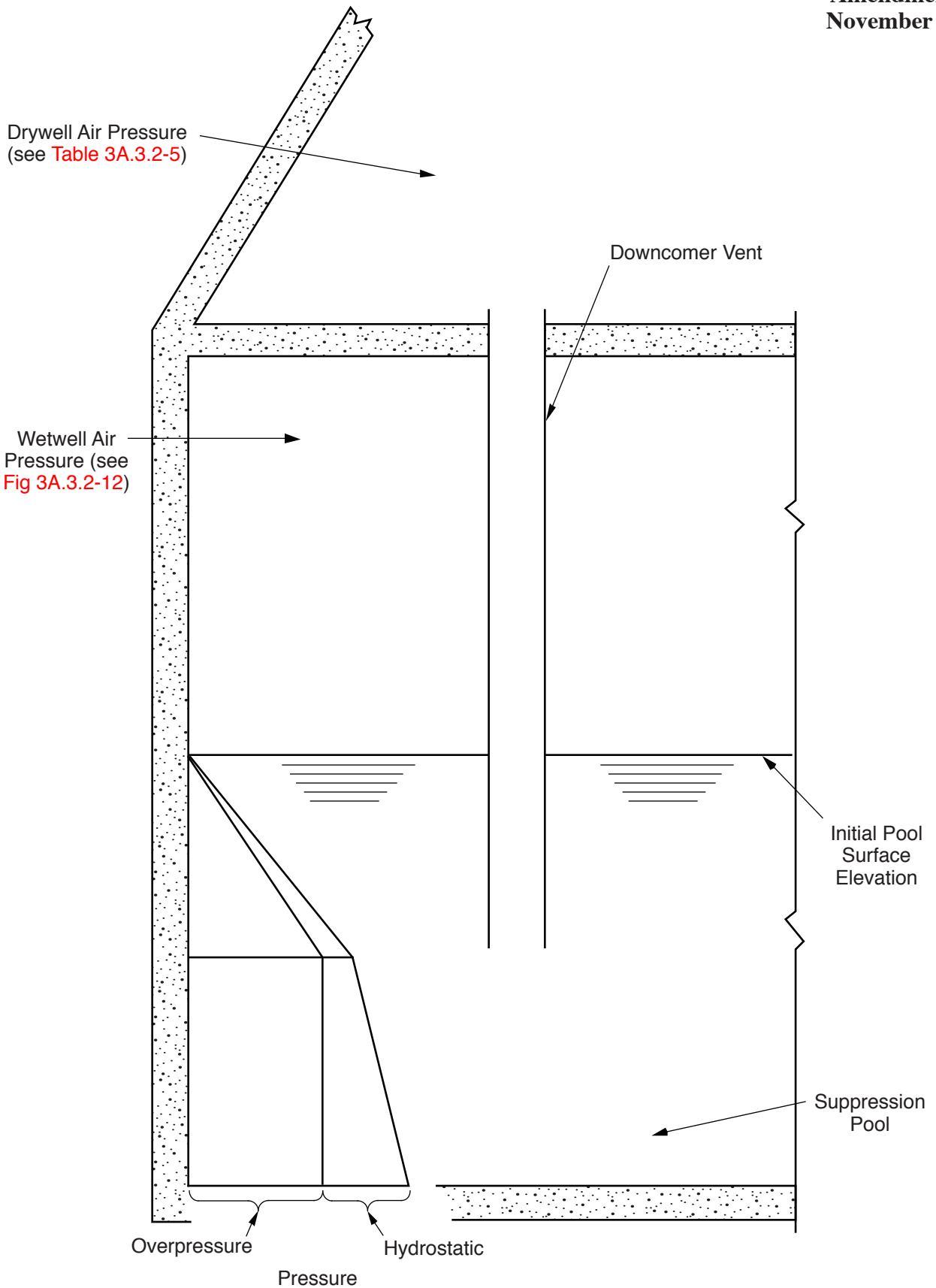
	LOCA Boundary Load Duration		
Columbia Generating Station **Final Safety Analysis Report**			
	Draw. No. **950021.87**	Rev.	Figure **3A.3.2-15**

Drywell Air Pressure
(see Table 3A.3.2-5)

Downcomer Vent

Wetwell Air
Pressure (see
Fig 3A.3.2-12)

Initial Pool
Surface
Elevation

Suppression
Pool

Overpressure

Hydrostatic

Pressure

Columbia Generating Station Final Safety Analysis Report	LOCA Boundary Load Distribution During Vent Clearing

| | Draw. No. 950021.88 | Rev. | Figure 3A.3.2-16 |
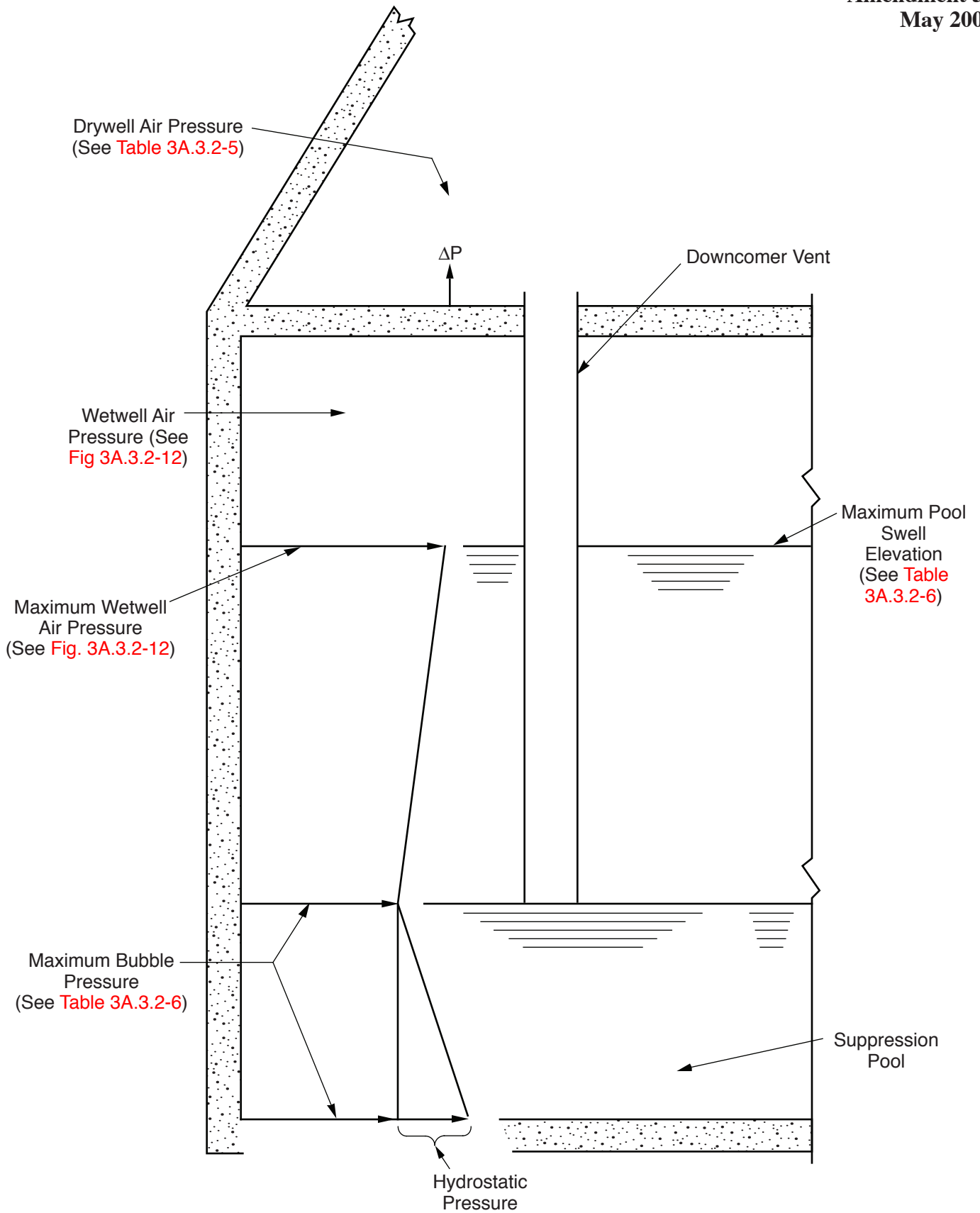
Form No. 960690

Drywell Air Pressure
(See Table 3A.3.2-5)

ΔP

Downcomer Vent

Wetwell Air
Pressure (See
Fig 3A.3.2-12)

Maximum Pool
Swell
Elevation
(See Table
3A.3.2-6)

Maximum Wetwell
Air Pressure
(See Fig. 3A.3.2-12)

Maximum Bubble
Pressure
(See Table 3A.3.2-6)

Suppression
Pool

Hydrostatic
Pressure

Columbia Generating Station Final Safety Analysis Report	LOCA Boundary Load Distribution During Pool Swell		
	Draw. No. 950021.89	**Rev.**	**Figure** 3A.3.2-17
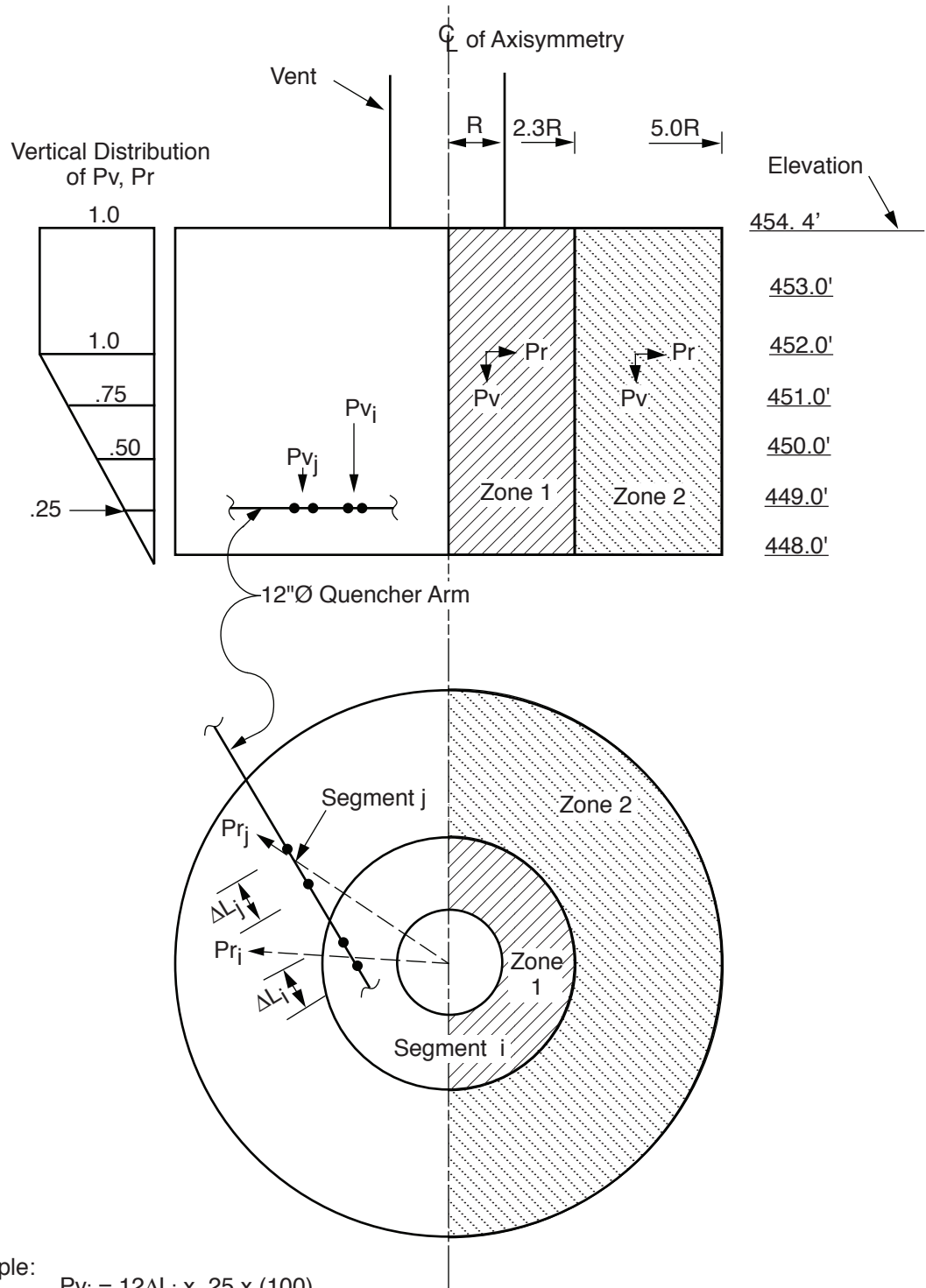
Example:

$$Pv_i = 12\Delta L_i \times .25 \times (100)$$
$$Pr_i = 12\Delta L_i \times .25 \times (\pm 60)$$
$$Pv_j = 12\Delta L_j \times .25 \times (-25)$$
$$Pr_j = 12\Delta L_j \times .25 \times (6)$$

Columbia Generating Station **Final Safety Analysis Report**	**Distribution of Short Term LOCA Loads on Structures Below El. 454.4 ft**		
	Draw. No. 950021.90	Rev.	Figure 3A.3.2-18

Water Level ▽   El. 466.4'

C L

12" Ø SRV Line

Containment Vessel →

Vent

C L

R

2.4R

Downcommer
Bracing Truss

Downcomer
Vent Exit
El. 454.4'

.6 psi/in.

.4 psi/in.

4R

Piping System 24"Ø
Entering Containment
at El. 452'

1.0 psi/in.

.6 psi/in.

4R

.8
psi/in.

A
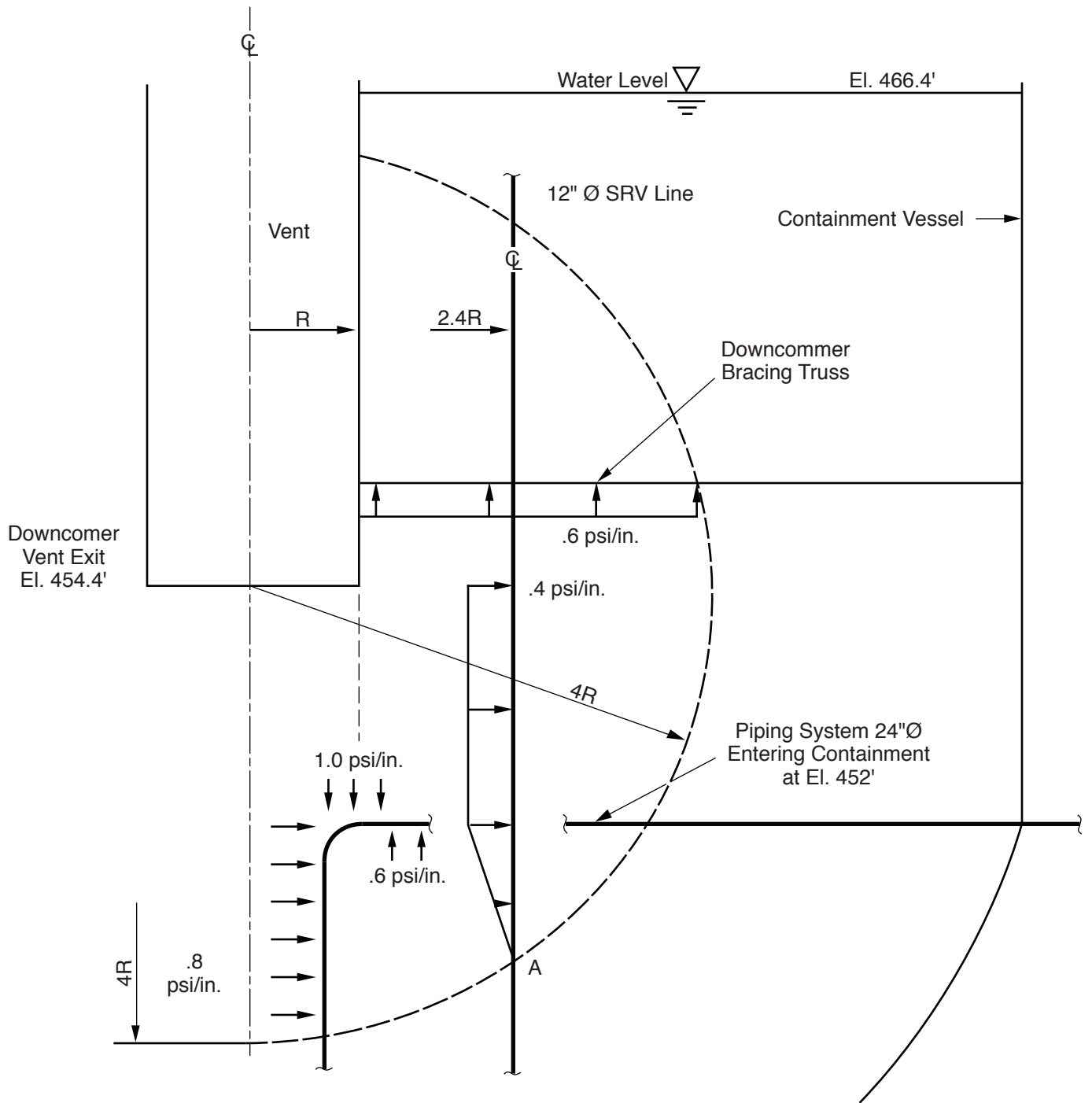
**Pressure Gradients Across Submerged Structures
Due to Chugging**

**Columbia Generating Station
Final Safety Analysis Report**

| Draw. No. 950021.91 | Rev. | Figure 3A.3.2-19 |
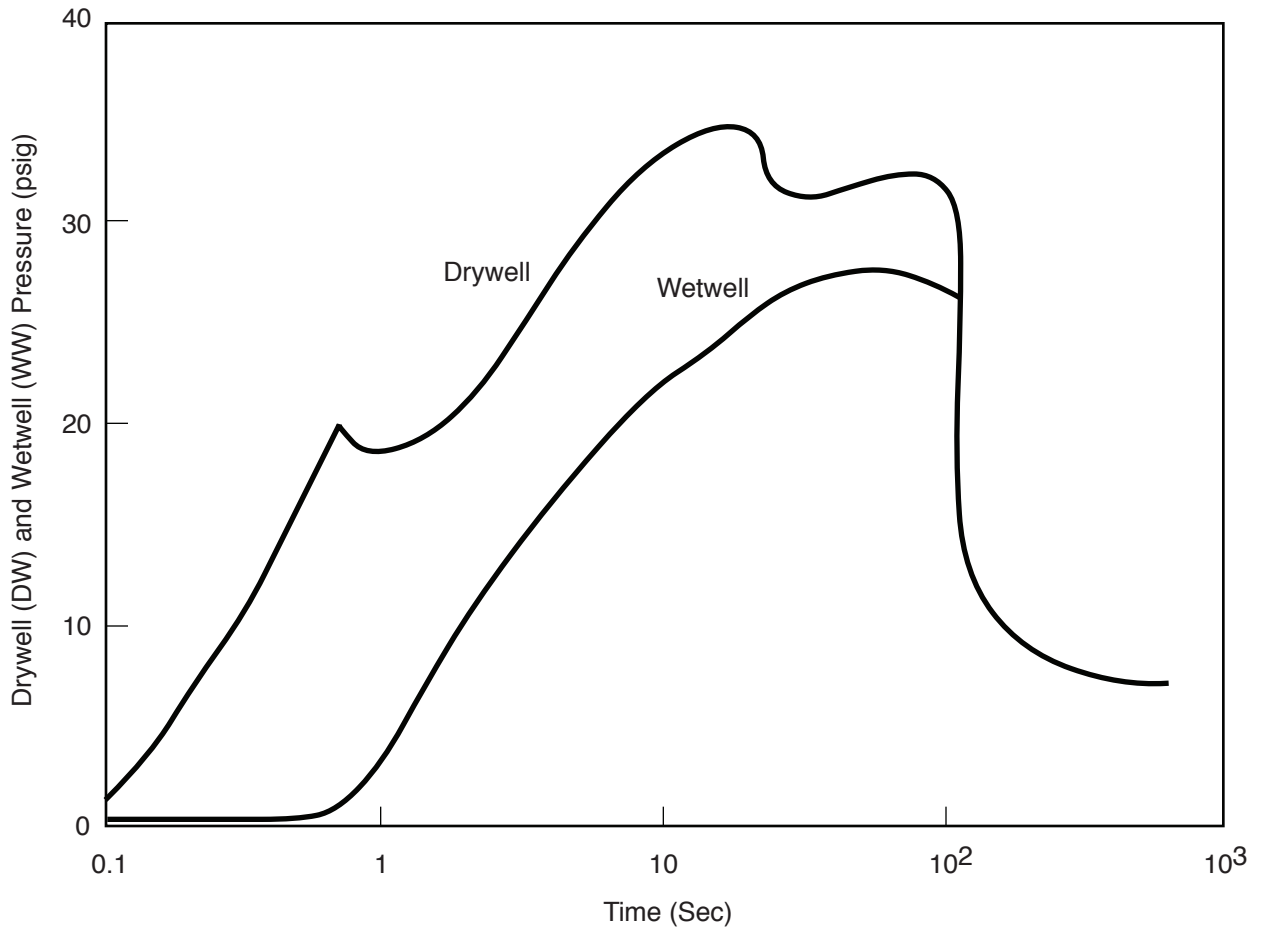
40

Drywell (DW) and Wetwell (WW) Pressure (psig)

30

20

10

0

Drywell

Wetwell

0.1   1   10 10^2 10^3

Time (Sec)

Columbia Generating Station **Final Safety Analysis Report**	**Large Recirculation Line Break - Pressure** **Response - Minimum ECCS**		
	Draw. No. 950021.92	Rev.	Figure 3A.3.2-20

a) 3 LPCI, 1 HPCS, 1 LPCS, 2 HX, KHX = 578
b) 1 LPCI, 1 HPCS,1 HX, KHX = 289
b) 1 LPCI, 1 HPCS,1 HX, KHX = 289, No Containment Spray

Containment Pressure (psig)

Time (Sec)

Columbia Generating Station Final Safety Analysis Report	Containment Pressure Response for Large Recirculation Line Break - Cases A, B, and C		
	Draw. No. 950021.93	**Rev.**	**Figure 3A.3.2-21**

Columbia Generating Station
Final Safety Analysis Report

Large Recirculation Line Break -
Temperature Response

| Draw. No. 950021.94 | Rev. | Figure 3A.3.2-22 |

Form No. 960690

a) 3 LPCI, 1 HPCS, 1 LPCS, 2 HX, KHX = 578
b) 1 LPCI, 1 HPCS,1 HX, KHX = 289
c) 1 LPCI, 1 HPCS,1 HX, KHX = 289, No Containment Spray

Drywell Temperature (°F)

Time (sec)

Columbia Generating Station Final Safety Analysis Report	Drywell Temperature Response for Large Recirculation Line Break - Cases A, B, and C

Draw. No. 950021.95	Rev.	Figure 3A.3.2-23

a) 2 HX, 3 LPCI, 1 HPCS, 1 LPCS, KHX = 589 W/Spray
b) 1 HX, 1 LPCI, 1 HPCS, KHX = 289, W/Spray
c) 1 HX, 1 LPCI, 1 HPCS, KHX = 289, No Containment Spray

Suppression Pool Temperature (°F)

Time (sec)

Columbia Generating Station Final Safety Analysis Report	Suppression Pool Temperature Response for Large Recirculation Line Break - Long Term Response
	Draw. No. 950021.96 **Rev.** **Figure 3A.3.2-24**
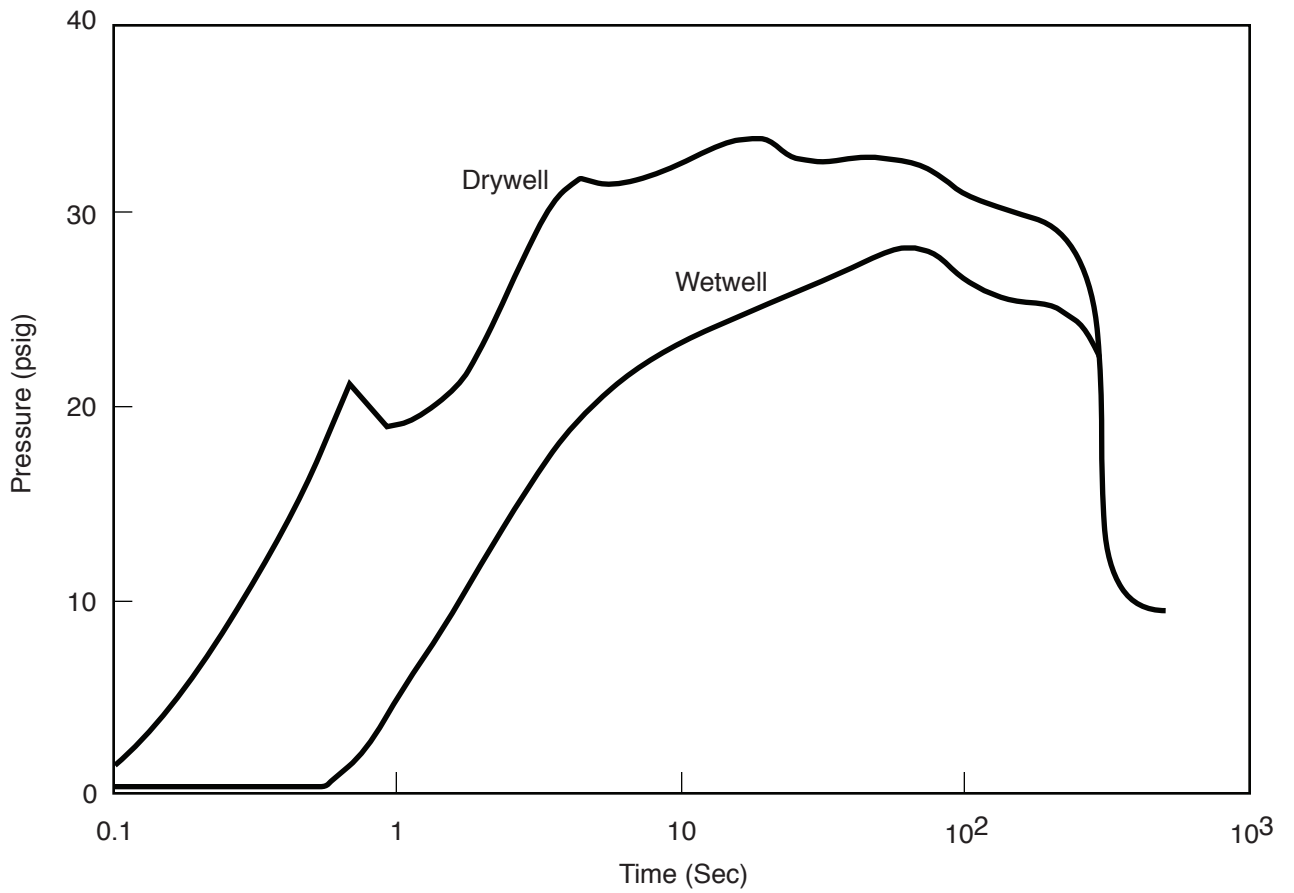
Pressure Response
Main Steam Line Break

Columbia Generating Station Final Safety Analysis Report	Pressure Response Main Steam Line Break		
	Draw. No. 950021.97	Rev.	Figure 3A.3.2-25

Form No. 960690

Temperature Response -
Main Steam Line Break -
Minimum ECCS

Columbia Generating Station
Final Safety Analysis Report

Draw. No. 950021.98	Rev.	Figure 3A.3.2-26

Form No. 960690

Temperature Response -
Recirculation Line Break (0.1 ft^2)
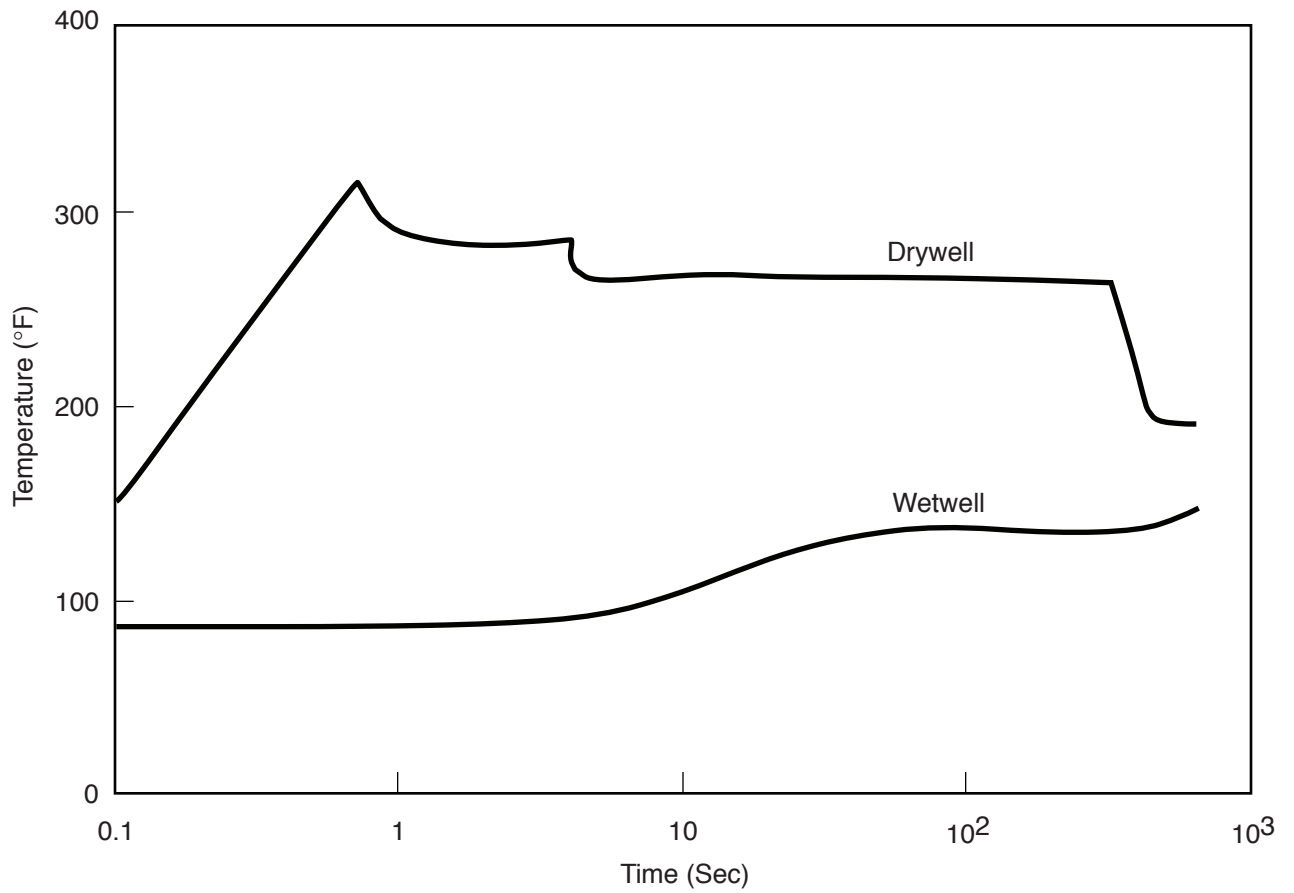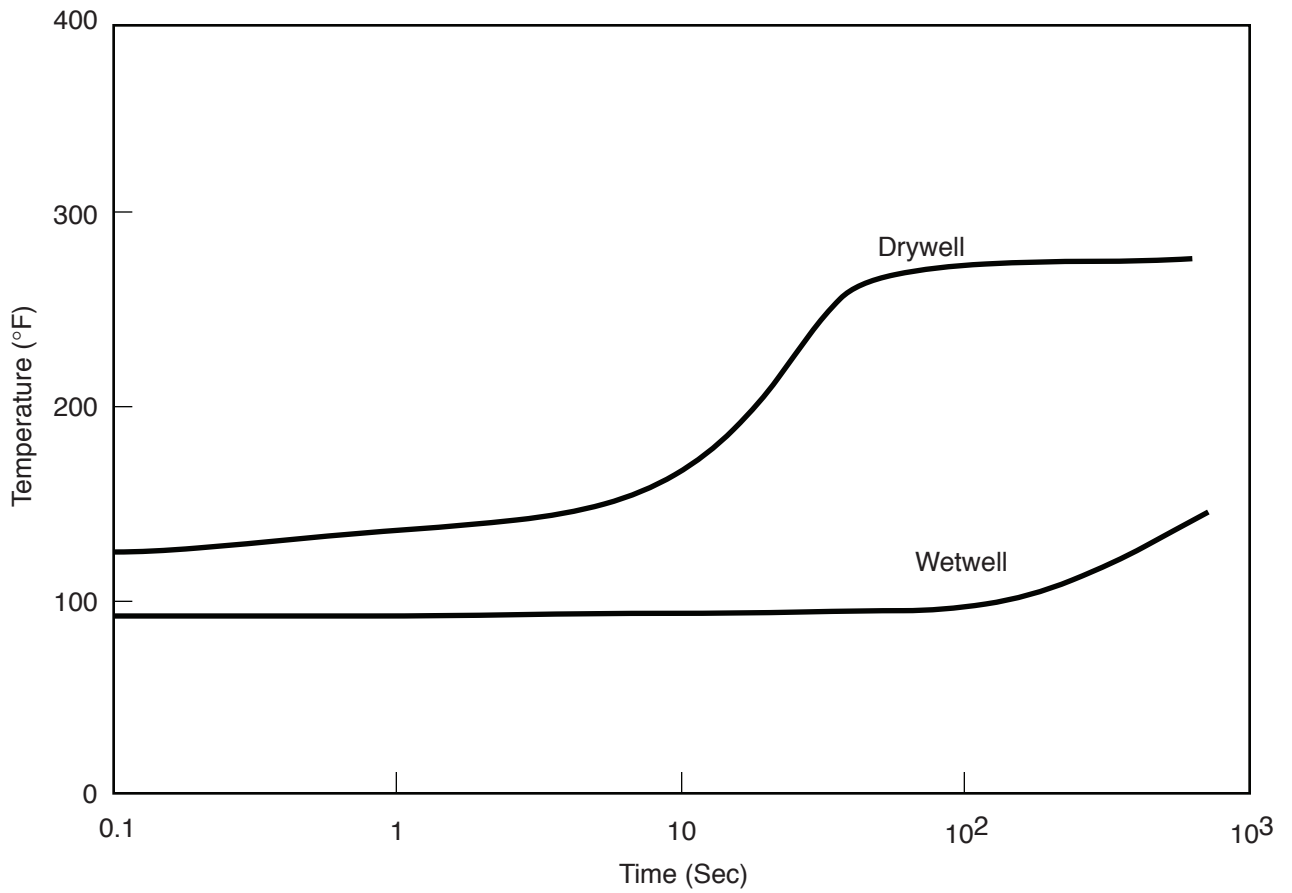
Columbia Generating Station Final Safety Analysis Report	Temperature Response - Recirculation Line Break (0.1 ft^2)		
	Draw. No. 950021.99	Rev.	Figure 3A.3.2-27

Pressure (psig)

Drywell

Wetwell

40

30

20

10

0

0.1   1   10 10^2 10^3

Time (Sec)
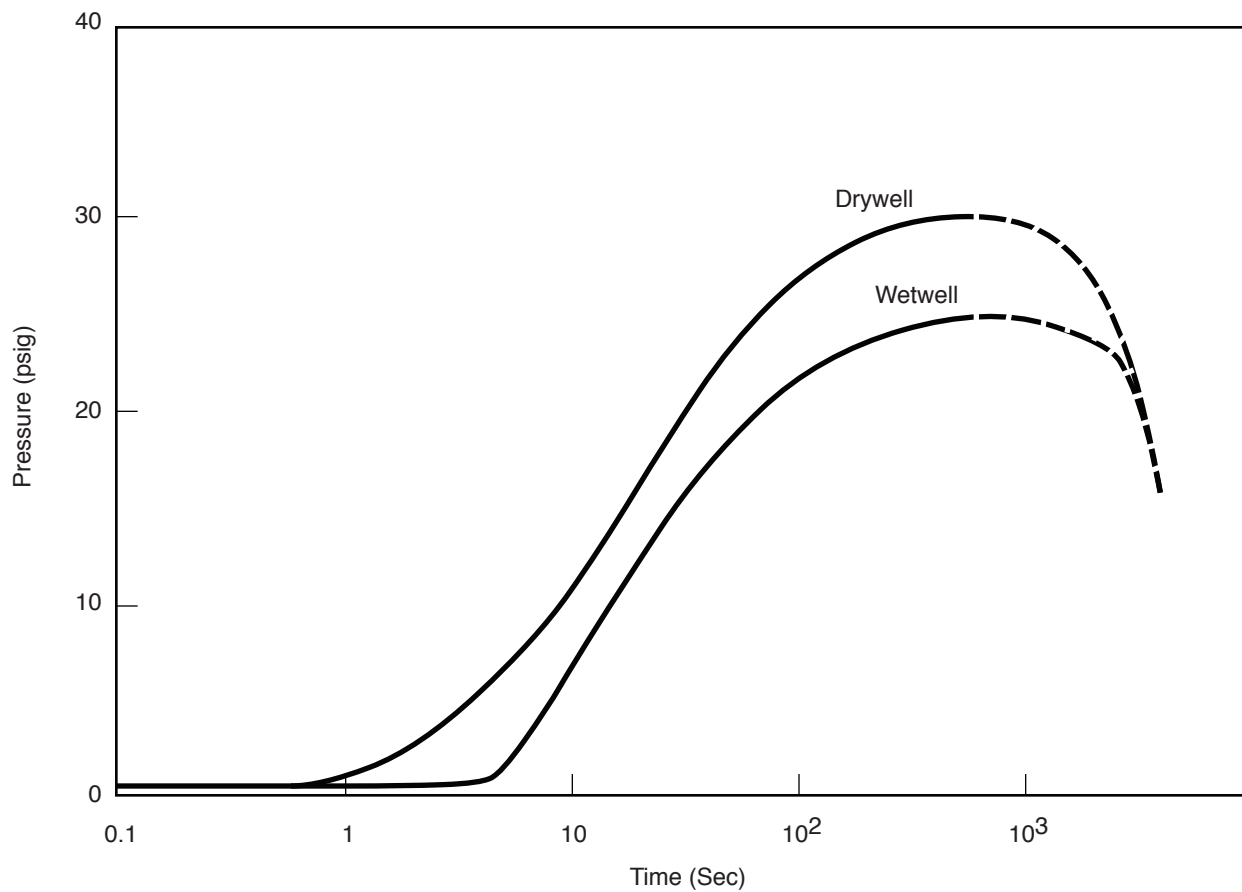
Columbia Generating Station Final Safety Analysis Report	Pressure Response - Recirculation Line Break (0.1 ft²)		
	Draw. No. 960222.84	Rev.	Figure 3A.3.2-28

3A.3.3   LOAD SUMMARY

A load summary is given in Table 3A.3.3-1 to provide guidance in identifying loads and to provide references to more detailed discussions of them. The table lists the loads being evaluated and the peak load magnitude directly applied to each structure, or a reference to the DAR sections where the information is derived. It also lists the classification of the load as primary or secondary as defined by NRC.

Table 3A.3.3-1[a]

Summary of Hydrodynamic Loads on Wetwell Structures

Load Category	Stl. Contain-ment	Vert. and Horiz. Tees (6)	Base-mat	Pedestal	Dia. Floor	Dia. Floor Seal	Down-comer Bracing	Column	Down-comer	SRV Piping System	Quencher	Plat-forms and Ladder	Fully Sub. (3)	Part. Sub.	In Pool Swell Zone (3)	DAR Ref. Sec.	Load Class
SRV																	
Water Clearing	sm	sm	sm	sm	N/A	N/A	sm	sm	sm	sm	sm	N/A	sm	sm	N/A	3.1.2.1	Sec.
Air Clearing	151	151	151	151	N/A	N/A	3.1.3.2	3.1.3.2	3.1.3.2	3.1.3.2	3.1.3.2	N/A	3.1.3.2	3.1.3.2	N/A	3.1.3	Prim.
Steam Cond.	sm	sm	sm	sm	N/A	N/A	sm	sm	sm	sm	sm	N/A	sm	sm	N/A	3.1.3.2	Sec.
LOCA																	
Vent Water Clearing	24	24	24	sm	N/A	N/A	sm	3.2.3.3	sm	3.2.3.3	3.2.3.3	N/A	3.2.3.3	sm	N/A	3.2.3	Prim.
Air Bubble Charging	21[b]	21[b]	21[b]	sm	N/A	N/A											

[a] Conformance to NRC acceptance criteria for each load in this table is presented in Attachment 3A.H.
[b] Values are in psig.

Notes:
1. Peak dynamic pressure.
2. Unless identified as dynamic pressure, the numerical value given is equivalent static peak pressure (i.e., includes a DLF).
3. All fully-submerged piping systems enter the pool below vent exit.
4. sm denotes load as small, not requiring consideration.
5. Between elevations 466 ft-4.75 in. and 484 ft-4.75 in.
6. LOCA induced vent, thrust loads are neglected as secondary loads (see Reference 3A.3.2-1).

3A.3.4   SEQUENCE OF DYNAMIC LOADS

The effects of various dynamic loads on structures are analyzed separately. It is important to establish the relative time sequence of all dynamic events to obtain a realistic assessment of design margins. The DFFR (Reference 3A.3.2-2) established relative sequence of dynamic loads during a single SRV discharge event and a postulated LOCA. It is noted that during an SRV actuation the water clearing loads, the air clearing loads, and the steam condensation loads occur in a sequence and the peak dynamic effects due to each need not be combined. Similarly, the LOCA water clearing, air clearing (bubble charging), pool swell impact, pool swell drag, pool fallback, and the high, intermediate, and low mass flux steam condensation occur in a sequence and the peak dynamic effects due to each need not be combined. During pool swell or fallback, drag pressure parallel to the flow and lift pressure normal to the flow occur simultaneously, and the two loads are combined. Also, for some submerged structures, pool swell impact occurs at the upper parts of the structure while pool swell drag and lift loads act on the lower parts of the structure. In this case, the three loads are combined. The continuity of short-term water and air clearing phases during an SRV discharge or during a LOCA and the pool swell impact and drag loads during a DBA LOCA is recognized either by specifying a conservative DLF for use with peak load value of the combined time history or by use of the combined time history in the dynamic analysis in assessing the structures.

The DFFR provides guidance about the SRV actuations occurring during the normal operation of the plant and during the small, intermediate, and large break LOCA. In absence of information about relative time sequence of the three events, the following conservative assumptions for submerged structures are made in combining the effects due to these events in this assessment:

a.   Short-term LOCA and SRV loads

For structures submerged in the pool, the direct hydrodynamic loads due to the LOCA jet, LOCA bubble, pool swell, and fallback are not combined with the direct hydrodynamic loads due to the SRV water jet or air bubbles. The presence in the pool of air bubbles from the SRV line is assumed to have negligible effect on short-term pool dynamics during a LOCA. The seismic effects are combined with the short-term LOCA load effects; and

b.   Long-term LOCA and SRV loads

For all miscellaneous submerged piping systems and major structures (columns, downcomer bracing, downcomers and SRV line with quencher) the worst case LOCA steam condensation loads are combined with seismic effects and with a single adjacent SRV actuation load or with the actuation of ADS valves.

3A.3.5   LOAD COMBINATIONS AND ACCEPTANCE CRITERIA

Load combinations and acceptance criteria for events which include suppression pool hydrodynamic loads are described in this section. Four categories of structural components affected by these events are identified and the applicable load combinations and acceptance for each category are listed. These structural categories are the steel containment structure (suppression chamber portion), reinforced concrete structures, steel structures, and piping and piping systems. Symbols representing generic load types are used in the load combinations; these symbols are defined below.

3A.3.5.1   <u>Steel Containment Structure</u>

3A.3.5.1.1   Definitions

D Dead loads

L Live loads

E_O Loads generated by operating basis earthquake

E_{SS} Loads generated by safe shutdown earthquake

H Loads associated with pool swell phenomenon following L the clearing of the downcomer vents including fallback

P Containment pressure associated with the large break A (DBA) LOCA

P_B Containment pressure associated with IBA or SBA

P Loads associated with chugging phenomena

P_E Design external pressure on the containment

P_O Normal operating pressure

P_{SR} Loads associated with main steam SRV actuation

P_V LOCA related hydrodynamic loads on suppression chamber, including H_L, P_c

R_A Pipe reactions under thermal conditions generated by the postulated accidents and including R_o

R_E Pipe reactions under thermal conditions during event causing external pressure

R_O Pipe reactions during startup, normal operating or shutdown conditions, based on the most critical transient or steady-state condition

R_R Reaction and jet forces associated with the pipe break

T_A Thermal loads under thermal conditions associated with LOCA

T_E Thermal loads under thermal conditions during event causing external pressure

T_O Thermal effects and loads during normal operation

3A.3.5.1.2   Load Combinations

The following load combinations for the CGS steel containment are in agreement with those specified in the NRC Standard Review Plan, 3.8.2, Revision 0, and properly include the new SRV and LOCA hydrodynamic loads.

(1) $D + L + P_O + T_O + R_O + P_{SR}$

(2) $D + L + E_O + P_O + T_O + R_O + P_{SR}$

(3) $D + L + E_O + T_A + R_A + (P_A \text{ or } P_B) + P_V + P_{SR}$

(4) $D + L + E_O + T_E + R_E + P_E + P_{SR}$

(5) $D + L + E_{ss} + P_O + T_O + R_O + P_{SR}$

(6) $D + L + E_{ss} + T_A + R_A + (P_A \text{ or } P_B) + P_V + P_{SR}$

(7) $D + L + E_{ss} + T_E + R_E + P_E + P_{SR}$

Notes:

1.   In all combinations the hydrostatic pressure due to the presence of water in the pressure-suppression chamber pool is considered with dead and live loads.

2.   Restraint due to the presence of filler material between the containment vessel and the biological shield wall (equivalent to an external pressure of 2 psi) is considered where critical.

3.   For independent, short duration, vibratory loads such as seismic, SRV discharge, chugging loads, the peak dynamic responses due to the individual loads are combined by the square-root-of-sum-of-the-squares (SRSS) method.

4.   For time relationship between concurrently applied loads in combinations (3) and (6) see Section 3A.3.4.

5.   In the case of P_{SR} and P_C both the axisymmetric and nonaxisymmetric loading conditions are investigated.

6.   Maximum equivalent static pressures for P_A, P_B, and P_V are given in Table 3A.3.5-1.

The design assessment of the containment vessel is made on the basis of the SRSS method as stated above. However, subsequent investigation indicates that if combination of peak dynamic responses due to seismic, SRV discharge loads, and chugging loads is done by the absolute sum method, the resultant design margins for the containment vessel are greater than 1.0.

3A.3.5.1.3   Acceptance Criteria

The design rules for the steel containment are in accordance with ASME Code Section III, 1971 Edition through the 1972 Summer addenda, Subsection NE, Class MC Components. The acceptance criteria for each load combination are summarized in Table 3A.3.5-2.

3A.3.5.2   Reinforced-Concrete Structures

Structures to which the criteria below apply include the basemat, the RPV pedestal, the columns supporting the diaphragm floor, and the diaphragm floor slab.

3A.3.5.2.1   Definitions

D   Dead loads

E_O Loads generated by operating basis earthquake

E_{SS} Loads generated by safe shutdown earthquake

H_L Hydrodynamic forces associated with pool swell phenomenon following the clearing of the downcomer vents including fallback forces

L   Live loads

P_A All loads associated with the large break (DBA) LOCA including drywell and suppression chamber transient pressure loads and H_L, P_c, and P_{co} as defined herein

P_B All loads associated with IBA or SBA type of LOCA including transient pressure loads and P_c

P_c Loads associated with chugging phenomena during LOCA

P_O Normal operating pressure

P_{SR} Loads associated with main steam SRV actuation

R_A Pipe reactions under thermal conditions generated by the postulated accidents and including R_O

R_O Pipe react ions during startup, normal operating or shutdown conditions, based on the most critical transient or steady-state condition

R_R Reaction and jet forces associated with the pipe break

T_A Thermal loads resulting from thermal conditions generated by postulated accidents and including T_O

T_O Thermal effects and loads during normal operation.

3A.3.5.2.2   Load Combinations

The load combinations for the basemat and for the reinforced concrete structures internal to the containment are listed in Table 3A.3.5-3. The following notes are applicable to Table 3A.3.5-3.

a.   In combinations 4, 4a, 5, 5a, 7, and 7a, the maximum values of P_A, P_B, T_A, R_A, and P_{SR} including a DLF are used unless a dynamic analysis is performed.

b.   Thermal loads may be neglected when it can be shown that they are secondary and self-limiting in nature.

c.   All the loads listed are not necessarily applicable to all the structures.

d.   For independent short duration vibratory loads such as seismic, SRV discharge loads and chugging loads, the peak dynamic responses are combined by the SRSS method. Also, peak responses due to SRV direct pressure loads and due to SRV building motion response spectra are combined by SRSS.

e.   The design assessment of the structures of Section 3A.3.5.2 is made on the basis
of the preceding notes. However, subsequent investigation indicates that if
combination of peak dynamic responses due to seismic, SRV discharge loads
and chugging loads is done by the absolute sum method, the resultant design
margins for the structures of Section 3A.3.5.2 are greater than 1.0.

3A.3.5.2.3   Acceptance Criteria

For all load combinations in Table 3A.3.5-3, the allowable limit on section strength is the
section strength required to resist design loads based on the strength design methods described
in ACI 318-77 (Reference 3A.3.5-1).

3A.3.5.3   Steel Structures

Structures to which the criteria below apply include the downcomer bracing system, the
diaphragm floor beams, and platforms and ladders attached to the containment shell.

3A.3.5.3.1   Definitions

Definitions of load symbols in Table 3A.3.5-4 are the same as those in 3A.3.5.2.1.

3A.3.5.3.2   Load Combinations

The load combinations for steel structures internal to the containment are listed in
Table 3A.3.5-4. Notes a, b, c, and d listed for Table 3A.3.5-3 in 3A.3.5.2.2 are also
applicable to Table 3A.3.5-4.

The design assessment of the structures of 3A.3.5.3 is made on the basis of the preceding
notes. However, subsequent investigation indicates that if combination of peak dynamic
responses due to seismic, SRV discharge loads and chugging loads is done by the absolute sum
method, the resultant design margins for the structures of 3A.3.5.3 are greater than 1.0.

3A.3.5.3.3   Acceptance Criteria

The allowable limits for structural acceptance for the load combinations of Table 3A.3.5-4
using the elastic working stress method are defined as follows.

Combination	Limit
1	S
2,3	1.5S
4,4a,5,5a,6	1.6S
7,7a	1.7S

In the above, S is the required section strength based on the elastic design methods and the allowable stresses defined in Part 1 of the AISC Specification (Reference 3A.3.5-2). The 33% increase in allowable stresses for concrete and steel due to seismic loadings is not permitted.

The allowable limits for structural acceptance for the load combinations of Table 3A.3.5-4 using the plastic design method are defined as follows:

Combination	Limit
1,2,3	Y
4,4a,5,5a,6,7,7a	0.9Y

In the above, Y is the section strength required to resist design loads based on the plastic design methods described in Part 2 of the AISC Specification (Reference 3A.3.5-2).

3A.3.5.4   Piping Systems

3A.3.5.4.1   Definitions

The loads for the piping components are: dead weight, seismic, and loads associated with SRV actuation and LOCA effects. The SRV and LOCA loads have been described in detail in previous sections of this report. A description of the symbols as they appear in the piping and component load combination table (Table 3A.3.5-5) follows:

Load Symbol	Load Description
P	Operating pressure
D.W.	Dead weight
OBE	Loads due to operational basis earthquake
SSE	Loads due to safe shutdown earthquake

SRV   Loads due to sequential pressure setpoint actuation of all (18) SRVs

      a.   SRV bubble loads on submerged piping and components in the suppression pool

      b.   Building motion induced loads.

SBA/IBA   Loads associated with SBA/IBA:

      a.   Chugging/CO loads on submerged structures. (Chugging bounds CO loads.)

      b.   Building motion due to chugging loads. (Chugging bounds CO loads.)

DBA   Loads associated with DBA:

      a.   Water jet

      b.   LOCA bubble

      c.   Pool swell

      d.   Fallback

      e.   Chugging loads on submerged structures. (Chugging bounds CO loads.)

      f.   Building motion induced loads due to CO and chugging. (Chugging bounds CO.)

3A.3.5.4.2   Load Combinations

Load combinations for the loads listed in Section 3A.3.5.4.1 are given in Table 3A.3.5-5. These load combinations are based on Table 6.1 of the DFFR (Reference 3A.3.2-11) and modified conservatively. For independent short duration vibratory loads such as seismic, SRV discharge loads, and chugging loads, the peak dynamic responses are combined by the SRSS method as described in the DFFR. The time relationship for the loads are described in Section 3A.3.4.

3A.3.5.4.3   Acceptance Criteria

Piping and components are designed for normal, upset, emergency, and faulted plant conditions, as delineated in the Load Combination Table using the stress values for the respective normal, upset, emergency, and faulted limits as defined in the appropriate subsection of the ASME Boiler and Pressure Vessel Code (Reference 3A.3.5-3).

3A.3.5.5   <u>References</u>

3A.3.5-1   "Building Code Requirements for Reinforced Concrete," ACI 318-71/77.

3A.3.5-2   "Specification for the Design, Fabrication, and Erection of Structural Steel for Buildings," American Institute of Steel Construction, February 12, 1969/ November 11, 1978.

3A.3.5-3   ASME Boiler and Pressure Vessel Code, Section III, Division 1, Subsection NC "Class 2 Components," American Society of Mechanical Engineers, 1971 through Winter 1973 Addenda.[*]

---

[*] Faulted conditions appeared for the first time in Winter 1976 addendum.

Table 3A.3.5-1

Equivalent Static Loads for Pressure Transients and
Loss-of-Coolant Accident Effects

Loading Combinations (See Section 3A.3.5.1.2)	P_A (Max) psig		P_B (Max) psig		H_L (Max) psig
	Drywell	Wetwell	Drywell	Wetwell	Vent Clearing Pressure
(1), (2), (4), (5), and (7)	-	-	-	-	-
(3) and (6)	+34	+28	+30	+25	+24

Acceptance Criteria for Containment Vessel
Allowable Stress Limits

Loading Combinations[a]	Primary Stresses			Secondary Stresses	Peak Stresses	Buckling
	General Membrane (P_m)	Local Membrane (P_L)	Bending+ Local Membrane (P_B+P_L)			
(1) and (2)	S_m	$1.5\ S_m$	$1.5\ S_m$	$3S_m$	Consider for fatigue analysis	Allowable given by ASME III Section NE-3133
(3) and (4)	S_m	$1.5\ S_m$	$1.5\ S_m$	N/A	N/A	Allowable given by ASME III Section NE-3133
(5), (6), and (7)						
For elements not integral and continuous	S_m	$1.5\ S_m$	$1.5\ S_m$	N/A	N/A	Allowable given by ASME III Section NE-3133
For elements integral and continuous	The greater of $1.2S_m$ or S_y	The greater of $1.8S_m$ or $1.5S_y$	The greater of $1.8S_m$ or $1.5S_y$	N/A	N/A	120% of Allowable given by ASME III Section NE-31311

[a] For definition of loading combinations, see Section 3A.3.5.1.

Notes:

1. Thermal stresses need not be considered in computing P_m, P_L, and P_B.

2. Thermal effects are considered in:
   a. Specifying stress intensity limits as a function of temperature.
   b. Analyzing effects of cyclic operation ASME III Section NE-3222.4

Table 3A.3.5-3

Load Combinations - Reinforced-Concrete Structures

Number	Load Condition	D	L	P_O	T_O	R_O	E_O	E_{SS}	P_B	P_A	T_A	R_A	P_{SR}	R_R
	Service Load Conditions													
1	Normal w/o temperature	1.4	1.7	1.0									1.5	
2	Normal w/ temperature	1.0	1.3	1.0	1.0	1.0							1.3	
3	Normal severe environment	1.0	1.0	1.0	1.0	1.0	1.25						1.25	
	Factored Load Conditions													
4	Abnormal (IBA/SBA)	1.0	1.0						1.25		1.0	1.0	1.25	
4a	Abnormal (DBA)	1.0	1.0							1.25	1.0	1.0	1.0[a]	
5	Abnormal (IBA/SBA) severe environment	1.0	1.0					1.1	1.1		1.0	1.0	1.1	
5a	Abnormal (DBA) severe environment	1.0	1.0					1.1		1.1	1.0	1.0	1.0[a]	
6	Normal extreme environment	1.0	1.0					1.0					1.0	
7	Abnormal (IBA/SBA) extreme environment	1.0	1.0					1.0	1.0		1.0	1.0	1.0	1.0
7a	Abnormal (DBA) extreme environment	1.0	1.0					1.0		1.0	1.0	1.0	1.0[a]	1.0

[a] Single valve actuation.

Note: See Section 3A.3.5.2.2.

Load Combinations - Steel Structures

Number	Load Condition	D	L	P_O	T_O	R_O	E_O	E_{SS}	P_B	P_A	T_A	R_A	P_{SR}	R_R
	Using Elastic Working Stress Design Method - Part 1 of AISC Specs, 1969													
	Service Load Conditions													
1	Normal w/o temperature	1.0	1.0	1.0									1.0	
2	Normal w/ temperature	1.0	1.0	1.0	1.0	1.0							1.0	
3	Normal sev. envir.	1.0	1.0	1.0	1.0	1.0	1.0						1.0	
	Factored Load Conditions													
4	Abnormal (IBA)	1.0	1.0						1.0		1.0	1.0	1.0	
4a	Abnormal (DBA)	1.0	1.0							1.0	1.0	1.0	1.0[a]	
5	Abnormal (IBA) sev. env.	1.0	1.0					1.0	1.0		1.0	1.0	1.0	
5a	Abnormal (DBA) sev. env.	1.0	1.0					1.0		1.0	1.0	1.0	1.0[a]	
6	Normal ext. env.	1.0	1.0	1.0	1.0	1.0		1.0						
7	Abnormal (IBA) ext. env.	1.0	1.0					1.0	1.0		1.0	1.0	1.0	1.0
7a	Abnormal (DBA) ext. env.	1.0	1.0					1.0		1.0	1.0	1.0	1.0[a]	1.0
	Using Plastic Design Method - Part 2 of AISC Specs, 1969													
	Service Load Conditions													
1	Normal w/o temperature	1.7	1.7	1.7									1.5	
2	Normal w/temperature	1.0	1.3	1.0	1.0	1.0							1.3	
3	Normal sev. env.	1.0	1.0	1.0	1.0	1.0	1.25						1.25	
	Factored Load Conditions													
4	Abnormal (IBA)	1.0	1.0						1.25		1.0	1.0	1.25	
4a	Abnormal (DBA)	1.0	1.0							1.25	1.0	1.0	1.25[a]	
5	Abnormal (IBA) sev. env.	1.0	1.0					1.1	1.1		1.0	1.0	1.1	
5a	Abnormal (DBA) sev. env.	1.0	1.0					1.1		1.1	1.0	1.0	1.1[a]	
6	Normal ext. env.	1.0	1.0	1.0	1.0	1.0		1.0					1.0	
7	Abnormal (IBA) ext. env.	1.0	1.0					1.0	1.0		1.0	1.0	1.0	1.0
7a	Abnormal (DBA) ext. env.	1.0	1.0					1.0		1.0	1.0	1.0	1.0[a]	1.0

[a] Single valve actuation.

Note: See Section 3A.3.5.2.2.

Table 3A.3.5-5

Load Combinations and Acceptance Criteria for ASME Code
Class 1, 2, and 3 Balance-of-Plant Piping and Equipment[a]

Load Cases	Load Combinations (1, 2, and 3)	Design Assessment Acceptance Criteria
1	P+D.W.	Normal (A)
2	N+OBE+SRV$_{ONE}$	Upset (B)
3	N+OBE+SRV$_{TWO}$	Upset (B)
4	N+OBE+SRV$_{ALL}$	Upset (B)
5	N+OBE+SRV$_{ALL}$+SBA	Emergency[b] (C)
6	N+OBE+SRV$_{TWO}$+SBA	Emergency[b] (C)
7	N+SSE+SRV$_{ADS}$+SBA/IBA	Faulted[b] (D)
8	N+SSE+SRV$_{TWO}$+SBA/IBA	Faulted[b] (D)
9	N+SSE+SRV$_{ONE}$	Faulted[b] (D)
10	N+SSE+SRV$_{TWO}$	Faulted[b] (D)
11	N+SSE+SRV$_{ALL}$	Faulted[b] (D)
12	N+SSE+DBA	Faulted[b] (D)

[a] Equipment includes pumps, valves, supports, and vessels. For bolting used in connection
with the support of ASME Code Class 1, 2, and 3 components, vendor load capacity data
sheets are used, or where design is by the architect engineer, stress levels are maintained less
than specified minimum yield at temperature.

[b] All ASME Code Class 1, 2, and 3 piping systems which are required to function for safety
shutdown under the postulated events shall meet the requirements of NRC's memorandum,
"Evaluation of Topical Report - Piping Functional Capability Criteria," date July 17, 1980.

Table 3A.3.5-5

Load Combinations and Acceptance Criteria for ASME Code
Class 1, 2, and 3 Balance-of-Plant Piping and Equipment[a] (Continued)

Notes:

1. As required by the appropriate subsection, i.e., NB, NC, or ND of ASME Section III, Division I. Other loads, such as thermal transient, thermal gradients, and anchor point displacement portion of the OBE or SRV, may require consideration in addition to those primary stress-producing loads listed.

2. SBA, IBA, and DBA include all event induced loads, as applicable, such as chugging, pool swell, drag loads, annulus pressurization, etc.

3. Seismic and hydrodynamic loads are combined by the SRSS technique and added to the applicable static loads.

Load Definition Legend

Normal (N)   Normal loads include internal pressure and dead weight

OBE   Operational basis earthquake loads

SSE   Safe shutdown earthquake loads

SRV_{TWO} SRV discharge induced loads from two adjacent valves

SRV_{ALL} The loads induced by actuation of all SRVs

SRV_{ADS} The loads induced by the actuation of SRVs associated with the automatic depressurization system

SRV_{ONE} The loads induced by the actuation of one SRV

3A.4   UNDERLINE DESIGN ASSESSMENT

3A.4.1   SUPPRESSION POOL BOUNDARY STRUCTURES

3A.4.1.1   Assessment of Steel Containment Structure

The primary containment structure in the suppression chamber area, as shown in
Figure 3A.4.1-1, is an orthogonally stiffened steel shell. See FSAR Section 3.8 for a
description of the steel containment structure.

The thickness of the steel shell plate in the suppression chamber region is approximately
1.5 in. and varies with height. Vertical "Tee" stiffeners, at a spacing of 40.5 in., are welded
to the inside face of the shell plate and extend about 8 ft beyond the knuckle (cylinder-cone
inter-face) elevation. In the pool region of the suppression chamber, additional horizontal
"Tee" stiffener rings at an approximate spacing of 36 in., are welded to the inside face of the
shell plate. The purpose of adding these tees (Figure 3A.4.1-4) is to increase the load carrying
capacity of the containment shell. The vertical tees are required for resisting compressive
loads due, mainly, to seismic effects. The horizontal tees are intended to carry the
hydrodynamic loads which were not considered in the original design of the containment shell.
There are no heavy attachments to the containment in the suppression chamber region.

The drywell floor slab is radially separated from the containment and the gap is sealed by
means of a radially and vertically flexible seal, as shown in Figure 3A.4.1-9. The slab is
connected to the containment in the tangential direction by means of shear lugs.

3A.4.1.1.1   Loads Used For Assessment

The methods used for calculating hydrodynamic loads on the pool boundary, as described in
Sections 3A.3.1 and 3A.3.2, provide a conservative definition of loads for design assessment.

3A.4.1.1.1.1 Safety/Relief Valve Loads. The suppression pool boundary pressure loading is
determined in accordance with procedures described in Reference 3A.4.1-1 on the basis of
operating conditions at CGS. A discussion on the derivation of the safety/relief valve
(SRV) load definition is provided in 3A.3.1.

Several different incidents may occur which would cause one or more SRVs to actuate. For
example, the valves may operate either manually, or on pressure setpoints following a turbine
trip, automatically through the automatic depressurization system (ADS) system.

The critical modes of SRV actuations considered in the design are detailed in
Reference 3A.4.1-1. For the purposes of design assessment, consideration is given to all the
SRV discharge cases that are postulated to occur during the life of the CGS plant. A summary
of the various cases is explained below.

3A.4.1.1.1.1.1 Single Valve Discharge Case. Actuation of any single SRV is postulated during a loss-of-coolant accident (LOCA) involving a large or intermediate break. Two possible cases of single SRV discharge are considered, the single inner quencher discharge and the single outer quencher discharge. A single inner quencher discharge is more likely to occur because of its lower pressure setpoint. However, a single outer quencher discharge is conservatively assumed for the assessment of the containment vessel.

3A.4.1.1.1.1.2 Two Valves Discharge Case. For this event, two SRVs are considered to discharge concurrently through two adjacent quenchers.

3A.4.1.1.1.1.3 Automatic Depressurization System Valves Discharge Case. The seven ADS valves for CGS are assigned to outer quenchers in a configuration that is nearly axisymmetrical. The ADS is characterized by an automatic and simultaneous actuation as discussed in the DFFR (Reference 3A.3.2-2). The ADS discharge is not considered to occur during a large pipe break LOCA. However, it is assumed that the ADS may discharge during an intermediate pipe break or a small pipe break LOCA.

3A.4.1.1.1.1.4 All Valves Discharge Case. Under certain plant conditions, the actuation of all 18 SRVs in CGS is assumed. Two different conditions may occur during this event: the axisymmetric all valves discharge conservatively assumes that all 18 SRVs discharge simultaneously; the nearly symmetric all valves discharge assumes that there is some imbalance during the discharge event. As discussed in the DFFR (Reference 3A.3.2-2), the all valves discharge is not considered to occur during a large pipe break LOCA. However, it is assumed that the all valves discharge may occur during an intermediate pipe break or a small pipe break LOCA.

3A.4.1.1.1.2 Loss-of-Coolant Accident Loads. Loss-of-coolant accidents are associated with postulated large pipe breaks [design basis accident (DBA)], intermediate pipe breaks [intermediate break accident (IBA)], or small pipe breaks [small break accident (SBA)]. Various transient LOCA pressure loads on the pool boundary considered in the assessment of the containment include vent water clearing jet loads, air bubble pressure loads, pool swell, fallback, drywell and wetwell pressure transients, and chugging loads.

3A.4.1.1.1.2.1 Chugging Loads. A general discussion of the chugging phenomenon is included in Section 3A.3.2.4. Design pool boundary loads discussed in Section 3A.3.2.4.2.1 are used for the structural assessment.

3A.4.1.1.1.2.2 High and Medium Mass Flux Condensation Oscillations. During the sequence of a LOCA event, condensation oscillations take place after pool swell and fallback. Depending on the steam mass flux rate, they are identified as either (a) high mass flux or (b) medium mass flux condensation oscillations. However, as noted in Section 3A.3.2.4.1.2, the controlling boundary pressure loads due to chugging exceed those due to condensation

oscillations. Therefore, condensation oscillation loads are not considered in the assessment of the containment vessel.

3A.4.1.1.1.2.3 <u>Other Loss-of-Coolant Accident Loads.</u> Loss-of-coolant accident loads, other than those due to condensation oscillations and chugging, include

    a.   Pressure and temperature transients

           These transients represent symmetric loadings. An equivalent static loading is used for a LOCA pressure transient which takes due account of the time history of the pressure buildup. Thermal effects (T_A) on stress intensities and cyclic operation have been considered. Pressure and temperature transients considered in the assessment are shown in Figures 3A.3.2-20 through 3A.3.2-28;

    b.   Reaction from downcomer vent horizontal exit load

           The horizontal loads acting at the downcomer exits are transmitted via the downcomer bracing system and result in tangential reactions at the steel containment structure;

    c.   Pool swell bubble pressure

           The air slug pressure in the suppression pool during pool swell acts symmetrically around the inside of the containment structure. Its time history, in relation to the appropriate period of the containment structure, is used in determining the dynamic load factor (DLF).

           In addition to the preceding case of symmetric loading, the case of an asymmetric bubble pressure acting on the submerged boundary in accordance with Reference 3A.3.2-5 is also included; and

    d.   Reactions from components supported by the steel containment structure

           Drag and impact loads occur on structural components supported by the steel containment structure as a result of pool swell and fallback. Reactions from these structural components are carried by the containment structure.

3A.4.1.1.1.3 <u>Other Significant Loads.</u>

    a.   Seismic loads

           Loads due to the operating basic earthquake (OBE) and the safe shutdown earthquake (SSE), developed in the project design, are applicable. Seismic

loads include the effect of the water in the suppression pool. The effects due to water sloshing (pressure load) have been accounted for in the containment pool swell assuming a concurrent seismic event (SSE) is insignificant;

b.　　Dead load, live load, and hydrostatic pressure

The hydrostatic pressure due to the suppression pool is included in the dead load; and

c.　　Design external pressure

An external pressure of 2 psi resulting from atmospheric conditions inside and outside the drywell is used. When external pressure governs the design, an additional external pressure of 2 psi due to the reaction of the compressible foam between the containment and the biological shield wall is used. This reaction results from the thermal expansion of the containment shell.

3A.4.1.1.2　　Controlling Load Combinations

The applicable load combinations for the pressure-suppression chamber portion of the steel containment structure are defined in Section 3A.3.5.1.2. Combinations presented therein are also applicable to the horizontal and vertical stiffening tees. Load combination (3), stated below, is found to control the design of the stiffened steel containment structure.

Load Combination (3):　　　$D + L + E_O + T_A + R_A + P_B + P_V + P_{SR}$

The interpretation and contribution of each of the terms depends on the event being considered. In considering the overall steel containment structure, the controlling combination of events involves ADS actuation during an intermediate break LOCA with clugging. Consequently, P_B and T_A refer to the IBA. In this load combination, T_A and R_A are relatively insignificant. The term P_{SR} refers to ADS pool boundary pressure loading. Thus, the effective controlling load combination involves:

$D + L + E_O + P_B + P_{SR} + P_C$

3A.4.1.1.3　　Acceptance Criteria

The acceptance criteria for design of steel containment structure, including horizontal and vertical tees, is in compliance with the 1971 ASME Code, Edition through the 1972 Summer Addenda, Section III, Division 1, Subsection NE is given in Section 3A.3.5.1.3.

3A.4.1.1.4   Method of Analysis

3A.4.1.1.4.1 <u>Formulation of the Problem.</u> In accordance with the methods presented in Sections 3A.3.1 and 3A.3.2 for defining hydrodynamic loads, it is assumed that the incident pressures on the pool boundary, resulting from bubble oscillations and steam condensation, are acting on the boundary as externally applied loads. In computing the responses of the structure, the fluid-shell interaction effects are accounted for by solving the coupled partial differential equations governing the fluid and the shell structure using finite elements. The stresses due to chugging used for assessing the containment structure are obtained by using the building model and the method of analysis presented in Section 3A.5.2. For SRV loads, a refined containment model described in Section 3A.5.1 is used.

For pool boundary hydrodynamic loads, since the vertical and horizontal tees are integrated in the model of the suppression chamber portion of the containment, the fluid-shell interaction analysis also gives the dynamic stresses in the tees.

3A.4.1.1.4.2 <u>Mathematical Model.</u> The mathematical model used in the containment analysis for SRV loads is discussed in Section 3A.5.1.1.2 and shown in Figure 3A.5.1-2. Prominent features of this axisymmetric model are discussed in Reference 3A.4.1-1. The mathematical model used in the containment analysis for chugging loads is discussed in Section 3A.5.2.1 and shown in Figure 3A.5.2-1. A detailed description of the chugging model can be found in Reference 3A.4.1-4.

3A.4.1.1.4.3 <u>Coupled Equations of Motion.</u>

  a. Shell equations

    The partial differential equations governing the motion of the containment shell are based on equations given in Reference 3A.4.1-3;

  b. Fluid equations

    The partial differential equations governing the dynamics of compressible fluid are the continuity equation and the equation of motion establishing the relationship between the pressure and the velocity of a particle in the fluid. For reasons cited in Reference 3A.4.1-4, the water in the suppression pool is considered to be compressible for the chugging model. However, for reasons cited in Reference 3A.4.1-1, the water is considered to be incompressible for the SRV model;

c.   Fluid boundary conditions

The fluid boundaries can be seen in Figure 3A.4.1-8. The pressure at the fluid
surface is specified to be zero. The continuity requirement at the fluid-structure
interface is satisfied by specifying the radial component of fluid motion at the
interface to be equal to that of the shell;

d.   Shell boundary conditions

As discussed in Section 3A.5.1.1.2, a refined containment model is used for the
analysis of the containment structure under SRV loading. This refined model is
connected to the overall building model at the following locations (see
Reference 3A.4.1-1): basemat in the radial, vertical, and circumferential
directions; diaphragm floor in the circumferential direction; and stabilizer truss
and refueling bellows in the radial and circumferential directions.

For the analysis of the containment structure due to chugging loads, the overall
building model discussed in Section 3A.5.2.1, is used;

e.   Geometric symmetry

The axisymmetric geometry of the containment shell-fluid system is utilized in
the solution of the equations in cylindrical coordinates. The azimuth coordinate
is eliminated from the governing equations by representing azimuthal
dependence of each variable by a Fourier series. The equations are thus solved
for each Fourier term or harmonic of the series and the final solution is obtained
by summation of solutions for each term.

3A.4.1.1.4.4 Numerical Solution. Numerical solutions to equations described in
Section 3A.4.1.1.4.3 are obtained by using finite elements. An integration time step of
0.001 sec is used in the analyses for both SRV and chugging loads.

3A.4.1.1.4.5 Computer Program. A Burns and Roe computer program "HYDI-2"
(Attachment 3A.F) was developed for Mark II containment configurations, and subsequently
used in the analysis of the containment structure due to chugging loads. The numerical
solutions were verified by the commercially available finite element program "NASTRAN"
(Attachment 3A.F). The analysis of the refined containment model for SRV loads was made
with the "NASTRAN" program.

3A.4.1.1.5   Results and Design Margin

3A.4.1.1.5.1 Results of Analysis. The hydrodynamic pressure loads, as described in
Section 3A.4.1.1.1, are applied to the containment wall of the fluid-shell interaction models

(Figures 3A.5.1-2 and 3A.5.2-1). Utilizing the Burns and Roe, Inc. computer program HYDI-2 for chugging loads, and the NASTRAN program for SRV loads, the responses of the containment are computed. The maximum stresses (in time) are evaluated in the applicable load combinations for determining the controlling load combination and corresponding design margin for the containment structure. Maximum time-wise profiles of radial displacements are presented in Figures 3A.4.1-2 and 3A.4.1-3 for the containment structure.

Responses to various loads discussed in Section 3A.4.1.1.1 are summarized below:

a.   ADS discharge case

        The ADS actuation combined with IBA or SBA is the most critical axisymmetric pressure load on the containment. For the purposes of assessment, the ADS pressure loading is conservatively assumed to be the same as the larger of each of the two all valves discharge pressure loadings, i.e., the design boundary pressure. Thus, the response of the containment to the ADS actuation is shown in Figure 3A.4.1-2. The resulting stresses are used in the controlling load combination for calculating the design margin of the containment structure;

b.   All valve discharge case

        In considering the two different all valves discharge events, the nearly symmetric pressure loading is slightly greater than the axisymmetric pressure loading (see References 3A.4.1-1 and 3A.4.1-2);

c.   Single valve discharge case

        Actuation of a single SRV combined with LOCA (DBA) loads results in the most critical non-axisymmetric pressure loading on the containment. However, responses of the containment to the resulting load combination is less severe than case (a), above;

d.   Two valves discharge case

        Responses of the containment to this load are conservatively assumed to be the same as case (c) (see Reference 3A.4.1-1);

e.   Chugging

        Reference 3A.4.1-4, described in Section 3A.3.2.4.2.2, presents the responses of the containment shell to the chugging pressure load. The resulting stresses are used in the controlling load combination for calculating the design margin of

the containment structure. As discussed in Section 3A.5.2.2, the nearly symmetric chugging load is used for assessment purposes. The response of the containment to these design chugging loads is shown in Figure 3A.4.1-3; and

    f.   High and medium mass flux condensation oscillations

           Condensation oscillation loads are not considered in the assessment of the containment structure since they are bounded by chugging loads.

3A.4.1.1.5.2 Assessment Results. The containment assessment performed in accordance with Sections 3A.3.5.1.2 and 3A.3.5.1.3 shows that in load combination (3) the general membrane stress intensity controls the containment design. Based on this calculation, the design margin for the containment shell is 1.29.

The buckling strength of the CGS containment in resisting the external pressure and axial compression acting on the suppression pool region increases substantially as a result of adding the horizontal stiffening rings. The most critical load combination under events causing net external pressure and axial compression is load combination (7). Under this load combination the ratio of the allowable buckling pressure load of the containment to the applied external pressure load is 3.1. The ratio of the allowable buckling axial load of the containment to the axial compressive load is 1.37. In this analysis, the interaction effect is accounted for by assuming that the horizontal stiffening tees resist only external pressure while the vertical stiffening tees resist only axial compression.

For the containment tees, the stress intensities for load combination (3) are governed by primary bending plus local membrane stresses. These stresses occur at the webs of the horizontal tees and at the root of the flange for the vertical tees. Based on these stress values, the design margins for the vertical and horizontal tees are 2.23 and 1.26, respectively.

The combined stresses in both the containment and tees are calculated for the controlling load combination by adding the stress resulting from static loads algebraically and stresses due to dynamic oscillating loads by the square-root-of-sum-of-the-squares (SRSS) method. The resulting design margin for the containment structure (including the horizontal and vertical tees) is 1.26.

3A.4.1.2   Basemat

The assessment of the capacity of the basemat relative to load combinations involving suppression pool hydrodynamic loads is made in this section. The basemat and adjoining structures are shown in Figures 3A.4.1-5 and 3A.4.1-6.

3A.4.1.2.1   Loads Used for Assessment

A complete description of all the hydrodynamic loads used in the assessment of the basemat is provided in Section 3A.3. Symbols, equations, and load combinations referred to in this section are detailed in Section 3A.3.5.2.

3A.4.1.2.1.1 Safety/Relief Valve Loads. Loads on the suppression pool boundary due to SRV actuations are detailed in Section 3A.3.1. Specific SRV loading cases considered in the basemat assessment include symmetric loads due to the actuation of all 18 valves and asymmetric loads due to the actuation of a single SRV. For both cases, dynamic stresses in the basemat (bending and shear) are developed on the basis of a time-history application of the loads. The analytical model used for the assessment is shown in Figure 3A.5.1-lb. Prominent features of the model, including the use of axisymmetric shell elements is discussed in Section 3A.5.1.

3A.4.1.2.1.2 Loss-of-Coolant Accident Loads. Loads on the suppression pool boundary due to a LOCA are detailed in Section 3A.3.2. Of all the LOCA loads, chugging pressures are the most significant with respect to the basemat. Other LOCA loads, including jet loads and bubble pressures, are not significant with respect to the basemat assessment. Dynamic stresses in the basemat (bending and shear) are developed on the basis of a time-history application of the loads. The analytical model used for the assessment is shown in Figure 3A.5.2-1. Prominent features of the model, including the use of axisymmetric shell elements, are discussed in Section 3A.5.2.

3A.4.1.2.1.3 Other Significant Loads. Seismic loads constitute a principal loading in the basemat assessment. The seismic loads on the basemat from the superstructure (exterior walls, biological shield wall, and pedestal) are the same as those used in the original building design. In that original design, a dynamic analysis was made using a discrete mathematical idealization of the entire reactor building. The stress resultants at the base of the superstructure (overturning moment, axial force) due to the OBE and the SSE as developed in the original design are used.

Dead and live loads as developed in the original structural design are also used.

3A.4.1.2.2   Applicable Load Combinations and Acceptance Criteria

The load combination and acceptance criteria described in Section 3A.3.5.2 are applicable to the basemat.

3A.4.1.2.3   Method of Analysis

The structural capacity of the basemat is investigated for the applicable load combinations with loads as listed above. The general approach in the basemat assessment is to determine the

values of the controlling stress resultants in the basemat (bending and shear) on the basis of elastic analysis under applied design loads and to calculate the capacity of the basemat in terms of these stress resultants by the strength method of the ACI 318-71 Code (Reference 3A.4.1-5). Critical sections for bending and shear are located with respect to the face of the biological shield wall in compliance with code requirements.

3A.4.1.2.3.1 <u>Effects of E_O, E_{SS}, D, L.</u> The investigation of the basemat for the combined effect of dead, live, and seismic loads is based on the analysis performed in the original building design. Depicted as a plate on an elastic foundation, the basemat is modeled as a series of plate elements while the supporting soil is modeled as a group of elastic springs situated at designated nodes. The effects of the seismic overturning moment and the vertical acceleration of the dead and live loads are converted to nodal loads. Resulting stresses from the model and loads described above are calculated with the use of the computer program NASTRAN. Values of the controlling bending moment, beam shear, and punching shear due to combined dead, live, and SSE loads are tabulated in Table 3A.4.1-1 for the critical section of the basemat.

3A.4.1.2.3.2 <u>Effect of P_{SR}, P_B.</u> The values of bending moments and shears at the critical section in the basemat due to SRV actuation and chugging are available from the analysis of the reactor building models described in Section 3A.5. The symmetric mode of SRV actuation and the nearly symmetric mode of chugging result in the comparatively larger values of stress resultants. The controlling stress resultants for these loads are tabulated in Table 3A.4.1-1 for the critical section.

3A.4.1.2.3.3 <u>Critical Load Combination.</u> Review of the stress resultant values in connection with the applicable load combinations shows that the critical load combination for all stress resultants is load combination (7); this combination is noted below with only the significant terms included.

$$(7) \quad D + L + E_{SS} + P_B + P_{SR}$$

3A.4.1.2.3.4 <u>Capacity.</u> The capacity of the basemat with respect to bending, beam shear, and punching shear is determined in accordance with the strength method of the ACI 318-71 Code (Reference 3A.4.1-5). These stress resultant capacities are listed in Table 3A.4.1-1.

3A.4.1.2.4 Results and Design Margins

Comparison of the design values for the stress resultants in Table 3A.4.1-1 with the capacity values in the table shows that the basemat provides adequate capacity. The ratio of bending capacity to design bending moment is 1.14. The ratio of beam shear capacity to design beam shear is 1.48. The ratio of punching shear capacity to design punching shear is 1.27.

3A.4.1.3   Pedestal

The assessment of the capacity of the reactor pressure vessel (RPV) pedestal relative to load combinations involving suppression pool hydrodynamic loads is made in this section. The pedestal and adjoining structures in the suppression chamber are shown in Figure 3A.4.1-7.

3A.4.1.3.1   Loads Used for Assessment

A complete description of all the hydrodynamic loads used in the assessment of the RPV pedestal is provided in Section 3A.3. Symbols, equations, and load combinations referred to in this section are detailed in Section 3A.3.5.2.

3A.4.1.3.1.1 Safety/Relief Valve Loads. Loads on the suppression pool boundary due to SRV actuations are detailed in Section 3A.3.1. Specific SRV loading cases considered in the pedestal assessment include symmetric loads due to the actuation of all 18 valves and asymmetric loads due to the actuation of a single SRV. For the asymmetric case, dynamic stresses in the pedestal are developed on the basis of time history application of the load. For the symmetric case, dynamic stresses are developed on the basis of applied pressures increased by an appropriate DLF which is determined from the time history analysis. The analytical model used for the assessment is shown in Figure 3A.5.1-lb. Prominent features of the model, including the use of axisymmetric shell elements, are discussed in Section 3A.5.1.

3A.4.1.3.1.2 Loss-of-Coolant Accident Loads. Loads on the suppression pool boundary due to LOCA are detailed in Section 3A.3.2. Of all the LOCA loads, chugging pressures are the most significant with respect to the pedestal. Other LOCA loads, including pool swell, jet loads, and bubble pressures are not significant with respect to the pedestal assessment. Dynamic stresses in the pedestal are developed on the basis of the model and load application described in Section 3A.4.1.2.1.2.

3A.4.1.3.1.3 Other Significant Loads. Seismic loads (E_O, E_{SS}) constitute a principal loading in the pedestal assessment. The seismic loadings and associated analysis in this assessment are the same as those used for the original design. A dynamic analysis was made using a discrete mathematical idealization of the entire reactor building including the pedestal. The stress resultants in the pedestal (overall bending moment, horizontal shear force, and axial force) due to the OBE (E_O) and the SSE (E_{SS}) as developed in the original design are used. Dead loads as developed in the original building design are also utilized.

3A.4.1.3.2   Applicable Load Combinations and Acceptance Criteria

The load combinations and acceptance criteria for internal reinforced concrete structures described in Section 3A.3.5.2 are applicable to the pedestal.

3A.4.1.3.3   Method of Analysis

The structural capacity of the pedestal is investigated for the load combinations with two types of loading, namely, asymmetric and symmetric. The general approach in the pedestal assessment is to determine the values of the controlling stress resultants on the basis of elastic analysis under design loadings and to calculate the capacity of the pedestal in terms of these stress resultants in accordance with the strength method of the ACI 318-71 Code (Reference 3A.4.1-5).

3A.4.1.3.3.1 Asymmetric Action. The loads which contribute to asymmetric action of the pedestal are seismic loads (E_O and E_{SS}), loads due to single SRV actuation (P_{SR}), and loads due to chugging phenomena (P_B). The significant stress resultants associated with these loads are overturning moment and total shear. For seismic loading, the values of these stress resultants in the original design are used. For P_{SR} and P_B, the stress resultants are obtained by integrating over the entire pedestal section the stresses obtained from the elastic analysis of the reactor building structural model. Controlling values of the stress resultants which occur at the base of the pedestal are tabulated in Table 3A.4.1-2.

Review of the stress resultant values in connection with the load combinations shows that the critical load combination for both moment and shear is load combination (7), stated below, with only the significant load terms included.

$$(7) \qquad D + E_{SS} + P_B + P_{SR}$$

The capacity of the pedestal relative to overturning moment and concurrent axial load is expressed by the interaction curve shown in Figure 3A.4.1-10. Points along the interaction curve representing different capacity combinations of axial load (P_u) and bending moment (M_u) have been calculated in line with the ACI 318-71 Code (Reference 3A.4.1-5). The minimum and controlling value of axial load occurs with upward seismic action; this axial load value (12,380 kips) and the controlling overturning moment from Table 3A.4.1-2 (212,380 ft kips) are also plotted in Figure 3A.4.1-10. As noted in the figure, the bending moment capacity coincident with the controlling axial load is 375,000 ft kips.

The capacity of the pedestal relative to overall horizontal (tangential) shear, calculated in accordance with the ACI 318-71 Code (Reference 3A.4.1-5), is 14,500 kips. From Table 3A.4.1-2, the controlling design shear is 2760 kips.

3A.4.1.3.3.2 Symmetric Action. Loads which contribute to symmetric action of the pedestal are due to actuation of all 18 SRVs (P_{SR}) and chugging phenomena (P_B). The hydrostatic pressure (D) also causes symmetric action. For P_{SR} and P_B, an appropriate DLF is included as noted in Section 3A.4.1.3.1.1. Symmetric action is investigated with respect to radial and circumferential normal stresses and with respect to the effect of the end fixity at the base.

To obtain the radial and circumferential normal stresses, the pedestal is analyzed as a thick walled cylinder. Maximum compressive stress (circumferential) occurs for load combination (1):

(1) $1.4D + 1.7L + 1.0P_O + 1.5P_{SR}$

In this load combination, terms L and P_O do not contribute to the stresses being considered and are omitted. For calculation purposes, the maximum values of D, and P_{SR} (positive value) are used. Maximum tensile stress (circumferential) occurs for load combination (4):

(4) $1.0D + 1.0L + 1.0T_A + 1.0R_A + 1.25 (P_B + P_{SR})$

In this load combination, L, T_A, and R_A are omitted as they do not affect the stress resultant under consideration.

Radial shear and moment occur under the symmetric loads due to the fixity of the pedestal at its junction with the basemat. The analysis is based on a general theory of the elastic behavior of cylindrical shells. Maximum values of radial shear and moment occur at the pedestal base with load combination (4).

In this load combination, L, T_A, and R_A are omitted as they do not affect the stress resultant under consideration.

3A.4.1.3.4   Results and Design Margins

Results for asymmetric loading are summarized below:

a.   The controlling value of the pedestal overturning moment under design loadings is less than the pedestal moment capacity. The ratio of the moment capacity to the controlling overturning moment is 1.77; and

b.   The controlling value of the pedestal base shear under design loadings is less than the pedestal shear capacity. The ratio of shear capacity to controlling applied shear is 5.25.

Results for symmetric loading are summarized below:

a.   The calculated normal stresses occurring during symmetric action are found to be less than the allowable strength values. The ratio of pedestal capacity to stress under controlling loading is 5.53 for tensile circumferential stress and 15.83 for circumferential compressive stress; and

b.   The calculated stresses due to radial shear and moment due to pedestal fixity at its base during symmetric action are found to be less than the allowable strength values. The ratio of radial shear capacity to maximum shear due to load is 1.11 and the corresponding ratio for radial moment is 5.06.

Review of the preceding results shows that the overall controlling design margin is 1.11 applicable to radial shear under symmetric loading.

3A.4.1.4   Diaphragm Floor

Assessment of the capacity of the diaphragm floor (see Figures 3A.4.1-6 and 3A.4.1-7) relative to load combinations involving suppression pool hydrodynamic loads is made in this section.

3A.4.1.4.1   Loads Used for Assessment

A complete description of all hydrodynamic loads is given in Section 3A.3. This subsection discusses the loads used for the assessment of the diaphragm floor.

3A.4.1.4.1.1 Safety/Relief Valve Actuation Loads. Safety/relief valve discharge does not result in pressure loads directly on the diaphragm floor, but causes dynamic horizontal pressure differentials across the downcomers, the SRV piping, and the columns, all of which are supported at the diaphragm floor, and dynamic vertical pressure differential across the downcomer bracing which is transferred to the diaphragm floor by the downcomers.

In addition, building response spectra from SRV discharge result in acceleration of the diaphragm floor which induces dynamic stresses in the components of the floor.

3A.4.1.4.1.2 Loss-of-Coolant Accident Loads. The maximum net downward pressure on the diaphragm floor during a DBA LOCA is 20 psi (see Section 3A.3.2.5.2). Since the time required to develop the maximum net downward differential pressure resulting from a recirculation line break is approximately 0.7 sec, dynamic effects are not significant and temperature transients at time of peak downward pressure differential do not contribute to the floor loading.

The maximum net upward pressure on the diaphragm floor is of short duration, and is due to wetwell atmosphere compression resulting from pool swell during a DBA LOCA (see Section 3A.3.2.5.2). A value of 5.5 psi maximum net upward pressure is considered in the assessment of the diaphragm floor (see Section 3A.3.2.3.1.3).

Pool swell and fallback drag loads on the downcomer bracing (see Section 3A.3.2.3.3.1) are transferred to the diaphragm floor by the downcomers.

Other significant LOCA loads include pipe break jet impingement and steam condensation accelerations obtained from the response spectra at the diaphragm floor support locations.

3A.4.1.4.1.3 <u>Other Significant Loads.</u> Other loads which result in significant stresses in the diaphragm floor are dead loads, live loads, and vertical seismic accelerations.

Dead leads include the weight of the diaphragm floor reinforced concrete slab and supporting steel beams, downcomers, horizontal run of SRV piping, including vertical supports, downcomer bracing supported vertically by the downcomers and, hence, the diaphragm floor. Live loads include personnel and equipment weights on the diaphragm floor. Seismic accelerations are obtained from the seismic response spectra at the support locations for the diaphragm floor.

3A.4.1.4.2   Controlling Load Combinations

The load combination criteria for structures internal to the pressure-suppression chamber (see Sections 3A.3.5.2 and 3A.3.5.3) are applicable to the diaphragm floor. In particular, the combinations for steel structures, using the elastic working stress design method with both service load conditions and factored load conditions, are investigated in the analysis for the structural steel components of the floor (see Section 3A.3.5.3). The combinations for reinforced concrete structures, using the ultimate strength design method with both service load conditions and factored load conditions, are investigated for the reinforced concrete slab component of the floor (see Section 3A.3.5.2). The controlling load combinations are specified in Section 3A.4.1.4.5.

3A.4.1.4.3   Acceptance Criteria

The acceptable stress levels for the steel components of the diaphragm floor are specified in Section 3A.3.5.3.3.

The acceptable allowable limit for the concrete components is the ultimate strength as determined by the ultimate strength design method of the ACI 318-71 Building Code (Reference 3A.4.1-5).

3A.4.1.4.4   Method of Analysis

The diaphragm floor components, consisting of the reinforced concrete slab, the structural steel circumferential and radial beams, and connections, were investigated individually for the effects of both the upward and downward loads. To determine design loads for each of the components, the diaphragm floor was analyzed as a slab (one-way); beam (circumferential beams), and girder (radial beams) structural system with the radial beams supported at the pedestal and on the columns, but not at the containment vessel shell.

3A.4.1.4.5   Results and Design Margins

The diaphragm floor reinforced concrete slab and the steel circumferential and radial beams, including connections, were found to have sufficient capacity to withstand the governing load combinations. The critical component under downward load, as defined by the governing load combination (7a) for steel structures, is the radial beam. The design margin (i.e., ratio of the allowable stress to the maximum absolute calculated stress) for the radial beam is 1.62, and is based on the following input into the loading combination (7a) for steel structures:

(7a) $1.7S \geq 1.0D + 1.0L + 1.0E_{SS} + 1.0P_A + 1.0T_A + 1.0R_A + 1.0P_{SR} + 1.0R_R$

$$D \quad = \quad 4.28 \text{ psi}$$

$$L \quad = \quad 6.94 \text{ psi}$$

$$E_{SS} \quad = \quad 1.52 \text{ psi}$$

$$P_A \quad = \quad 20 \text{ psi}$$

$$T_A \quad = \quad 0$$

$$R_A \quad = \quad 0$$

$$P_{SR} \quad = \quad 1.65 \text{ psi}$$

$$R_R \quad = \quad 534,000 \text{ lb}$$

where D, L, E_{SS}, P_A, T_A, R_A, P_{SR}, and R_R are as defined in Section 3A.3.5.2.

The critical components under upward load are the anchor bolts at the radial beam to column connection. The design margin (i.e., ratio of the allowable stress to the maximum absolute calculated stress) far the anchor bolts is 1.27, based on the following input into the governing loading combination (4a) for reinforced concrete structures:

(4a) $U \geq 1.0D + 1.0L + 1.25P_A + 1.0T_A + 1.0R_A + 1.0P_{SR}$

$$D \quad = 4.28 \text{ psi}$$

$$L \quad = 0$$

$$P_A \quad = 5.57 \text{ psi}$$

$$T_A \quad = 0$$

$$R_A = 0$$

$$P_{SR} = 1.65 \text{ psi}$$

where D, L, P_A, T_A, R_A, and P_{SR}, are as defined in Section 3A.3.5.2.

3A.4.1.5   Diaphragm Floor Seal

The diaphragm floor seal is located at the inside surface of the primary containment vessel periphery at el. 493 ft 5 in. It provides a flexible, pressure tight seal between the primary containment vessel and the diaphragm floor and is capable of accommodating differential thermal expansion between them. The diaphragm floor seal is a 270° omega-shaped configuration of stainless steel and is drained to the floor drain system with four drain pipes, as shown in Figure 3A.4.1-9.

3A.4.1.5.1   Loads Used for Assessment

   a.   Normal plant condition

         This condition is defined as reactor startup, operation at power, and normal reactor cold shutdown. These loads are due to thermal expansion of the component and thermal displacement between the concrete diaphragm floor and primary containment during normal plant operation;

   b.   SRV loads

         These loads are not directly applied to the diaphragm floor seal, but do cause displacement of the primary containment shell relative to the diaphragm floor resulting in stress in the seal;

   c.   LOCA loads

         The LOCA combination governing the design of the seal includes the effects of relative thermal displacement, differential pressure, and hydrodynamic effects. Other LOCA effects, given in Section 3A.3.2, include the temperature and pressure transients, pool swell air compression load, and primary containment displacement due to building response. A discussion of direct load, i.e., temperature and pressure transients and pool swell phenomenon is presented in Section 3A.4.1.5.2; and

d.　　　Other loads

The effect of dead load, OBE, and SSE seismic loads, as applicable, are included in the analysis. Loads from the drain pipes are also included.

3A.4.1.5.2　　Controlling Load Combination

The controlling load combination for the diaphragm floor seal is that which includes loads due to a DBA. The load due to pool swell air compression is given in Section 3A.3.2.3. The LOCA pressure and temperature transients are described in Section 3A.3.2.5.

The following individual loads were utilized for load combinations, per ASME Code Section III, Subsection NE in the design of the diaphragm floor seal. The load combinations used are defined in Table 3A.3.5-5.

a.　　　Normal Plant Conditions,

b.　　　OBE,

c.　　　SSE,

d.　　　LOCA,

e.　　　SRV loads with all four valve actuations,

f.　　　Piping loads due to all dynamic loads listed above,

g.　　　The maximum differential pressure, and

h.　　　Relative displacement due to the movement of the primary containment vessel and diaphragm floor.

The fatigue evaluation was performed conservatively using the cycles in Table 3A.4.1-3.

3A.4.1.5.3　　Acceptance Criteria

The acceptance criteria for the analysis of the diaphragm floor seal is as follows:

a.　　　Achieving a positive margin of safety on critical elastic buckling of the seal when considering the maximum convex pressure on the seal due to hydrodynamic loads;

b.   Stress based on elastic analysis of the seal is not to exceed the following:

1.   Average membrane stress intensity is not to exceed the allowable values
defined in ASME Code Section III 1971 through Summer 1972 Addenda
Paragraph NE 3320;

c.   The cumulative usage factor as defined in ASME Code Section III, 1971
through Summer 1972 Addenda, Paragraph NB 3222.4(e) is not to exceed
unity.

3A.4.1.5.4   Method of Analysis

The ANSYS (see Attachment 3A.F) finite element model of the diaphragm floor seal consists
of a 5.2° segment of the omega shaped configuration and the weldolet welding fitting for the
drain pipe. Refer to Figure 3A.4.1-10. Unit differential pressure, unit displacements in the
vertical and radially horizontal directions to represent the differential displacement of the
primary containment vessel and diaphragm floor, unit piping loads at the weldolet, and a
linearized thermal gradient are specified load steps in the analysis. Stresses are calculated by
applying scaling factors to the unit load analyses and superimposing the results. Note that
circumferential differential displacement of the primary containment vessel and the diaphragm
floor in the horizontal plane is prevented by shear lugs furnished along the outer periphery of
the diaphragm floor.

3A.4.1.5.5   Results and Design Margins

The differential displacements, differential pressures, and the piping loads for the critical
loading combinations, as tabulated in Section 3A.4.1.5.2, were used to perform the stress
analysis. The design margin on the elastic buckling of the omega seal as described in
Section 3A.4.1.5.3.a is 34.7. The calculated stress intensity and fatigue values are presented
in Tables 3A.4.1-4 and 3A.4.1-5 respectively.

3A.4.1.6   References

3A.4.1-1   "SRV Loads - Improved Definition and Application Methodology for Mark II
Containments," technical report, Burns and Roe, Inc. Transmitted to NRC by
letter GO2-80-172 dated August 8, 1980.

3A.4.1-2   Letter GO2-82-35, "Responses to CSB Open Items 44 through 48,"
G. D. Bouchey (WPPSS) to A. Schwencer (NRC), January 13, 1982.

3A.4.1-3   Gosh, S. and Wilson, E., "Dynamic Stress Analysis of Axisymmetric Structures
Under Arbitrary Loading," University of California at Berkeley, EEEC,
69-September 10, 1969.

3A.4.1-4   "Chugging Loads - Revised Definition and Application Methodology for Mark II Containments (Based on 4TCO Test Results)," technical report, Burns and Roe, Inc. Transmitted to NRC by letter GO2-81-189 dated July 22, 1981.

3A.4.1-5   ACI Standard 318-71/77, Building Code Requirements for Reinforced Concrete, American Concrete Institute.

Table 3A.4.1-1

Basemat - Stress Resultants at Critical Sections

	Bending Moment (kips per ft)	Beam Shear (kips per ft)	Punching Shear (kips per ft)
D+L+E$_{SS}$	3132	125	315
P$_{SR}$	511	32	32
P$_{B}$	76	1	20
Comb. 7	3649	157	353
Capacity	4230	232	465

Table 3A.4.1-2

Pedestal - Stress Resultants at Base

Load	Overturning Moment - M (ft - kips)	Base Shear - H (kips)
E_O	123,600	1,530
E_{SS}	212,300	2,665
P_{SR}	2,825	719
P_B	5,088	29
(Comb. 7)	212,380	2,760
Capacity	375,000	14,500

Table 3A.4.1-3

Equivalent Stress Cycles for Fatigue Evaluation

Load	Number of Events	Number of Equivalent Stress Cycles per Event	Total Number of Stress Cycles
Operating basis earthquake	5	10	50
Safe shutdown earthquake	1	10	10
SRV[a]	4,478	3	13,434
Chugging	1	1,000	1,000

[a] This includes the cycles due to building motion, direct pressure, and fluid transients during SRV actuations.

Table 3A.4.1-4

Summary of Stress Intensities for Diaphragm Floor Seal

Loading Condition Table 3A.3.5-5	Primary Membrane Stress Intensity				Primary Membrane Plus Secondary Stress Intensity				
	Calculated Stress Int. Pm (ksi)	ASME Allowable		Design Margin	Calculated Stress Int. Pm + Q Range (ksi)	ASME Allowable		Design Margin/ Remarks
		Limit	Stress (ksi)			Limit	Stress (ksi)	
Normal	4.46	Sm	16.56	3.71	26.83	3 Sm	49.68	1.85
Upset	11.84	Sy	25.0	2.11	44.36	3 Sm	49.68	1.12
Emergency	12.89	1.2 Sm	19.9	1.54				Evaluation not required
Faulted	13.82	1.2 Sy	30.0	2.17				Evaluation not required

$$\text{Design Margin} = \frac{\text{Allowable Stress}}{\text{Calculated Stress}}$$

Table 3A.4.1-5

Cumulative Usage Factor Calculation
for Diaphragm Floor Seal

Load Combination Set[a]	Expected Number of Cycles (ni)	Alt. Stress Salt (psi)	Allowable Number of Cycles N	Calculated Usage Factor $U_i = \dfrac{n_i}{N_i}$
1	1	387.0	33	0.03
2	9	204.0	150	0.06
3	50	178.5	250	0.2
4	60	153.4	350	0.172
5	880	74.0	3700	0.238
6	12,434	18.0		0.0

Cumulative Usage Factor U = 0.7 < 1

[a] Load combination set definition

1 - NPC + LOCA + SSE + SRV + CHUGGING
2 - NPC + SSE + SRV + CHUGGING
3 - NPC + OBE + SRV + CHUGGING
4 - NPC + SRV+ CHUGGING
5 - SRV + CHUGGING
6 - SRV

Maximum Water Level. El. 466' - 4 3/4"

Containment
Shell

3' - 2"

Horizontal Tee
Stiffener Ring

WT 8x18   3' - 2"

18"

Typical Detail

2' - 10"

1 1/2"

Vertical Tee
Stiffener WT 8x18

3' - 0"

Containment
Shell

3' - 0"

Typical Detail

2' - 10"

20"   1 1/2"

El. 446'

1' - 8"

	Stiffened Containment in Wetwell Region	
Columbia Generating Station **Final Safety Analysis Report**		
	Draw. No. **960222.85**	Rev.	Figure **3A.4.1-1**

Distance from Base (Inches) — vertical axis: 0, 40, 80, 120, 160, 200, 240, 280, 320, 360, 400, 440, 480, 520, 560, 600, 640, 680

El. 446.0'

Radial Displacement (Inches) — horizontal axis: 0.0, .02, .04, .06, .08, .10

Columbia Generating Station
Final Safety Analysis Report

Displacement Profile
SRV Load - All Valves

Draw. No. **960222.86** | Rev. | Figure **3A.4.1-2**

El. 446.0'

Distance from Base (Inches)

Radial Displacement (Inches)
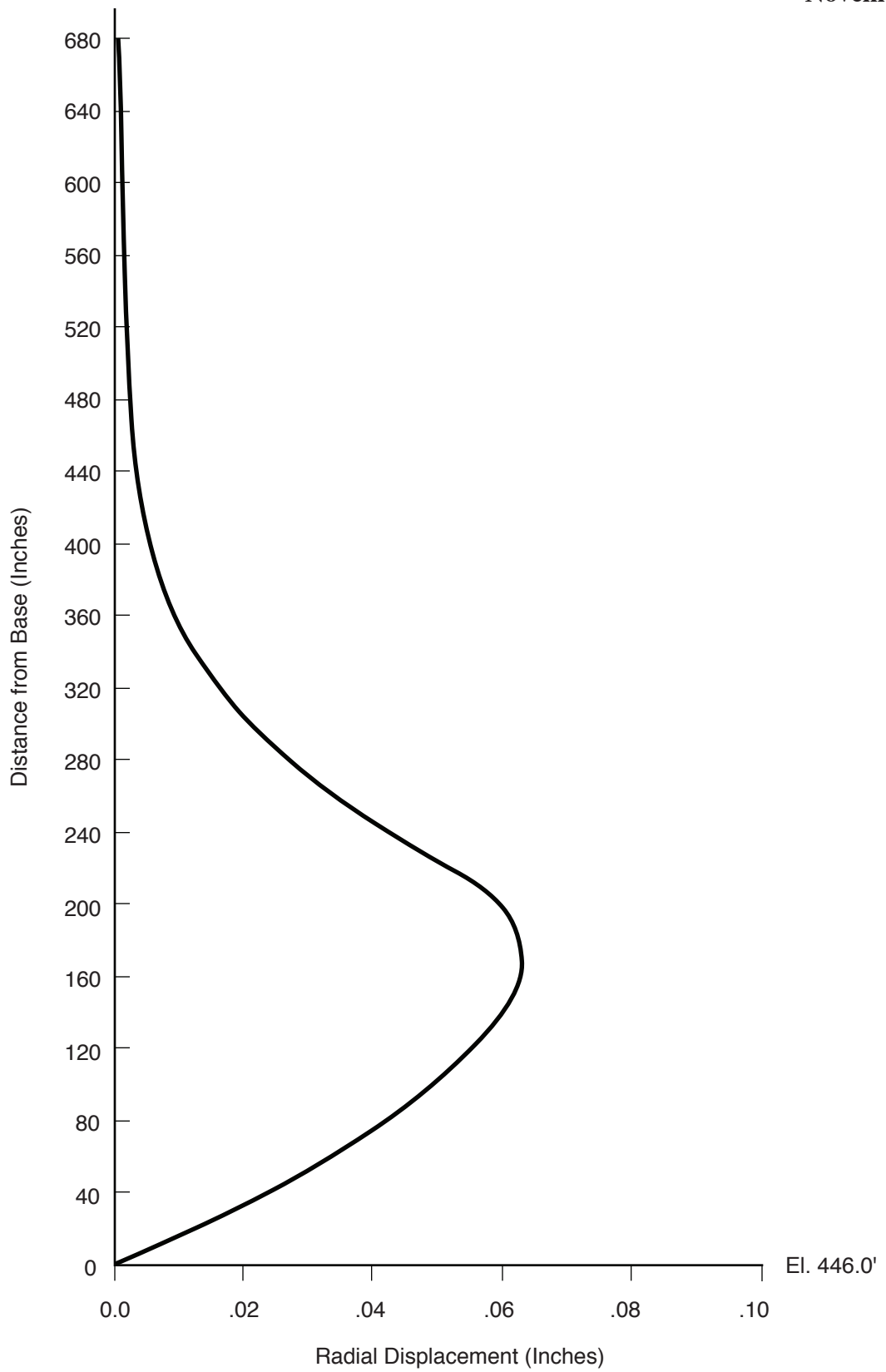
| Columbia Generating Station Final Safety Analysis Report | Displacement Profile Nearly Symmetric Chugging |

Draw. No. **960222.87**   Rev.   Figure **3A.4.1-3**

Form No. 960690

Vertical Tee Stiffener

Containment Shell

Horizontal Tee
Stiffener Ring
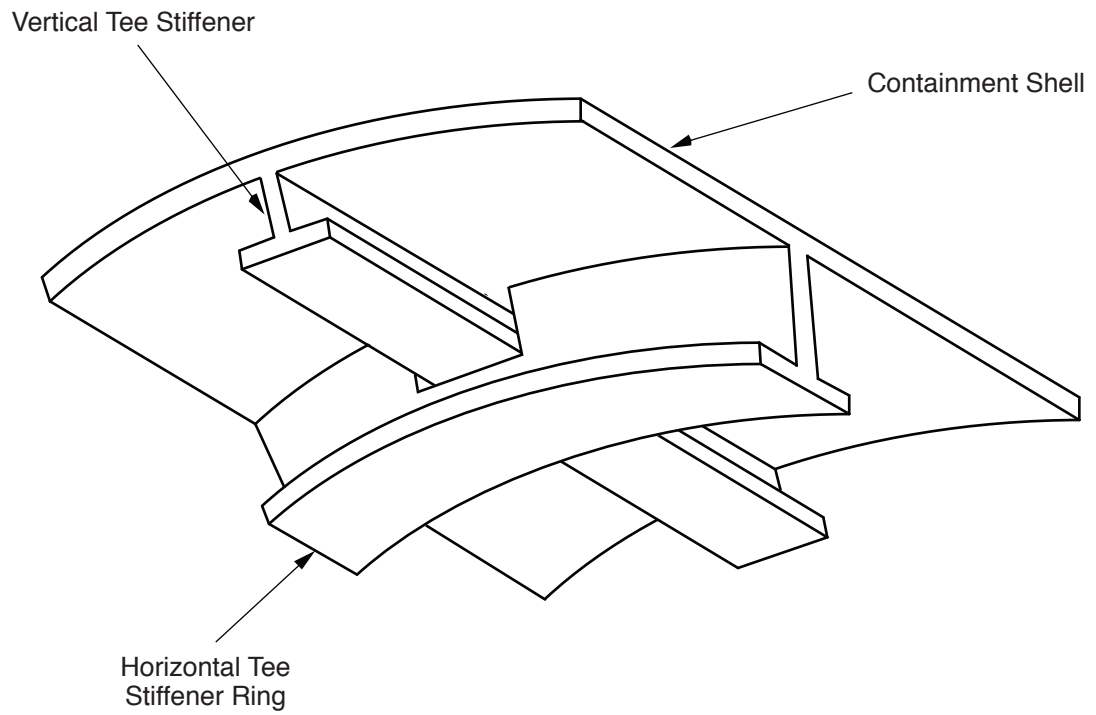
	Stiffener Configuration	
Columbia Generating Station **Final Safety Analysis Report**		
Draw. No. 970187.22	**Rev.**	**Figure 3A.4.1-4**
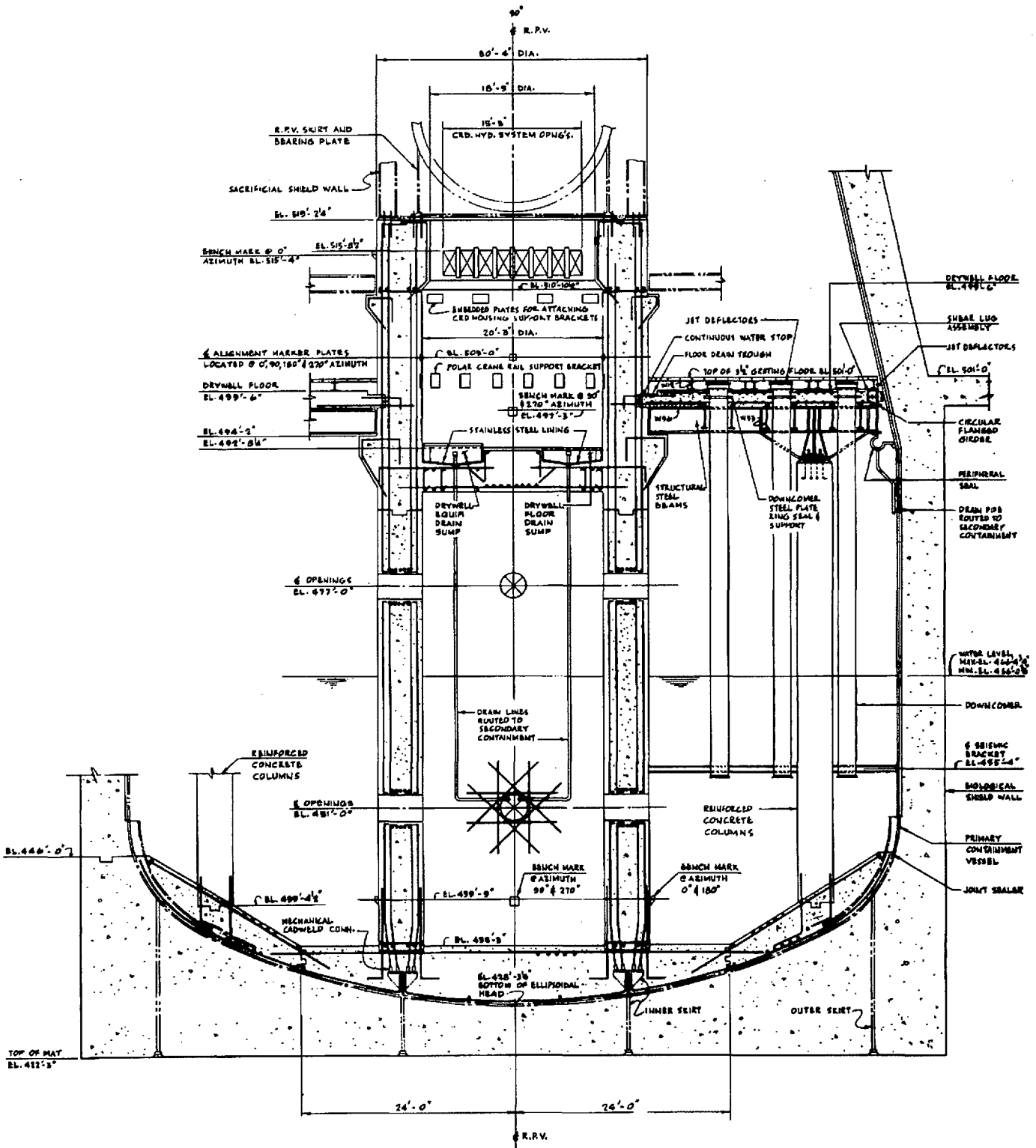
SECTIONAL ELEVATION LOOKING EAST

Columbia Generating Station
Final Safety Analysis Report

Reactor Pedestal, Diaphragm Floor and Columns

| Draw. No. 020361.19 | Rev. | Figure 3A.4.1-7 |

Form No. 960690

Pu: Axial load in KIPS x 10^3

$\begin{cases} Pu = 30,000^k \\ Mu = 513,000^{ft\text{-}k} \end{cases}$

Ao $\begin{cases} P'u = 12380^k \\ M'u = 212,380^{ft\text{-}k} \end{cases}$

P'u = Minimum

$\emptyset = .7$

0.1Po = 19400^k

$\begin{cases} Pu = 12380^k \\ Mu = 375,000^{ft\text{-}k} \end{cases}$

$\ell = M/P = Constant$

$.9 \geq \emptyset \geq .7$

Mu: Bending Moment in Foot-KIPS x 10^4
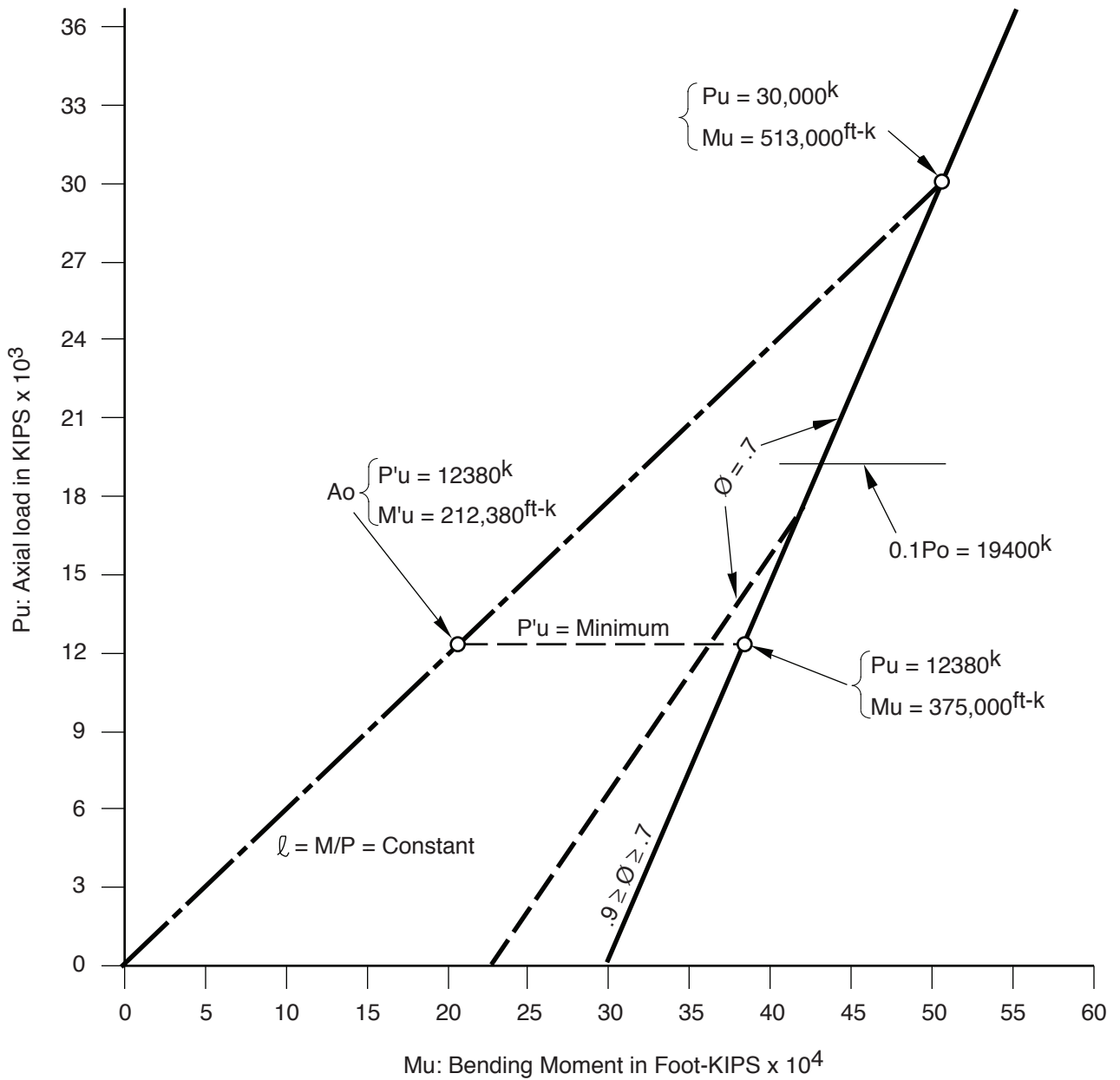
Columbia Generating Station **Final Safety Analysis Report**	**Pedestal-Interaction Diagram** **Axial Load Versus Moment**

| **Draw. No. 960222.90** | **Rev.** | **Figure 3A.4.1-8** |

Form No. 960690

R = 40' - 5 9/16"

Cover P̲L

Jet Deflector P̲L

Curb P̲L

El. 499' - 6"

Male Shear Lug

Female Shear Lug

Containment
Vessel Shell

Continuous P̲L

W 36
Radial Beam

2' - 0"

3' - 0 3/4"

Diaphragm Floor Seal

El. 493' - 5"

2" Drain

R = 41' - 6"
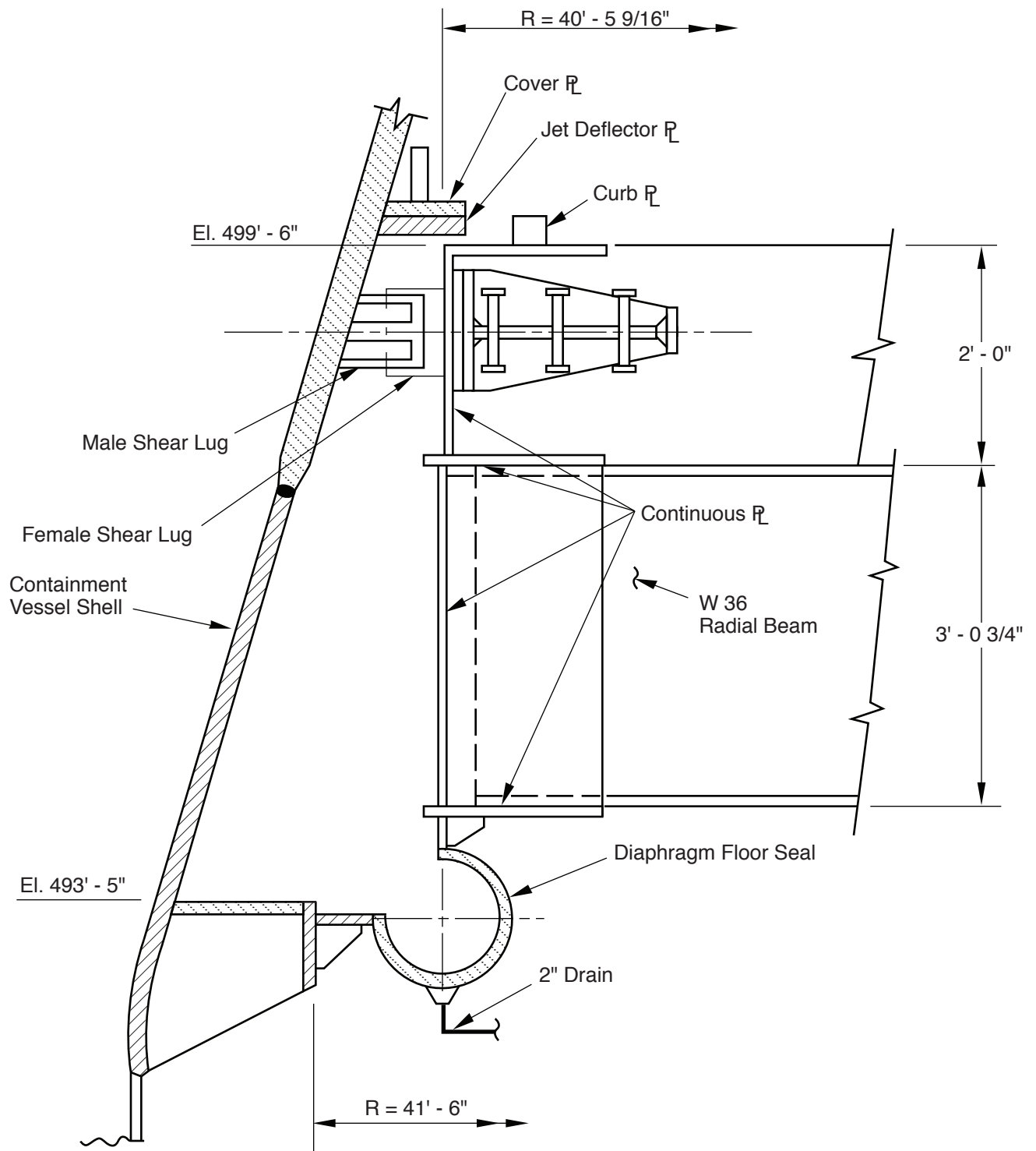
Drywell Diaphragm Floor Seal

Columbia Generating Station
Final Safety Analysis Report

| Draw. No. 960222.88 | Rev. | Figure 3A.4.1-9 |

Diaphragm
Floor Seal

Weldolet Welding Fitting
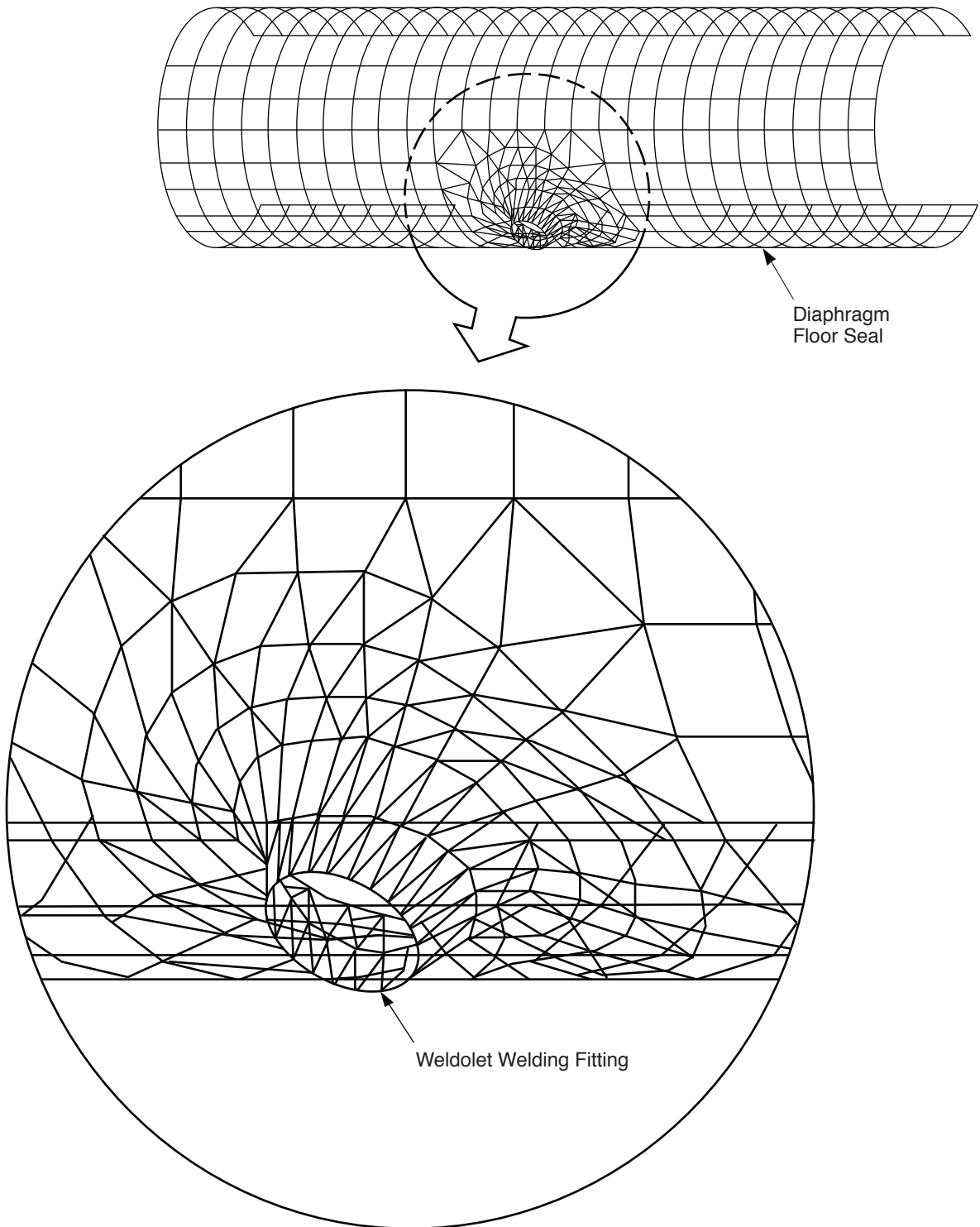
	Finite Element Model Diaphragm Floor Seal
Columbia Generating Station **Final Safety Analysis Report**	
	Draw. No. 990578.01 Rev. Figure 3A.4.1-10

3A.4.2   SUPPRESSION POOL MAJOR STRUCTURES AND COMPONENTS

Assessment of the capacities of the major structures and components of the suppression pool chamber relative to load combinations involving suppression pool hydrodynamic loads is made in this section. The structures considered are downcomer bracing systems columns, downcomers, SRV piping system, quenchers, and platforms.

3A.4.2.1   Downcomer Bracing System

An assessment was made of the capacity of the original design of the downcomer bracing system relative to load combinations involving suppression pool hydrodynamic loads. It was determined that this original bracing, consisting of a system of radial beams, had inadequate capacity. Consequently, a replacement pipe truss bracing system was designed and installed. The assessment of the capacity of this pipe truss system relative to the load combinations involving suppression pool hydrodynamic loads is made in this section.

3A.4.2.1.1   Description of System

The pipe truss system of downcomer bracing is shown in Figure 3A.4.2-1. Like the original system, the function served by the pipe truss system is to provide horizontal support for the 102 downcomers, (three of which are capped as discussed in Sections 3A.3.2.1 and 3A.3.2.2) and the 18 SRV discharge pipes at a level near the lower end of the downcomers.

The pipe truss system consists of a horizontal planar truss located with center line at the same elevation as the original system. The model of the truss used in the structural analysis is shown in Figure 3A.4.2-2. In the truss system, the downcomers and the SRV lines are located at the truss nodes. Structural rings are provided around each downcomer and each SRV pipe for connections by the truss members. The truss members are 4-in. and 6-in. double extra strong steel pipes. Connections of the truss to the RPV pedestal and to the containment vessel are at the same connection points as the original radial beams.

As described in Section 3A.4.2.1.2, the pipe truss system is subjected to both horizontal and vertical loads. Horizontal reactions from the downcomers and from the SRV pipes are applied to the encircling structural rings which form the truss nodes. Horizontal forces applied directly to the truss members are also carried by the members to the truss nodes. By truss actions these horizontal loads are transmitted to the supports at the RPV pedestal and at the containment vessel. The pedestal connection can sustain both radial and circumferential reaction components due to horizontal loading; however, the vessel reaction is circumferential because the connection is free to move radially.

Vertical loadings, due to the various causes listed in Section 3A.4.2.1.2, act directly on the pipe truss system. To carry these vertical loadings, supports are provided against upward and downward motion at each of the downcomers; also the connections to the pedestal and vessel

are restrained vertically. Vertical forces acting on each truss member are carried to its ends at the structural rings, pedestal, or vessel connections. The structural rings around the downcomers are independent of the downcomers but stops are welded to the downcomers to prevent differential vertical motion. The structural rings around the SRV lines are independent of these lines and no restraint against differential vertical motion is provided. Vertical loads from the rings on the downcomers are transmitted by the downcomers to the drywell floor.

3A.4.2.1.2   Loads Used for Assessment

A complete description of all hydrodynamic loads is given in Section 3A.3. In this section only the loads used for the assessment of the bracing system are discussed. Symbols used in this section are defined in Section 3A.3.5.3 in connection with load combinations.

3A.4.2.1.2.1 Safety/Relief Valve Actuation Loads. Safety/relief valve actuation causes horizontal and vertical loading on the bracing system as unbalanced pressures and induced accelerations of supported components occur. The pressures and accelerations acting on the downcomers, the SRV pipe lines, and the bracing members cause the horizontal loading; the vertical loading is due to these actions on the bracing system alone. The spatial distribution of these loads is discussed under Methods of Analysis (Section 3A.4.2.1.4).

Loads due to the SRV pressures and induced accelerations are applied to the bracing system as equivalent static loads. The magnitudes of the loadings from the downcomers and SRV lines are based on analyses of each of these components as described in the assessments of the components in Sections 3A.4.2.3 and 3A.4.2.4 respectively. The pressure loadings on the bracing members proper are equivalent static pressures as defined in Section 3A.3. Reactions due to the pressures on the downcomers, SRV lines, and truss members are applied at the truss nodes.

The forces due to the induced accelerations of the downcomers, SRV lines, and bracing members are obtained by analysis of these structures using the response spectra developed for SRV actuation. These forces from downcomers, SRV lines, and bracing members are also applied as reactions at the truss nodes.

3A.4.2.1.2.2 Loss-of-Coolant Accident Loads. Loss-of-coolant accidents are characterized by several phenomena causing nonconcurrent loadings on the bracing system. The principal nonconcurrent loadings are short-term pool swell pressure and fallback pressure loads and long-term chugging loads. Other significant loads are short-term jet and bubble loads and long-term condensation oscillation loads. Pool swell and fallback are basically vertical motions and generally applied vertical pressures are associated with each. The chugging loads result from lateral forces at the downcomer exits, from horizontal and vertical accelerations induced by building motion, and from chugging pressures on the wetwell components supported by the bracing system. The horizontal accelerations of the downcomers, SRV lines,

and bracing members contribute to the horizontal loading of the bracing, whereas the vertical acceleration of only the bracing members causes vertical loading of the bracing.

a.   Pressure due to pool swell

The pool swell pressures acting on the bracing system are determined to be 25 psi upward and 5 psi horizontal including the DLF, applied concurrently;

b.   Pressure due to fallback

Fallback pressures acting on the bracing system are determined to be 25 psi downward and 5 psi horizontal including the DLF, applied concurrently;

c.   Lateral forces at downcomer exits

The characteristics of these lateral exit loads are described in Section 3A.3.2.4.4. As noted therein, the lateral exit loads are dynamic loads whose amplitude depends on the size of the downcomer and the number of concurrently loaded downcomers. For an assumed number of concurrently loaded downcomers, the axial forces in the members of the bracing system and the reactions at the supports are determined by dynamic analysis of the system. Determination of the critical number of downcomer exits which are subjected simultaneously to lateral force is described subsequently under Methods of Analysis (Section 3A.4.2.1.4);

d.   Induced accelerations due to chugging

The forces due to the induced accelerations of the downcomers, SRV lines, and bracing members are obtained by analyses of these structures using the response spectra developed for chugging action. Forces from these components are applied on the bracing system as reactions at truss nodes;

e.   Chugging pressures

Chugging pressures are applied on the members of the bracing system and on the inner row SRV lines as described in Section 3A.3.2.4.3.2. Equivalent static loads constituting the end reactions due to the pressures on these components are applied at the truss nodes; and

f.   Other LOCA loads

The other LOCA loads mentioned above are now considered. It is noted that the short-term loads due to LOCA jet and bubble are smaller in magnitude than

the previously considered SRV pressure loads which cannot occur simultaneously with them. Hence, these short-term loads are not controlling. Similarly, it is determined that the long-term condensation oscillation loads are smaller than loads due to chugging which occur subsequently. Therefore, the condensation oscillation loads also are not controlling.

3A.4.2.1.2.3 Other Significant Loads. Seismic forces represent a significant loading on the bracing system. The forces due to the seismic accelerations of the downcomers, SRV lines, and bracing members are obtained by analysis of these structures using the response spectra developed for OBE and SSE. The forces from downcomers, SRV lines, and bracing members are applied as reactions at the truss nodes.

Dead load of the bracing system and thermal loads are also included in the assessment. Thermal loads result from temperature change of the bracing system and from reactions on the bracing system from supported piping.

3A.4.2.1.3   Controlling Load Combinations and Acceptance Criteria

The load combinations and acceptance criteria pertinent to the downcomer bracing are those listed in Section 3A.3.5.3. Based on the results of the analysis, it is determined that, for the loading conditions involved, the controlling combinations with associated allowable stresses are those listed below. Only the significant load terms are included.

Service load conditions:

$$(1) \qquad S \geq D + P_{SR}$$

Factored load conditions:

$$(5) \qquad 1.6\, S \geq D + T_A + E_O + P_B + P_{SR}$$

$$(7) \qquad 1.7\, S \geq D + T_A + E_{SS} + P_B + P_{SR}$$

Further description as to the loads included in the design loading conditions is presented under Method of Analysis.

3A.4.2.1.4   Method of Analysis

Structurally, the pipe truss downcomer bracing system is treated as a plane truss with respect to horizontal loads and as an assembly of beams with respect to vertical loads. The horizontal planar pipe truss is supported externally at 17 equally spaced points around the pedestal and at an equal number of points at the containment vessel. Prior to the truss analysis, the reactions due to the distributed loads along the downcomers and along the SRV lines and bracing

members are calculated and these reactions are applied directly at the truss nodes. The
analysis methods, design loading conditions, and principal results are described below.

3A.4.2.1.4.1 Analysis for Horizontal Loads.

    a.   The analysis uses the proprietary computer program "Mc Auto STRUDL".

    b.   The structural model used in the analysis is shown in Figure 3A.4.2-2. The
model represents the actual configuration of the north half of the symmetrical
structure except for adjustments along the omitted half structure.

    c.   The truss and its connections are treated as pin connected so that the truss
members carry only axial load.

    d.   All loads are taken to act at the nodes in the truss analysis. The effect of truss
member bending under distributed normal loads is considered in member design
where combined axial load and member bending is provided for.

    e.   The STRUDL analysis furnishes truss member axial loads and reaction
components as well as displacements of nodes.

3A.4.2.1.4.2 Analysis for Vertical Loads.

    a.   Vertical loads on the bracing system, i.e., on bracing members and on rings,
are transmitted through bending and shear to supports on the downcomers and at
the pedestal and vessel. Combined axial load and member bending is provided
for in the design.

    b.   Downcomers and diaphragm floor are investigated for the resultant vertical
loads.

3A.4.2.1.4.3 Design Load Conditions. The spatial distribution, direction, and magnitudes of
possibly coincident loads as described below are used in the controlling load combinations;
two critical loading conditions are adopted as a conservative basis of design. By these loading
conditions it is intended to maximize stresses and reactions in specific portions of the
half-structure. These critical stresses and reactions are then utilized to design all similar
members and supports around the entire structure. The two conditions utilized in the design are
noted below.

    a.   Condition 1: Maximum Horizontal Loading

        This loading is intended to result in greatest stresses in the members and
supports in the vicinity of the north-south and east-west axes. The directions of

building motions and applied pressures and loads are selected so as to maximize overall loading in the south to north and west to east directions. (Refer to truss layout in Figure 3A.4.2-2.) Associated vertical loads are also included.

1. SRV actuation

    a) Building motions due to all valve actuation and due to single valve actuation are considered. The building motions cause reactions at all downcomers and SRV lines and accelerations of all truss members. Radial forces and accelerations are directed outward; circumferential forces and accelerations are clockwise. Reactions of downcomers, SRV lines, and members act on the truss nodes.

    b) Unbalanced pressures due to all valve and single valve actuation are included. Varying pressures depending on distance from the active nodes are applied to all downcomers, SRV lines, and bracing members. The resulting reactions from these components act at the truss nodes. The direction of reactions from downcomers and SRV lines is generally along the line from the active node to the structure. For the bracing member, the pressures and reactions are normal to the bracing member.

    c) Vertical loads on the pipe truss are due to dead load, building motion induced acceleration, and unbalanced pressure.

2. Long-term LOCA loads (chugging)

    a) In the analysis, the number of downcomers subjected to lateral exit loads is varied from one to all 51 downcomers in the model structure. Two directions of load application are considered: south to north and west to east. It is determined that controlling effects are always due to loading of a single vent. In this regard it is noted that the lateral load definition in Section 3A.3.2.4.4 provides a high intensity load for single vent loading as compared to multiple vent loading.

    b) Building motion due to chugging causes reactions at all downcomers and SRV lines and accelerations of all truss members. Radial forces and accelerations are directed outward; circumferential forces and accelerations are clockwise. Reactions of the downcomers, SRV lines, and truss members act on the truss nodes.

      c)   Chugging pressures on the interior SRV lines result in radially outward reactions applied at the truss nodes.

      d)   Vertical loads on bracing members are due to building motion induced accelerations and chugging pressure. In addition, inclination of bracing members during LOCA caused by downcomer temperature growth results in vertical component of member axial force as an additional reaction on the downcomer.

3.   Seismic

      a)   Eastward, northward, and vertical seismic actions are included. Both OBE and SSE are considered.

      b)   In west-east seismic action, all downcomers and SRV lines react against the bracing towards the east. All bracing members have accelerations eastward. Corresponding northward effects result from south-north seismic action.

      c)   Vertical loads on bracing members are due to vertical accelerations;

b.   Condition 2: Maximum Vertical Loading

The vertical loads associated with Condition 1 which involve controlling horizontal loads have been previously stated. To determine the maximum vertical loading, short-term LOCA events are investigated. Loads included under Condition 2 are described below.

1.   SRV actuation

The acceleration and pressure loads due to single valve actuation are included.

2.   Pool swell or fallback

The vertical statically equivalent pressures due to pool swell or fallback are 25 psi on pipe truss members and on truss rings at downcomers and SRV lines.

3.   Seismic

Horizontal and vertical loadings are the same as described above for Condition l.

4.   Additional DBA effects

Inclination of bracing members during DBA caused by downcomer temperature growth results in a vertical component of member axial force as an additional reaction on the downcomers. Also, building motion results in vertical acceleration of the bracing members. However, this acceleration has relatively small magnitude.

5.   Coincident member axial loads

Such axial loads are caused by single SRV actuation and by seismic loading.

3A.4.2.1.5   Results and Design Margin

The principal results of the analysis and the resultant design margins are stated below.

3A.4.2.1.5.1 Principal Results.

a.   Bracing members

These members are designed for combined stress involving axial force and biaxial bending. Members connecting to the pedestal are 6-in. double extra strong steel pipe; all other members are 4-in. double extra strong steel pipe;

b.   Node rings

These rings are designed for a combination of radial loads which is conservative based on the design loading conditions. As a result of this analysis, built-up H-sections 5 in. wide by 7 in. high at the downcomers and 4 in. wide by 6 in. high at the SRV lines are used. Material is high strength structural steel (ASTM A 572, Fy = 60 k.s.i.);

c.   Pedestal connections

The existing embedded plates for the original radial beam system are utilized in the pipe truss system. Additional strengthening was installed based on the design loading conditions. Six concrete anchors were added at each pedestal connection; and

d.   Containment vessel connection

The pipe truss end bearing at the containment vessel fits into the existing socket provided for the original radial beams. The containment vessel redesign includes the reactions due to the downcomer bracing design loading conditions.

3A.4.2.1.5.2 Design Margins. The design margins provided by the pipe truss bracing system are discussed in this section. The design margin for a structural component or system refers to the controlling design parameter such as bending stress for a flexural member and sum of the amplified stress ratios for the case of combined axial and bending stress. The design margin is then defined as the ratio of the permissible value of the design parameter to the value of the design parameter under design loading.

Table 3A.4.2-1 lists the controlling design margins for each of the six principal structural components of the pipe truss bracing system, namely, 6-in. pipe members, 4-in. pipe members, pedestal connection, vessel connection, downcomer ring, and SRV line ring. The calculated design margins are listed in the table for the cases of maximum horizontal or vertical loading (Conditions 1 or 2), under both service load and factored load conditions.

3A.4.2.2   Columns

The assessment of the capacity of the columns relative to load combinations involving suppression pool hydrodynamic loads is presented in this section. The columns and adjoining structures are shown in Figure 3A.4.2-3.

3A.4.2.2.1   Loads Used for Assessment

A complete description of all hydrodynamic loads is given in Section 3A.3. Seismic loads are described in Section 3A.3.5. In this section, only the loads used for the assessment of the columns are discussed. Symbols used in this section are defined in Section 3A.3.5.2 in connection with load combinations.

3A.4.2.2.1.1 Safety/Relief Valve Actuation Loads. Actuation of the SRVs results in four different load effects on the columns. These are unbalanced bubble pressure on the columns, column accelerations associated with resultant building motions, quencher discharge water jet loads, and secondary effects from pressure loading of the downcomer bracing truss.

Maximum bubble pressures applied laterally on the column are defined for two cases, namely, initial actuation and subsequent actuation. The spatial distributions of the maximum pressure loading on the column corresponding to these two cases are shown in Figure 3A.3.1-8. The DLFs associated with these maximum pressure loadings are functions of the column modal frequencies as shown in Figure 3A.3.1-10. The maximum dynamic column reactor loads for the subsequent actuation load case are documented by Reference 3A.3.1-9 and are tabulated in Table 3A.4.2-2. The structural model used for the dynamic analysis of the column under lateral load is described in Section 3A.4.2.2.3 and shown in Figure 3A.4.2-4.

The horizontal and vertical accelerations due to building motion are based on the response spectra developed for SRV actuation in Section 3A.5.1. The horizontal (lateral) accelerations are used in the dynamic analysis of the column by the response spectrum method in conjunction with the structural model described in Section 3A.4.2.2.3 and shown in Figure 3A.4.2-4. The axial (vertical) forces in the column are obtained from the vertical response spectra by a dynamic analysis by the response spectrum method; a structural model, which includes both the diaphragm floor beam and the column, is used and is shown in Figure 3A.4.2-5.

The quencher jet drag load on the column is small in comparison with the bubble load. Since the two loadings do not occur simultaneously, the jet loading is not a controlling loading. The direct vertical pressure loading on the downcomer bracing members is transmitted into the diaphragm floor by the downcomers. The diaphragm floor in turn loads the column. The net loading on the column during the phase of maximum bubble pressure on the column is small and is included in the assessment.

3A.4.2.2.1.2 Loss-of-Coolant Accident Loads. Both short-term and long-term LOCA loads are significant in the assessment of the columns.

Several axial loads on the columns due to short-term LOCA events are considered in the analysis. The overall pressure transient in the drywell and wetwell results in a net downward pressure (20.55 psi equivalent static) on the diaphragm floor and hence an axial compressive column load. The design net upward pressure (5.50 psi) on the diaphragm floor during the pool swell transient causes an upward load on the columns. During LOCA, vertical pressures act on the downcomer bracing system due to bubble charging and due to pool swell and fallback. The resultant vertical forces are transmitted via the downcomers and the diaphragm floor into the columns. However, these forces are not controlling in comparison with the aforementioned net downward and upward pressures on the diaphragm floor. In addition to the pressure loads, the load on the column, due to pipe break/jet impingement on the diaphragm floor, is included in the assessment.

The significant lateral loads associated with LOCA, which are included in the column assessment, are those due to chugging. Lateral loads due to water clearing and due to air

clearing are negligible. The loads due to condensation oscillation are less critical than those due to chugging, and consequently, are omitted from the assessment. The effects of chugging include both direct horizontal pressures on the columns and induced horizontal and vertical accelerations associated with building motions, but only the effects due to building accelerations are significant.

The horizontal and vertical accelerations due to chugging are based on the response spectra described in Section 3A.5.2. Column loading is then developed by dynamic analysis of the column by the response spectrum method in the manner described above for SRV induced building motion. The analysis for horizontal loading uses the structural model of Figure 3A.4.2-4, and the analysis for vertical loading uses the structural model of Figure 3A.4.2-5.

3A.4.2.2.1.3 <u>Other Significant Loads.</u> Dead load, live load, seismic loads, and loads due to annulus pressurization constitute additional significant loads included in the column analysis. The dead load of the diaphragm floor and columns is carried as an axial column load. The live load on the diaphragm floor is transmitted to the columns as an axial load. Horizontal and vertical column loadings are obtained from the seismic response spectra in the same manner as described above for the SRV and LOCA response spectra.

Pressurization of the annulus between the RPV and the sacrificial shield wall, due to a postulated break in either the circulation line or the feedwater line, as described in 6.2.1.2 of the FSAR, results in building motions with associated response spectra. Horizontal and vertical column loadings are obtained from the response spectra in the same manner as described above for the SRV and LOCA response spectra.

3A.4.2.2.2   Applicable Load Combinations and Acceptance Criteria

The load combinations and acceptance criteria for internal reinforced-concrete structures described in Section 3A.3.5.2 are applicable to the columns.

3A.4.2.2.3   Method of Analysis

The structural capacity of the column is investigated for the applicable load combinations with loads as listed above. The general approach in the column assessment is to determine the values of the controlling stress resultants in the column (bending moment, axial force, and shear) on the basis of elastic analysis under design loads and to calculate the capacity of the column in terms of these stress resultants by the strength method of the ACI 318-71 Code (Reference 3A.4.1-5). Three loading cases are investigated. Because of the shape of the column interaction curve for bending and axial load, maximum bending in the column is checked first with minimum coincident axial load and then with maximum coincident axial load. The third loading case involves maximum shears.

The moments, shears, and axial forces are obtained for each of the significant loads. The column is analyzed dynamically via a modal time-history technique (Reference 3A.3.1-9) for the directly applied SRV pressures and for the loads due to the building motion accelerations as defined by the SRV chugging, seismic, and annulus pressurization response spectra; dynamic analysis is by the response spectrum method. In the analysis, the column is treated as fixed at its base and simply supported at its top in accordance with actual construction. For the dynamic analysis under lateral (horizontal) loading, the actual structure is modeled as a 17-node beam as shown in Figure 3A.4.2-4. Masses are lumped at the nodes with additional mass provided below pool level to account for the effect of the suppression pool. The axial (vertical) column forces are determined by the dynamic analysis using a structural model which represents the diaphragm floor beam - column system. As shown in Figure 3A.4.2-5, the diaphragm floor mass is included in 26 nodes along the beam and the column mass is 14 nodes along the column. Dynamic analysis for lateral loads and for vertical loads are made using the commercial computer programs STRUDL and IMAGES-3D.

The critical locations along the column for bending moment and shear are determined from the analysis results. Maximum bending moments and shear occur at the column base. The magnitude of the horizontal shear at the top of the column is also noted to verify the adequacy of the top connection. The values of the controlling bending moments, shears, and axial force are listed for each significant loading in Table 3A.4.2-2.

a.   Maximum bending moment with minimum axial load

It is determined that the controlling values of maximum bending moment with coincident minimum axial load occur for load combination (1). This combination is stated below for minimum axial load with only the significant load terms listed.

(1) $1.0 D + 1.5 P_{SR}$

The maximum bending moment is caused by the direct lateral pressure on the column, due to SRV subsequent actuation, and the associated horizontal building motion acceleration. The coincident minimum compression axial load occurs with dead load (D) and upward load due to the vertical building motion acceleration caused by the SRV actuation (P_{SR}). The controlling values of bending moment and axial load are 17.67 ft kips and 173.3 kips (compression), respectively.

The column capacity for combined loading and axial load is determined in accordance with the strength design method of the ACI 318-71 Code (Reference 3A.4.1-5). From the applicable interaction curves, the bending moment capacity of the column, with the above axial load of 173.3 kips, is found to be 2182.0 ft kips;

b.   Maximum bending moment with maximum axial load

The controlling coincident values of bending moment and axial load occur for
load combination (1). This combination is stated below for maximum axial load
with only the significant load terms listed.

(1) $1.4\,D + 1.7\,L + 1.5\,P_{SR}$

The maximum bending moment is caused by SRV subsequent actuation as in
(a) above. The coincident maximum compressive axial load is due to dead load
(D), live load (L), and downward load due to the SRV actuated building motion
(P_{SR}). The controlling value of the axial load is 745.2 kips. As a result of
moment magnification due to the axial load, the controlling value of the bending
moment is increased from 1700 ft kips to 1869 ft kips. Utilizing the column
interaction curves, the bending moment capacity is found to be 2230.5 ft kips;

c.   Maximum shear

As noted previously, maximum column shear occurs at the column base.
Column shear capacity is affected by the axial force at the section. The
controlling load combination for column shear is load combination (1) which is
stated below for minimum axial load with only the significant loads listed.

(1) $1.0\,D + 1.5\,P_{SR}$

The maximum shear is caused by the same event as in (a) above, namely, SRV
subsequent actuation (P_{SR}). The coincident minimum compressive axial load
occurs with dead load (D) and SRV actuation (P_{SR}). The controlling values of
shear and axial load are 142.4 kips and 173.3 kips (compression), respectively.
Utilizing the strength design method of the ACI 318-71 Code
(Reference 3A.4.1-5), the column shear capacity is calculated to be 376.9 kips;
and

d.   Column top shear connection

The controlling top horizontal reaction in relation to the capacity of the top
connection in shear occurs with load combination (1) with minimum axial
(compressive) load. This combination is stated below.

(1) $1.0\,D + 1.5\,P_{SR}$

The top horizontal reaction is caused in this case by SRV initial actuation (P_{SR}); its magnitude is 62.1 kips.

The shear capacity of the top connection is due to shear friction associated with the connecting anchor bolts and the superimposed axial load. Conservatively, the superimposed load is due to dead load (D) reduced by the upward load due to SRV actuation (P_{SR}). Utilizing the strength design method of the ACI 318-71 Code (Reference 3A.4.1-5), the shear capacity of the top connection is 75.5 kips.

3A.4.2.2.4   Results and Design Margins

It is determined that the columns have adequate capacity with regard to the applicable load combinations involving suppression pool hydrodynamic loads. The design margins with respect to the significant stress resultants are noted below:

a.   Maximum bending moment with minimum axial load - The smallest design margin representing the ratio of column bending capacity to applied bending moment, with minimum axial load, is 1.54;

b.   Maximum bending moment with maximum axial load - The smallest design margin representing the ratio of column bending capacity to applied bending moment, with maximum axial load, is 1.49;

c.   Maximum column shear - The smallest design margin representing the ratio of the column shear capacity to the applied shear is 3.23; and

d.   Column top shear connection - The smallest design margin representing the ratio of the capacity of the column top connection in shear to the applied top shear is 1.18.

3A.4.2.3   Downcomers

The primary function of the downcomer vent system is to channel the steam accumulating in the drywell chamber during a LOCA into the wetwell chamber to accomplish pressure suppression (see Section 3A.3.2.1).

The downcomer vent system consists of eighty-three 24-in. OD and sixteen 28-in. OD standard schedule carbon steel pipes running vertically downward from the diaphragm floor (except that the ends of the downcomers are stainless steel as described in FSAR Section 3.8.3.4). Originally 102 downcomers were provided, but three (one 24-in. and two 28-in.) were capped, as discussed in Sections 3A.3.2.1 and 3A.3.2.2. The downcomers are embedded in the diaphragm floor and extend down to el. 454 ft 4.75 in. All downcomers

are restrained laterally at el. 455 ft 4 in. by the downcomer bracing system, which is vertically restrained by the downcomers. Vertical loads are imposed by the bracing system onto the downcomers and transmitted to the diaphragm floor. (See Figures 3A.2.1-5 and 3A.2.1-6.)

Nine of the 24-in. OD downcomers have an extra strong welding tee at el. 491 ft 11 in. to accommodate 24-in. dual inline vacuum breaker valves. In addition, to provide extra strength, the eighteen 28-in. downcomers have been stiffened by the insertion of a 4-ft 8-in. long by 2-in. thick spool piece. This piece accommodates the penetration for the main steam SRV (MSRV) piping which is welded to these downcomers at el. 493 ft 0 in.

Figure 3A.2.1-4 shows locations where the vacuum breaker valve assemblies and the MSRV piping penetrate the downcomers just below the diaphragm floor.

3A.4.2.3.1   Loads Used for Assessment

The downcomer piping is subjected to static, dynamic, and hydrodynamic loads under the various plant operating conditions identified as normal, upset, emergency, and faulted. Each of these loads in various combinations is identified in Section 3A.3.5.4.

The individual loads acting on the downcomers are identified below:

　　　a.　　Deadweight (W)

　　　b.　　Thermal expansion and thermal transient

　　　c.　　Pressure (P)

　　　　　　The pressure differential between the drywell and suppression chamber atmospheres produces loads on the downcomer walls since it acts as a pressure retaining boundary during a LOCA.

　　　d.　　OBE

　　　e.　　SSE

　　　f.　　SRV discharge dynamic loads

　　　　　　The spatial distribution of the maximum direct bubble pressure loading used for downcomer assessment was obtained by multiplying a dynamic pressure load (Figure 3A.3.1-7) by the maximum DLF.

　　　　　　A maximum DLF of 4.2 was conservatively obtained from the response spectrum of DLFs shown in Figure 3A.3.1-10.

The inertia loading effects due to the acceleration of the structure are described in Section 3A.5.1. The response spectra used for downcomer assessment are the enveloped spectra which were developed by enveloping the spectra due to four SRV actuation cases at the appropriate locations for the downcomers.

g.   LOCA loads

The loads on the downcomer associated with LOCA are chugging pressure, condensation oscillation pressure, and the building response loading during LOCA event.

The spatial distribution of condensation oscillation and chugging pressure loadings on downcomers are considered as equivalent static pressure loads.

The pressure distribution for the condensation oscillation on downcomers is bounded by chugging load and therefore is not a controlling load.

The LOCA jet, LOCA bubble, pool swell, and fallback loads are identified to be negligible on downcomers as described in Section 3A.3.2, hence, these loads are not considered in downcomer analysis.

The input response spectra for chugging and condensation oscillation are based on the spectra described in Section 3A.5.2 and are enveloped in the same manner as described in the previous section for SRV load.

3A.4.2.3.2   Load Combination and Acceptance Criteria

The resultant stresses experienced by the downcomers are considered acceptable if they satisfy the ASME Boiler and Pressure Code, Section III, Subsection NC (Reference 3A.4.2-1).

The allowable stress "S_h" for both the 24-in. and 28-in. OD downcomers is 15,000 psi. This value was obtained from the tabulated values in Section III, Attachment 3A.I for "S_h" at a design temperature of 340°F, for carbon steel SA 155 KCF 70 and SA 106, GR.C.

Allowable Stress Limits (Equation 9 of NC-3652 and NC-3611, Reference 3A.4.2-1)

The stress includes the primary membrane plus the primary bending stresses. The limits of these stresses depend on the loading conditions as follows :

a.   The limit of stress under the upset condition is $1.2S_h$ = 18,000 psi,
b.   The limit of stress under the emergency condition is $1.8S_h$ = 27,000 psi, and
c.   The limit of stress under the faulted condition is $2.4S_h$ = 35,000 psi.

3A.4.2.3.3   Method of Analysis

Downcomers were analyzed for the appropriate loading combination using the computer program ADLPIPE (Attachment 3A.F).

The mathematical model for the downcomer is a vertical pipe anchored at the underside of the drywell floor and guided at the downcomer bracing system. The inertia effect of water surrounding the submerged portion of the downcomer was obtained by the addition of a virtual mass of water distributed along the submerged portion. The mass of water inside the submerged portion of the downcomers was conservatively considered in the model for all dynamic loadings. The SRV discharge lines were incorporated in the model of the 28-in. downcomer.

3A.4.2.3.3.1   Static Analysis.   Static analysis techniques were used to determine the stresses due to dead weight, internal pressure, thermal and hydrodynamic loads using an equivalent static pressure load, or an appropriate DLF, as shown in Figure 3A.3.1-10.

3A.4.2.3.3.2   Response Spectrum Analysis.   The response spectrum method of analysis was performed, for seismic and hydrodynamic loads, using the ADLPIPE program. Modal responses were combined in accordance with Regulatory Guide 1.92 while damping values were selected per Regulatory Guide 1.61.

Spatial components were combined by the SRSS method, with the exception of seismic which used the higher of the absolute sum of (a) north-south and vertical or (b) east-west and vertical (see Section 3.7 of the FSAR).

3A.4.2.3.4   Results and Design Margin

The downcomers were analyzed for all load combinations described in Section 3A.3.5.4. The stresses in the 24-in. OD and 23-in. OD downcomers pipe show that they are structurally adequate for all plant operating conditions. The design margins for the 24-in. and 28-in. downcomers in each criteria category are summarized below. The lowest design margin is shown to be 1.08.

<div align="center">24-in. Downcomer</div>

Acceptance Criteria From Table 3A.3.5-5	Allowable Stress	Calculated Stress	Design Margin
Upset	18,000	15,513	1.16
Emergency	27,000	15,709	1.72
Faulted	36,000	18,810	1.91

<u>28-in. Downcomer</u>

Acceptance Criteria From Table 3A.3.5-5	Allowable Stress	Calculated Stress	Design Margin
Upset	18,000	16,654	1.08
Emergency	27,000	16,744	1.61
Faults	36,000	18,371	1.96

Design margin is defined as follows:

$$DM = \frac{\text{Allowable Stress}}{\text{Calculated Stress}}$$

3A.4.2.3.5   Fatigue Evaluations

The fatigue evaluation presented below was an NRC request and is not an ASME requirement.

The fatigue evaluation of 24-in. and 28-in. downcomer lines in the wetwell air volume was performed using ASME Section III, Class 1 rules (NB-3600). A governing loading scenario, based on the DFFR (Reference 3A.3.2-1), was developed. The loadings which were evaluated are:

a.   Internal pressure,
b.   Thermal expansion and transients,
c.   Seismic,
d.   Pressure differential effects between drywell and suppression chamber,
e.   SRV pool load and building response, and
f.   Chugging pool load and building response.

Equivalent numbers of fatigue cycles were determined for dynamic loads. The 24-in. and 28-in. downcomers were analyzed for the appropriate load combinations and their associated number of cycles as presented in Table 3A.4.1-3. The combined stresses and corresponding equivalent stress cycles were computed to obtain the fatigue usage factor. The maximum fatigue usage factor for both downcomers are presented in Tables 3A.4.2-4 and 3A.4.2-5.

3A.4.2.4   <u>Safety/Relief Valve Piping Systems</u>

The MSRV piping in the suppression chamber consists of 18 independent piping systems, each comprised of 10-in. and 19-in. OD Schedule 80 carbon steel pipe. The wetwell portion of each SRV piping system in the wetwell originates from a 28-in. downcomer (anchor point),

which penetrates at el. 493 ft 0 in., and then runs horizontally for a sufficient length to provide enough thermal flexibility. The horizontal run also allows the quenchers to be distributed evenly about the suppression pool. The piping then drops vertically downward to the quencher body which is bolted to the quencher support at el. 447 ft 0 in. The quencher support is modeled as an integral part of the SRV piping system and as such has flexibility taken into account. A schematic showing a typical SRV piping layout is shown in Figure 3A.4.2-6. Lateral guides are provided at the downcomer bracing.

3A.4.2.4.1   Loads Used for Assessment

The SRV piping systems are subjected to static, dynamic, and hydrodynamic loads due to normal, upset, emergency, and faulted plant operating conditions. The loading cases and combinations are described in Section 3A.3.5.4.

The hydrodynamic loads resulting in significant effects on the SRV piping are listed below. For a description of these loads see Section 3A.4.2.3.1.

    a.   Deadweight (w),
    b.   Thermal,
    c.   Pressure (P),
    d.   OBE,
    e.   SSE,
    f.   SRV pressure (Figure 3A.3.1-9),
    g.   SRV building response,
    h.   SRV blowdown,
    i.   LOCA jet (Figure 3A.3.2-18 and Table 3A.3.2-8),
    j.   LOCA bubble (Figure 3A.3.2-18 and Table 3A.3.2-8),
    k.   Chugging drag (Figure 3A.3.2-19), and
    l.   Chugging building response.

The SRV pressure used in the analysis is applied in the same manner as described in Section 3A.4.2.3.1 for the downcomers. The building response loads are based on the spectra described in Section 3A.5.

3A.4.2.4.2   Load Combination and Acceptance Criteria

The stresses within the SRV piping are acceptable if they satisfy the ASME Boiler and Pressure Vessel Code, Subsection NC. The allowable stress "S_h" used for primary stress evaluation is 15,000 psi. This value was obtained from the tabulated values in Section III, Attachment 3A.I for "S_h" at a design temperature of 475°F for carbon steel.

3A.4.2.4.3   Allowable Stress Limits (Equation 9 of NC-3652 and NC-3611,
                         Reference 3A.4.2-1)

The stress for the SRV piping includes the primary membrane plus the primary bending
stresses. The limits of these stresses depend on the loading conditions as follows:

    a.   The limit of stress under the upset condition is $1.2S_h = 18,000$ psi,
    b.   The limit of stress under the emergency condition is $1.8S_h = 27,000$ psi, and
    c.   The limit of stress under the faulted condition is $2.4S_h = 36,000$ psi.

3A.4.2.4.4   Method of Analysis

The SRV piping was analyzed for the appropriate loading combinations (Table 3A.3.5-5) using
the computer programs ADLPIPE and ANSYS (Attachment 3A.F). Analysis was performed
for all 18 SRV lines. The quencher towers were included in the piping models to account for
quencher tower flexibility. The inertial effects of water were accounted for in the same matter
as described in Section 3A.4.2.3.3. Analysis results are summarized in Section 3A.4.2.4.5.

3A.4.2.4.4.1 Static Analysis. Static analysis techniques were used to determine the stresses
due to dead weight, internal pressure, thermal and hydrodynamic loads using an equivalent
static pressure load or an appropriate DLF, as shown in Figure 3A.3.1-10.

3A.4.2.4.4.2 Response Spectrum Analysis. The ADLPIPE program was utilized to perform
dynamic response spectra analyses. Modal responses were combined in accordance with
Regulatory Guide 1.92 while damping values were selected per Regulatory Guide 1.61.

3A.4.2.4.4.3 Time History Analysis. The ANSYS program was utilized as required for
critical SRV lines in order to obtain more realistic piping response for SRV building response
loads. For SRV blowdown transient loads, ADLPIPE was used to perform a force time
history analysis.

3A.4.2.4.5   Results and Design Margin

The calculated stresses for the design configuration of all SRV piping systems show that the
piping is structurally adequate for all plant operating conditions. The maximum calculated
stresses and the resulting minimum design margins for the SRV piping systems for the
controlling load combinations from Section 3A.3.5.4 are shown below.

Acceptance Criteria from Table 3A.3.5-5	Allowable Stress (psi)	Calculated Stress (psi)	Design Margin
Upset	18,000	17,206	1.05
Emergency	27,000	17,207	1.57
Faulted	36,000	17,280	2.08

Design margin is defined as follows:

$$\text{DM} = \frac{\text{Allowable Stress}}{\text{Calculated Stress}}$$

3A.4.2.4.6   Fatigue Evaluations

The fatigue evaluation presented below was an NRC request and is not an ASME requirement.

The fatigue evaluation on all 18 SRV lines in the wetwell air volume was performed using ASME Section III, Class 1 rules (NB-3600). A governing loading scenario, based on the DFFR (Reference 3A.3.2-11), was developed. The loadings which were evaluated are:

   a.   Internal pressure,
   b.   Thermal expansion and transients,
   c.   Seismic,
   d.   SRV blowdown,
   e.   SRV pool load and building response, and
   f.   Chugging pool load and building response.

Equivalent numbers of fatigue cycles were determined for dynamic loads. All 18 SRV discharge lines in the wetwell region were analyzed for the appropriate load combinations and their associated number of cycles as presented on Table 3A.4.1-3. The combined stresses and corresponding equivalent stress cycles were computed to obtain the fatigue usage factor. The maximum fatigue usage factor for all 18 SRV discharge lines in the wetwell air volume was found to be below ASME allowable limits. The results of the maximum usage factors is presented on Table 3A.4.2-6.

3A.4.2.5   Quencher

Quenchers have been installed on the discharge end of the SRV lines to reduce air clearing loads and to promote effective heat transfer between the suppression pool water and the discharging steam-air mixture during SRV actuation. The quenchers are an integral part of the SRV piping system and are bolted to the quencher support at the base plate. The quencher support assessment is included in the SRV piping system assessment, Section 3A.4.2.4.

3A.4.2.5.1　　Loads Used for Assessment

The quenchers, in common with the other piping components, are subjected to static, dynamic, and hydrodynamic loads due to normal, upset, emergency, and faulted plant conditions. The loading cases arc described in Section 3A.3.5.4.

The mechanical loads are from Table 3-16 of the DFFR (Reference 3A.4.2-2) and modified to account for CGS plant specific conditions. The load from DFFR Table 3-16, which are not plant specific, are the quencher arm and body loads arising from the SRV water and air clearing transients. These generic bounding loads are described in the DFFR (Reference 3A.4.2-2). The other loads on Table 3A.3-16 of the DFFR are modified to account for (a) quencher arm loads caused by the various submerged hydrodynamic loading described in Section 3A.3, and (b) the static and dynamic loads resulting from the SRV piping system analysis described in Section 3A.4.2.4.

3A.4.2.5.2　　Load Combination Acceptance Criteria

The assessment of the quenchers for the plant loads is performed in accordance with ASME Section III, Subsection NC (Reference 3A.4.2-1). The code stamp and hydrotest requirements are not applicable since the quencher is not a pressure retaining component. The code jurisdiction ends at the weld between the SRV discharge piping and the quencher inlet nozzle (12 in. x 24 in. reducer).

3A.4.2.5.3　　Evaluation

The quencher body and the quencher arms are examined to determine their adequacy for conditions of loading described above.

The quencher body together with the quencher arms were modeled through finite element program ANSYS. The model uses a quadrilateral shell element which has both bending and membrane capabilities. The element has six degrees of freedom at each node. This element also has an option for variable thickness. The modeled structure is shown in Figures 3A.4.2-7 and 3A.4.2-8.

Element loading capabilities include surface temperatures and pressures. Also, concentrated loads can be applied at each node point. The significant loads affecting quencher body and the quencher arms are

      a.　　　The loads arising from the SRV water and air clearing transients,

      b.　　　The SRV loads caused by pool velocity and acceleration fields from an adjacent firing quencher, and

c.   SRV induced building response loads.

The quencher assembly was analyzed statically with the load vectors related to type of loads as discussed above and for load combinations presented in Section 3A.4.2.5.2. Since the quencher has linear properties the superposition of load combinations was used for evaluation of results.

The calculated stress intensities for the various loading conditions are presented in Table 3A.4.2-3. The tabulated design margins for the governing upset condition indicate the quencher assembly is structurally adequate.

3A.4.2.6   Platforms and Ladders

The assessment of the capacities of the platforms and ladder relative to load combinations involving suppression pool hydrodynamic loads is made in this section.

3A.4.2.6.1   Loads Used for Assessment

Complete description of all hydrodynamic loads has been given in Section 3A.3. The loads used for the assessment of the platforms and ladder are discussed below.

3A.4.2.6.1.1 Safety/Relief Valve Operation Loads. No direct loads on the platforms at el. 472 ft 4 in. and el. 486 ft 8 in. or the ladder between el. 472 ft 4 in. and 490 ft 1 in. result from operation of the SRV system. However, building response to dynamic pressures at the pool boundary during SRV discharge result in dynamic stresses in the platform and ladder components which are supported from the steel containment structure.

3A.4.2.6.1.2 Loss-of-Coolant Accident Loads. As discussed in Section 3A.3.2.3, a LOCA results in pool swell impact and drag loads and fallback drag loads on the platform at el. 472 ft 4 in. and the ladder between el. 472 ft 4 in. and el. 484 ft 4.75 in. Also, the ladder and the knee braces below the platform at el. 472 ft 4 in. are subjected to a horizontal lift load caused by both pool swell and fallback.

Additional LOCA loads include building responses to condensation oscillation and chugging which are obtained from response spectra at tile points of attachment of the platforms and ladder to the containment vessel. Since the condensation oscillation load is bounded by the chugging load, no separate platform assessment has been performed for the condensation oscillation loading condition.

3A.4.2.6.1.3 Other Significant Loads. Other loads which result in significant stresses in the platform and ladder components are dead loads, live loads, and seismic accelerations.

Dead loads include the weights of the platforms and ladder. Live loads include personnel on the platforms and ladder, equipment weights on the platforms, and the monorail loads on the platform at el. 486 ft 8 in. Seismic accelerations are obtained from seismic response spectra at the points of attachment of the platforms and ladder to the containment vessel.

3A.4.2.6.2   Controlling Load Combinations

The load combination criteria for structures internal to the suppression chamber (see Section 3A.3.5.3) are applicable to the platforms and ladder. In particular, the combinations for steel structures using the elastic working stress method are investigated for both service load conditions and factored load conditions.

3A.4.2.6.3   Acceptance Criteria

The acceptable stress level for the platform and ladder components using the elastic working stress method is as defined for the loading combinations in Section 3A.3.5.3.

3A.4.2.6.4   Method of Analysis

Both platforms and the ladder were investigated for the effects of the loading combinations in Section 3A.3.5.3. The components of the platform at el. 472 ft 4 in. and the ladder were analyzed individually, whereas the platform at el. 486 ft 8 in. is above the effects of pool shell and therefore was not reanalyzed. As noted in Section 3A.3.2.3, the grating does not sustain impact loads. Therefore, the only significant load on the grating is the drag load component. The supporting beams and bracing members were analyzed for drag and lift pool swell/fallback loads. The portion of the ladder between el. 472 ft 4 in. and 404 ft 4.75 in. was analyzed for impact loading on the highest rung in the pool swell region and drag and lift on all rungs below the rung with impact.

3A.4.2.6.5   Results

The governing load combination (5a) for steel structures is given below with corresponding input for the platform at el. 472 ft 4 in. and the portion of the ladder between el. 472 ft 4 in. and 484 ft 4.75 in.:

(5a) $1.6S \geq 1.0D + 1.0L + 1.0E_o + 1.0P_A + 1.0T_A + 1.R_A + 1.0P_{SR}$

$D = 0.10$ psi

$L = 0$

$E_o = 0.11$ psi

P_A = 8.4 psi (drag on gross area of grating)

= 25.0 psi (drag on ladder rungs and bracing members)

= 44.0 psi (impact on ladder rungs)

= small (horizontal lift pressure on supporting bars and handrail members)

= 11.0 psi (horizontal lift pressure on bracing members)

= 5.0 psi (horizontal lift pressure on ladder rungs)

= small (impact and drag on supporting bars and handrail members)

T_A = 0

R_A = 0

P_{SR} = 0.05 psi

where D, L, E_o, P_A, T_A, R_A, and P_{SR} are as defined in Section 3A.3.5.2.

The portion of the ladder between el. 472 ft 4 in. and 484 ft 4.75 in. was found to have sufficient capacity to withstand the governing load combination with a design margin (i.e., ratio of the allowable stress to the maximum absolute calculated stress) of 2.15. However, the existing platform at el. 472 ft 4 in. was found to be deficient (under the above load combination. The critical component is the grating under upward load. To make the grating sufficient, every other bearing bar (instead of every fourth as is in the original design) has been welded to all supporting members including the platform member supporting the ladder. With this reinforcement a design margin for the grating of 1.80 is attained. Also, two platform members have been reinforced, and the rectangular bracing members have been replaced with circular members. With this reinforcement the critical supporting member has a design margin of 1.18.

3A.4.2.7   References

3A.4.2-1   ASME Boiler and Pressure Vessel Code, Section III, Division 1,
              Subsection NC, "Class 2 Components," American Society of Mechanical
              Engineers, 1971 through Winter 1973 Addenda.[*]

_____

[*] Faulted conditions appeared first in Winter 1976 Addenda.

3A.4.2-2   Mark II Containment Dynamic Forcing Functions Information Report (DFFR),
NEDO-21061, Revision 2, September 1976.

Table 3A.4.2-1

Downcomer Bracing System Controlling Design Margins

Component	Service Load Conditions Maximum Horizontal Loading	Factored Load Maximum Horizontal Loading	Conditions Maximum Vertical Loading
6 in. D.E.S. pipe	3.45		2.96
4 in. D.E.S. pipe	2.5		1.68
Pedestal connection	2.00	2.02	
Vessel connection	5.26		2.75
Downcomer ring	1.92	1.95	
SRV line ring	3.39	4.12	

Notes:

1.   For service load conditions, load combination (1) controls. Only maximum horizontal loading is applicable.

2.   For factored load conditions, load combination (5) controls. Only the design margin for the controlling loading is listed.

Table 3A.4.2-2

Controlling Stress Resultants in Column

		Shear (kips)		Axial Force[a] (kips)	
	Base Moment (ft kips)	Base	Top	Base	Top
Safety/Relief Valve Actuation					
All valves initial	771.1	70.2	41.4	±102.1	±86.4
1 valve subsequential	1133.0	94.9	48.9	±37.1	±37.1
Loss-of-Coolant Accident					
Chugging	13.5	2.5	1.4	±11.7	±10.2
Annulus pressurization	136.4	11.1	6.5	±6.4	±5.3
Pipe break jet				±745.0	±745.0
Pool swell				-172.0	-172.0
Transient pressure difference (drywell-wetwell)				+642.0	+642.0
Seismic					
Operating basis earthquake	127.1	9.9	5.7	±31.2	±27.1
Safe shutdown earthquake	164.2	12.8	7.4	±46.1	±39.6
Dead				+229.0	+134.0
Live				+217.0	+217.0

[a] Positive axial force is compressive; negative is tensile.

Table 3A.4.2-3

Results Summary - Safety/Relief Valve Quencher

Loading Condition	Stress Category	Principal Stress (psi)			Critical Stress Intensity (psi)	Allowable Stress (psi)	D.M. (1)
		1	2	3			
Normal	P_m	2525	1390	-275	2800	15,978	5.71
	P_L	11,092	1204	-275	11,367	23,967	2.11
	$P_L + Q$	13,678	1052	0	13,678	47,934	3.50
Upset	$P_L + Q$	28,399	6985	0	38,399	47,934	1.25
	P_m	4102	535	-275	4377	17,576	4.01
	P_L	13,480	2540	-275	13,755	26,364	1.92
Emerge	P_m	3989	1392	-275	4264	23,967	5.62
	P_L	16,964	1711	-275	17,239	28,761	1.67
Fault (1)	P_m	3994	1395	-275	4267	31,956	7.48
	P_L	16,982	1712	-275	17,257	38,347	1.99
Fault (2)	P_m	3334	1223	-275	3609	31,956	8.85
	P_L	14,738	1633	-275	15,013	33,347	2.55

[a] Generally the maximum stresses occurs between the quencher arms, where the arms meet the body.

Notes:

1. Design margin is defined as follows:

    $$DM = \frac{\text{Allowable Stress}}{\text{Calculated Stress}}$$

2. The definition of the above terms is proved in ASME Code Section III, Paragraph NC-3217 of Winter 1976 Addenda.

Cumulative Usage Factor Calculation at 24 in. Downcomer Anchor

Load Combination[a] Set	Expected Number of Cycles (ni)	Bending Moment Mi lb/ft	Peak Stress Sp (psi)	Alt. Stress Salt (psi)	Allowable Number of Cycles N	Calculated Usage Factor $U_i = \dfrac{n_i}{N_i}$
1	1	244,008	60,116	30,058	20,000	0.0001
2	9	244,008	32,575	16,288	200,000	0.0001
3	50	202,180	26,991	13,496	300,000	0.0002
4	940	216,065	28,845	14,422	300,000	0.0031
5	12,434	183,244	24,463	12,232	400,000	0.0311

Cumulative Usage Factor U= 0.0346 < 1.0

[a] Load combination set definition

1 - NPC + LOCA + SSE + SRV + CHUGGING

2 - SSE + SRV + CHUGGING

3 - OBE + SRV

4 - SRV + CHUGGING

5 - SRV

Table 3A.4.2-5

Cumulative Usage Factor Calculation at 28 in. Downcomer Anchor

Load Combination[a] Set	Expected Number of Cycles (ni)	Bending Moment Mi lb/ft	Peak Stress Sp (psi)	Alt. Stress Salt (psi)	Allowable Number of Cycles N	Calculated Usage Factor $U_i = \dfrac{n_i}{N_i}$
1	1	346,771	61,562	30,781	18,000	0.0001
2	9	346,771	33,775	16,888	150,000	0.0001
3	50	307,359	29,937	14,968	200,000	0.0002
4	940	557,714	54,321	27,161	30,000	0.0313
5	12,434	275,671	26,850	13,425	400,000	0.0311

Cumulative Usage Factor U = 0.0629 < 1.0

[a] Load combination set definition

1 - NPC + LOCA + SSE + SRV + CHUGGING

2 - SSE + SRV + CHUGGING

3 - OBE + SRV

4 - SRV + CHUGGING

5 - SRV

Table 3A.4.2-6

Maximum Usage Factors Table

	First Actuation	Second Actuation	Subsequent Actuations	Total Cumulative Usage Factor
Low set SRV lines (MSRV-1C) (MSRV-1B)	0.626	0.033	0.237	0.896
Non-low-set SRV lines	0.527	0.202	N/A	0.729

GENERAL NOTES.

LEGEND.

GRAPHIC SCALES

DETAIL D-982

DETAIL D709
(TYPICAL FOR 28" DOWNCOMERS)

SECTION 4837-4837

DETAIL D708

SECTION 4965-4965

PLAN OF DOWNCOMER BRACING SYSTEM EL 455'-4"

ALL WORK ON THIS DRAWING SHALL BE QUALITY CLASS I

CONTAINMENT VESSEL

REACTOR PEDESTAL

INSIDE FACE CONTAINMENT VESSEL

Columbia Generating Station	**Downcomer Bracing System - Plan and Details**
Final Safety Analysis Report	Draw. No. **S1060** Rev. **7** Figure **3A.4.2-1**

Typical Column

Typical Downcomer

Typical Joint At Containment

Typical Member Number

Typical Node Number

Typical SRV Line

RPV Pedestal

North
0°

Y

X

90° East
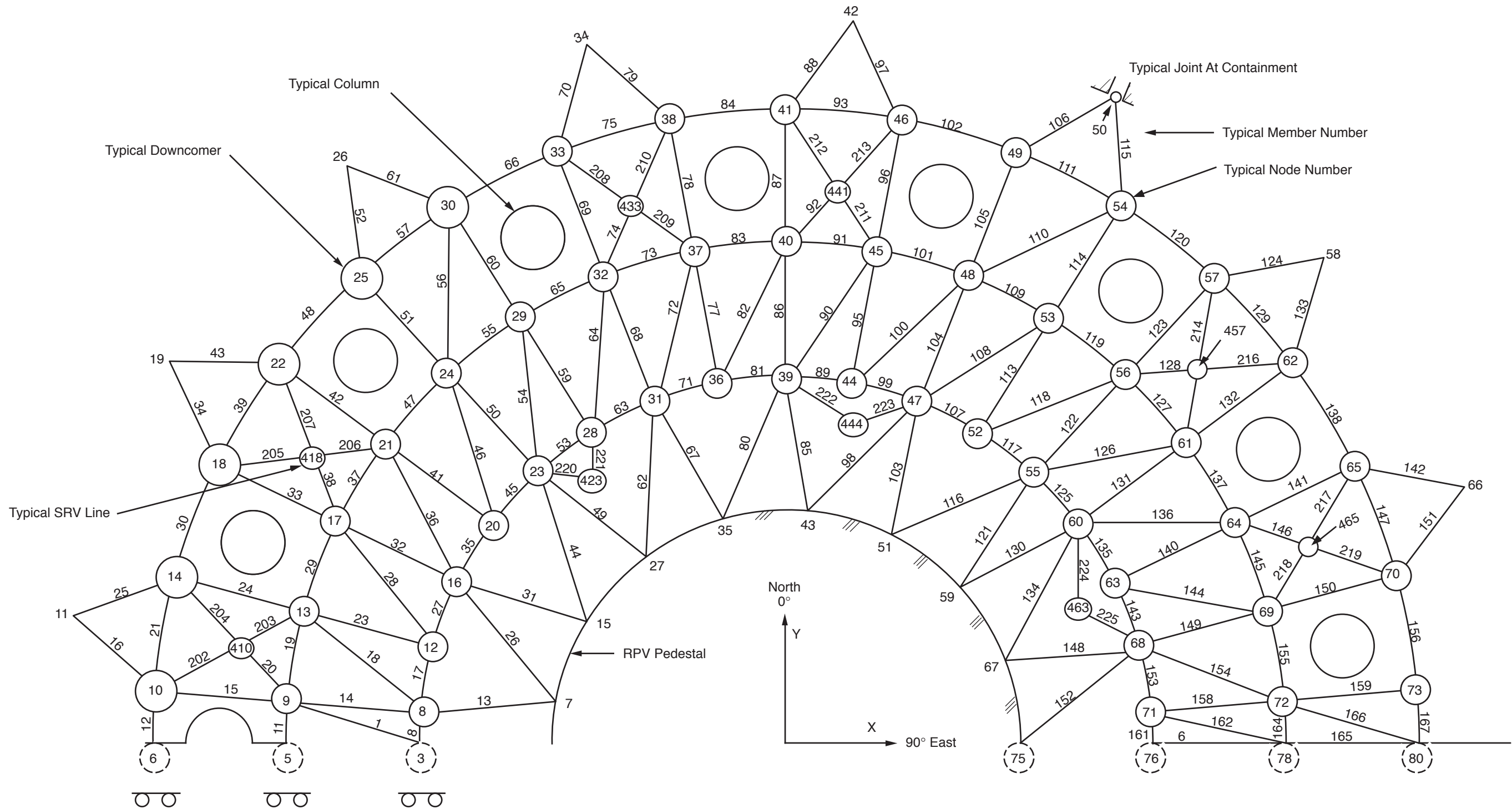
Columbia Generating Station Final Safety Analysis Report	Downcomer Bracing System - Model For Structural Analysis		
	Draw. No. **950021.61**	Rev.	Figure **3A.4.2-2**
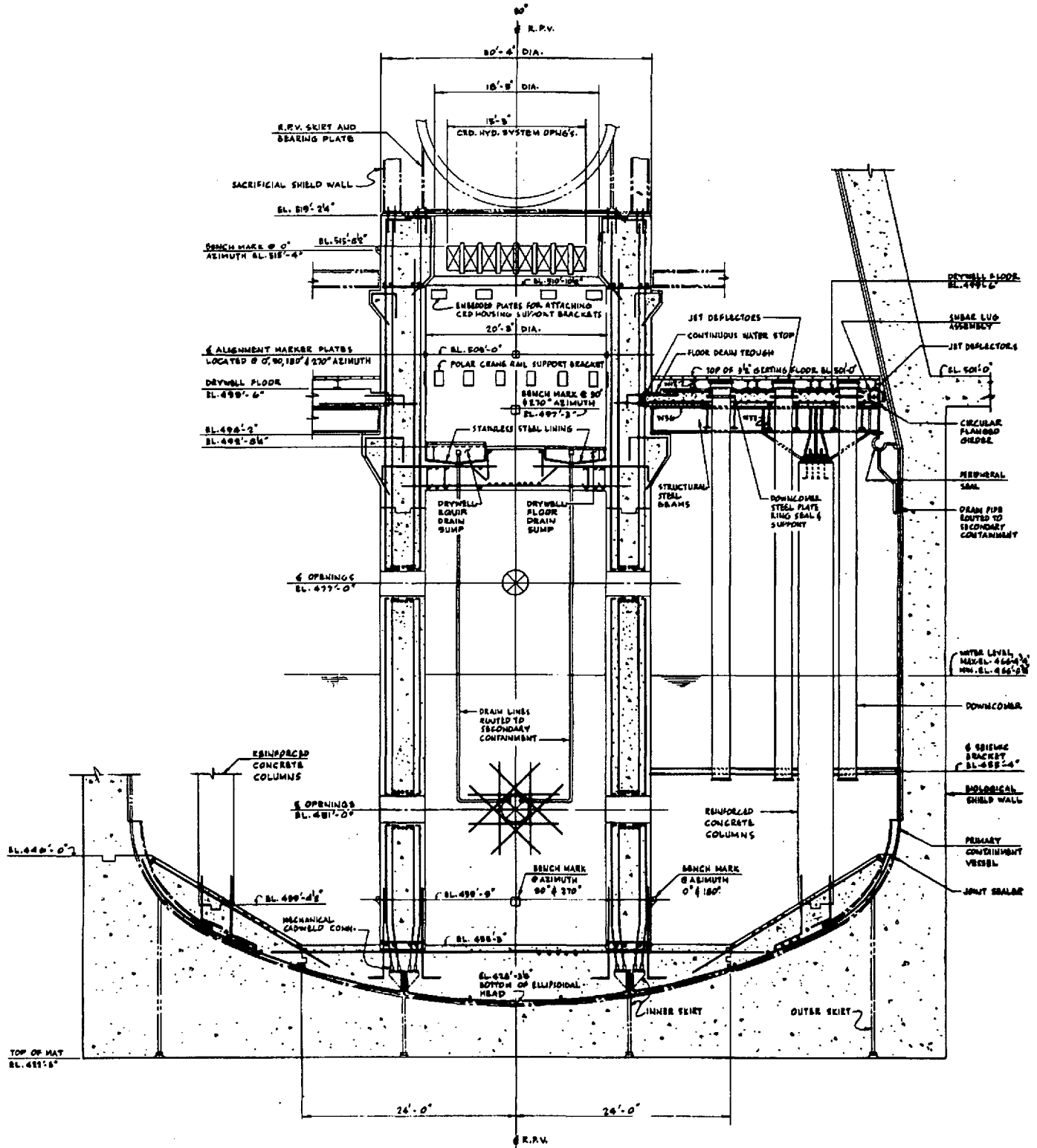
Form No. 960690

SECTIONAL ELEVATION LOOKING EAST

Columbia Generating Station Final Safety Analysis Report	Diaphragm Floor Columns and Adjoining Structures		
	Draw. No. 020361.20	Rev.	Figure 3A.4.2-3

Pinned at Top

Diaphragm Floor

El. 491' - 4"

17

16
16

15
15

14 — Typical Member No.

14 — Typical Node No.

13
13

12
12

11
11

10
10 — El. 466' - 4"
Water Surface

9
9

8
8

7
7

6
6

5
5

4
4

3
3

2
2

1
1 — El. 439' - 4"

Fixed at Base

4 at 4' = 16'

52' - 0"

12 at 3' = 36'

Model for Horizontal Loads

Columbia Generating Station Final Safety Analysis Report	Diaphragm Floor Column Model for Dynamic Analysis		
	Draw. No. 950021.62	Rev.	Figure 3A.4.2-4

Form No. 960690

Member: 1   4   8   12   16   20   24

Node: 1 2 6 10 14 18 22 26

1' - 6"

26

27

1' - 4"   17 at 1' = 17'   7 at 1' = 7'

18' - 4"

27

28

28

29

29

30

30

31

31

32

32

33

33

34

34

35

35

36

36

37

37

38

38

39

39

40

13 at 4' = 52'

Model for Vertical Loads

Columbia Generating Station
Final Safety Analysis Report

Structural Model of Diaphragm
Floor Beam and Column

| Draw. No. 950021.63 | Rev. | Figure 3A.4.2-5 |

Rigid Restraint
(Vertical Only)

El. 493' - 0"

Anchor at 28" Ø
Downcomer

El. 489' - 5"

El. 493' - 0"

12x10
Reducer

Upper Guide

Water Level

El. 466' - 3 1/4"

Downcomer
Bracing

El. 455 '- 4"

El. 435' - 3"

Columbia Generating Station Final Safety Analysis Report	SRV Piping System Inner Ring Quencher Support		
	Draw. No. **960222.91**	Rev.	Figure **3A.4.2-6**

Temp. Design = 474°F
Press. Design = 550 psig

12" Sch.80 Pipe
T = .687"

12.75"

Reducer, 1 1/4" Thk. Rolled
SA155 KCF 70

2.6565"

10°

12" Sch. 80 Pipe
SA312, Type 304,
or SA358, Type 304,
Cl. 1

24" Sch.160 Pipe
SA376, Type 304

1.1927"

5.5989'

6"

17"

1/2"

2.343"

4.4375'

18.5"

1"

24" - 600# Blind Flg., F.F., F&D
SA182, GR.F 304

Columbia Generating Station **Final Safety Analysis Report**	**Quencher Assembly**		
	Draw. No. 960222.92	**Rev.**	**Figure** 3A.4.2-7

24" Sch. 160 Pipe
(Quencher Body)

12" Sch. 80 Pipe
(Quencher Arm)

24"-600# Blind Flange
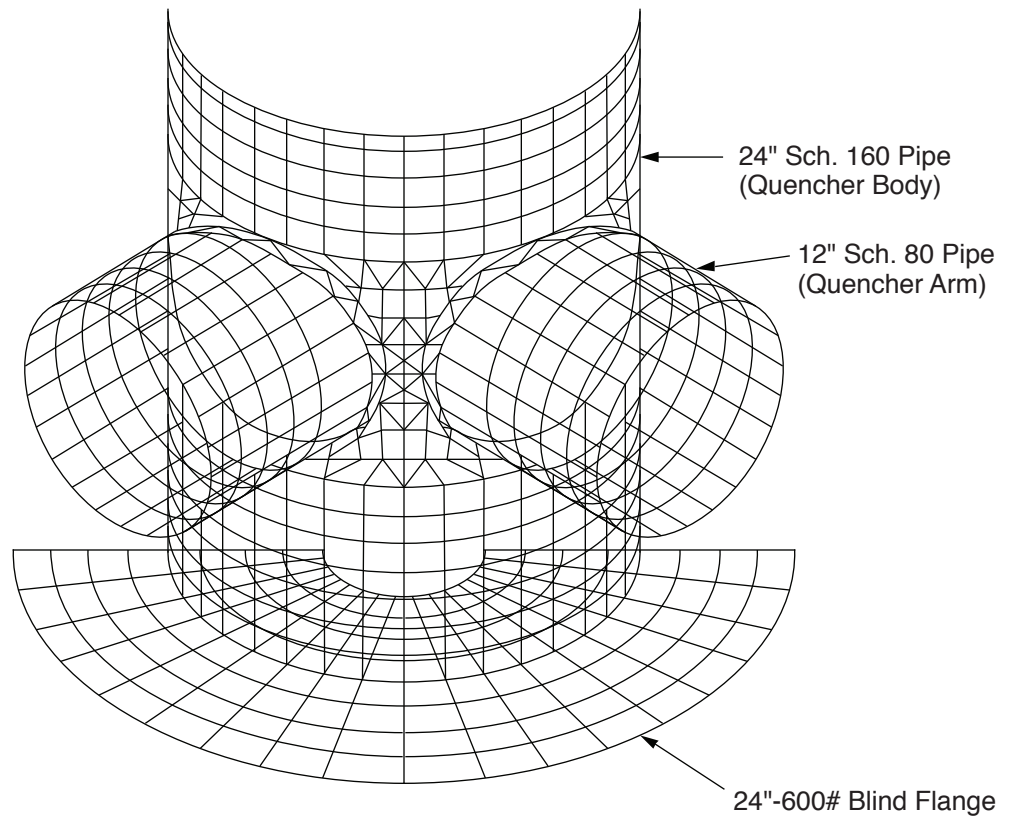
Columbia Generating Station Final Safety Analysis Report	SRV Quencher Assembly		
	Draw. No. **960222.93**	Rev.	Figure **3A.4.2-8**

3A.4.3　　MISCELLANEOUS SUPPRESSION POOL PIPING SYSTEMS

A tabulation of the miscellaneous systems located in the suppression chamber is given in Table 3A.4.3-1. The results of the stress analysis for suppression pool piping other than SRV piping and downcomers is presented in Table 3A.4.3-3.

Depending upon the location in the wetwell, the suppression pool piping will be subjected to different loading associated with SRV discharge and LOCA. For identification purposes, the miscellaneous wetwell piping has been broken into four zones, i.e., fully submerged piping, partially submerged piping, piping in the pool swell zone, and piping above the pool swell zone (Figure 3A.4.3-1). Piping in each zone is noted in Table 3A.4.3-1.

3A.4.3.1　　Loads Used for Assessment

The wetwell piping systems are subjected to static, dynamic, and hydrodynamic loads due to normal, upset, emergency, and faulted plant operating conditions. Each zone is characterized by certain applicable loads shown in Table 3A.4.3-2. A description of each of these loads is provided in Sections 3A.3 and 3A.5.

3A.4.3.2　　Load Combination and Acceptance Criteria

The design limits, as set forth in the ASME Boiler and Pressure Vessel Code (ASME Code) Section III, Subsection NC (Reference 3A.4.2-1) were utilized for the assessment of the suppression pool piping systems. The various piping systems are considered acceptable if they satisfy the equations of Paragraph NC-3652 of Section III of the ASME Code.

The piping, as listed on Table 3A.4.3-1, is fabricated of low alloy carbon steel pipe having an allowable stress "S_h" primary evaluation of 15,000 psi up to a temperature of 275°F.

Allowable Stress Limits (Equation 9 of NC-3652 and NC-3611, Reference 3A.4.2-1)

The stress for the miscellaneous wetwell piping includes the primary membrane plus bending stresses. The limits of these stresses, depending on loading conditions, are the same as those listed in Section 3A.4.2.4.3.

3A.4.3.3　　Method of Analysis

The miscellaneous suppression pool piping systems were analyzed for the appropriate loading combinations using ADLPIPE and ANSYS computer programs (Attachment 3A.F). Hand calculation methods were used to analyze short cantilevered pipes attached to the primary containment. Static and response spectrum analyses were handled in the same manner as described in Section 3A.4.2.3.3. However, displacement time history analyses were performed, as required, to obtain more realistic piping responses due to SRV building response

loads. For residual heat removal (RHR) blowdown transient loads, ADLPIPE was used to perform force time history analysis.

3A.4.3.4   Results and Design Margins

Table 3A.4.3-3 presents pipe stress results and design margins for piping systems in the wetwell. The pipe supports for the wetwell were also assessed and determined to be within acceptable limits.

Table 3A.4.3-1

Miscellaneous Wetwell Piping

Ref. Penetration Number X-	Line/Description	Penetration Elevations	Penetration Azimuths	Remarks
Zone I - Fully Submerged Piping				
33	8 in. RCIC Pump Suction	452 ft-0 in.	336°	
100	6 in. Fuel pool cleanup	452 ft-0 in.	295°	
35	24 in. RHR pump "A" suction	452 ft-0 in.	276° - 49 ft	Similar in config. to X-32
32	24 in. RHR pump "B" suction	452 ft-0 in.	263° - 11 ft	
31	24 in. HPCS pump suction	452 ft-0 in.	97° - 36 ft	
34	24 in. LPCS pump suction	452 ft-0 in.	66° - 05 ft	Similar in config. to X-36
36	24 in. RHR pump C suction	452 ft-0 in.	45° - 39 ft	
88	3 in. instrumentation	455 ft-0 in.	180°	
86B	2 in. instrumentation	462 ft-0 in.	45°	Short length of pipe
87B	2 in. instrumentation	462 ft-0 in.	245°	Short length of pipe
N/A	4 in. FPC - SYPHON	N/A	N/A	
Zone II - Partially Submerged Piping				
64	1.5 in. RCIC vacuum pump discharge	467 ft-9 in.	345°	Similar in config. to X-65
4	10 in. RCIC line (24 in. header)	467 ft-9 in.	318°	
65	2 in. RCIC pump min. flow	467 ft-9 in.	312°	
101	6 in. RPC test	467 ft-9 in.	0°	
47	18 in. RHR pump A test	467 ft-9 in.	288.7°	Similar in config. to X-48
117	18 in. RHR pressure relief	467 ft-9 in.	279°	Similar in config. to X-11B
118	18 in. RHR pressure relief	467 ft-9 in.	261°	
48	18 in. RHR pump B test	467 ft-9 in.	251.29°	
23	3 in. EDR equipment drain	467 ft-9 in.	132°	
24	3 in. FDR floor drain	467 ft-9 in.	111°	
49	12 in. HPCS pump test	467 ft-9 in.	103° - 31 ft	
63	12 in. LPCS pump test	467 ft-9 in.	60°	Similar in config. to X-49
26	18 in. RHR pump "C" test	467 ft-9 in.	20°	

Table 3A.4.3-1

Miscellaneous Wetwell Piping (Continued)

Ref. Penetration Number X-	Line/Description	Penetration Elevations	Penetration Azimuths	Remarks
Zone III - Pool Swell Zone				
87A	2 in. instrumentation	471 ft-6 in.	245°	Short length of pipe
86A	2 in. instrumentation	471 ft-6 in.	45°	Short length of pipe
51	42 in. HATCH	473 ft-6 in.	155°	Short length of pipe
107B	12 in. electrical line	475 ft-0 in.	240°	Short length of pipe
107A	12 in. electrical line	475 ft-0 in.	52° - 30 ft	Short length of pipe
66	24 in. CSP	475 ft-0 in.	222° - 30 ft	Short length of pipe
116	12 in. RCIC	477 ft-6 in.		Short length of pipe
81	14 in. instrumentation	479 ft-4 in.	235°	Short length of pipe
82	10 in. CAS	479 ft-4 in.	230°	
83	10 in. instrumentation	479 ft-4 in.	240°	
84	10 in. instrumentation	479 ft-4 in.	40°	Similar in config. to X-83
Zone IV - Above Pool Swell Zone				
67	24 in. CEP	491 ft-0 in.	0°	Short length of pipe
102	6 in. Plugged (4 in. CAC pipe)		240°	Short length of pipe
103	6 in. Plugged (4 in. CAC pipe)		180°	Short length of pipe
104	6 in. Plugged (4 in. CAC pipe)		323°	Short length of pipe
105	6 in. Plugged (4 in. CAC pipe)		140°	Short length of pipe
57	12 in. SPARE		47°	Short length of pipe
58	12 in. SPARE		132°	Short length of pipe
59	12 in. SPARE		258°	Short length of pipe
60	12 in. SPARE		280°	Short length of pipe
25A	6 in. RHR		70°	
25B	6 in. RHR		235° - 30 ft	
119	24 in. vacuum breaker		151°	Short length of pipe

Table 3A.4.3-2

Piping Zone Versus Loads

Loading	Zone			
	Fully Submerged	Partially Submerged	Pool Swell Zone	Above Pool Swell Zone
Deadweight	X	X	X	X
Thermal	X	X	X	X
Pressure	X	X	X	X
Operating basis earthquake	X	X	X	X
Safe shutdown earthquake	X	X	X	X
SRV pressure	X	X		
SRV response spectra	X	X	X	X
LOCA jet	X	X		
LOCA bubble	X	X		
Pool swell and fallback	X	X	X	
Chugging pressure	X	X		
Chugging response spectra	X	X	X	X

Table 3A.4.3-3

Summary of Results and Design Margins for
Miscellaneous Wetwell Piping

Penetration Number	Controlling Load Case	Allowable Stress (psi)	Calculated Stress (psi)	Design Margin
X-33	Upset	18,000	12,264	1.46
X-100	Upset	18,000	5,231	3.44
X-32	Upset	18,000	9,923	1.81
X-31	Upset	18,000	14,096	1.28
X-36	Upset	18,000	11,687	1.54
X-4	Emergency	27,000	14,453	1.86
X-101	Faulted	36,000	19,826	1.81
X-47 and X-117	Emergency	27,000	16,952	1.59
X-23	Upset	18,000	13,963	1.28
X-49	Emergency	27,000	13,001	2.07
X-26	Emergency	27,000	19,580	1.37
X-24	Emergency	27,000	19,344	1.39
X-35	Upset	18,000	9,923	1.81
X-34	Upset	18,000	17,939	1.003
X-48 and X-118	Emergency	27,000	24,400	1.03[a]
		For Most Severe Condition		
X-104	Emergency	27,000	17,687	1.53
X-82	Upset	18,000	14,388	1.25
X-25A and X-25B	Upset	18,000	17,500	1.03[b]
X-83	Faulted	44,640	33,084	1.35

Table 3A.4.3-3

Summary of Results and Design Margins for
Miscellaneous Wetwell Piping (Continued)

Penetration Number	Controlling Load Case	Allowable Stress (psi)	Calculated Stress (psi)	Design Margin
X-84	Faulted	44,640	33,084	1.35
X-88	Upset	22,700	16,508	1.37
X-63	Faulted	36,000	6,220	5.78
X-64	Upset	18,000	15,193	1.19
X-65	Upset	18,000	14,271	1.26
4 in. FPC	Upset	18,000	2,774	6.49

[a] The design margin for this line in reality is larger because of the conservative approach taken, that the flexibility of the containment was not considered for the governing load in this case - RHR transient.

[b] The design margin for this line is also larger due to conservatism in the envelope spectrum analysis for SRV and chugging as compared to multi-input or time-history analysis that could have been utilized.

Notes:

1.   The effects of short pipes cantilevered from the containment to hydrodynamic loads is considered minimal. These short stubs are listed in Table 3A.4.3-1.

2.   The information provided within this table are the maximum stresses between the nozzle and the termination of the pipe within the wetwell.

3.   Results of the stresses at the shell will be provided later.
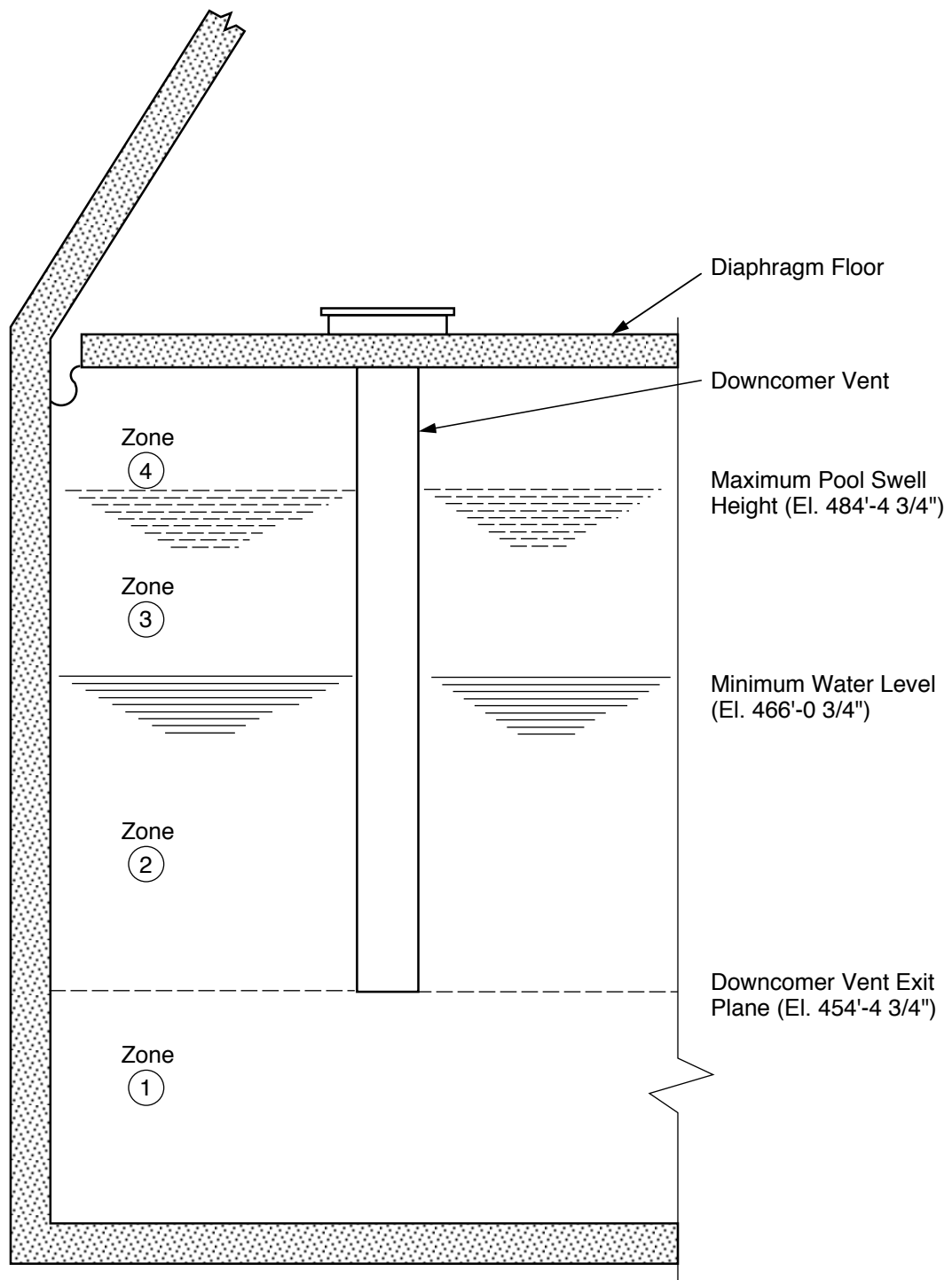
Diaphragm Floor

Downcomer Vent

Zone
(4)

Maximum Pool Swell
Height (El. 484'-4 3/4")

Zone
(3)

Minimum Water Level
(El. 466'-0 3/4")

Zone
(2)

Downcomer Vent Exit
Plane (El. 454'-4 3/4")

Zone
(1)

	Hydrodynamic Loading Zones		
Columbia Generating Station **Final Safety Analysis Report**			
	Draw. No. 960222.94	**Rev.**	**Figure 3A.4.3-1**

3A.5   EFFECTS DUE TO BUILDING RESPONSES TO SAFETY/RELIEF VALVE
DISCHARGE AND LOSS-OF-COOLANT ACCIDENT LOADS

Response spectra generated at each floor location define the input motions used for
qualification and assessment of all the safety-related piping and equipment. In load
combinations which include safety/relief valve (SRV) discharge and seismic loads, or
loss-of-coolant accident (LOCA) steam condensation and seismic loads, seismic response
spectra based upon a finite element soil-structure model were used in design and plant
assessments for structures, piping, and equipment. The use of the finite element soil-structure
model generally results in lower structural responses than the soil spring and dashpot model
used in the original seismic design.

3A.5.1   BUILDING RESPONSES TO SAFETY/RELIEF VALVE DISCHARGE LOADS

This section presents the dynamic responses of the containment and internal structures
subjected to loads resulting from SRV discharge as defined in Section 3A.3.1.3. The
analytical model and method of analysis for determining the building structural response to
SRV discharge loads are described in the following sections.

3A.5.1.1   Analytical Model

3A.5.1.1.1   Overall Building Model

Figure 3A.5.1-1a presents the soil-structure model. Figure 3A.5.1-1b presents the
axisymmetric overall building model of the CGS reactor building. It should be noted that the
thick reactor pressure vessel (RPV) pedestal and building mat were accounted for in the model
by utilizing multiple layer axisymmetric solid elements.

These models were utilized to determine the response to the loading conditions stated in
Section 3A.3, and provided responses at the RPV pedestal, foundation mat, biological shield
wall, and in the reactor building walls and floors outside of primary containment.

3A.5.1.1.2   Steel Containment Shell Model

Figure 3A.5.1-2 shows the more refined three-dimensional finite element model of the
containment shell. This model is interconnected to the rest of the building at the basemat
(el. 446 ft), diaphragm floor (el. 503 ft), stabilizer truss (el. 565 ft), and the refueling bellows
(el. 583 ft).

3A.5.1.2   Method of Analysis

The containment shell model was analyzed for SRV rigid wall pressure loads acting on the
wetwell boundary and specified displacements at all the points where the shell is connected to

the rest of the building. The displacements were obtained from the solutions of the overall building model. The refined containment shell model, as discussed in Section 3A.5.1.1.2, was used to determine the response of the steel shell.

A more detailed discussion of the two models, analytical approach, and results are found in "SRV Loads - Improved Definition and Application Methodology" (Reference 3A.3.1-1).

3A.5.1.3   Safety/Relief Valve Discharge Load Cases

Several SRV discharge cases were considered for CGS design evaluation as discussed below.

3A.5.1.3.1   Response to All Valve Discharge

All 18 SRVs are conservatively assumed to discharge during certain plant conditions.

Two design conditions are associated with all the valves discharge case - the "axisymmetric" condition and the "nearly symmetric" condition. Each of these loading conditions is applied in load combinations involving the all valves discharge case. The axisymmetric loading condition assumes all valves will discharge simultaneously in the pool, thus maximizing the response of the axisymmetric features of the containment and reactor pedestal. The nearly symmetric loading condition assumes some imbalance may occur during actuation of all SRVs. The imbalance may occur from sequential discharging at different set points, variability in valve opening time, differences in SRV discharge line geometry, etc.

Listed below is a sample of the response spectra used in plant assessments involving the axisymmetric loading condition. For the "nearly symmetric" loading condition, the response spectra used are constructed by adding 0.5 times the axisymmetric response spectra to 0.6 times the single valve response spectra.

Location	Direction	Figure
Top of RPV Pedestal, el. 520 ft Mass No. 44	Radial	3A.5.1-3a, 3A.5.1-3b
Top of RPV Pedestal, el. 520 ft Mass No. 44	Vertical	3A.5.1-4a, 3A.5.1-4b
Basemat at RPV Pedestal, el. 435 ft Mass No. 141	Radial	3A.5.1-5a, 3A.5.1-5b
Basemat at RPV Pedestal, el. 435 ft Mass No. 141	Vertical	3A.5.1-6a, 3A.5.1-6b

Top of Sac. Shield Wall, el. 567 ft Mass No. 14	Radial	3A.5.1-7a, 3A.5.1-7b
Top of Sac. Shield Wall, el. 567 ft Mass No. 14	Vertical	3A.5.1-8a, 3A.5.1-8b
RPV, el. 545 ft Mass No. 27	Radial	3A.5.1-9a, 3A.5.1-9b
RPV, el. 545 ft Mass No. 27	Vertical	3A.5.1-10a, 3A.5.1-10b
Containment Vessel, el. 547 ft Mass No. 60600	Radial	3A.5.1-11a, 3A.5.1-11b
Containment Vessel, el. 547 ft Mass No. 60600	Vertical	3A.5.1-12a, 3A.5.1-12b
Containment Vessel, el. 448 ft Mass No. 50100	Radial	3A.5.1-13a, 3A.5.1-13b
Containment Vessel, el. 448 ft Mass No. 50100	Vertical	3A.5.1-14a, 3A.5.1-14b

Notes: 1. Figures denoted "a" refer to the conventional [single frequency pressure (SFP)] load case while the figures denoted "b" refer to the multiple frequency pressure (MFP) load case (see Reference 3A.3.1-1 for details).

2. The tangential loads were also utilized in the assessment of CGS. The tangential values are not included in this submittal as they are much smaller in magnitude then the presented valves.

3A.5.1.3.2   Automatic Depressurization System Valves Discharge Case

This case corresponds to the discharge of the SRVs of the automatic depressurization system (ADS) which are automatically actuated. For assessment purposes, the more conservative all valves response spectra values were utilized.

3A.5.1.3.3   Two Valves Discharge Case

In this case, two SRVs are considered to discharge concurrently through two adjacently located quenchers. For assessment purposes, the more conservative single outer valve discharge response spectra were utilized.

3A.5.1.3.4   Single Valve Discharge

The single outer quencher discharge, which is less likely to happen, is considered in the assessment because it is found to be more conservative, both for containment and pedestal response.

Location	Direction	Figure
Top of RPV Pedestal, el. 520 ft Mass No. 44	Radial	3A.5.1-15a, 3A.5.1-15b
Top of RPV Pedestal, el. 520 ft Mass No. 44	Vertical	3A.5.1-16a, 3A.5.1-16b
Basemat at RPV Pedestal, el. 435 ft Mass No. 141	Radial	3A.5.1-17a, 3A.5.1-17b
Basemat at RPV Pedestal, el. 435 ft Mass No. 141	Vertical	3A.5.1-18a, 3A.5.1-18b
Top of Sac. Shield Wall, el. 567 ft Mass No. 14	Radial	3A.5.1-19a, 3A.5.1-19b
Top of Sac. Shield Wall, el. 567 ft Mass No. 14	Vertical	3A.5.1-20a, 3A.5.1-20b
RPV, el. 545 ft Mass No. 27	Radial	3A.5.1-21a, 3A.5.1-21b
RPV, el. 545 ft Mass No. 27	Vertical	3A.5.1-22a, 3A.5.1-22b
Containment Vessel, el. 547 ft Mass No. 60600	Radial	3A.5.1-23a, 3A.5.1.23b
Containment Vessel, el. 547 ft Mass No. 60600	Vertical	3A.5.1-24a, 3A.5.1-24b

Containment Vessel, el. 448 ft   Radial   3A.5.1-25a,
Mass No. 50100   3A.5.1-25b

Containment Vessel, el. 448 ft   Vertical   3A.5.1-26a,
Mass No. 50100   3A.5.1.26b

Notes: 1. Figures denoted "a" refer to the conventional (SFP) load case while the
                figures denoted "b" refer to the MFP load case (see Reference 3A.3.1-1 for
                details).

            2. The tangential loads were also utilized in the assessment of CGS. The
                tangential values are not included in this submittal as they are much smaller in
                magnitude then the presented valves.

See Enlarged Detail
Fig. 3A.5.1-1b

El. 427.75'

El. 374.25'

El. 331.25'

El. 281.25'

El. 206.75'

El. 106.25'

3 at 48.0' = 144.0'   60.0'   96.0'
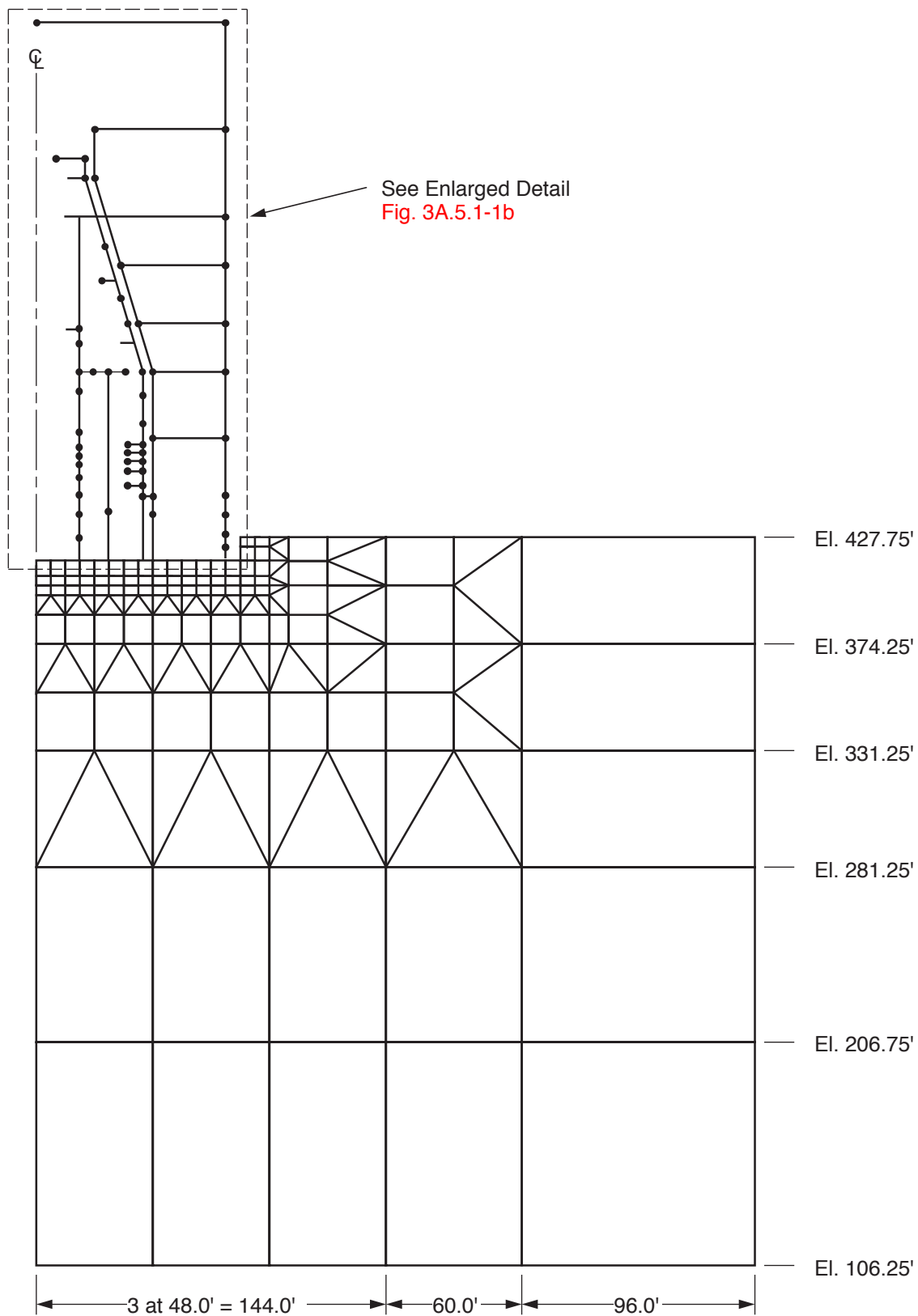
Columbia Generating Station Final Safety Analysis Report	Axisymmetric Model of the Reactor Building and Soil Foundation
	Draw. No. 960222.95	Rev.	Figure 3A.5.1-1a

Figure Not Available For Public Viewing

Figure Not Available For Public Viewing

Figure Not Available For Public Viewing

Figure Not Available For Public Viewing

Figure Not Available For Public Viewing

Figure Not Available For Public Viewing

Figure Not Available For Public Viewing

Figure Not Available For Public Viewing

Figure Not Available For Public Viewing

3A.5.2 BUILDING RESPONSES TO LOSS-OF-COOLANT ACCIDENT LOADS

The analysis of the containment under the action of long-term LOCA loads and the resultant responses are described in this section. The LOCA loads considered are those described in Section 3A.3.2.4, namely, chugging and condensation oscillation. However, the condensation oscillation load is not a governing load as compared to the chugging load, therefore it was not considered in the design assessment. The discussion in this section applies to the effects of chugging only. A complete definition of the chugging loads and the methodology of their application to the reactor building is contained in Reference 3A.3.2-15.

3A.5.2.1 Analytical Model

The mathematical model used for the analysis of the structure subjected to chugging loads includes the reactor building and the supporting soil. The model of the reactor building is shown in Figure 3A.5.2-1. The model of the supporting soil is the same as that shown in Figure 3A.5.1-1a in connection with the analysis for SRV discharge loads. The soil is represented by solid axisymmetric elements with asymmetric load capability. Spatial variation of soil shear modulus and unit weight and soil-structure interaction are accounted for.

As shown in Figure 3A.5.2-1, two types of finite elements have been used in modeling of the building, namely, axisymmetric conical shell elements and axisymmetric solid elements; both types of elements have asymmetric loading capability. The wetwell columns, stabilizer trusses, bellows, and shear lugs between the diaphragm floor and containment are modeled using springs.

In the suppression pool region, where the hydrodynamic loads are applied and where a more accurate representation is required, the node locations are closely spaced. The horizontal rings attached to the containment vessel are treated as discrete rings and the additional stiffness due to the vertical stiffeners is included with the vessel properties.

The RPV and internals are represented by axisymmetric shell elements. The dynamic coupling effect of the fluid in the RPV is accounted for by adding hydrodynamic masses to the nodal points of the mathematical model.

3A.5.2.2 Method of Analysis and Building Response

The structural response of the reactor building, when subjected to the chugging phenomenon, is determined from the application of the seven distributions of the chugging pressures on the wetwell pool boundary in the analytical model. These seven distributions of pool boundary pressures result from the seven design chugging sources developed for the multivent chugging definition described in Section 3A.3.2.4.2.1. Two loading cases are considered for each of the seven design sources, namely, nearly symmetric and asymmetric conditions. Detailed

analytic methods for determination of the structural response are given in
Reference 3A.3.2-15.

As described in Reference 3A.3.2-15, the nearly symmetric and asymmetric results are
comparable. For the purpose of this assessment, the nearly symmetric loading condition is
used.

The response of the building is obtained in terms of acceleration response spectra. These were
calculated for significant locations in the reactor building for the nearly symmetric and
asymmetric loading conditions. The envelope spectrum curves were plotted with peaks spread
by $\pm 15\%$ for damping values of 0.5%, 1.0%, 2.0%, and 4.0% of critical damping. Nearly
symmetric response spectra plots for different locations in the building are illustrated in the
figures listed below.

It should be noted that the design values presented in Figures 3A.5.2-2 through 3A.5.2-10
were increased by a factor of 1.10 to account for the differences in vent size (28 in. for
Columbia Generating Station as compared to 24 in. for the 4T and 4TCO test) and an
additional factor of 1.16 over the values presented in the chugging report.

3A.5.2.2.1   Reactor Building Response, Nearly Symmetric Loading - Acceleration
              Response Spectra

Location	Direction	Figure
Containment Vessel, el. 448 ft Mass No. 152	Radial	3A.5.2-2
Containment Vessel, el. 448 ft Mass No. 152	Vertical	3A.5.2-3
Containment Vessel, el. 459 ft Mass No. 123	Radial	3A.5.2-4
Containment Vessel, el. 459 ft Mass No. 123	Vertical	3A.5.2-5
RPV Support on Pedestal, el. 519 ft Mass No. 57	Radial	3A.5.2-6
RPV Support on Pedestal, el. 519 ft Mass No. 57	Vertical	3A.5.2-7

Containment Vessel, el. 583 ft
Mass No. 12   Radial   3A.5.2-8

Building Wall, el. 521 ft
Mass No. 55   Radial   3A.5.2-9

Building Wall, el. 521 ft
Mass No. 55   Vertical   3A.5.2-10

Note that the tangential loads were also utilized in the assessment of CGS. The tangential values are not included in this submittal as they are much smaller in magnitude then the presented values.

Figure Not Available For Public Viewing

Attachment 3A.B

THREE-DIMENSIONAL SOURCE FLOWS IN EXACT CONTAINMENT GEOMETRY

3A.B.1   INTRODUCTION AND SUMMARY

The method specified in Reference 3A.B-1 to calculate the flow field due to bubbles [caused by a loss-of-coolant accident (LOCA) or safety/relief valve (SRV) actuation] in a Mark II suppression pool is the method of images (MOI). The MOI is a potential flow technique and uses point source(s) or sink(s) to represent the bubble(s) and a number of image sources and/or sinks to simulate flow at the pool boundaries to satisfy the kinematical boundary conditions. The MOI has the following limitations with regard to its application to CGS:

      a.   The annular suppression pool geometry needs to be idealized into a rectangular pool using an "equivalent radius" concept,

      b.   The sloping suppression pool bottom needs to be idealized into a flat bottom, and

      c.   Computer flow field calculation costs are high.

In view of these limitations, the MOI is not used to calculate the potential flow field due to stationary source(s) in the CGS suppression pool. Instead, a numerical method is used to determine three-dimensional potential flows induced by source(s) in the exact CGS containment geometry.

The principle of the method can be stated rather simply. The three-dimensional potential flow induced by sources in any arbitrary suppression pool geometry is provided by solution of Laplace's equation for the velocity potential, ϕ. This is done by splitting the function ϕ into two components: ϕ_s which is due to all the sources and sinks (representing expanding or contracting bubbles) and is calculated analytically, and $\hat{\phi}$, which is a smooth function that is calculated numerically. The function $\hat{\phi}$ calculated from the original boundary conditions for ϕ with the boundary values of ϕ_s subracted off. Single ϕ_s analytically known elsewhere and $\hat{\phi}$ can be determined from its boundary conditions by iteration, the total value of the velocity potential, ϕ, can be easily determined.

This attachment describes the formulation of the problem, the method of solution, the numerical procedures utilized, and presents and analyzes some results. Section 3A.B.2 discusses the problem formulation and the solution method, Section 3A.B.3 discusses the numerical procedure, Section 3A.B.4 discusses how the flow field is calculated,

Section 3A.B.5 discusses the initial estimate to start the iteration solution for $\hat{\phi}$.

Section 3A.B.6 discusses the convergence and accuracy of the method, and Section 3A.B.7 presents and analyzes some results for single and multiple bubble cases.

3A.B.2 PROBLEM FORMULATION AND SOLUTION METHOD

For a potential flow, the fluid velocity components may be expressed in terms of a velocity potential function, as shown below:

$$V_x = -\frac{\partial \phi}{\partial x} \; , \qquad V_y = -\frac{\partial \phi}{\partial y} \; , \qquad V_z = -\frac{\partial \phi}{\partial z}$$

The negative sign is purely a convention and means that the fluid flows in the direction of potential drop (Reference 3A.B-2).

The formulation of the boundary value problem for the potential is:

$\nabla^2 \phi = 0$ everywhere in the fluid except appropriate delta functions at sources and sinks,

$\dfrac{\partial 0}{\partial n} = 0$ on the rigid boundaries (containment wall, basemat, and pedestal), and

$\phi = 0$ on the free surface (follows from pressure = 0).

The velocity potential, ϕ is split into two parts:

$$\phi = \phi_s + \hat{\phi}$$

The function ϕ_s represents contributions from the singularities (sources and/or sinks) and its analytical expression at any point within the fluid is given below:

$$\phi_S = \sum_v \phi_S$$

$$o_S = \frac{Q_v}{4\pi_{\rho v}}$$

where Q_v represents the source strength of the vth source or sink and ρ_v represents the distance from the vth source or sink to the point in question (Reference 3A.B-1).

The function $\hat{\phi}$ is a smooth function and satisfies the boundary value problem:

$$\nabla^2 \hat{\phi} = 0 \qquad \text{everywhere,}$$

$$\frac{\partial \phi}{\partial n} = -\frac{\partial \phi_s}{\partial n} \qquad \text{on the rigid boundaries and any planes of symmetry, and}$$

$$\hat{\phi} = -\phi_s \qquad \text{on the free surface.}$$

The boundary values for $\hat{\phi}$ were derived by subtracting the boundary values of ϕ_s from the original boundary value conditions far the total velocity potential, ϕ. Because $\hat{\phi}$ is extremely smooth, it can be accurately calculated by finite differences.

3A.B.3   NUMERICAL PROCEDURE

The geometry of the Columbia Generating Station suppression pool and the location of quenchers and downcomers are shown in Figures 3A.2.1-1 through 3A.2.1-8, inclusive. A cylindrical grid of points is overlayed such that all boundaries with $\partial \phi / \partial n = 0$ (i.e., walls and symmetry planes) are all centered between planes of grid points, while the water surface $z = z_{max}$ is a plane of grid points. Figures 3A.B-1 and 3A.B-2 show how the suppression pool geometry has been modeled for a single SRV actuation case and a LOCA bubble case to take advantage of symmetry.

The lengths between grid points in the r, ϕ, and z direction are denoted by Δr, $\Delta \phi$, and Δz and are indexed in the three directions by i, j, and k, respectively.

$$r_i = r_{min} = (i - 1.5) \Delta r$$

$$\phi_j = (j - 1.5) \Delta \phi$$

$$z_k = (z - 1.5) \Delta z$$

Any function, f, when regarded as a function defined on the grid points will be denoted as $f(r_i, \phi_j, z_k) = f_{i,j,k}$. The coordinates of the source(s) are indicated by the subscript s_v.

As mentioned before, the potential ϕ is split into $\phi_s + \hat{\phi}$. ϕ_s is the source potential (or the sum of each source's contribution in the multi-bubble cases):

$$\phi_s = \sum_v \frac{Q_v}{4\pi \rho_v}$$

where

$$\rho_v = ((r \cos \theta - r_v)^2 + (r \sin\theta)^2 = (z-z)) \, 1/2$$

ϕ_s is evaluated exactly on all grid points. The numerical procedure of calculating ϕ is by the standard cover-relaxation method, which is summarized succinctly here. $\hat{\phi}$ satisfied the Laplace equation which, in cylindrical coordinates, is (Reference 3A.B-2):

$$\nabla^2 0 = \frac{1}{r} \frac{\partial}{\partial r} \frac{(r \partial 0)}{\partial r} + \frac{1}{r^2} \frac{\partial^2 0}{\partial \theta^2} + \frac{\partial^2 \hat{\phi}}{\partial z^2} = 0 \qquad (3A.B\text{-}1)$$

The finite difference approximation of equation 3A.B-1 is chosen as (∇_f^2 = finite aprrox. of $\nabla^2 2$):

$$\nabla_f^2 \hat{\phi} = \frac{(r_{i+1} + r_i)(\hat{\phi}_{i+1,j,k} - \hat{\phi}_{i,j,k}) - (r_i - r_{i-1})(\hat{\phi}_{i,j,k} - \hat{\phi}_{i-1,j,k})}{2r_i(\Delta r)^2} +$$

$$\frac{\hat{\phi}_{i,j+1,k} + \hat{\phi}_{i,j-1,k} - 2\hat{\phi}_{i,j,k}}{r_i^2(\Delta\theta)^2} + \frac{\hat{\phi}_{i,j,k+1} + \hat{\phi}_{i,j,k-1} - 2\hat{\phi}_{i,j,k}}{(\Delta z)^2} = 0 \qquad (3A.B\text{-}2)$$

where:

$$i=2,3\ldots i_{max}\text{-}1, \ j=2,3\ldots j_{max}\text{-}1, \ k=2,3\ldots k_{max}\text{-}1$$

Equation 3A.B-2 constitutes a linear system of (i_{max}-2) x (j_{max}-2) x (k_{max}-2) equations. The number of unknowns is larger, since they are unknowns at the boundaries, which are to be related by the boundary conditions.

As stated before, the boundary conditions for ϕ are:

$$\hat{\phi} = -\phi_s \text{ on the water surface and } \frac{\partial \hat{\phi}}{\partial n} = -\frac{\partial \phi_s}{\partial n} \text{ on walls, bottom, and planes of}$$

symmetry.

For planes of symmetry a simplification from $\partial \hat{\phi} / \partial n = -\partial \phi_s / \partial n$ to $\partial \hat{\phi} / \partial n = 0$ occurs.

The finite difference equations have corresponding boundary conditions for flat bottom containments:

$$\hat{\phi}_{i,j,k_{max}} = -\phi_{s\,i,j,k_{max}} \qquad \text{(on the free surface),}$$

$$\hat{\phi}_{i,j,1} - \hat{\phi}_{i,j,2} = -\phi_{s\,i,j,1} + \phi_{s\,i,j,2} \qquad \text{(on basement floor),}$$

$$\hat{\phi}_{1,j,k} - \hat{\phi}_{2,j,k} = -\phi_{s\,1,j,k} + \phi_{s\,2,j,k} \qquad \text{(on the pedestal wall),}$$

$$\phi_{i_{max},j,k} - \phi_{i_{max}-1,j,k} = -\phi_{i_{max},j,k} + \phi_{i_{max}-1,j,k} \qquad \text{(on the containment wall),}$$

$$\hat{\phi}_{i,1,k} = \hat{\phi}_{i,2,k} \qquad \text{(on the surface } \theta = 0^{\circ}\text{), and}$$

$$\hat{\phi}_{i,j_{max},k} - \hat{\phi}_{i,j_{max}-1,k} = -\phi_{s\,i,j_{max},k} + \phi_{s\,i,j_{max}-1,k} \qquad \text{(on the surface } \theta = \theta_{max}\text{).}$$

These equations, coupled with equation 3A.B-2, now provide a complete system of i_{max}, k_{max} equations for the same number of unknowns.

There are many techniques available to solve the finite-difference equations generated from the Laplace equation. Some, using fast Fourier transform techniques or direct elimination techniques, are indeed very fast. The successive over-relaxation procedure (SOR) was selected because it is adequate in speed; in addition, it can handle general boundaries, whereas, use of other (possibly faster) methods require rectangular domains, periodic boundary conditions, or other restrictions.

Equation 3A.B-2 is solved for the center point in terms of the values at the neighboring points by iterating: (Superscript (n) indicates the nth iteration, $(n+1)$ the next iteration, etc.)

$$\hat{\phi}_{i,j,k}^{(n+1)} = \frac{\hat{\phi}_{i,j+1,k} + \hat{\phi}_{i,j-1,k}}{r_i^2(\Delta\theta)^2} + \frac{\overline{\phi}_{i,j,k+1} = \hat{\phi}_{i,j,k-1}}{(\Delta z)^2} + \frac{(r_{i+1} + r_i)}{2r_i(r)^2}\hat{\phi}_{i+1,j,k} +$$

$$\frac{(r_{i-1} + r_i)}{2r_i(\Delta\theta)^2}\hat{\phi}_{i-1,j,k} - \frac{2}{2r_i(\Delta\theta)^2} + \frac{2}{(\Delta z)^2} + \frac{2}{(\Delta r)^2}$$

or $$\hat{\phi}^{(n+1)} = V_o\hat{\phi}^{(n)}$$

where:

       V_o denotes an "averaging" operator.

Whenever a point is updated, the new value is to be used in calculating its neighboring points $\left(\hat{\phi}^{(n+1)} = V_1\hat{\phi}^{(n)} + V_2\hat{\phi}^{(n+1)}\right)$. This is straightforward iteration or relaxation. In SOR, which is much faster, the change is anticipated by using an acceleration parameter, (Reference 3A.B-3):

$$\hat{\phi}^{(n+1)} = \hat{\phi}^{(n)} + \omega\left(V_{0_{\phi^{(n)}-\phi^{(n)}}}\right) \tag{3A.B-3}$$

Numerical analysis theory shows that convergence occurs for $0 < \omega < 2$, but the optimal depends on the geometry. Various test runs for the single SRV bubble, and for the three bubble LOCA geometries were run with $\omega = 1.98$ chosen for rapid convergence (Section 3A.B.6 gives more details on convergence).

(Note: for $\omega = 1$, equation 3A.B-3 becomes $\hat{\phi}^{(n+1)} = V_0\hat{\phi}^{(n)}$ which is the straightforward iteration case).

3A.B.4   CALCULATION OF FLOW FIELD

3A.B.4.1   Steady State Flow Field Calculation

The calculation of the velocity due to a potential function is performed by taking the negative gradient of the total potential, ϕ. As discussed earlier, the total potential is determined by summing ϕ_s, the potential due to the singularities plus $\hat{\phi}$, which is a smooth function. To ensure accuracy near singularities the velocity field is also calculated as the sum of two components:

$$V = -\nabla\phi = -\nabla\left(\phi_s + \hat{\phi}\right) = V_s + \hat{V}$$

The velocity field due to the smooth function $\hat{\phi}$ is determined numerically at points one-half a grid distance away from the velocity potential grid system as shown in Figure 3A.B-3a. Essentially this scheme averages values of $\hat{\phi}$ in the two neighboring grid planes that are normal to the direction of the desired velocity component. Once these two averages are established, the velocity component is determined by subtracting the two values and dividing by the grid width (Δr, $r\Delta\theta$, Δz) in the appropriate direction (a representative example is given in Figure 3A.B-3). The r, θ, and z velocity components due to $\hat{\phi}$ are shown below:

$$V_{r\,i,j,k} = \left(\hat{\phi}_{i,j,k} + \hat{\phi}_{i,j+1,k} + \hat{\phi}_{i,j,k+1} + \hat{\phi}_{i,j+1,k+1}\right) -$$
$$\left(\hat{\phi}_{i+1,j,k} + \hat{\phi}_{i+1,j+1,k} + \hat{\phi}_{i+1,j,k+1} + \hat{\phi}_{i+1,j+1,k+1}\right) \,/\, (4 \cdot \Delta r)$$

$$V_{0\,i,j,k} = \left(\hat{\phi}_{i,j,k} + \hat{\phi}_{i+1,j,k} + \hat{\phi}_{i,j,k+1} + \hat{\phi}_{i+1,j,k+1}\right) -$$

$$\left(\hat{\phi}_{i,j+1,k} + \hat{\phi}_{i+1,j+1,k} + \hat{\phi}_{i,j+1,k+1} + \hat{\phi}_{i+1,j+1,k+1}\right) / (4 \cdot r \cdot \Delta 0)$$

$$V_{z\,i,j,k} = \left(\hat{\phi}_{i,j,k} + \hat{\phi}_{i+1,j,k} + \hat{\phi}_{i,j+1,k} + \hat{\phi}_{i+1,j+1,k}\right) -$$

$$\left(\hat{\phi}_{i,j,k+1} + \hat{\phi}_{i+1,j,k+1} + \hat{\phi}_{i,j+1,k+1} + \hat{\phi}_{i+1,j+1,k+1}\right) / (4 \cdot \Delta z)$$

The velocity field due to a source is determined analytically at the same grid points used for the velocity field due to the smooth function. The magnitude of the total velocity at a point due to a source is defined as:

$$|V_s| = \frac{Q}{4\pi\rho^2}$$

The x, y, z velocity components are defined by:

$$Vx_s = |V_s| \cdot \frac{x - x_s}{\rho}$$

$$Vy_s = |V_s| \cdot \frac{y - y_s}{\rho}$$

$$Vz_s = |V_s| \cdot \frac{z - z_s}{\rho}$$

and the cylindrical components are defined by:

$$Vr_s = Vx_s \cos\theta + Vy_s \sin\theta$$
$$V\theta_s = Vy_s \cos\theta - Vs_s \sin\theta$$
$$Vz_s = Vz_s$$

For multiple sources, the velocity component are determined by summing the contribution of each of the sources. The total velocity magnitude is determined by the square root of the sum of the squared of the three components.

The usual way of calculating the velocity field is by differentiating the total potential function ϕ by the use of finite differences in exactly the same manner as was describe for the smooth function's velocity calculation. The defect here is that the resultant velocity field becomes inaccurate as one approaches the source(s). This is due to the singularity in ϕ and the resultant inability of a finite difference scheme to approximate a derivative. Also, finite differences taken across the source(s) will be totally inaccurate and meaningless. The above method of calculating the velocity field avoids this problem because (1) the velocities due to

ϕ_s are an exact solution and, (2) $\hat{\phi}$ is a smooth function which allows for a good approximation of a derivative by finite differences.

3A.B.4.2   Transient Flow Field Calculation

The flow field due to a time varying source can be calculated by assuming that the source strength varies with time. Since the velocity field is now a function of time and space, an acceleration field can also be calculated:

$$V(r, \theta, z, t) = -Q(t)\nabla\phi(r, \theta, z)$$
$$V(r, \theta, z, t) = -Q(t)\nabla\phi(r, \theta, z)$$

where:

  $Q(t)$ is the equivalent time varying point source strength representing the hydrodynamic source.

  $\dot{Q}(t)$ is the time rate of change of $Q(t)$.

  $\nabla\phi(4, \theta, z) = $ gradient of the velocity potential at a given point due to a normalized point source strength.

  $V(r, \theta, z, t) = $ total velocity at a given point.

  $\dot{V}(r, \theta, z, t) = $ total acceleration at a given point.

3A.B.5   INITIAL ESTIMATE FOR ITERATION

Since $\partial\hat{\phi}/\partial n$ connects two grid planes which make up a rigid boundary, it is a "soft" boundary condition and "clamps" down the solution less than does a $\hat{\phi}$ boundary condition. With $\hat{\phi}$ known at only one out-of-six possible boundaries, it is necessary to start the iterations with as good an estimate as possible for the initial function $\hat{\phi}^{(0)}$. For single source cases, the initial function $\hat{\phi}^{(0)}$ is easy to construct: simply take $\hat{\phi} - \phi_s$ on the surface, and $\hat{\phi} = 0$ on the basemat, and interpolate linearly in z along each vertical line. Subsequent convergence for $\hat{\phi}$ is not too far from zero on all the boundaries.

For the multi-bubble LOCA cases, the situation is quite different. Above the sources the flow is essentially a vertical slug with uniform velocity up to the surface, while below the sources the flow is very small. Thus ϕ rises from zero on the surface to some large value near the

bubbles. From this knowledge of the phenomenon the following construction for the initial function was developed:

(1)   Calculate the average surface velocity:

$$V_{surf} \;=\; \Sigma Q/\text{area of surface}$$

(2)   The total ϕ behaves like:

$$\phi \;\cong\; V_{surf}(z_{surf} - z) \qquad\qquad \text{far above the sources}$$
$$\phi \;\cong\; \phi \text{ sources} \qquad\qquad\qquad\quad \text{near the source}$$
$$\phi \;\cong\; V_{surf}(z_{surf} - z_s) \qquad\qquad \text{far below the source}$$

(3)   From (2) above use:

$$\hat{\phi} \;=\; V_{surf}(z_{surf} - z) - \phi_s \qquad\qquad \text{above the source}$$
$$\hat{\phi} \;=\; V_{surf}(z_{surf} - z_s) - \phi_{s'}\,, \qquad\qquad |z - z_s| < 12''$$
$$\hat{\phi} \;=\; V_{surf}(z_{surf} - z_s)\,, \qquad\qquad\quad |z - z_s| < -12''$$

The prescription is designed to obtain the correct $\hat{\phi}$ away from the sources quickly, and not to introduce any singular parts into $\hat{\phi}$ near the sources. Naturally, such estimates are arbitrary, but absolute accuracy of the initial estimates are not required anyway.

3A.B.6   CONVERGENCE AND ACCURACY

This section is concerned with the accuracy of the finite difference solution. A good numerical solution is one that accurately approximates the exact solution. The approach of the numerical solution to the exact solution as the grid is refined is called convergence of the numerical solution. If an iterative scheme is used, as in our case, convergence of the iterations is defined by the difference between any two iterations approaching zero as the number of iterations is increased.

For this scheme, theory assures us that both kinds of convergence take place (Reference 3A.B-3) provided $0 < \omega < 2$ (see Section 3A.B.3) and provided small enough grids and large enough number of iterations are used. The real questions, of course, are whether small enough grids and enough iterations have been used to guarantee an accurate enough approximate solution.

To check convergence of the numerical solution LOCA bubble charging, SRV, etc. were recalculated with several different grid sizes until the change in the solution was insignificant. Figure 3A.B-4 shows the results of several different grids. Figure 3A.B-1 shows the geometry for a single SRV case.

Convergence of iterations is easier to check by printing the total percent change between two successive iterations, and ascertaining that this change is not more than 0.001% (for single bubble, 300 iterations, for LOCA, 2000 iterations). Note that this suggests accuracy, but does not guarantee it, for even such small changes can be accumulated over a large number of steps and can cause divergence of the solution.

(For example: $\dfrac{M}{\Sigma}\dfrac{1}{n}$ diverges as M approaches infinity but the percent change between successive terms n=1 approaches zero.)

There are additional checks made, namely, overall conservation. To do this, the flow $\iint (\partial\phi/\partial n)ds$ over all the surface areas due to the singular part of the potential, ϕ_s and the smooth part of the potential, $\hat{\phi}$ are calculated. On the solid walls, they are equal and opposite and add up to zero (this is exactly so on vertical walls and on the flat bottom, but only closely so on the slant bottom). On the free surface, the sum of the two should equal exactly the total of all the sources. For the number of iterations performed the solutions are always within 0.1%.

In addition, the integral $\iiint \overline{V}^2\phi dV$ is calculated. For the smooth part, this should equal zero, while for the singular part, this should equal the total flow of N sources, $(N \cdot 4\pi)$. The first is accurate always to within 0.1 in.^{3}/sec, the latter agrees with the sum of the free surface flows to within 0.1%. This however, is not coincidental, since the finite difference approximation of the Laplacian operator has been chosen to be "conservative", i.e., the Gauss theorem holds for the difference approximation.

Finally, the integral, $\iiint_3 \left|\overline{V}^2\phi\right|dV$, is also calculated and vanished to within 0.1 in.^{3}/sec for the smooth part. This same integral is calculated for the singular part and should also equal the total source flows which in fact it does not. This is unimportant, since the singular part is never calculated by finite difference except at the boundary, and the finite difference Laplacian is not expected to be accurate for the singular functions.

3A.B.7   RESULTS

In this section, some computed results for two representative cases are presented and analyzed: (a) slanted bottom pool, LOCA bubble charging event and, (b) flat bottom pool, LOCA bubble charging event.

In all the velocity results presented, the source strengths have been normalized to:

$$Q/4\pi = 10,000 \text{ in.}^3/\text{sec}$$

i.e., the flow velocity is 100 in./sec at a radius of 10 in. from the source center, or the total flow is $4\pi \times 10^4 \text{ in.}^3/\text{sec}$. However, to keep the potentials in a more manageable range, the printed values are 1/10 of the potentials corresponding to the above normalized source strength (i.e., the reader should multiply all printed potentials by 10 to get the correct value).

3A.B.7.1   Loss-of-Coolant Accident Bubble Charging

Loss-of-coolant accident bubble charging calculations were made under the assumption that all bubbles are of the same strength ($Q/4\pi = 10,000$). Then by symmetry, it suffices to perform the calculation for a wedge of angle $2\pi/34 = 10.6^\circ$ radius (since there are three rows of 34 downcomers). By further symmetry, it suffices to consider just a half-wedge, or 5.29°, since the plane exactly halfway between two downcomer planes is a symmetry plane. Figure 3A.B-2 gives the geometry of the LOCA bubble charging calculations. The flat bottom calculations used 16 points in r, 26 points in z, and 10 points in θ; corresponding to grid sizes of $\Delta r = 23.75 \text{ in.}$, $\Delta \theta = 0.01155 \text{ rad}$, and $\Delta z = 15.26 \text{ in.}$ Figure 3A.B-5 shows the potential distribution at a plane near the sources and Figure 3A.B-6 shows the same at the plane midway between two source planes. Figures 3A.B-7 and 3A.B-8 show the velocity in the planes $\theta = 0^\circ$ and $\theta = 5.29^\circ$, respectively.

There are some physically interesting features revealed in these calculations. (a) In contrast to one or a few single bubbles, when LOCA bubbles grow in phase, flow below the source is essentially negligible. (b) There is very little variation in the flow pattern in the azimuthal (θ) direction, except of course, at the exact elevation of the sources. (c) Although the sources have the same strength, the innermost source has a stronger influence on the flow than does the outermost one, simply because of the increased density of the bubbles as one approaches the pedestal. (d) From calculations for three-dimensional LOCA flow for the flat bottom case (Figure 3A.B-9) the smallness of the velocities (or essentially constant ϕ values) below the source levels, indicates that the effect of the slant bottom is negligible.

3A.B.8   REFERENCES

3A.B-1   Analytical Model for Estimating Drag Forces on Rigid Submerged Structures
             Caused by LOCA and SRV Ramshead Air Discharges, General Electric
             Company, NEDE-21471 (Proprietary), September 1977.

3A.B-2   Theoretical Hydrodynamics, by L. M. Milne-Thompson, the Macmillan
             Company, N.Y., 1950.

3A.B-3   <u>Analysis of Numerical Methods</u>, by E. Isaacson and H. B. Keller, John Wiley & Sons, Inc., N.Y., 1966.

A) Plan View of Suppression Pool
   Showing Single SRV Symmetry
   About θ = 0° to 180°
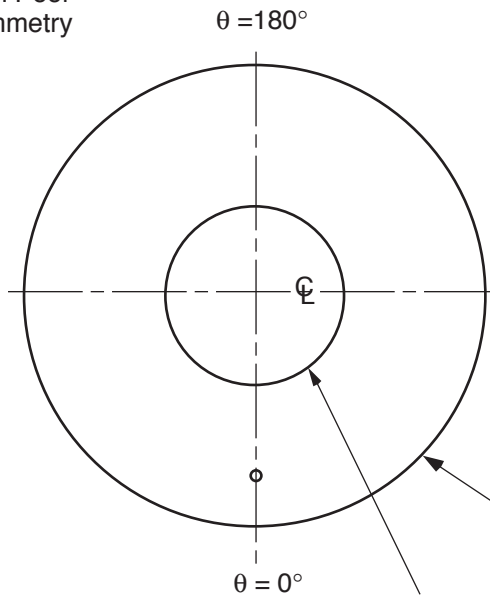
θ =180°

C̶L

θ = 0°

Pedestal Wall   Containment Wall

B) Conceptualization Showing
   Geometry that was Modeled

C̶L

θ =180°   j Max   k Max   θ = 0°

i Max

i,j,k = 1

165.0"

Z

θ

r   395.125"
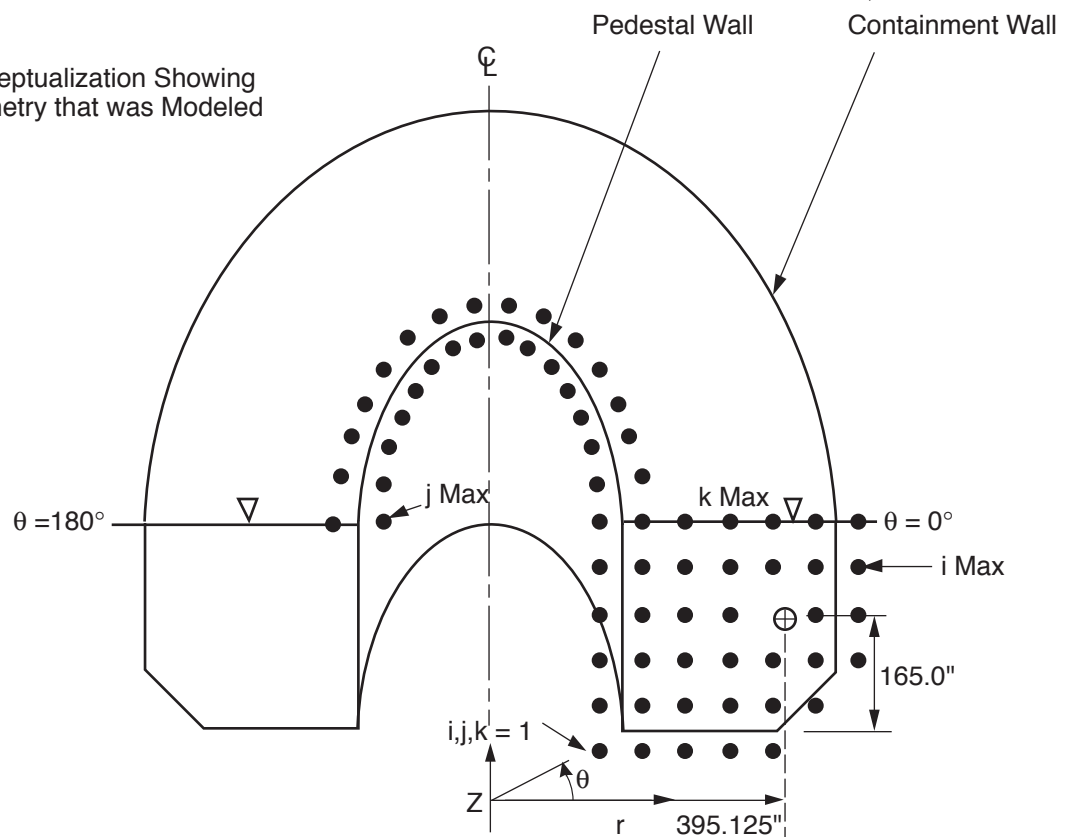
Notes:

1) ○ Indicates Downcomer Location

2) ⊕ Indicates Source/Bubble Location

3) C̶L Indicates Suppression Pool Centerline

4) ● Indicates Velocity Potential Grid Points

Geometry for Single SRV Case

Columbia Generating Station
Final Safety Analysis Report

| Draw. No. 900547.82 | Rev. | Figure 3A.B-1 |

A) Plan View of Suppression Pool
Showing Downcomer Symmetry
About θ = 0°
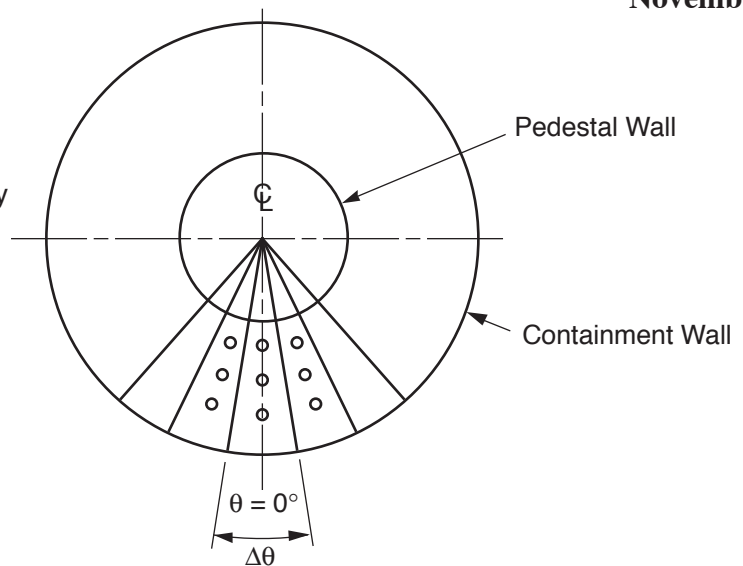
Pedestal Wall

Containment Wall

θ = 0°

Δθ

B) Conceptualization
Showing Geometry that
was Modeled

i,j = 1
k = kMax

Pedestal Wall

iMax, jMax, kMax

Containment Wall

Δθ/2

θ = 0°

217.75"

Z

r1 = 276" r2 = 360" r3 = 444"

32.5°
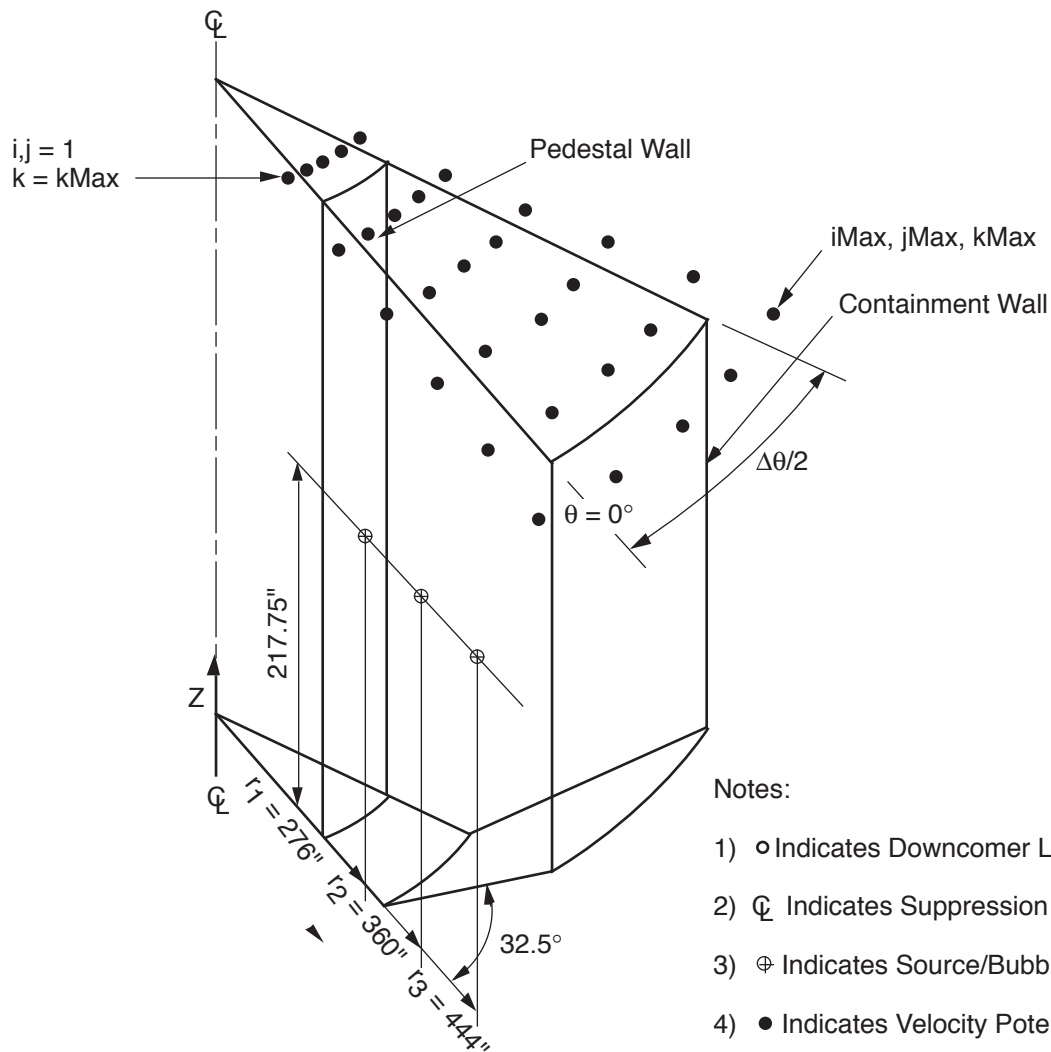
Notes:

1) ○ Indicates Downcomer Location

2) ₵ Indicates Suppression Pool Center Line

3) ⊕ Indicates Source/Bubble Location

4) ● Indicates Velocity Potential Grid Points

Columbia Generating Station
Final Safety Analysis Report

Geometry for LOCA Bubble Charging Case

Draw. No. 900547.81 | **Rev.** | **Figure** 3A.B-2

Form No. 960690

A) Relationship of Velocity Potential
Grid Versus Velocity Grid

$\hat{\varnothing}_{i, j+1, k+1}$

$\hat{\varnothing}_{i+1, j+1, k+1}$

$\hat{\varnothing}_{i, j, k+1}$

$\hat{\varnothing}_{i+1, j, k+1}$

$v_{i, j, k}$

Δz

$\hat{\varnothing}_{i, j+1, k}$

$r\Delta\theta$

k

j

i

$\hat{\varnothing}_{i,j,k}$

$\hat{\varnothing}_{i+1, j, k}$

Δr
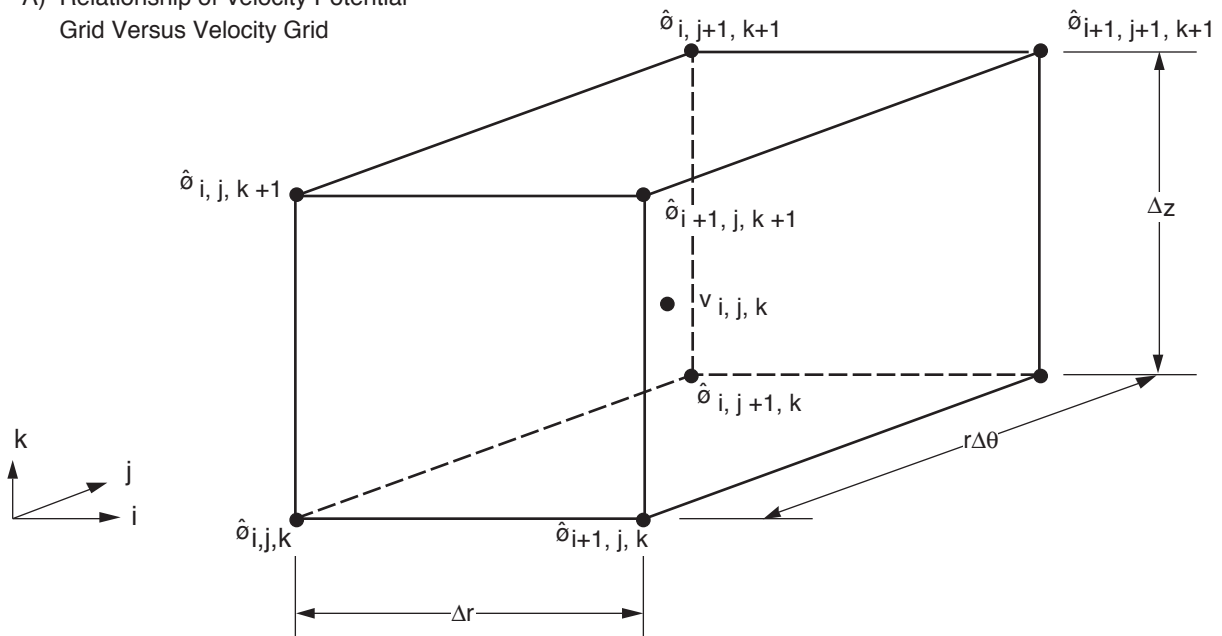
B) Conceptualization of How
$v\hat{\theta}$ Is Calculated.

$\hat{\varnothing}$ Averaged
on This Wall
Equal $\varnothing_2$

$v\hat{\theta}_{i,j,k}$

$\hat{\varnothing}$'s Averaged
on This Wall
Equal $\varnothing_1$

$r\Delta\theta$

k

j

i
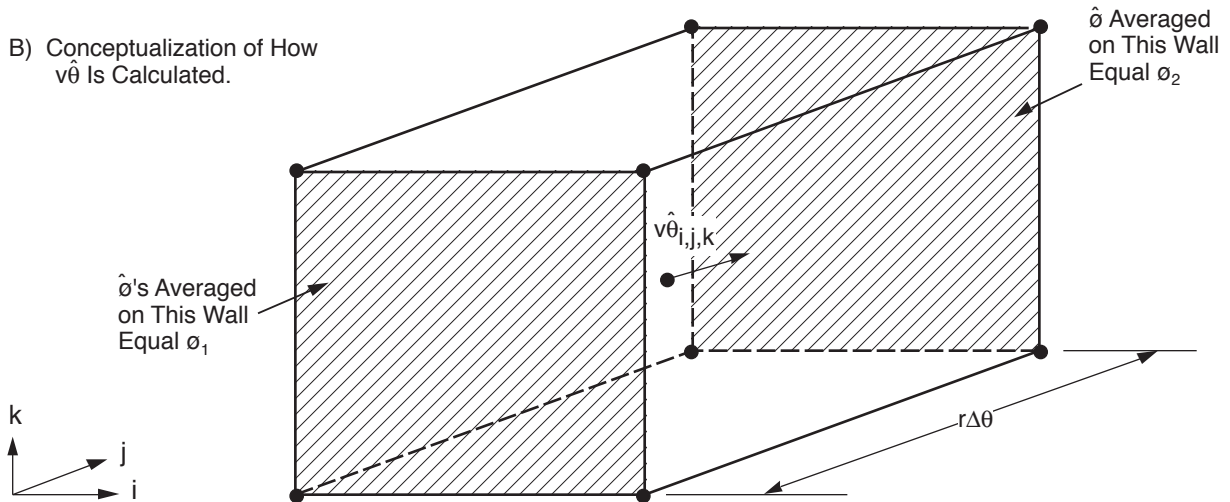
$\varnothing_1 = (\hat{\varnothing}_{i, j, k} + \hat{\varnothing}_{i+1, j, k} + \hat{\varnothing}_{i+1, j, k+1} + \hat{\varnothing}_{i, j, k+1})/4$

$\varnothing_2 = (\hat{\varnothing}_{i, j+1, k} + \hat{\varnothing}_{i, j+1, k+1} + \hat{\varnothing}_{i+1, j+1, k+1} + \hat{\varnothing}_{i+1, j+1, k})/4$

$v\hat{\theta} = \dfrac{\hat{\varnothing}_1 - \hat{\varnothing}_2}{r\Delta\theta}$
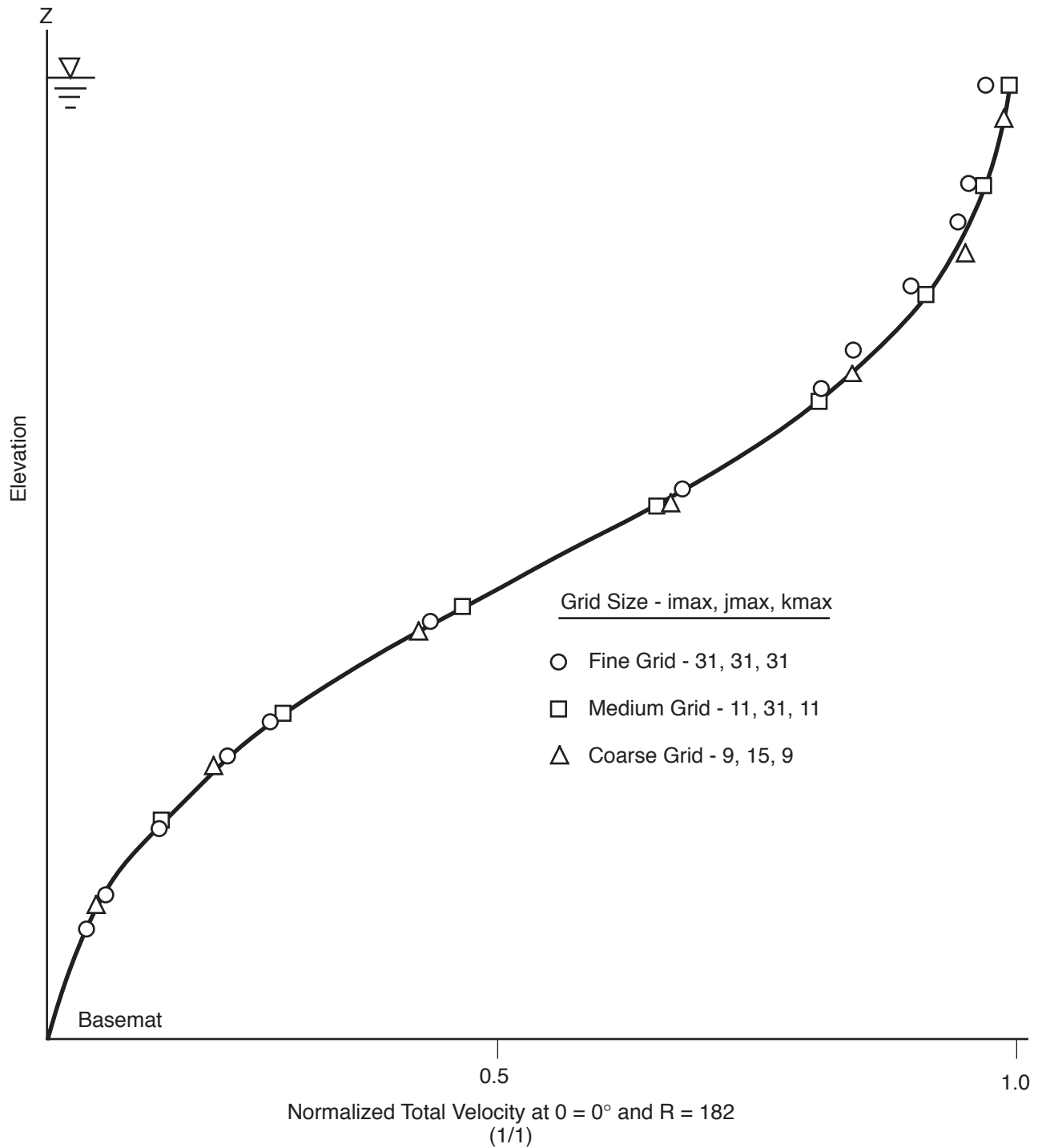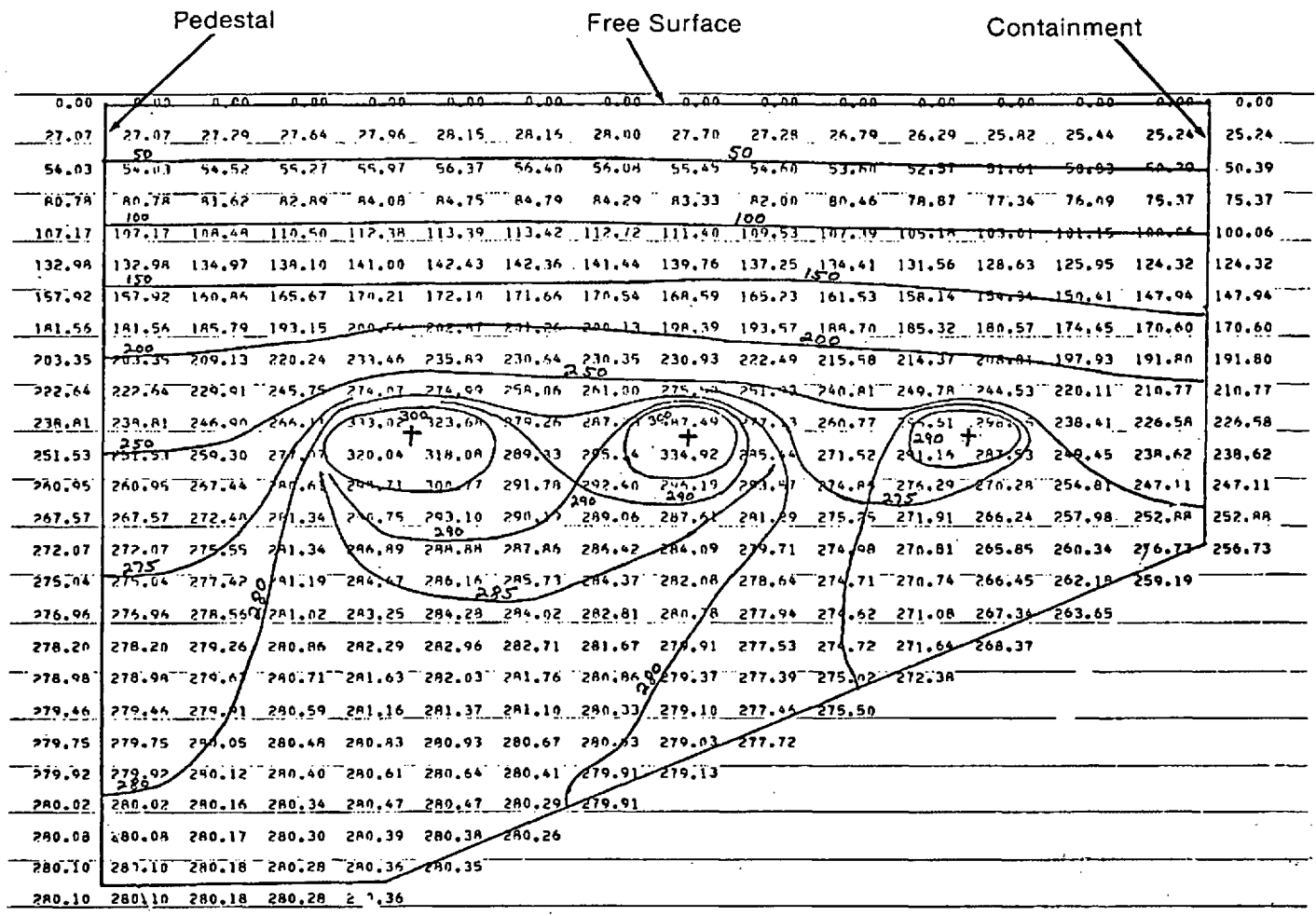
Columbia Generating Station
Final Safety Analysis Report

Velocity Grid

Draw. No. **900547.83** | Rev. | Figure **3A.B-3**

Form No. 960690

Z

Elevation

Basemat

Grid Size - imax, jmax, kmax

○   Fine Grid - 31, 31, 31

□   Medium Grid - 11, 31, 11

△   Coarse Grid - 9, 15, 9

0.5

1.0

Normalized Total Velocity at 0 = 0° and R = 182
(1/1)

Columbia Generating Station
Final Safety Analysis Report

Grid Convergence Test

Draw. No. **900547.80**   **Rev.**   **Figure** **3A.B-4**

Form No. 960690

Φ Units: in²/sec for a Point Source of Strength 10^{+3} in³/sec

Pedestal   Free Surface   Containment

Notes:
1. + indicates radial and vertical locations of the sources.
2. See Figure 3A.B-2 for geometry.

Columbia Generating Station Final Safety Analysis Report	Velocity Potential, Φ, in Plane 0.33° Away from Sources for LOCA Bubble Slant Bottom Case

Draw. No. 020361.23	Rev.	Figure 3A.B-5
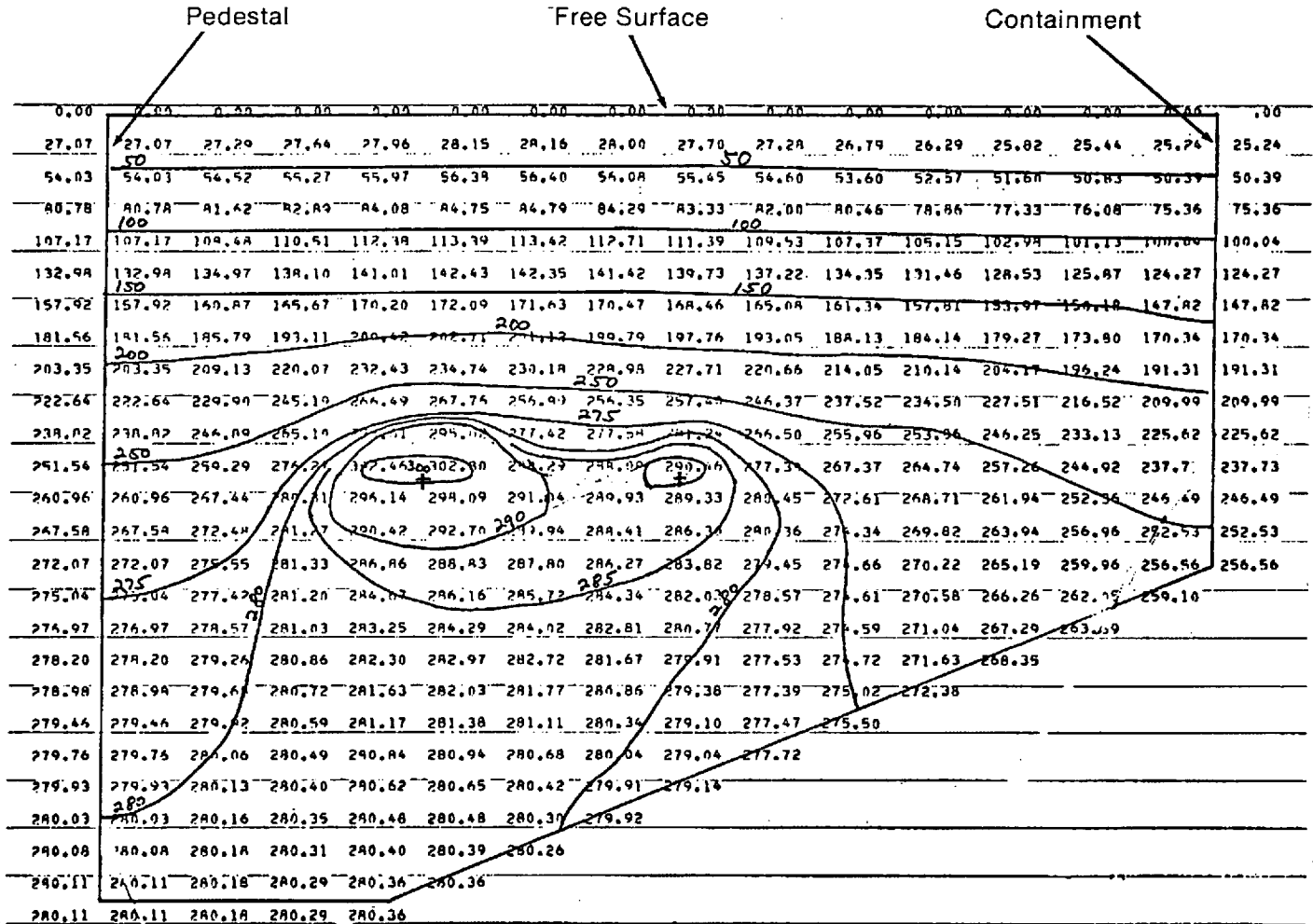
Form No. 960690

Φ Units: in²/sec for a Point Source of Strength 10^{+3}in³/sec

Pedestal   Free Surface   Containment

Notes:
1. + indicates radial and vertical locations of the sources.
2. See Figure 3A.B-2 for geometry.

Columbia Generating Station Final Safety Analysis Report	Velocity Potential, Φ, in Plane 4.96° Away from Sources for LOCA Bubble Slant Bottom Case
	Draw. No. 020361.24 Rev. Figure 3A.B-6

∇Φ Units: in/sec for a Point Source of Strength 10^{+4} in³/sec

Pedestal   Free Surface   Containment
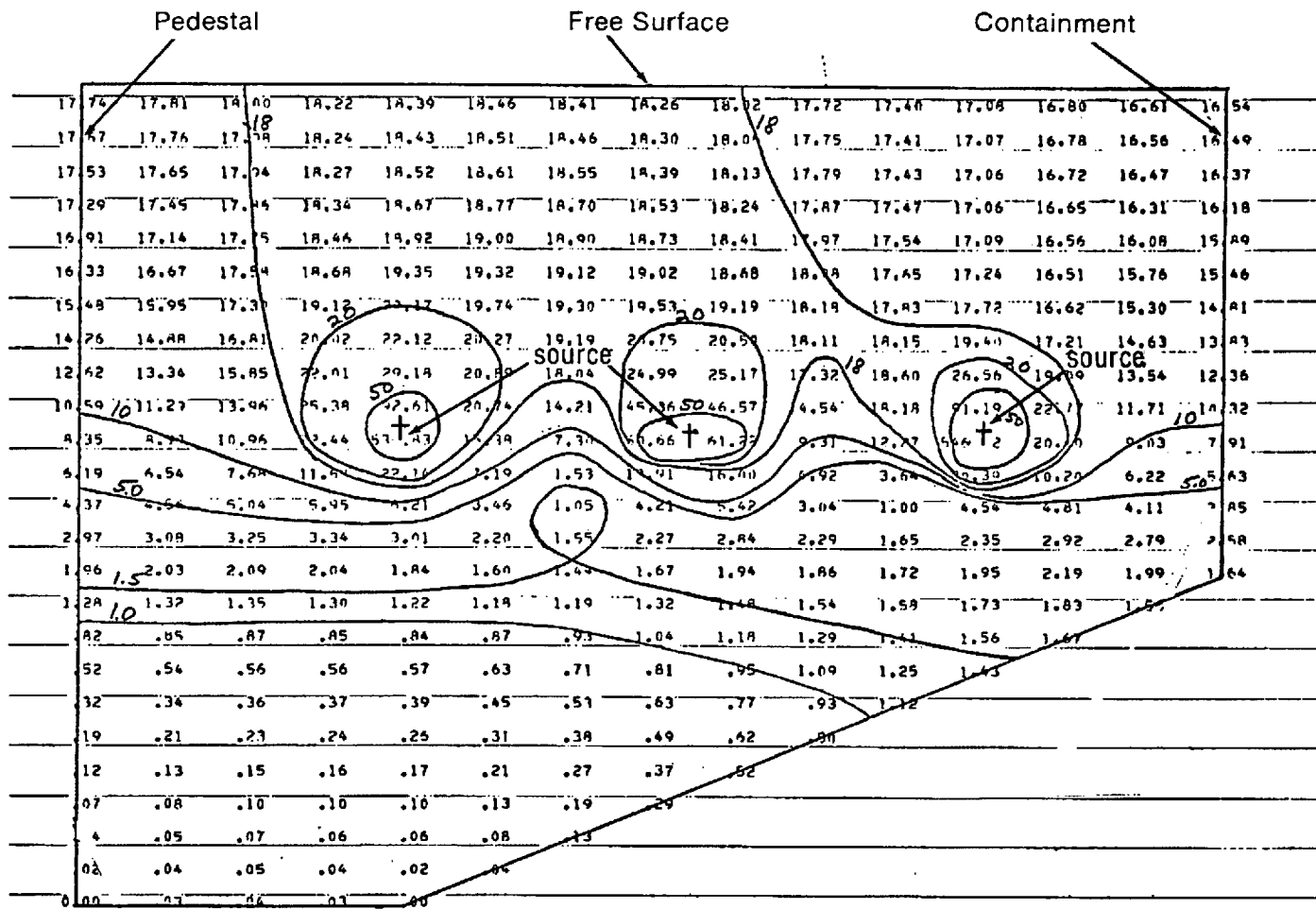
source   source

Note:
1. Figure 3A.B-2 shows geometry.

Columbia Generating Station Final Safety Analysis Report	Total Velocity Gradient, ∇Φ, in Source Plane for LOCA Bubble Slant Bottom Case
	Draw. No. 020361.25 Rev. Figure 3A.B-7

Form No. 960690

∇Φ Units: in/sec for a Point Source of Strength 10^{+4}in³/sec

Pedestal   Free Surface   Containment

17	74	17.81	18.00	18.22	18.39	18.46	18.41	18.26	18.02	17.72	17.40	17.08	16.80	16.61	16	54
17	47	17.76	17.98	18.24	18.43	18.51	18.46	18.30	18.06	17.75	17.41	17.07	16.77	16.56	16	49
17	53	17.65	17.94	18.28	18.52	18.61	18.56	18.39	18.13	17.79	17.43	17.06	16.72	16.46	16	37
17	29	17.45	17.87	18.34	18.67	18.77	18.70	18.53	18.24	17.86	17.46	17.05	16.63	16.30	16	17
16	91	17.15	17.76	18.46	18.92	19.00	18.89	18.72	18.39	17.95	17.50	17.04	16.52	16.06	15	88
16	33	16.67	17.55	18.68	19.33	19.32	19.11	18.97	18.61	18.03	17.54	17.05	16.37	15.70	15	62
15	48	15.95	17.32	19.09	20.05	19.70	19.24	19.27	18.87	18.01	17.48	17.07	16.14	15.15	14	74
14	27	14.90	16.84	19.77	21.26	20.01	18.99	19.49	19.11	17.64	17.09	16.94	15.79	14.30	13	72
12	43	13.36	15.85	20.64	22.75	19.67	17.53	18.93	18.74	16.32	15.73	16.06	14.87	12.95	12	22
10	58	11.31	13.91	19.57	19.81	16.63	13.51	15.10	15.68	13.19	12.41	13.04	12.71	10.95	10	23
8	35	8.82	10.77	13.08	7.06	9.53	7.18	6.55	9.04	6.54	7.36	7.78	9.29	8.45	7	95
6	19	4.53	7.56	9.06	4.76	4.68	1.74	.54	4.83	4.75	3.30	4.00	6.15	6.03	5	76
4	34	4.55	4.00	5.50	4.15	2.89	.89	1.73	3.35	2.98	1.98	2.81	4.11	4.14	3	98
2	96	3.07	3.24	3.30	2.72	2.10	1.43	1.84	2.46	2.28	1.89	2.34	2.92	2.95	2	66
1	96	2.03	2.09	2.04	1.80	1.58	1.43	1.59	1.87	1.86	1.78	2.01	2.24	2.03	1	68
1	54	1.32	1.15	1.31	1.22	1.18	1.19	1.30	1.47	1.55	1.60	1.76	1.86	1.39		
	82	.85	.87	.85	.84	.87	.93	1.04	1.17	1.29	1.42	1.57	1.69			
	51	.54	.56	.56	.58	.63	.71	.81	.95	1.09	1.25	1.44				
	32	.34	.36	.37	.39	.45	.51	.63	.77	.93	1.12					
	19	.21	.23	.24	.26	.31	.38	.49	.62	.80						
	12	.13	.15	.16	.17	.21	.27	.37	.52							
	07	.08	.10	.10	.10	.13	.19	.29								
	14	.05	.07	.06	.06	.08	.13									
	02	.04	.05	.04	.02	.04										
0	00	.03	.04	.03	.00											

Note:
1. **+** indicates radial and vertical locations of the sources.

Columbia Generating Station **Final Safety Analysis Report**	**Total Velocity Gradient, ∇Φ, in Source Plane 5.29°** **Away from Sources for LOCA Bubble Slant Bottom** **Case**
	Draw. No. 020361.26 | Rev. | Figure 3A.B-8

Φ Units: in²/sec of a Point Source of Strength 10⁺⁹in³/sec

Pedestal   Free Surface   Containment
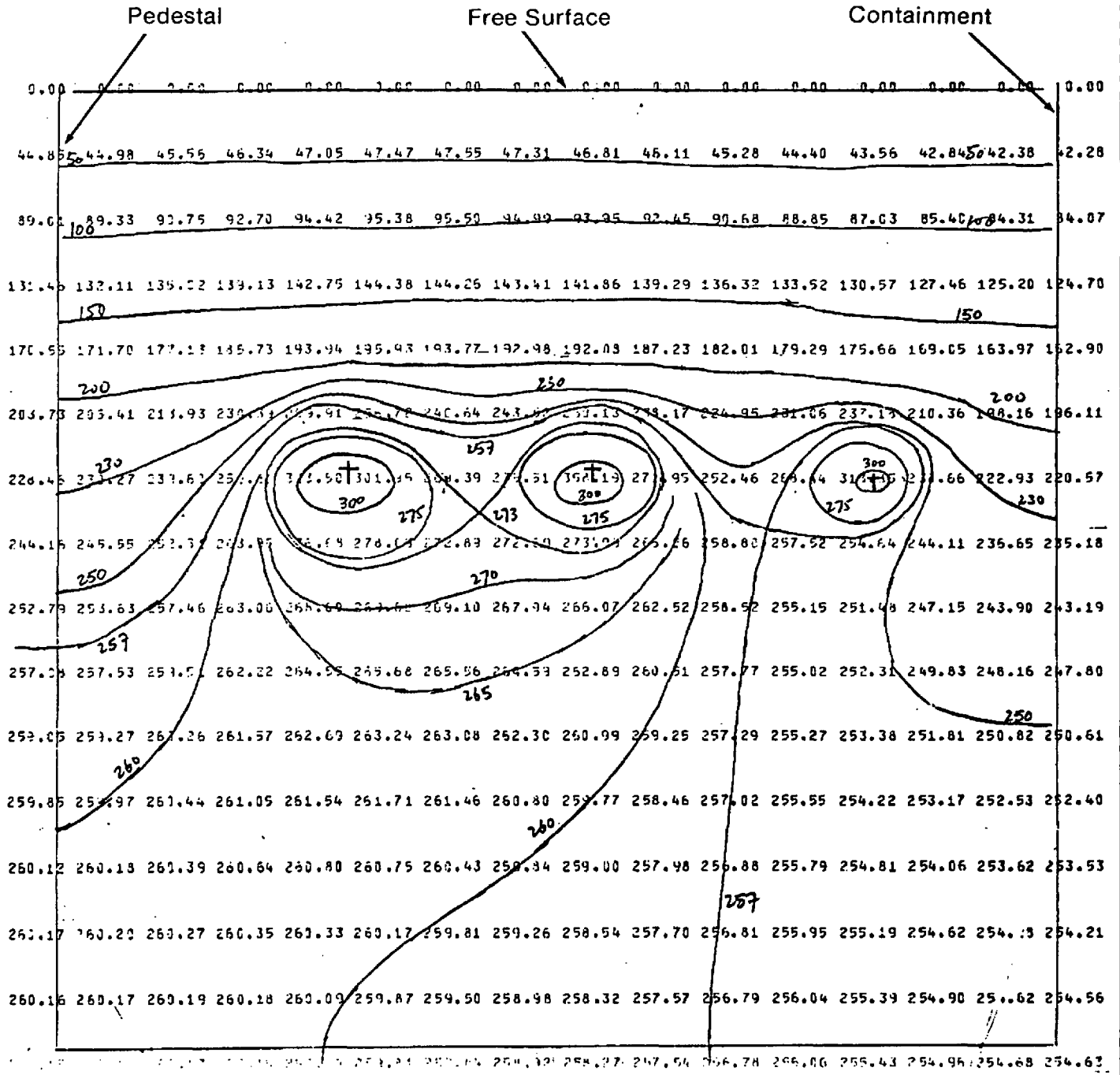
Notes:
1. + indicates radial and vertical locations of the sources.
2. Figure 3A.B-2 shows approximate geometry.

Columbia Generating Station Final Safety Analysis Report	Velocity Potential, Φ, in Plane 0.33° Away from Sources for LOCA Bubble Flat Bottom Case
	Draw. No. 020361.27 Rev. Figure 3A.B-9

Form No. 960690

Attachment 3A.C

CONCEPT OF DRAG FORCES DUE TO HYDRODYNAMIC FLOW FIELDS

3A.C.1   CONCEPT

The concept of drag forces is described in Reference 3A.C-1 as a means to estimate loads on submerged structures due to flow fields created in a Mark II containment suppression pool by the hydrodynamic events described in Section 3A.3. Loads resulting from the actual distorted flow around a structure may be estimated by postulating an equivalent locally uniform flow field due to the safe forcing function in the pool without any structures. This uniform flow is characterized by the velocity and acceleration fields present at the geometric center of the structure or structural segment. The loads on submerged structures are characterized by drag forces due to locally uniform velocity and acceleration fields. The velocity field causes a standard drag force and a lift force, and the acceleration field causes an acceleration drag force. The total load on the structure or structural component is obtained by the vectorial summation of these forces.

Information essential for calculating the drag loads is identified below.

3A.C.2   FORMULAS FOR DRAG LOADS

In the following three sections, formulas are presented to calculate velocity drag load, acceleration drag load, and lift load. The methodology described below is in general agreement with Reference 3A.3.2-4.

Long structures are divided into segments for more precise evaluation. This is done to account for the variations of the velocity and acceleration along the structure.

3A.C.2.1   Velocity Drag Load

The velocity drag load is calculated using the following formula:

$$P_s = \frac{1}{2}\rho \ C_D \ V_{max}^2$$

where:

P_s = velocity drag pressure amplitude (psi). This pressure acts in the flow direction.

ρ = mass density of water (lb sec^2/in.^{4}).

C_D = standard drag coefficient. Numerical values for C_D are given in the applicable sections of Section 3A.3.

V_{max} = maximum velocity in the direction of flow (in./sec).

3A.C.2.2   Acceleration Drag Load

The acceleration drag load is calculated using the following formula:

$$P_A = \rho\, C_M\, \frac{\pi}{4}\, D\, V_{max}^2$$

where:

A = acceleration drag pressure amplitude (psi). This pressure acts in the flow direction.

C_M = acceleration drag coefficient. Numerical values for C_M are given in the applicable sections of Section 3A.3.

D = diameter of cylindrical structure (in.). If the structure is not cylindrical, D is the diameter of a cylinder circumscribing the structure.

V_{max} = maximum acceleration in the direction of flow (in./sec^2).

3A.C.2.3   Lift Load

The lift load is calculated using the following formula:

$$P_L = \frac{1}{2}\, \rho\, C_L\, V_{max}^2$$

where:

P_L = lift pressure amplitude (psi). This pressure is normal to the flow direction.

C_L = lift coefficient. Numerical values for C_L are given in the applicable sections of Section 3A.3.

3A.C.3   REFERENCES

3A.C-1   "Analytical Model for Estimating Drag Forces on Rigid Submerged Structures caused by LOCA and Safety/Relief Valve Ramshead Air Discharges," General Electric Company, NEDO-21471, September 1977.

Attachment 3A.D

CALCULATION MODELS FOR SHORT-TERM
LOSS-OF-COOLANT ACCIDENT PHENOMENA

3A.D.1   INTRODUCTION

This attachment provides additional information concerning the numerical techniques used to model short term hydrodynamic phenomena. The vent clearing, pool swell, and loss-of-coolant accident (LOCA) bubble numerical models are discussed in Sections 3A.D.2, 3A.D.3, and 3A.D.4 respectively. In each section, the model assumptions, equations, numerical techniques, and verification are either discussed in detail or referenced to the appropriate General Electric document.

3A.D.2   DOWNCOMER VENT CLEARING MODEL

The pool swell analytical model (PSAM), (Reference 3A.D-1), models the pool swell event subsequent to downcomer vent water clearance. Initial conditions required to start the PSAM include the time of vent clearing and the pool surface displacement, velocity, acceleration, and wetwell pressure at the time of vent clearing. In order to provide a time history of the suppression pool surface during the downcomer vent clearing process and a conservative input to the PSAM, the computer code VENT was developed. VENT is a subroutine for the PSAM computer code SWELL (see Section 3A.D.3). By continuity the downcomer vent exit water velocity and acceleration time histories are also calculated. These transients are used as conservative input to the LOCA water jet code (see Section 3A.3.2.3.1.1).

Section 3A.D.2.1 discusses the downcomer vent clearing model development and Section 3A.D.2.2 discusses the experimental verification and the conservatism of the model.

3A.D.2.1   Model Development

Assumptions used in developing the vent clearing model are as follows:

      a.   The frictional losses of the pool system are conservatively neglected,

      b.   The wetwell free air volume is isentropically compressed by the upward moving water slug,

      c.   Heat losses are neglected,

      d.   The air velocity within the downcomers is small, therefore the air pressure in the vents is conservatively assumed to equal the current drywell pressure,

e.   Downcomer vent losses are conservatively neglected, and

f.   Viscous effects are neglected.

Figure 3A.D-1 shows a schematic of the vent clearing model. The mathematical derivation of this model is similar to the model in Reference 3A.D-2 with the exception that the vent clearing model described here couples the equation of motion for the vent system with the equation of motion for the pool system.

3A.D.2.1.1   Drywell Pressure

The time varying drywell pressure, P_D, is the driving function for the vent clearing analysis. P_D is not calculated by VENT but is input as data.

3A.D.2.1.2   Water in the Downcomer Vents

The mass of water within the downcomer vents, m', that is being accelerated downward by the increasing drywell pressure transient is given by:

$$m' = \rho_w(H_o - h)A_V \qquad \text{(3A.D-1)}$$

where

ρ_w = the density of water

A_V = the total downcomer vent exit area

H_o = the initial submergence of the downcomers

h = the displacement of the internal downcomer water surface.

3A.D.2.1.3   Water Slug in the Suppression Pool

The mass of the water slug in the suppression pool, m, which is being accelerated upward by the increasing drywell pressure is given by:

$$m = \rho_w(H_o + z)A_p \qquad \text{(3A.D-2)}$$

where

A_p = the net suppression pool water surface area

z = the displacement of the pool surface.

3A.D.2.1.4 Suppression Chamber Air Space

From assumption 2, the transient pressure in the suppression chamber air space, P_s, is calculated from:

$$P_s = P_{so}(V_{so}/V_s)^k$$

where

V_s = $V_{so} - A_v h$

V_{so} = initial wetwell free air space volume

P_{so} = initial wetwell air pressure

k = specific heat ratio of air.

Combining and solving yields:

$$P_s = P_{so}(V_{so}/(V_{so} - A_v h))^k$$

3A.D.2.1.5 Fluid Dynamics

Refer to Figure 3A.D-1. From Newton's second law, MA = F, the equation of motion for the water inside of the vents is:

$$m' \frac{d^2h}{dt^2} = (P_D - P_\infty)A_v = \rho_w A_v (H_o - h)g$$

where

P_∞ = the pressure at the downcomer vent exit.

Combining with equation 3A.C-1 and solving for $\dfrac{P_D - P_\infty}{\rho_w}$ yields:

$$\frac{P_D - P_\infty}{\rho_w} = \left(H_o - h\right)\frac{d^2n}{dt^2} - \left(H_o - h\right)g \qquad\qquad (3A.D-3)$$

Also from Newton's second law, the equation of motion for the water outside of the vents is:

$$m\frac{d^2z}{dt^2} = \left(P_\infty - P_s\right)A_p - \rho_w A_p\left(H_o + z\right)g$$

Combining with equation 3A.D-2 and solving for $\dfrac{P_\infty - P_s}{\rho_w}$ yields:

$$\frac{P_\infty - P_s}{\rho_w} = \left(H_o + z\right)\frac{d^2z}{dt^2} + \left(H_o + z\right)g \qquad\qquad (3A.D-4)$$

Substituting $h\,A_v/A_p$ for z (see Figure 3A.D-1) in equation 3A.D-4 and then summing equations 3A.D-3 and 3A.D-4 and solving for d^2h/dt^2 yields:

$$\frac{d^2h}{dt^2} = \frac{\dfrac{P_D - P_s}{\rho_w} - g\,h\left(1 + A_v/A_p\right)}{H_o\left(1 + A_v/A_p\right) - h\left(1 - \left(A_v/A_p\right)^2\right)} \qquad\qquad (3A.D-5)$$

Integration of d^2h/dt^2 yields the downcomer vent water velocity, dh/dt, and displacement, h, transients:

$$\frac{dh}{d5} = \int_0^t \frac{d^2h}{dt^2}\,dt \qquad\qquad (3A.D-6)$$

$$h = \int_0^t \frac{dh}{dt}\,dt \qquad\qquad (3A.D-7)$$

where

      t   = time after LOCA initiation.

The pool surface acceleration, velocity, and displacement transients are related by continuity to the vent water transients by a factor of A_v/A_p (see Figure 3A.D-1). It is important to note that at $h = H_o$, equation 3A.D-5 is the same as the equation of motion used in the PSAM (Reference 3A.D-7). This implies that equation 3A.D-5 plus the PSAM will provide a continuous and consistent time history of the suppression pool surface displacement during a LOCA.

3A.D.2.1.6   Numerical Integration

Sections 3A.D.2.1.1 and 3A.D.2.1.4 show that the drywell pressure, P_D, and the wetwell air space pressure, P_S are functions of time and vent water displacement, respectively. From equation 3A.D-5 this shows that the downcomer vent water acceleration, d^2h/dt^2, is a function of time and vent water displacement only. This means that equation 3A.D-5 is a second order differential equation of the functional form: $d^2h/dt^2 = f(t,h)$, where $h = h(t)$ by equation 3A.D-7. This allows numerical integration of equation 3A.D-5 using a fourth order Runge-Kutta technique given by equation 25.5.22 of Reference 3A.D-3. Integration of d^2h/dt^2 gives dh/dt and h (equations 3A.D-6 and 3A.D-7, respectively).

3A.D.2.1.7   Termination of Vent Clearing Analysis

Termination of the vent clearing analysis occurs when $H_o - h \leq O$. This is the moment that the vent clearing is completed; or t_o, vent clearance time.

3A.D.2.1.8   Input Data and Results

Input to the VENT subroutine requires data on the following plant characteristics: net pool area (A_p), total downcomer vent exit area (A_v), initial submergence of the downcomers (H_o), initial wetwell pressure (P_{so}), initial wetwell free air volume (V_{so}), and the drywell pressure transient (P_D). Table 3A.3.2-3 shows the CGS input data for the VENT computer code.

The vent exit water velocity and acceleration calculated by VENT are increased by 10% as indicated by the NRC in Reference 3A.3.2-1. The velocity and acceleration time histories (including the 10% increase) are shown in Figures 3A.3.2-2 and 3A.3.2-3, respectively.

3A.D.2.2   Experimental Verification

VENT has been verified against downcomer vent water displacement data from the 4T Test Series 5101, runs 21, 22, 24, and 37 (Reference 3A.D-4). These runs were chosen because they ran the full range of Mark II submergences and drywell pressurization rates. In each run, three conductivity probes were used to determine the displacement of the downcomer vent air/water interface. These probes, shown in Figure 3-3 of Reference 3A.D-5, sense the difference in conductivity between air and water. For each test, the three probes were located

in each downcomer at 0.5 ft, 6.5 ft, and 9.5 ft above the downcomer vent exits (see Figure 3-2 of Reference 3A.D-5).

Tables 3A.D-1 and 3A.D-2 show the input data to VENT for the verification runs. Table 3A.D-3 shows the measured and calculated 4T Test downcomer vent probe water clearing times. Figure 3A.D-2 summarizes the data in Table 3A.D-3 and shows that the comparison is excellent.

3A.D.3   POOL SWELL ANALYTICAL MODEL

In order to conservatively calculate the pool swell transient, the computer code SWELL was developed after the model discussed in References 3A.D-1, 3A.D-6, and 3A.D-7. The equations used in the SWELL computer code are documented in those references. The PSAM is schematically shown in Figure 3A.D-3 and its verification against empirical data and its conservatism is discussed in References 3A.D-1, 3A.D-6, 3A.D-7, and 3A.D-8. Input to SWELL requires data on the following plant characteristics: net pool area, total downcomer vent exit area, initial submergence of the downcomers, initial drywell air pressure, initial wetwell air pressure, initial drywell air temperature, initial wetwell free air volume, initial drywell humidity, downcomers loss coefficient, time of vent clearing, vent clearing velocity, and drywell air pressure transient.

Figures 3A.D-4 through 3A.D-9 are plots of pool surface velocity and pool surface elevation obtained with SWELL for the three benchmark plants presented in Reference 3A.D-7. (Note: for these verification runs, the vent clearing subroutine described in Section 3A.D.2 is not used since the vent clearing velocity and time are given in Reference 3A.D-7.) These plots are provided for comparison with the data included in Reference 3A.D-7 as benchmark problems for the SWELL code and show good agreement.

3A.D.4   LOSS-OF-COOLANT ACCIDENT BUBBLE CHARGING MODEL

The one-dimensional PSAM (see Section 3A.D.3) describes the bulk flow process in the suppression pool during a postulated pool swell event. This model assumes a flow field in the vertical direction only. The assumption of predominately vertical flow has been verified by small scale multivent pool swell tests. However, observation of these tests have shown that prior to LOCA bubble coalescence and the forming of an air blanket under the pool water slug, a significant three-dimensional flow field is developed. In response to these observations, new analytical techniques were developed in order to model the LOCA bubble charging event. The purpose of the LOCA bubble charging model, therefore, is to describe the three-dimensional flow fields during the early portion of the pool swell phenomenon.

In order to calculate the transient flow fields in the CGS suppression pool during the LOCA bubble charging portion of a postulated pool swell event, the computer code SOURCE was developed (see Attachment 3A.B). The application of the SOURCE code to the LOCA bubble

charging phenomenon is schematically shown in Figure 3A.B-2. This method uses point sources with the appropriate source strength to represent the LOCA bubble charging event in the exact CGS suppression pool geometry. In using this method it is assumed that all vents uniformly charge air into spherical bubbles with centers one downcomer radius below the vent exits. To calculate the transient LOCA bubble charging flow field, the rate of bubble growth is determined by continuity from the pool surface rise obtained from the PSAM. A comparison of the similarity between this method and the method discussed in Reference 3A.D-9 is provided in Table 3A.D-4.

3A.D.4.1   Potential Flow Field

The three-dimensional potential flow field calculation method that is the basis for the SOURCE computer code is described in Attachment 3A.B. Also described in Attachment 3A.B are the numerical techniques, the flow field calculation procedure, and the conservation, convergence, and accuracy checks of the method. Results for the CGS LOCA bubble charging case is discussed in Sections 3A.B.7 and 3A.3.2.

Although both methods use the same assumptions of potential flow, point sources to represent bubbles, and uniformly charging spherical bubbles, the SOURCE code is used instead of the method of images (MOI) (Reference 3A.D-9) to determine finite pool effects. This is because the SOURCE code models the exact CGS suppression pool geometry, whereas the MOI has to idealize the pool's annular boundaries and sloping floor characteristics.

3A.D.4.2   Source Strength Calculation

The rate of air charging (and, therefore, the rate of bubble radius growth) is determined by continuity from the pool surface rise obtained from the PSAM. In using this method, it is assumed that all vents uniformly charge air into spherical bubbles with centers 1 ft 0 in. below the vent exits. The PSAM method of calculating a transient source strength for use in determining the flow field during LOCA bubble charging is used for the CGS instead of the method presented in Reference 3A.D-9. Source strengths calculated using both methods are presented in the following sections where it is shown that the PSAM method is preferable to the method of Reference 3A.D-9 in that it is more conservative and has experimental verification. General Electric has developed a method to calculate the equivalent bubble charging velocity and acceleration source strengths for a point source in a finite pool. It is described in Reference 3A.D-9. Air bubbles at the downcomer vents during the LOCA bubble charging process are assumed to be spherical. The bubble radius growth time history is obtained by assuming the bubble dynamics are represented by the Rayleigh equation coupled with a mass and energy balance for the bubble. Because the Rayleigh equation models the bubble dynamics in an infinite pool, a factor "K" must be solved for each bubble to correct for finite pool boundary effects. This factor is then multiplied by the Rayleigh bubble velocity and acceleration source strengths to solve for the finite pool velocity and acceleration source strengths at each bubble as shown in Figure 3A.D-10. Table 3A.D-5 provides some CGS

LOCA bubble charging pool surface velocities and accelerations obtained using the source strength method or Reference 3A.D-9 along with the SOURCE computer code. Extensive small scale multivent pool swell tests have shown that the pool surface remains relatively flat during the LOCA bubble charging process. For CGS, the pool surface transient is calculated by the PSAM (see Section 3A.D.3). It is evident in References 3A.D-1 and 3A.D-7 that the PSAM estimates of the pool surface transient during the early portion of pool swell (which is LOCA bubble charging) consistently bounds all experimental data. The small scale multivent pool swell tests also indicate bubble sphericity during the early portion of the transient.

With these observations it is possible to obtain the bubble velocity and acceleration source strengths from the PSAM calculated pool surface transient by continuity as shown in Figure 3A.D-11. Table 3A.D-5 provides some LOCA bubble charging pool surface velocities and accelerations obtained for CGS using the Reference 3A.D-9 method and the PSAM methods for comparison. It is seen that while pool surface accelerations are similar, the pool surface velocities from the Reference 3A.D-9 method are less than 50% of the PSAM values. Therefore, for CGS the PSAM method is conservatively accepted for LOCA bubble source strength definitions.

Figure 3A.3.2-7 shows the velocity, $Q(t)$ and acceleration, $\dot{Q}(t)$, source strengths which are used in CGS load calculations.

3A.D.5   REFERENCES

3A.D-1   Ernst, R. J., Ward, M. G., Mark II Pressure Suppression Containment Systems: An Analytical Model of the Pool Swell Phenomenon, General Electric Company, NEDE-21544-P (Proprietary), December 1976.

3A.D-2   The General Electric Pressure Suppression Containment Analytical Model, General Electric Company, NEDM-10320, April 1971.

3A.D-3   Handbook of Mathematical Functions with Formulas, Graphs, and Mathematical Tables, National Bureau of Standards - Applied Mathematics Series .55, May 1968.

3A.D-4   Phases I, II, and III of the Temporary Tall Tank Test (4T) Program, an Applications Memorandum, Preliminary Draft, General Electric Company, December 1976.

3A.D-5   Mark II - Pressure Suppression Test Program, General Electric Company, NEDE-13442-P-01, May 1976.

3A.D-6   Response to NRC Question 020.68, Appendix A, WNP-2, DAR, Revision 2,
             August 1979.

3A.D-7   Mark II Containment Dynamic Forcing Functions Information Report (DFFR),
             General Electric Company, NEDE-21061, Revision 3, June 1978.

3A.D-8   Comparison of the 1/13 Scale Mark II Containment Multivent Pool Swell Data
             with Analytical Methods, General Electric Company, NEDO-21667,
             August 1977.

3A.D-9   Moody, F. J., Analytical Model for Estimating Drag Forces on Rigid
             Submerged Structures Caused by LOCA and Safety Relief Valve Ramshead Air
             Discharges, General Electric Company, NEDE-21471 (Proprietary),
             September 1977.

Table 3A.D-1

Vent Clearing Analytical Model Input Data

Parameter	21	22	24	37
Net pool area[a], ft^2	35.17	35.17	35.17	35.17
Downcomer vent flow area, ft^2	2.0211	2.0211	2.0211	2.0211
Downcomer submergency, ft	13.15	9.0	13.5	11.0
Integration time step, sec	0.0001	0.0001	0.0001	0.0001
Initial wetwell free air volume, ft^3	950	1108	950	1038
Drywell pressure time history, psia	See Table 3A.D-2			

[a] Excludes area of downcomer.

Table 3A.D-2

Measured 4T Test Series 5101 Drywell Dome
Pressure Time History

Run 21		Run 22		Run 24		Run 37	
Time (sec)	Pressure (psia)	Time (sec)	Pressure (psia)	Time (sec)	Pressure (psia)	Time (sec)	Pressure (psia)
0.	14.63	0.	14.57	0.	14.55	0.	14.54
0.037	14.65	0.037	14.80	0.040	14.53	0.041	14.52
0.055	15.12	0.058	15.30	0.058	14.66	0.060	14.60
0.076	15.61	0.079	15.87	0.076	15.35	0.078	14.93
0.097	15.73	0.097	16.16	0.097	16.12	0.096	16.04
0.115	15.91	0.115	16.42	0.113	16.52	0.114	17.28
0.134	16.18	0.133	16.70	0.133	17.11	0.133	17.91
0.152	16.42	0.152	17.01	0.154	17.80	0.153	18.46
0.170	16.54	0.170	17.47	0.173	18.41	0.174	19.35
0.189	16.80	0.191	17.98	0.191	19.04	0.193	19.94
0.210	17.27	0.212	18.47	0.210	19.54	0.211	20.44
0.230	17.80	0.230	10.89	0.228	20.03	0.230	20.97
0.249	13.10	0.249	19.42	0.246	20.52	0.248	21.54
0.267	18.41	0.267	19.79	0.267	21.07	0.266	22.21
0.285	13.79	0.285	20.33	0.288	21.67	0.287	23.00
0.303	19.08	0.304	20.80	0.306	22.22	0.308	23.77
0.322	19.32	0.324	21.29	0.324	22.73	0.326	24.40
0.343	19.70	0.345	21.87	0.343	23.19	0.344	24.99
0.363	20.03	0.364	22.36	0.361	23.64	0.363	25.54
0.382	20.37	0.382	22.95	0.380	24.11	0.381	26.16
0.400	20.64	0.400	23.29	0.400	24.68	0.400	26.77
0.419	20.94	0.419	23.72	0.421	25.12	0.420	27.40
0.437	21.27	0.437	24.23	0.440	25.61	0.441	27.91
0.455	21.69	0.458	24.75	0.458	26.10	0.460	28.40
0.476	22.06	0.479	25.34	0.476	26.68	0.478	29.00
0.497	22.46	0.497	25.85	0.494	27.21	0.496	29.63
0.515	22.81	0.515	26.30	0.513	27.78	0.514	30.24
0.534	23.15	0.533	26.78	0.533	28.33	0.533	30.81
0.552	23.46	0.552	27.23	0.554	28.87	0.553	31.40
0.570	23.80	0.570	27.76	0.573	29.32	0.574	31.95
0.539	24.13	0.591	28.14	0.591	29.79	0.593	32.43
0.610	24.51	0.612	28.61	0.610	30.21	0.611	32.90
0.630	24.88	0.630	28.99	0.628	30.70	0.630	33.37
0.649	25.26	0.649	29.40	0.646	31.10	0.668	33.79
0.667	25.59	0.667	29.81	0.667	31.63	0.666	34.22
0.685	25.91	0.685	30.21	0.688	32.14	0.687	34.80
0.703	26.22	0.704	30.68	0.706	32.57	0.708	35.35
0.722	26.58	0.724	31.16	0.724	33.01	0.726	35.78

Table 3A.D-2

Measured 4T Test Series 5101 Drywell Dome Pressure
Time History (Continued)

Run 21		Run 22		Run 24		Run 37	
Time (sec)	Pressure (psia)	Time (sec)	Pressure (psia)	Time (sec)	Pressure (psia)	Time (sec)	Pressure (psia)
0.743	27.01	0.745	31.61	0.743	33.44	0.744	36.23
0.763	27.33	0.764	31.98	0.761	33.90	0.763	36.71
0.782	27.61	0.782	32.32	0.780	34.37	0.781	37.08
0.800	27.86	0.800	32.58	0.800	34.78	0.800	37.46
0.819	29.18	0.819	32.87	0.821	35.20	0.820	37.79
0.837	28.39	0.837	33.11	0.840	35.49	0.841	38.05
0.855	28.81	0.858	33.31	0.858	35.81	0.860	38.25
0.876	29.12	0.878	33.52	0.876	36.13	0.878	38.35
0.897	29.48	0.897	33.68	0.894	36.52	0.896	38.52
0.915	29.78	0.915	33.80	0.913	36.84	0.914	38.68
0.934	30.07	0.933	33.88	0.933	37.17	0.933	38.78
0.952	30.39	0.952	33.96	0.954	37.47	0.953	33.84
0.970	30.66	0.970	34.36	0.973	37.74	0.974	38.88
0.989	30.92	0.991	34.10	0.991	37.96	0.993	38.98
1.010	31.29	1.102	34.15	1.010	38.18	1.011	39.00
1.030	31.57	1.030	34.21	1.028	38.31	1.030	39.04
1.049	31.87	1.049	34.19	1.046	38.41	1.048	39.06
1.067	32.08	1.067	34.17	1.067	38.57	1.066	39.08
1.085	32.26	1.085	34.17	1.088	38.59	1.087	39.11
1.103	32.54	1.104	34.18	1.106	38.61	1.108	39.10
1.122	32.67	1.124	34.08	1.124	38.65	1.126	39.08
1.142	32.85	1.145	34.38	1.143	38.65	1.144	39.08
1.163	33.07	1.169	34.32	1.161	38.63	1.163	39.06
1.182	33.19	1.182	33.90	1.180	38.61	1.181	39.06
1.200	33.33	1.200	33.88	1.200	38.61	1.200	39.06
1.219	33.38	1.218	33.80	1.221	38.55	1.220	39.02
1.237	33.44	1.237	33.76	1.240	38.49	1.241	38.94
1.255	33.50	1.258	33.64	1.258	38.43	1.260	38.92
1.276	33.60	1.278	33.54	1.276	38.35	1.278	38.90
1.297	33.60	1.297	33.50	1.294	38.26	1.296	38.88
1.315	33.66	1.315	33.44	1.313	38.20	1.314	38.84
1.333	33.62	1.333	33.35	1.333	38.08	1.353	38.89
1.352	33.56	1.352	33.29	1.354	37.98	1.353	38.89
1.370	33.46	1.370	33.19	1.373	37.92	1.374	38.82
1.389	33.42	1.391	33.13	1.391	37.78	1.393	38.82

Table 3A.D-3

Comparison of Measured and Calculated 4T Test
Probe Water Clearing Times

Probe Elevation Above Downcomer Exit (ft)	Probe Water Clearing Time (sec)			
	21[a]	22[a]	24[a]	37[a]
9.5	0.667 (0.687)	Initially dry	0.573 (0.582)	0.381 (0.388)
6.5	0.800 (0.811)	0.458 (0.467)	0.688 (0.688)	0.533 (0.533)
0.5	0.952 (0.961)	0.667 (0.654)	0.800 (0.813)	0.687 (0.670)

[a] 4T run number.

Note: Unbracketed numbers are measured data. Bracketed Numbers are calculated data.

Table 3A.D-4

Comparison Between Source Method
and the Reference 3A.D-9 Method for Calculation
of the Loss-of-Coolant Accident Bubble Charging Event

	Item	Source	Reference 3A.D-9	Comments
1.	Uses potential flow assumption	Yes	Yes	Same
2.	Uses point source to represent charging LOCA bubbles	Yes	Yes	Same
3.	All vents assumed to charge uniformly into spherical bubbles one radius below downcomers	Yes	Yes	Same
4.	Finite pool effects	Uses numerical scheme discussion in Attachment 3A.B of this Report	Uses MOI	-
5.	Models CGS annular suppression pool geometry	Yes	No	For MOI, the CGS annular pool geometry must be idealized into a rectangular pool using an "equivalent radius" concept.
6.	Models CGS sloping pool bottom	Yes	No	For MOI, the CGS sloping pool bottom needs to be idealized into a flat pool bottom.
7.	Transient source strength	Determined by continuity from pool surface rise obtained from the PSAM	Determined from Rayleigh bubble dynamics equation in an infinite pool and a finite pool correction factor "K"	Source method results in the same conservatism as PSAM flow field calculations. Source method yields higher velocities and accelerations than the method discussed in Reference 3A.D-9.
8.	Experimental verification of source strength	Yes	No	Source method determined directly from PSAM. PSAM has extensive experimental verification as to its conservatism.

Table 3A.D-5

Comparison of Results of Source and Method
of Reference 3A.D-9 Bubble Charging
Source Strength Methods

Time After Vent Clearing (sec)	GE Method[a]		PSAM Method[b]	
	V(ft/sec)	$\dot{V}$ (ft/sec^2)	V(ft/sec)	$\dot{V}$ (ft/sec^2)
0.	1.215	83.136	5.308	80.977
0.066[c]	4.872	81.767	10.613	79.772
0.24[d]	-	-	22.074	53.983

V = average pool surface velocity

$\dot{V}$ = average pool surface acceleration

[a] Source strength method documented in Reference 3A.D-9. Flow field data from SOURCE code.

[b] Data obtained from Figures 3A.3.2-4 through 3A.3.2-7.

[c] Near bubble coalescence by Reference 3A.D-9 method.

[d] Bubble coalescence time by SOURCE.
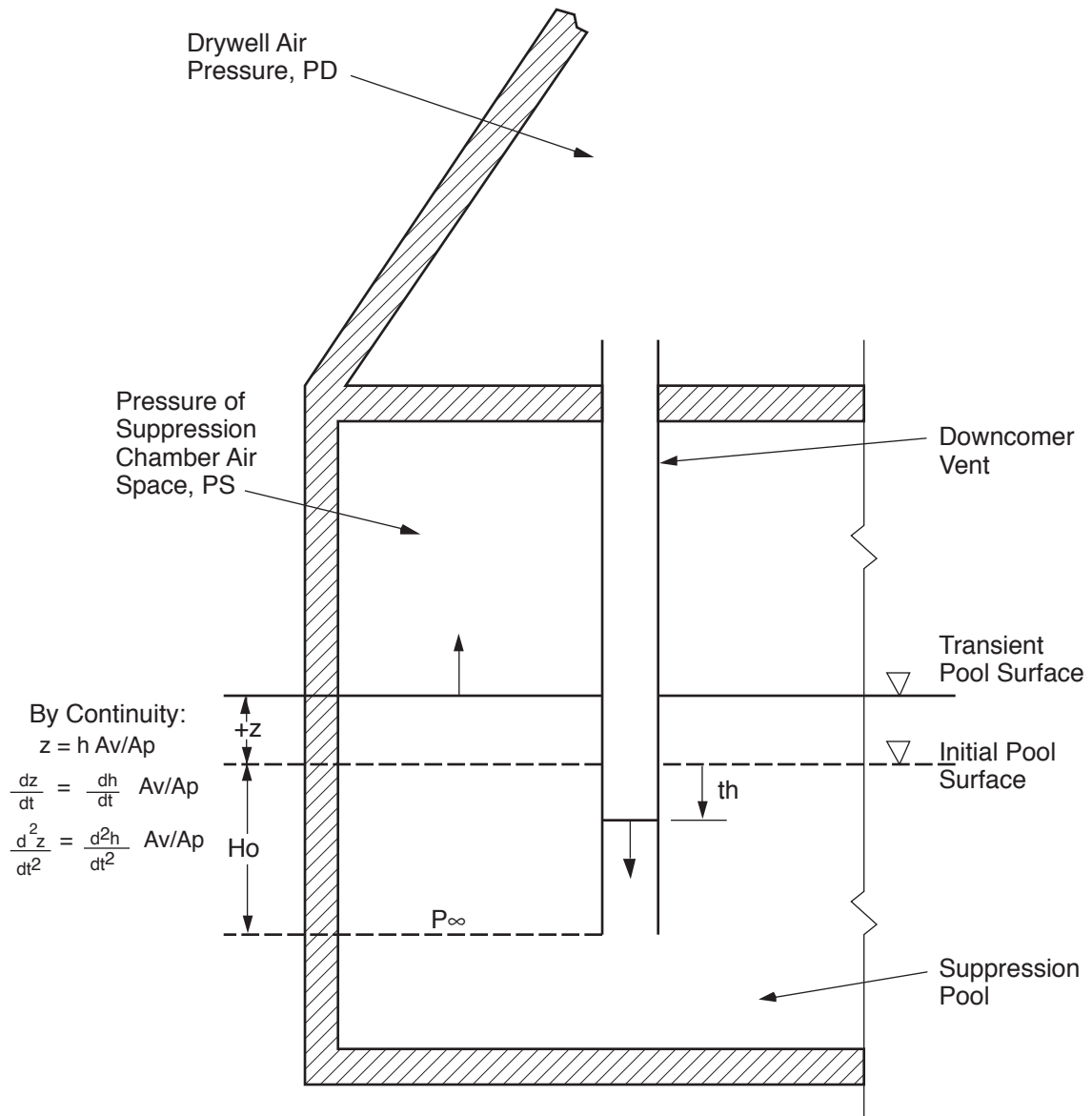
Drywell Air Pressure, PD

Pressure of Suppression Chamber Air Space, PS

Downcomer Vent

Transient Pool Surface

Initial Pool Surface

By Continuity:

$z = h \, A_v/A_p$

$$\frac{dz}{dt} = \frac{dh}{dt} \, A_v/A_p$$

$$\frac{d^2z}{dt^2} = \frac{d^2h}{dt^2} \, A_v/A_p$$

$+z$

H_0

th

P_∞

Suppression Pool

Columbia Generating Station
Final Safety Analysis Report

Schematic Representation of the Vent Clearing Model

| **Draw. No.** 900547.84 | **Rev.** | **Figure** 3A.D-1 |

Legend:
○ Probe 9.5 feet above downcomer vent exit
□ Probe 6.5 feet above downcomer vent exit
△ Probe 0.5 feet above downcomer vent exit

Calculated Time, t_c (Sec)

$t_c = 1.0047t_m + 0.0013$
(Least Squares Linear Regression Curve Fit)

$t_c = t_m$

Measured Time, t_m (Sec)

Columbia Generating Station
Final Safety Analysis Report

Comparison of Measured and Calculated 4T Test Probe Water Clearing Times

Draw. No. **900547.85**   Rev.   Figure **3A.D-2**

Form No. 960690

Drywell Air Pressure, PD

Pressure of
Suppression Chamber
Air Space, PS

Downcomer Vent

Vw

Pool Surface At
▽ Any Time, t

y

▽ t = 0 Initial
Pool Surface

Water Slug

H_o

Air Slug
Pressure, PB

Bubble Volume
VB

Suppression Pool

Columbia Generating Station
Final Safety Analysis Report

Schematic Representation of the
Pool Swell Model

Draw. No. 900547.86 | **Rev.** | **Figure** 3A.D-3
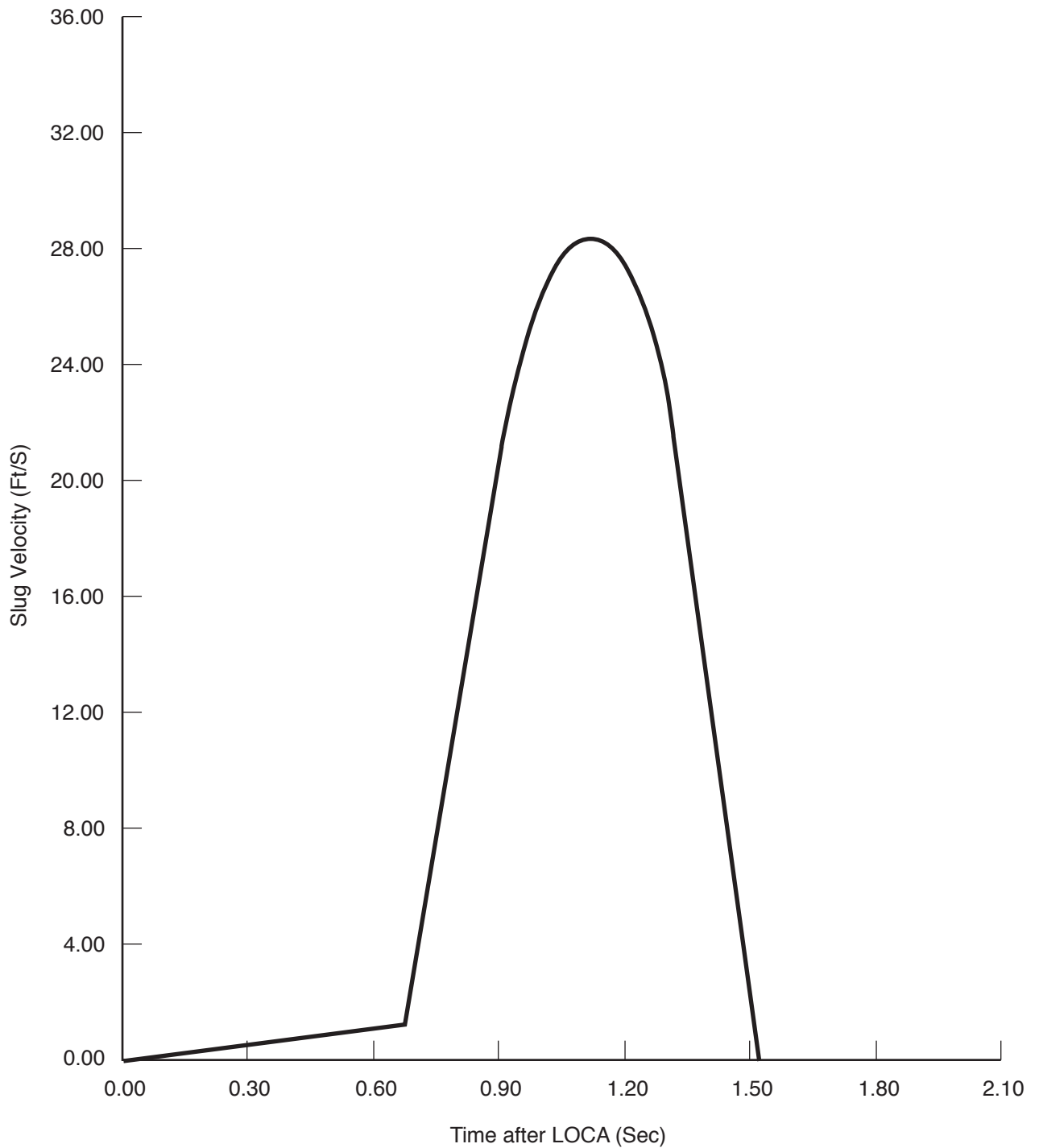
Slug Velocity (Ft/S)

Time after LOCA (Sec)

| Columbia Generating Station Final Safety Analysis Report | Benchmark I Plant - Slug Velocity Versus Time |

| Draw. No. 900547.87 | Rev. | Figure 3A.D-4 |

Form No. 960690

Slug Velocity (Ft/S) vs Slug Displacement (Ft)

	Columbia Generating Station Final Safety Analysis Report	Benchmark I Plant - Slug Velocity Versus Displacement

Draw. No. 900547.88	Rev.	Figure 3A.D-5

Form No. 960690

36.00

32.00

28.00

24.00

20.00

16.00

12.00

8.00

4.00

0.00

Slug Velocity (Ft/S)

0.00   0.30   0.60   0.90   1.20   1.50   1.80   2.10

Time after LOCA (Sec)

**Columbia Generating Station
Final Safety Analysis Report**

Benchmark II Plant - Slug Velocity Versus Time
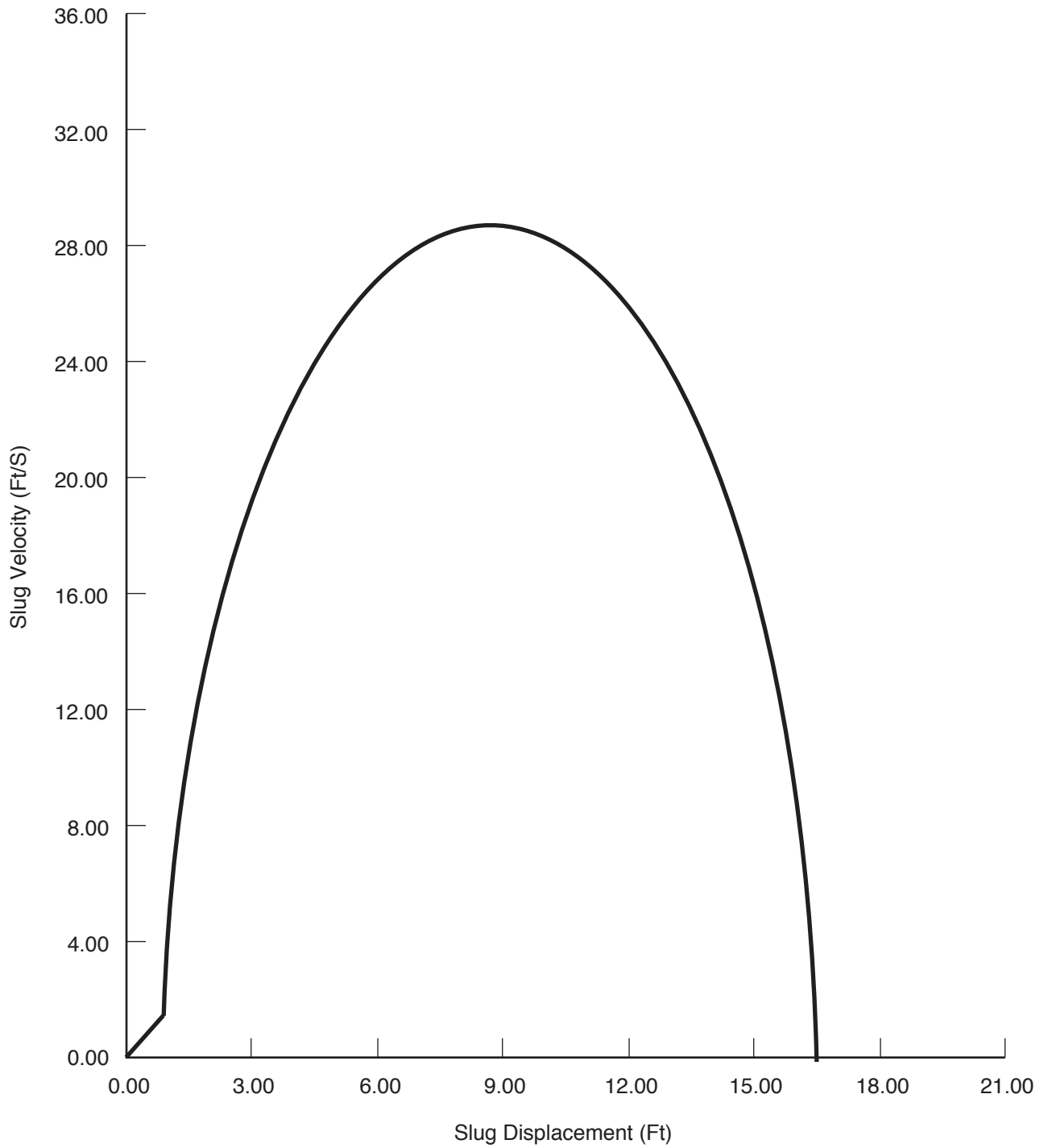
Draw. No. **900547.89**   Rev.   Figure **3A.D-6**
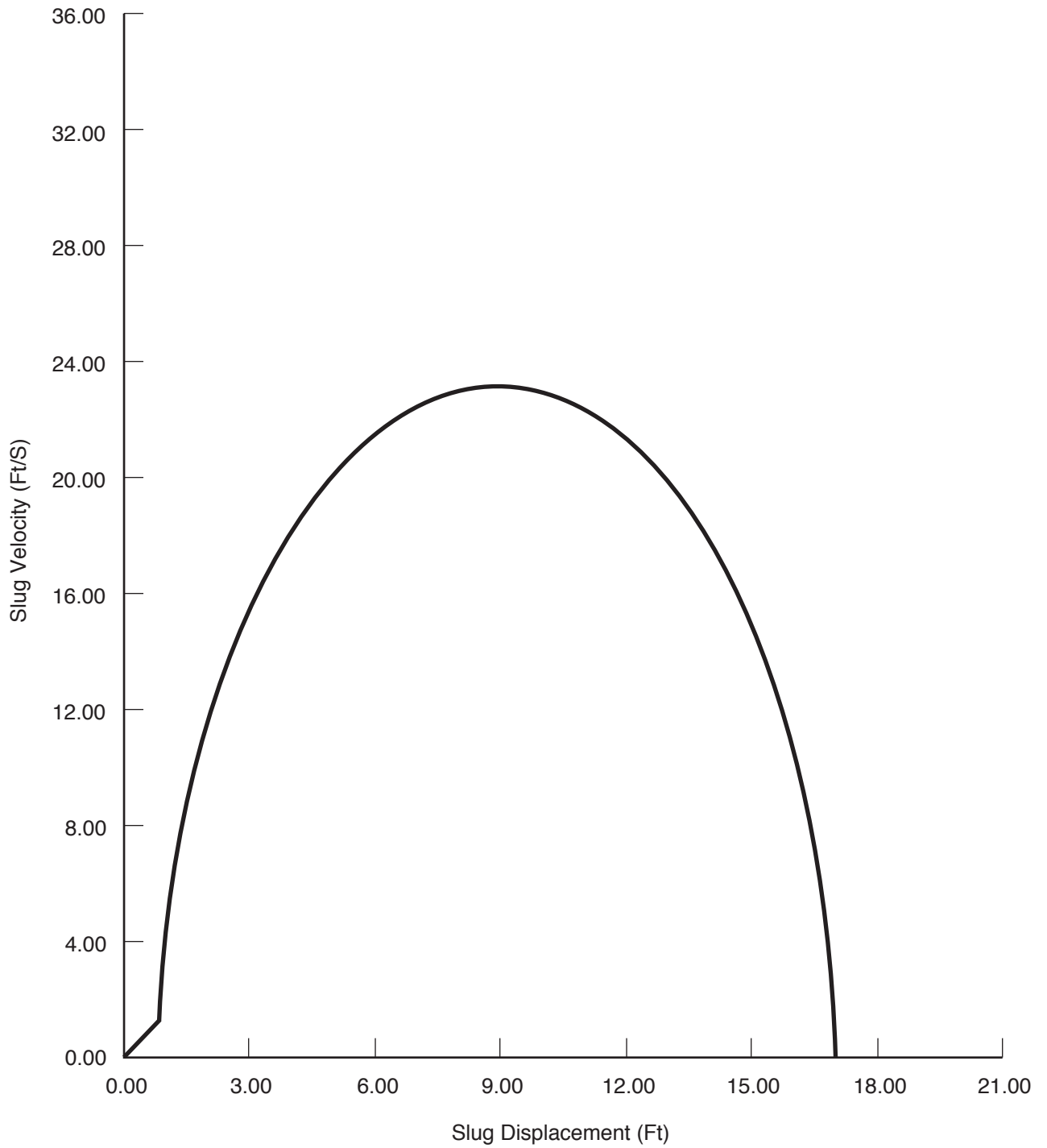
Form No. 960690

Slug Velocity (Ft/S)

Slug Displacement (Ft)

Columbia Generating Station Final Safety Analysis Report	Benchmark II Plant - Slug Velocity Versus Displacement
	Draw. No. 900547.90	**Rev.**	**Figure** 3A.D-7

Form No. 960690

Slug Velocity (Ft/S)

Time after LOCA (Sec)

Columbia Generating Station Final Safety Analysis Report	Benchmark III Plant - Slug Velocity Versus Time	
	Draw. No. **900547.91**	Rev.	Figure **3A.D-8**
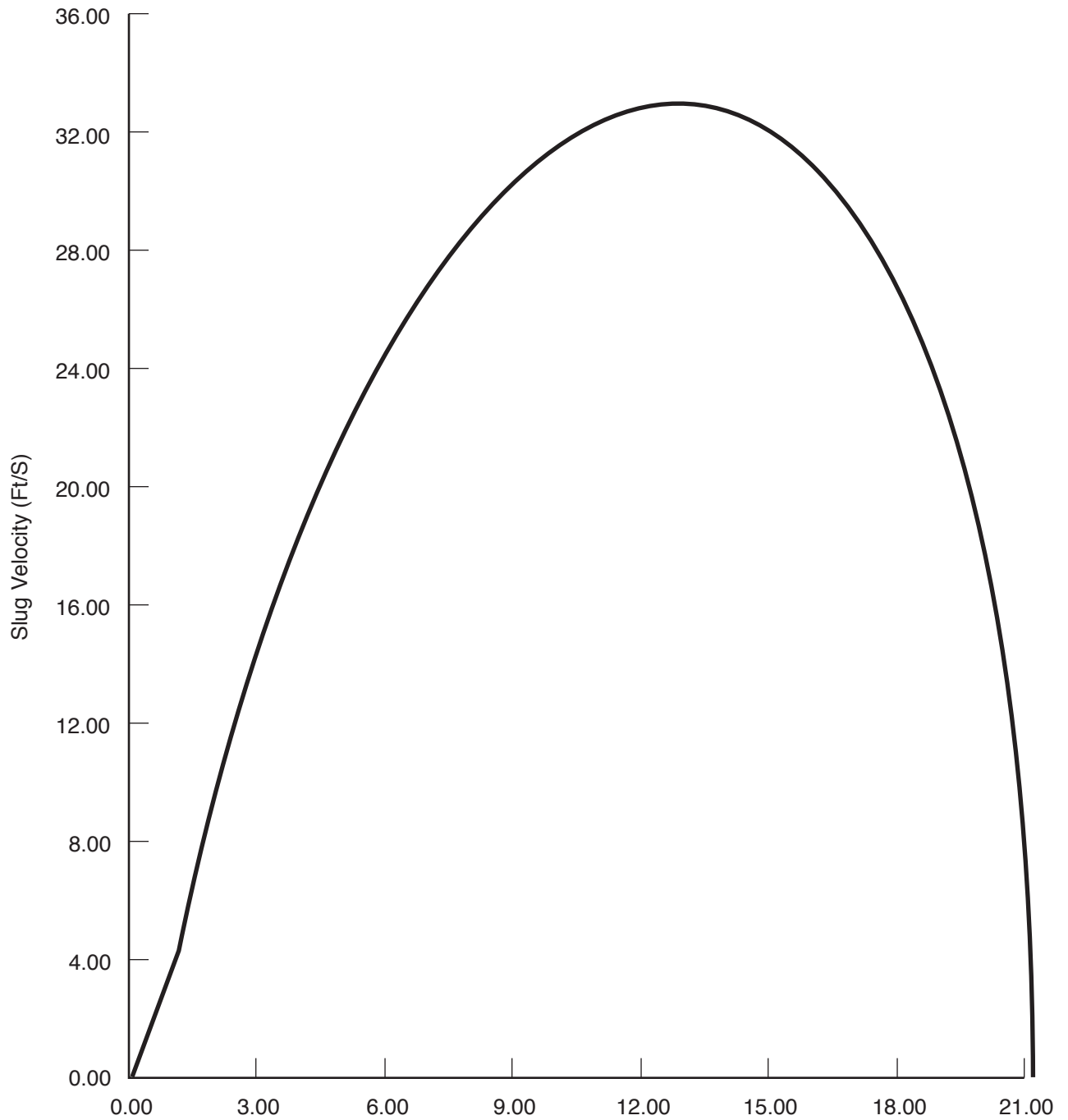
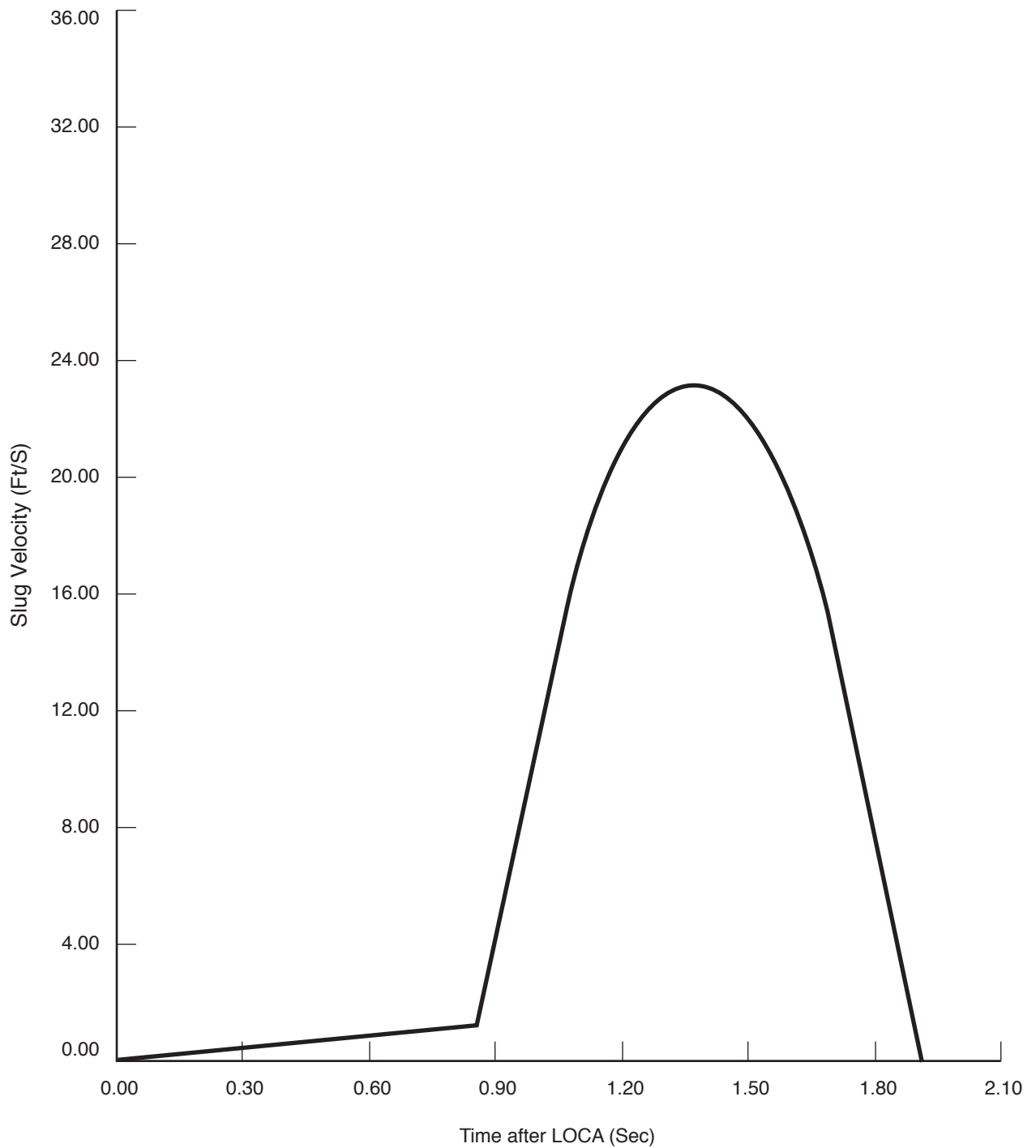Slug Velocity (Ft/S) versus Displacement axis (0.00 to 21.00)

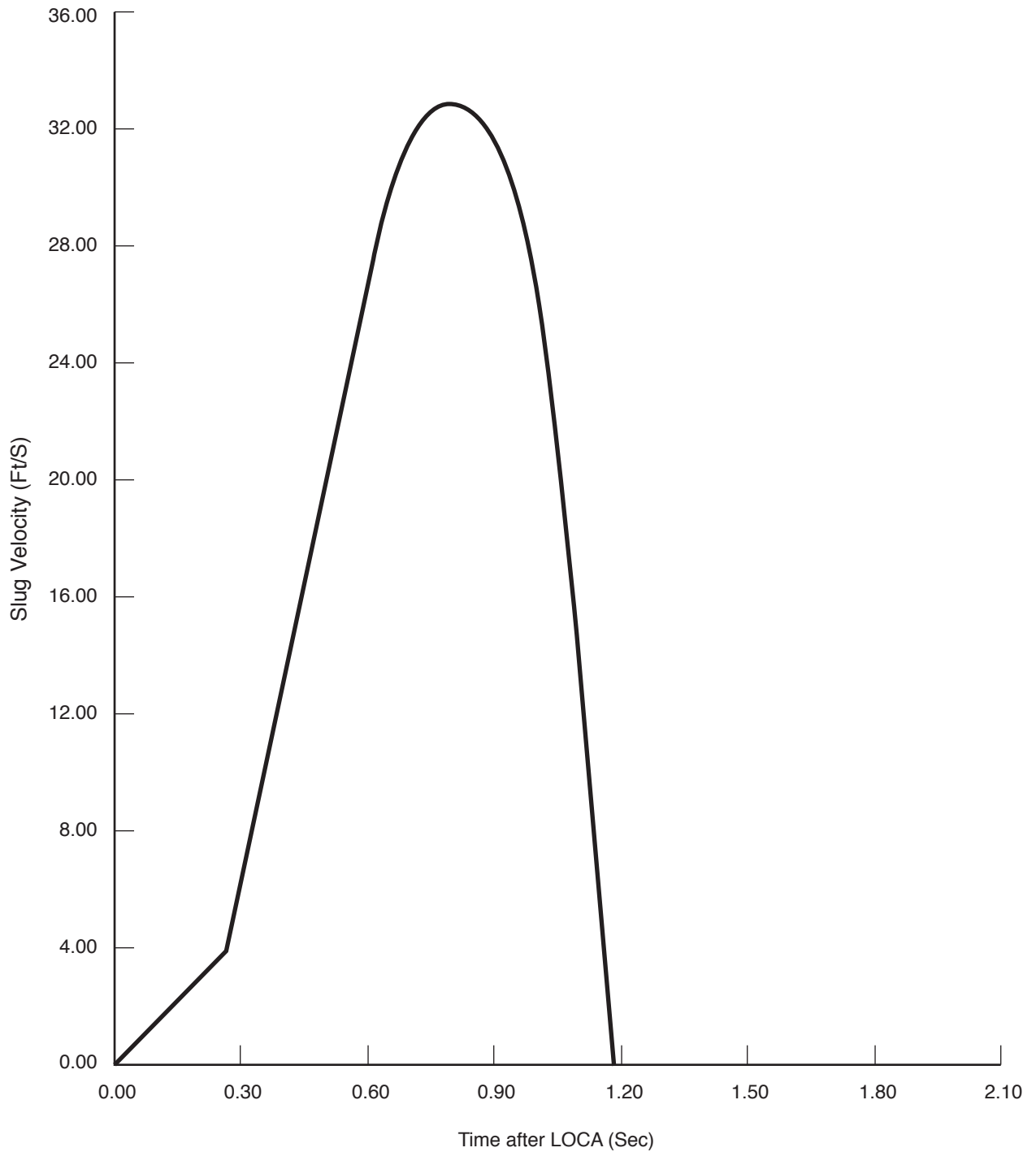| Columbia Generating Station Final Safety Analysis Report	Benchmark III Plant - Slug Velocity Versus Displacement
	Draw. No. **900547.92** Rev. Figure **3A.D-9**

Infinite Pool:

Steps

i) Spherical Bubble Dynamics
    Governed By Rayleigh Equation:

$$R\ddot{R} + \frac{3}{2}\dot{R}^2 = \frac{gc}{\ell}(P_B - P_\infty)$$

ii) From R, $\dot{R}$, And $\ddot{R}$ Get Source
    Strengths For Each Bubble

$$Q_i(t) = R^2\dot{R}$$
$$\dot{Q}_i(t) = R^2\ddot{R} + 2R\dot{R}^2$$
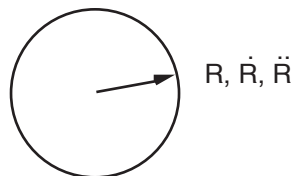
Note: $R \equiv R(t)$

$$\dot{R} \equiv \frac{dR}{dt}$$
$$\ddot{R} \equiv \frac{d^2R}{dt^2}$$

$R, \dot{R}, \ddot{R}$

Application To Finite Pool:

iii) Determine "K_i" Factor for
    Each Bubble to Account for
    Finite Pool and Other
    Bubble Effects

iv) Modify Source Strength for
    Each Bubble to Account for
    Finite Pool and Other
    Bubble Effects:

$$Q_i(t) = R^2\dot{R}K_i$$
$$Q_i(t) = R^2\dot{R} + 2R\dot{R}^2)K_i$$

v) Superposition Of All
    Bubbles To Get Flow Field:
    Velocity V, and Acceleration $\dot{V}$

$$V = -\sum_{i=1}^{102} Q_i(t)\,\nabla\phi_i$$
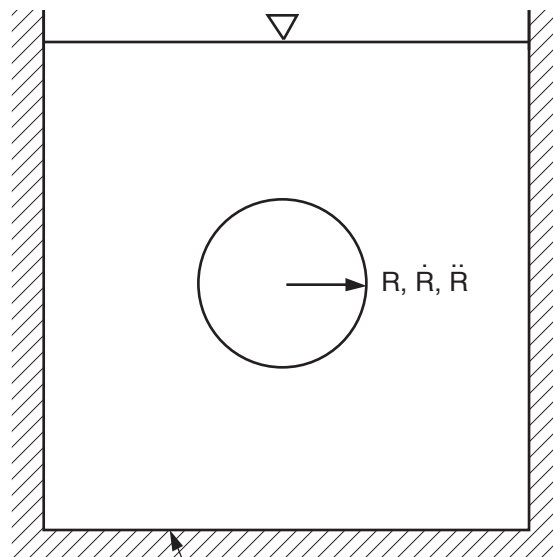
$$\dot{V} = -\sum_{i=1}^{102} \dot{Q}_i(t)\,\nabla\phi_i$$

$R, \dot{R}, \ddot{R}$

Containment
Boundary

Method of Images

Columbia Generating Station
Final Safety Analysis Report

Draw. No. 900547.93	Rev.	Figure 3A.D-10

Attachment 3A.E

SUPPRESSION POOL TEMPERATURE MONITORING SYSTEM

3A.E.1   DESIGN BASES

The suppression pool temperature monitoring (SPTM) system monitors the suppression pool bulk temperature with sensors distributed around the suppression pool. This system provides the main control room operator with the information necessary to avoid the conditions which might lead to the high-temperature steam quenching vibration phenomena mentioned below and discussed in detail in Section 3.5 of Reference 3A.E-1. This phenomena is not expected to occur when using a quencher discharge device. However, precautions using the SPTM system are designed to further make the occurrence of the vibrations impossible. Temperatures in the suppression pool are recorded and alarmed in the main control room.

The design basis for the SPTM system alarm setpoints provides the operator with adequate time to take the necessary action required to ensure that the conditions which are postulated to lead to high-temperature steam quenching vibrations do not occur. The design also provides the operator with the necessary information regarding localized heat-up of the pool water while the reactor vessel is being depressurized using the safety/relief valves (SRVs) when the SRVs are selected for actuation, they may be chosen so as to ensure mixing and uniformity of heat energy injection to the pool by monitoring the temperature sensors.

3A.E.1.1   High-Temperature Steam Quenching Vibrations

Boiling water reactor plants take advantage of the large thermal capacity of the suppression pool during plant transients which require SRV actuation. The discharge steam from each SRV is directed through a discharge line and a quencher device to the suppression pool where it is condensed. This results in an increase in pool water temperature, but a negligible increase in containment pressure.

However, certain events such as small pipe break have the potential for substantial energy addition to the suppression pool and could result in a high local pool temperature and the phenomenon of steam quenching vibration if timely corrective action is not taken. Suppression pool structural vibrations would occur during this condensing mode which would be forced by the periodic pulsation of the steam jet at the discharge.

The onset of the high-temperature steam quenching vibration phenomenon is a function of both the local suppression pool water temperature and the steam mass flux rate. The steam mass flux in the SRV piping in turn, is a function of the reactor vessel pressure.

3A.E.2   SYSTEM DESCRIPTION

The CGS SPTM system conformance to the criteria set by paragraph III.c of
Reference 3A.E-2 is as discussed below. Specifically, the criteria for the upper ring of the
sensors are:

1.   Each monitoring location has two redundant type thermocouples monitored in
the control room;

2.   There are eight monitoring locations equally spaced about the outer containment
perimeter;

3.   The sensors are mounted 7 in. below the minimum technical specification water
level;

4.   All sensors are monitored and recorded in the control room;

5.   Instrument setpoints for alarms will be set at the technical specification
temperature values such that the plant can be shutdown and depressurized prior
to the water in the suppression pool reaching a temperature at which
condensation instabilities are postulated to occur; and

6.   The SPTM system monitors are Seismic Category 1, Quality Class 1. The
electrical power is Class 1E. Divisional separation is maintained.

In addition to the sensors described above which monitor bulk temperature, there is a second,
lower ring of sensors. The lower ring meets Criteria 2, 4, 5, and 6, above. The degree of
conformance to Criteria 1 and 3 for the lower ring of sensors is as follows:

1.   Each monitoring location has one thermocouple Division 1 and 2 at alternate
locations, and

3.   The sensors are mounted at el. 447 ft 10.25 in., the approximate elevation of
the quencher discharge devices.

Since warmer water is more buoyant, the upper ring provides a more conservative value for
bulk temperature than the lower ring. The lower ring of sensors is provided to allow the
operator to assess if significant vertical thermal stratification occurs.

3A.E.3   REFERENCES

3A.E-1   Mark II Containment Dynamic Forcing Function Information Report (DFFR),
NEDO-21061, Revision 3, June 1978.

3A.E-2   Mark II Containment Lead Plant Program Load Evaluation and Acceptance
Criteria, Nuclear Regulatory Commission, NUREG-0487, October 1978.

Attachment 3A.F

COMPUTER PROGRAMS

The following are the programs referenced in this report:

3A.F.1   COMMERCIALLY AVAILABLE PROGRAMS

ANSYS

ANSYS is a large scale general purpose finite element computer program used for the solution of several classes of engineering analysis problems. Analytical capabilities include: static and dynamic analyses; plastic, creep and swelling analyses; and steady state and transient heat transfer analyses.

NASTRAN

NASTRAN is a large scale general purpose finite element computer program used for the solution of several classes of engineering analysis problems. Analytical capabilities include: static and dynamic analyses; thermal analyses; and the determination of eigenvalues for use in vibration analyses.

MCAUTO-STRUDL

MCAUTO-STRUDL is a commercially available computer program with general capability for the static and dynamic analysis of structures. The program, which is serviced and maintained by the McDonnell Douglas Automation Company, St. Louis, Missouri, has had wide commercial usage for many years.

ADLPIPE

ADLPIPE is a commercially available program used for the analysis of piping systems. Analytical capabilities include: static and dynamic analyses; and thermal analyses including thermal transient and fatigue evaluations for Class 1 piping systems.

FLUSH

FLUSH is a non-linear plain strain finite element seismic analysis program for soil-structure interaction analysis.

3A.F.2   BURNS AND ROE DEVELOPED PROGRAMS

<u>BESSEL</u>

BESSEL is a computer program which computes semi-analytical hydrodynamic added masses (incompressible fluids) for cylindrical and annular geometries

<u>HYDI-1</u>

HYDI-1 is a finite element program which computes hydrodynamic added masses and incident pressures for compressible fluids in three dimensional geometries.

<u>FOX/HYDI-2</u>

FOX/HYDI-2 is a finite element computer program used for the dynamic analysis for axisymmetric structures. The program performs the analysis by determining structural displacements in the frequency domain.

<u>SWELL</u>

This program is discussed in detail in Attachment 3A.D.

<u>VENT</u>

This program is discussed in detail in Attachment 3A.D.

<u>SOURCE</u>

This program is discussed in detail in Attachment 3A.B.

Attachment 3A.H

CONFORMANCE OF CGS DESIGN TO NRC ACCEPTANCE CRITERIA

Table 3A.H-1 is a summary of the CGS position for each of the pool dynamic loads. This table provides a description of each load or phenomenon, the Mark II Owner's Group load specification, the NRC evaluation reference, and the CGS position on the acceptance criteria for each load.

Load or Phenomenon	Mark II Owners Group Load Specification	NRC Evaluation	CGS Position on Acceptance Criteria
I. Loss-of-coolant accident (LOCA)-related hydrodynamic loads			
A. Submerged boundary loads during vent clearing	24 psi over-pressure added to local hydrostatic below vent exit (walls and basemat) - linear attenuation to pool surface.	II.A.1 [a]	Acceptable
B. Pool swell loads			
1. Pool swell analytical model (PSAM)			
a) Air bubble pressure	Calculated by the PSAM used in calculation of submerged boundary loads.	III.B.3.a [b]	Acceptable
b) Pool swell elevation	Use PSAM with polytropic exponent of 1.2 to a maximum swell height which is the greater of 1.5 vent submergence or the elevation corresponding to the drywell floor uplift P per NUREG 0487 criteria I.A.4. The associated maximum wetwell air compression is used for design assessment.	II.A.2 [c]	Acceptable

Table 3A.H-1

Conformance of CGS Design to NRC Acceptance Criteria (Continued)

Load or Phenomenon	Mark II Owners Group Load Specification	NRC Evaluation	CGS Position on Acceptance Criteria
c) Pool swell velocity	Velocity history vs. pool elevation predicted by the PSAM used to compute impact loading on small structures and drag on gratings between initial pool surface and maximum pool elevation and steady-state drag between vent exit and maximum pool elevation. Analytical velocity variation is used up to maximum velocity. Maximum velocity applies thereafter up to maximum pool swell. PSAM predicted velocities multiplied by a factor of 1.1.	III.B.3.a.3 [a]	Acceptable
d) Pool swell acceleration	Acceleration predicted by the PSAM. Pool acceleration is utilized in the calculation of acceleration loads on submerged components during pool swell.	III.B.3.a.4 [b]	Acceptable
e) Wetwell air compression	Wetwell air compression is calculated by PSAM.	II.A.2 [c]	Acceptable
f) Drywell pressure	Methods of NEDM-10320 and NEDO-20533 Appendix B. Utilized in PSAM to calculate pool swell loads.	III.B.3.a.6 [b]	Acceptable

Table 3A.H-1

Conformance of CGS Design to NRC Acceptance Criteria (Continued)

Load or Phenomenon	Mark II Owners Group Load Specification	NRC Evaluation	CGS Position on Acceptance Criteria
2. Loads on submerged boundaries	Maximum bubble pressure predicted by the PSAM added uniformly to local hydrostatic below vent exit (walls and basemat) liner attenuation to pool surface. Applied to walls up to maximum pool elevation.	III.B.3.b [b]	Acceptable
3. Impact loads			
a) Small structures	1.35 x pressure-velocity correlation for pipes and I beams based on PSTF impulse data and flat pool assumption. Variable pulse duration.	III.B.3.c.1 [b]	Acceptable
b) Large structures	None - Plant-unique load where applicable.	III.B.3.c.6 [b] Criteria A.5 [a]	Acceptable. CGS has no large structures in the pool swell zone
c) Grating	No impact load specified. P drag vs. open area correlation and velocity vs. elevation history from the PSAM. P drag multiplied by dynamic load factor.	III.B.3.c.3 [b] Criteria A.3 [a]	Acceptable

Load or Phenomenon	Mark II Owners Group Load Specification	NRC Evaluation	CGS Position on Acceptance Criteria
4. Wetwell air compression			
a) Wall loads	Direct application to the PSAM calculated pressure due to wetwell compression.	III.B.3.d.1 [b]	Acceptable
b) Diaphragm floor upward loads	5.5 psid for diaphragm floor loadings only.	2.12.7 [a]	Acceptable
5. Asymmetric pool LOCA	Use 20% of maximum pressure statistically applied to 1/2 of the submerged bubble.	II.A.3 [c] Criteria A-4 [a]	Acceptable
C. Steam condensation and chugging loads			
1. Downcomer lateral loads			
a) Single vent loads (24 in.)	Use single vent dynamic lateral load developed in NEDE-23806.	2.3.3.2 [a] Criteria B.1.a [a]	Acceptable
b) Multiple vent loads (24 in.)	Use multivent dynamic lateral load developed in NEDE-24106-P and NEDE-24794-P.	2.3.3.3 [a]	Acceptable
c) Single/multiple vent loads (28 in.)	Multiply basic vent loads by factor f=1.34	2.3.2.1 [a] B.1.b [a]	Acceptable

Conformance of CGS Design to NRC Acceptance Criteria (Continued)

Load or Phenomenon	Mark II Owners Group Load Specification	NRC Evaluation	CGS Position on Acceptance Criteria
2. Submerged boundary loads			
a) High/medium steam flux condensation oscillation (CO) load	Use method described in NEDE-24288-P[d]	2.2.2.1.3 [a]	CO loads are not governing design condition for CGS
b) Low steam flux chugging loads	Representative pressure fluctuation taken from 4TCO (NEDE-24285-P) test added to local hydrostatic	2.2.2.3 [a]	Plant unique. Chugging report entitled "Chugging Loads-Revised. Definition and Application Methodology for Mark II Containments" submitted July 1981
- Uniform loading conditions	Use method described in NEDE-24302-P[d]		See above
- Asymmetric loading	Representative pressure fluctuation taken from 4TCO test [NEDE-24285-P] applied as described in NEDE-24822-P.		See above

Load or Phenomenon	Mark II Owners Group Load Specification	NRC Evaluation	CGS Position on Acceptance Criteria
II. Safety/relief valve (SRV)-related hydrodynamic loads			
A. Pool temperature limits for X-quencher	20°F subcooling at quencher elevation for steam mass flux of 42 lb/ft^2-sec or less. 200°F for steam flux greater than 94 lb/ft^2-sec.	6.2.1.8.8 (5) A (4)	Acceptable
B. Quencher air clearing loads	Mark II plants utilizing the four arm quencher, use quencher load methodology described in DFFR.	Criteria II.2 [b]	CGS Plant unique SRV (x-quencher) load report entitled "SRV Loads - Definition and Application Methodology for Mark II Containments" submitted August 1980
C. Quencher arm and tie-down loads	Includes vertical and lateral arm load transmitted to the basemat via the tie-down.	III.C.2.e.2 [b]	Acceptable
1) X-quencher arm loads	Vertical and lateral loads developed on the basis of bounding assumption for air/water discharge from the quencher and conservative combinations of maximum/ minimum bubble pressure acting on the quencher.	III.C.2.e.1	Acceptable

Conformance of CGS Design to NRC Acceptance Criteria (Continued)

Load or Phenomenon	Mark II Owners Group Load Specification	NRC Evaluation	CGS Position on Acceptance Criteria
2. X-quencher tie-down loads	II.C.1 above plus vertical transient wave and thrust loads. Thrust load calculated using a standard momentum balance. Vertical and lateral moments for air or water clearing are calculated based on conservative clearing assumptions.	III.C.2.e.2 [b]	Acceptable
III. LOCA/SRV submerged structure loads			
A. SRV air bubble loads			
1. Standard drag in Accelerating flow fields	Drag Coefficients are presented in Attachment 1.k of the Zimmer FSAR.	Acceptable with the following modification: 1) Use $C_H = C_M - 1$ in the F_A formula 2) For noncylindrical structures use lift coefficient for appropriate shape or $C_L = 1.6$	Generic methodology acceptable. (Amplitudes for SRV loads verified by CAORSO data on submerged structures).

Load or Phenomenon	Mark II Owners Group Load Specification	NRC Evaluation	CGS Position on Acceptance Criteria
		3) The standard drag coefficient for pool swell and SRV oscillating bubbles should be based on data for structures with sharp edges	
2. Equivalent uniform flow velocity and acceleration	Structures are segmented into small sections such that $1.0 \leq L/D \leq 1.5$. The loads are then applied to the geometric center of each segment.	Acceptable	See III. A.1. above
3. Interference effects	A detailed methodology is presented in Attachment 1.k of the Zimmer FSAR.	Acceptable	See III. A.1 above
B. LOCA jet loads	Calculated by the Ring Vortex Model.	2.2.4.3 [a]	Acceptable

Conformance of CGS Design to NRC Acceptance Criteria (Continued)

Load or Phenomenon	Mark II Owners Group Load Specification	NRC Evaluation	CGS Position on Acceptance Criteria
C. Steam condensation drag loads	No generic load methodology provided	CGS load specification and NRC review is addressed in CGS SER	Generic "drag load" methodology acceptable Plant unique flow fields are consistent with I.C.2.a and I.C.2.b of this table. (See DAR Attachment 3A.I)
IV. Secondary loads			
A. Sonic wave load	Negligible load - none specified	Acceptable	Acceptable
B. Compressive wave load	Negligible load - none specified	Acceptable	Acceptable
C. Post swell wave load	No generic load provided	Plant unique load specification addressed in CGS SER	
D. Seismic slosh load	No generic load provided	Plant unique load specification addressed in CGS SER	

Table 3A.H-1

Conformance of CGS Design to NRC Acceptance Criteria (Continued)

Load or Phenomenon	Mark II Owners Group Load Specification	NRC Evaluation	CGS Position on Acceptance Criteria
E. Fallback load on submerged boundary	Negligible load - none specified	Acceptable	Acceptable
F. Thrust loads	Momentum balance	Acceptable	Acceptable
G. Friction drag loads on vents	Standard friction drag calculations	Acceptable	Acceptable
H. Vent clearing loads	Negligible load - none specified	Acceptable	Acceptable

[a] NRC Acceptance Criteria set forth in NUREG-0808.

[b] NRC Acceptance Criteria set forth in NUREG-0487.

[c] NRC Acceptance Criteria set forth in Supplement 1 of NUREG-0487.

[d] NRC Acceptance Criteria set forth in WNP-2 SER NUREG (0892).

Attachment 3A.I

SAFETY/RELIEF VALVE AND LOSS-OF-COOLANT ACCIDENT LOADS
ON SUBMERGED STRUCTURES

3A.I.1   INTRODUCTION

The loss-of-coolant accident (LOCA)/safety/relief valve (SRV) discharge devices and other submerged structures are shown in Figures 3A.2.1-2, 3A.2.1-6, 3A.2.1-7, and 3A.2.1-8 and identified in Table 3A.I-1.

The most significant hydrodynamic load for each structure is identified in Table 3A.I-1.

3A.I.2   SUMMARY OF METHODOLOGY USED FOR DEFINING LOSS-OF-COOLANT ACCIDENT JET/BUBBLE LOADS

Loss-of-coolant accident jet/bubble loads are defined using the ring vortex model. The pool is divided into zones and to ensure conservatism in design, the largest velocity and acceleration values seen by a submerged structure are assumed equal to the maximum calculated values anywhere in the applicable zone. The LOCA bubble charging model is used to verify/ensure that the design values are conservative.

3A.I.3   SUMMARY OF METHODOLOGY USED FOR DEFINING LOSS-OF-COOLANT ACCIDENT STEAM CONDENSATION LOADS

Generic "drag load" methodology and plant unique flow fields are used for LOCA steam condensation loads on submerged structures in compliance with the NRC acceptance criteria. Plant unique flow fields are defined consistently with steam condensation boundary loads.

The generic methodology identifies three components of flow induced loads on submerged structures: acceleration dependent and velocity square dependent in-line loads, velocity square dependent lift load (normal to the direction of flow).

Representative plant unique chugging flow fields show that the chugging loads on submerged structures are due to acceleration or pressure gradients established in the pool during the impulsive chugging phenomenon, i.e., velocity dependent loads are small.

3A.I.4   SUMMARY OF METHODOLOGY USED FOR DEFINING SAFETY/RELIEF VALVE LOADS

Caorso SRV test data on submerged structures are examined to supplement theoretical approaches of the acceptance criteria. The data and their correlation with theoretical approaches of the acceptance criteria confirm that SRV loads are primarily due to pressure

gradients established in the pool during the SRV discharge, i.e., velocity dependent loads are small.

The dynamic pressure gradients measured across Caorso column, vent and SRV line are used to define the peak load values (at quencher elevation), the spatial distribution of the load and its time dependence.

The pressure time histories recorded on submerged structures show waveform characteristics similar to those recorded at pool boundary. The SRV loads on submerged structures are defined consistently with the plant unique boundary loads.

The SRV loads on Columbia Generating Station structures are calculated using the following formula:

$$P = \left[\frac{\pi D^2}{4} \right] \left[\frac{d_{Caorso}^2}{d_{WNP2}^2} \right] \alpha \, P_b \, L$$

where:

P = load on a structure (force/unit length)

D = diameter of the structure

α = a load gradient factor established using Caorso SRV test data on submerged structures. The method to calculate (α) is explained in the notes for and in Figure 3A.I-1

d_{Caorso} = horizontal distance of the structure from the nearest actuating quencher in Caorso plant

d_{WNP2} = horizontal distance of the structure from the nearest actuating quencher

P_b = boundary pressure load definition from Reference 3A.I-1 including any modifications agreed upon with the NRC

L = load margin = minimum value of 1.4 is used for all piping which are adequately braced and a value of 2.0 is used for the column which is the only unbraced structure and is closest to the nearest quencher

Notes on Figure 3A.I-1

1. The SRV load gradient is obtained from Caorso data as follows:

$$A = \frac{P_f - P_{ba}}{D} = \alpha P_{19}$$

where:

A $=$ measured gradient across the cylindrical structure

P_f $=$ P_{front}

P_{ba} $=$ P_{back}

2. P_{19}, P_f, P_{ba} waveform characteristics are similar.

3. The value of (α) for each set of P_f (P_{42}, P_{41}, P_{33}, P_{24}) and P_{ba} (P_{40}, P_{39}, P_{53}) is obtained from Caorso SRV test data (single and multiple valve actuations).

4. For miscellaneous piping which run along the suppression pool boundary, the load gradient factor (α) equal to that for the column is specified.

3A.I.5   REFERENCES

3A.I-1   "SRV Loads - Improved Definition and Application Methodology for Mark II Containments," Technical Report (Proprietary), prepared by Burns and Roe, Inc. for application to Washington Public Power Supply System Nuclear Project No. 2, submitted to the Nuclear Regulatory Commission on 7/29/80.
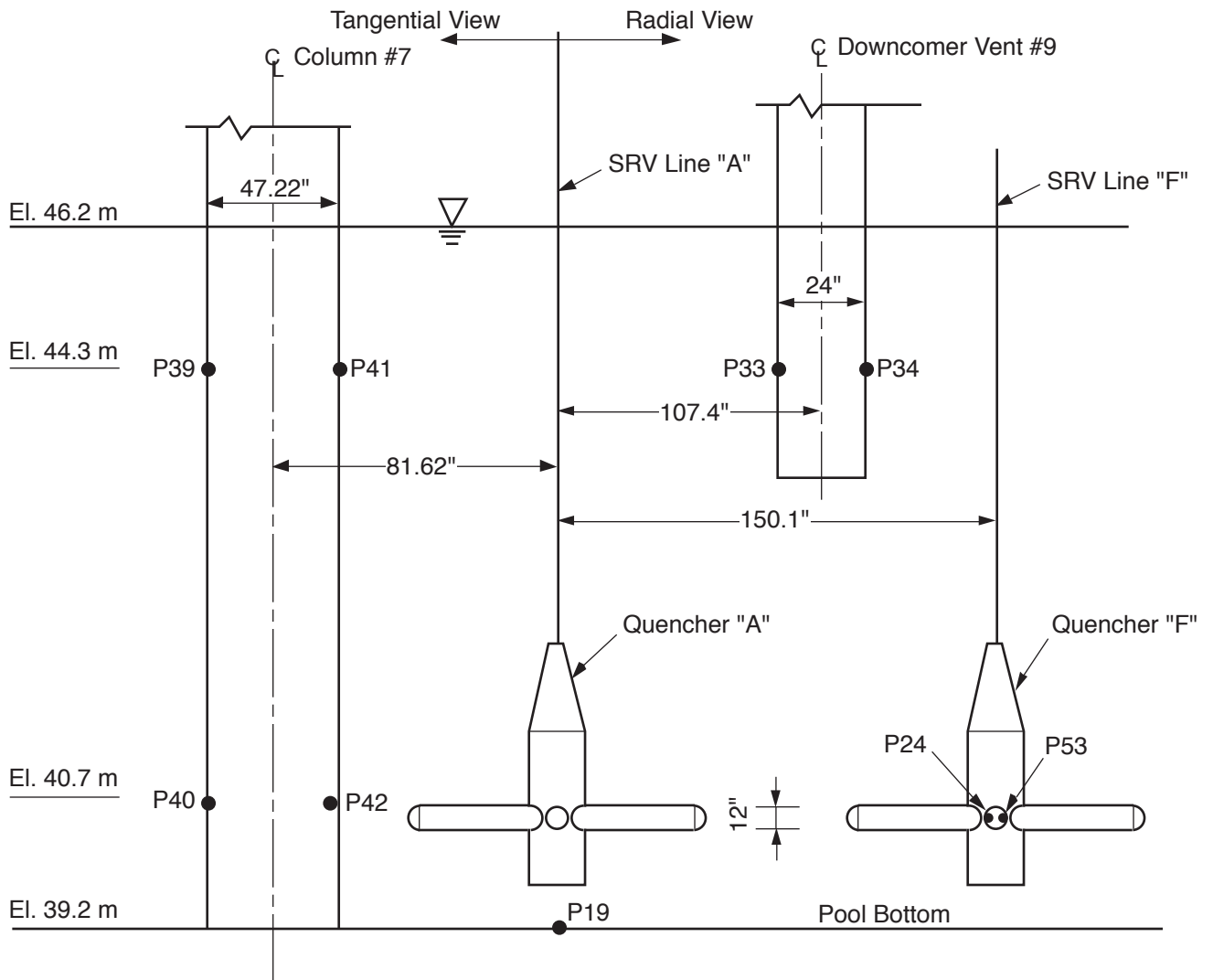
Table 3A.I-1

Loss-of-Coolant Accident/Safety/Relief Valve Loads
on Submerged Structures

Identification of Structures	Identification of Most Significant Hydrodynamic Load
1. (a) SRV line	SRV (due to actuation of adjacent SRV) [a]
(b) Quencher [b]	LOCA jet on arms
(c) Quencher Support [b]	None significant
2. Downcomer vents	SRV
3. Concrete columns	SRV
4. Bracing truss [b] at vent exit	Pool swell drag
5. Platform with grating (at el. 472 ft 4 in., 78% open area)	Pool swell drag
6. Miscellaneous piping, penetrations and supports along containment boundary	
(a) Below vent exit (el. 454 ft 4.75 in.)	LOCA jet and SRV [a]
(b) Above vent exit, below initial pool surface (el. 466 ft 4.75 in.)	Pool swell drag
(c) Above initial pool surface, below maximum pool swell (el. (484 ft 4.75 in.)	

[a] See also discussion presented in Reference 3A.3.1-8.

[b] Loads on discharge devices and their supports during discharge through the devices are addressed elsewhere.

Tangential View — Radial View

Ͼ Column #7

Ͼ Downcomer Vent #9

SRV Line "A"

SRV Line "F"

47.22"

El. 46.2 m

24"

El. 44.3 m   P39 ● ●P41   P33 ● ●P34

107.4"

81.62"

150.1"

Quencher "A"   Quencher "F"

P24   P53

El. 40.7 m   P40 ● ●P42   12"

El. 39.2 m   P19   Pool Bottom

Columbia Generating Station **Final Safety Analysis Report**	**Location of Pressure Transducers on Caorso Submerged Structures**		
	Draw. No. 900547.95	**Rev.**	**Figure 3A.I-1**